Sveriges geologiska undersökning

FoU rapport: Projekt nummer 35100

Utveckling av mjukvara till ett nytt portabelt radiomagnetotellurik (RMT) instrument

Mehrdad Bastani
2009

SGUs eget finansierad FoU projekt

SGU-rapport 2009:18

Utveckling av mjukvara till ett nytt portabelt radiomagnetotellurik (RMT) instrument

Mehrdad Bastani

2009

Contents

Förord

Som ett led inom berggrundsundersökningar genomför SGU geofysiska markmätningar på viktiga och intressanta magnetiska-, strålnings- och elektromagnetiska anomalier. Magnetfälts- och elektromagnetiska mätningar utförs längs profiler tvärs över långsträckta anomalier. Den välkända VLF metoden används i de elektromagnetiska mätningarna. VLF bandet täcker frekvensområdet mellan 16 till 30 kHz. I Europa kan mätas signal från 26 VLF sändare som fungerar endast tidvis. VLF instrumentet som SGU använder, är Wadi från ABEM AB. Instrumentet är ganska lätt att bära och bekvämt att hantera. Mättiden på varje punkt är kort och tar ca 5 sekunder. Wadi instrumentet mäter signalen från endast en utvald sändare. Insamlade data har därför relativt dåligt djupupplösning. Andra huvud problem med Wadi instrumentet är att hitta rätt sändare i korrekt riktning i förhållande till anomalins riktning. Ibland är det omöjligt att hitta en VLF sändare i rätt riktning. Vi har använt Wadi instrumentet för bergkvalitets- och berggrundsundersökningar inom olika projekten bl. a. norra Göteborg och BÄST. I första projektet genomfördes VLF- och magnetfältsmätningar för att kartlägga några av de största sprickzonerna i undersökningsområdet. Insamlade data längs två profiler var oanvändbara på grund av för svag VLF-signal.
Parallellt med VLF mätningar använde vi EnviroMT^{TM} instrumentet som utvecklades på Uppsala Universitet (Bastani, 2001).

I det här projektet utvecklade vi bearbetningsmjukvara för ett nytt instrument. Det nya instrumentet har samma noggrannhet och upplösning som EnviroMT^{TM} och är nästan lika enkelt att använda som Wadi. Instrumentet skulle vara lätt att bära och skulle kunna hanteras av en person i fält. Instrumentets hårdvara konstruerades på Uppsala Universitet. Dynesius m. fl. (2004) gav en detaljerad beskrivning av den nya hårdvaran och av mätmetodiken. Vi använde bearbetningsprogrammet av EnviroMT^{TM}s instrumentet som en grund. Nya insamlings- och bearbetningsparametrar justerades till den nya hårdvaruplattformen och ett användargränssnitt som kontrollerar datainsamling, databearbetning och presentation av data planerades och implementerades. Ingångsparametrar till bearbetningsprogrammet optimerades för att förenkla fältmätningen. I programmet finns möjligheter att välja två mätmetodiker en som använder endast magnetfält komponenter och en som använder både magnetiska- och elektriska fältkomponenter. Ett annat program skall göras för att kontrollera signalkvaliteten och filtrera brus. Även kalibrering av instrumentet kommer att utföras med hjälp av ett nytt program. Programmet ska använda kalibreringsdata som genereras med en HP signalgenerator.

En postprocesseringsmjukvara har utvecklats för att visualisera och tolka data efter fältarbete. Tolkningsmjukvaran innehåller 1D och 2D modelleringsprogram. Mjukvaran är användarvänlig och förbereder data i Oasismontaj format för att kunna visualisera data och resultat som kartor och profiler i standardformat som SGU använder.

I den här rapporten beskriver jag detaljer om olika program som har utvecklats inom ramen av det här projektet. Rapporten innehåller delar av examensarbetes rapporter av studenter på Uppsala Universitet som jag har handledat. Därför skrivs rapporten på engelska.

INTRODUCTION

1. Introduction

This document is the final report on the internal research project entitled "Development of software for a new portable Radio Magnetotelluric (RMT) instrument" that is financed by the Geological Survey of Sweden (SGU). The instrument makes use of several radio transmitters covering frequency range 10-350 kHz to map the electrical resistivity of the ground below the measuring point(s). The instrument is called Multi Frequency Receiver (MFR). The project was originally defined as collaboration between Uppsala University (UU) and SGU. UU was mainly responsible for the design and development of hardware and hardware-control-software. SGU had the task to design and make all the in-field and post-processing software. Pedersen et al. (2008) have reported details about the hardware and control-software in a separate report. The present report contains the details about parts of the hardware and the software developed for the MFR. First fundamentals about the RMT method and data processing used are briefly explained to show the key concepts behind the project. The structure of MFR data acquisition software in different measuring modes is then presented to make a link between the theory and application. Graphical user interface (GUI), calibration software, and database program are described to show the steps taken to convert the raw data to the resistivity models at each measuring point or along a given profile. Finally, the results from preliminary ground and airborne measurements are presented. I have used parts the reports written by the master students that I have supervised in the frame of this project. I have addressed their work and names in this report where necessary.

1.1 Electrical resistivity

The electrical resistivity (or the inverse conductivity) of most Earth materials ranges from a few tenth of Ωm to several tens of thousands Ωm (Bastani, 2001). Thus there can be huge contrasts in resistivity between neighboring geological structures. For example in an environmental context the electrical resistivity contrast between the target zone and intact host media is often so high that it can be used in mapping and resolving boundaries (e.g., salt-fresh underground water boundaries in the case of seawater intrusion). Table 1.1 represents the resistivity range of some rocks given by Reynolds (1997).

Material	Nominal resistivity (Ωm)
Granite	3.0×10^{2} - 1.0×10^{6}
Granite (weathered)	30 - 5.0×10^{2}
Schists (calcareous and mica)	20 - 1.0×10^{4}
Schist (graphite)	10 - 1.0×10^{2}
Slates	6.0×10^{2} - 4.0×10^{7}
Marble	1.0×10^{2} - 2.5×10^{8}
Consolidated shales	20 - 2.0×10^{3}
Conglomerates	2.0×10^{3} - 1.0×10^{4}
Sandstones	1 - 7.4×10^{8}
	Table 1.1continued
Limestones	5.0×10 - 1.0×10^{7}
Dolomite	3.5×10^{2} - 5.0×10^{3}
Marls	3 - 7.0×10
Clays	1 - 1.0×10^{2}
Alluvium and sand	10 - 8.0×10^{2}

Moraine	10 - 5.0 × 10^{3}
Soil (40% clay)	8
Lias clay	10 - 15
Boulder clay	15 - 35
Clay (very dry)	50 - 150
Merica mudstone	20 - 60
Coal measures clay	50
Middle coal measures	> 100
Chalk	50 - 150
Coke	0.2 - 8
Gravel (dry)	1400
Gravel (saturated)	100
Quaternary /Recent sands	50 - 100
Ash	4
Pulverised fuel ash	50 - 100
Laterite	800 - 1500
Lateritic soil	120 - 750
Dry sandy soil	80 - 1050
Sand clay / clayey sand	30 - 215
Sand and gravel	30 - 225
Unsaturated landfill	30 - 100
Saturated landfill	15 - 30
Acid peat waters	100
Acid mine waters	20
Rainfall runoff	20 - 100
Landfill runoff	< 10 - 50
Glacier ice (temprate)	2.0 × 10^{6} - 1.2 × 10^{8}
Glacier ice (polar)	5.0 × 10^{-5} - 3.0 × 10^{5}
Permafrost	1.0 × 10^{3} - > 1.0 × 10^{4}

Table 1.1: *Range of electrical resistivity of some minerals and rocks.*

The variations seen in the resistivities are a function of different conditions of formation, chemical composition, texture of the rock, crystallization, fluid and clay content, etc.

1.2 **Electromagnetic methods**

Electromagnetic methods are powerful, versatile, and widespread geophysical methods that can be employed to delineate the electrical resistivity/conductivity of Earth materials. There are two main subdivisions in electromagnetics, namely time-domain electromagnetic (TDEM) or transient electromagnetic (TEM) methods and frequency-domain electromagnetic methods (FDEM). Here we will concentrate on the plane wave frequency domain electromagnetic methods (PWEM) and specifically on the Magnetotelluric (MT)

1.2.1 **Magnetotelluric (MT) method**

MT using natural sources is the oldest among the PWEM methods. In a very useful summary Vozoff (1991) describes the MT sources and the interaction of their electric and magnetic fields with the Earth. The use of natural sources is necessary for deep crustal and upper

mantle studies. However, due to weak source fields at higher frequencies above 1000 Hz the method is hardly used at frequencies higher than 1000 Hz and due to manmade noise below 1000 Hz in industrialized areas considerable efforts must be made to suppress the influence of manmade signals on the impedance estimates (Larsen et al, 1996).

Goldstein and Strangway (1974) originally employed the Controlled Source Audio Magnetotelluric (CSAMT) technique using a grounded electric dipole source. In this technique the transmitting frequency can be selected and controlled by the operator. Zonge and Huges (1991) describe several types of controlled sources that can be used.

Technique	Source Type	Frequency range	Application
MT	Natural	10^{-4} Hz - 1 kHz	Deep sounding to study lithosphere
CSAMT	Artificial controlled source	Variable	Shallow environmental to deep crust sounding
Conventional VLF	VLF transmitters	15-25 kHz	Mapping structures
VLF resistivity	VLF transmitters	15-25 kHz	Low resolution shallow sounding
RMT	VLF and Radio transmitters	10-250 kHz	Shallow sounding for engineering and environmental studies

Table 1.2: *PWEM techniques, sources, frequency band, and their applications in geophysical prospecting*.

When the source is sufficiently far away from the receiver such that the transmitted wave can be considered as a plane wave, then all MT theory is valid for the CSAMT technique. According to Zonge and Hughes (1991) the CSAMT technique has given remarkable results in the exploration for massive sulfides, base and precious metals, geothermal resources, petroleum, and ground water contamination, as well as for geotechnical investigations.

In the conventional VLF method, first introduced and utilized by Paal (1965), the sources are the powerful Very Low Frequency (VLF) radio transmitters operating in frequency range 15-25 kHz. In this method the two horizontal and the vertical components of the magnetic field are measured. The transfer function between the horizontal and vertical magnetic field components reflects lateral changes in conductivity along the profile and its neighborhood. An interesting new development in airborne measuring techniques making use of at least two transmitters have provided maps of transfer functions unbiased by transmitter directions (Pedersen, 1994). Recently, new interpretation techniques have been developed to transform these maps into maps of electrical resistivities (Becken, 2000).

In the VLF Resistivity (VLF-R) method, using the same source as in conventional VLF method, one or two horizontal components of electric field are also measured and the scalar apparent resistivities and phase are calculated for each station. The narrow frequency range (15-25 kHz) of the method limits its depth range and vertical resolution.

The Radio MagnetoTelluric (RMT) method is similar to VLF-resistivity, but the frequency range (15-250 kHz) used in the method is much wider because in addition to the VLF

transmitters use is made of the Long Wave (LW) radio transmitters which - at least in Europe are numerous. Therefore the depth resolution of the technique is far better than for the VLF-R technique. The VLF methods use KHz but during the recent years it has been extended to also involve frequencies in the so called Low Frequency (LF) band (30 – 300 kHz). The method that uses both the VLF- and LF band is called radio magnetotelluric (RMT) and is similar to the VLF method. Since RMT has a broader frequency range it resolves the upper as well as the lower parts of the structure better than VLF. This method is therefore very useful in investigations of shallow depth with high lateral and/or vertical resolution. The source for VLF measurements is transmitters used for submarine communication while the source for LF is radio transmitters used for e.g. aircraft communication. During the last years some of the active VLF transmitters have been shut down and are not in use anymore. In Sweden and in Europe as a whole there are no more than 30 transmitters lying in the VLF frequency band 15 – 30 kHz. For transmitters that are using VLF and LF-frequencies, 15 – 250 kHz, there are a few hundreds of transmitters in Europe. The location for these transmitters can be seen in Figure 1.1

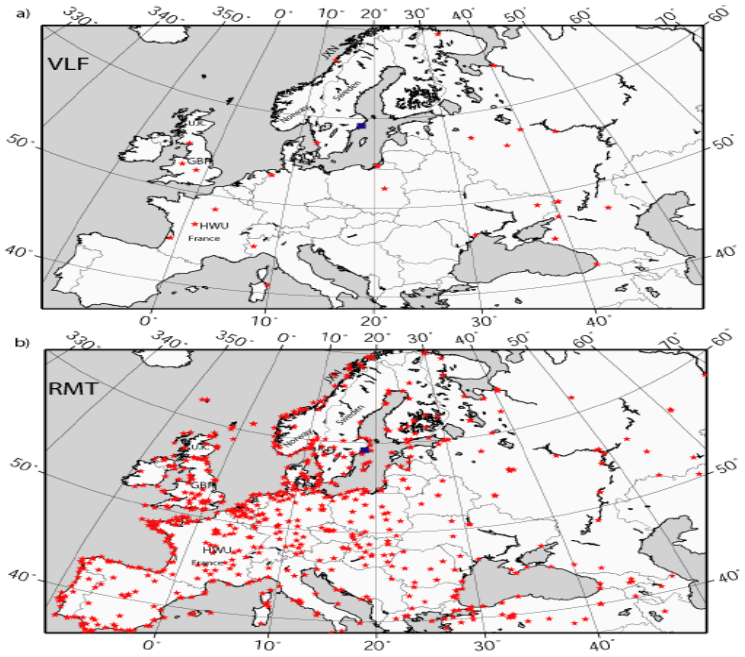

Figure 1.1 The location of a) VLF (15-30 kHz) and b) RMT (30-300 kHz) transmitters in Europe.

THEORY

2. Theory

In order to be able to describe the concepts behind magnetotelluric methods we have to start by looking at the fundamentals of the electromagnetic theory.

2.1 **Maxwell's equations**

There are four equations that summarize the theoretical content of electrodynamics. These are called Maxwell's equations. Assuming time dependence as $e^{i\omega t}$ in the frequency domain they can be described as:

$$\nabla \cdot \mathbf{D} = \rho \qquad \textit{Gauss's law} \qquad (2\text{-}1)$$

$$\nabla \cdot \mathbf{B} = 0 \qquad \textit{Gauss's law for magnetism} \qquad (2\text{-}2)$$

$$\nabla \times \mathbf{E} = -i\omega\mathbf{B} \qquad \textit{Faraday's law} \qquad (2\text{-}3)$$

$$\nabla \times \mathbf{H} = J + i\omega\mathbf{D} \qquad \textit{Ampere's law with Maxwell's correction} \qquad (2\text{-}4)$$

where in the SI system

E = electrical field intensity (V/m)

D = dielectric displacement (C/m^2)

B = magnetic flux density (T)

H = magnetic field intensity (A/m)

J = electric current density (A/m^2)

$\omega = 2\pi f$ = angular frequency (Hz)

ρ = electric charge density (C/m^3)

These vector fields for a linear, isotropic medium are related through their constitutive relationships:

$$\mathbf{D} = \varepsilon\mathbf{E} \qquad (2\text{-}5)$$

$$\mathbf{B} = \mu\mathbf{H} \quad (2\text{-}6)$$

$$\mathbf{J} = \sigma\mathbf{E} \quad (2\text{-}7)$$

where

ε = electric permittivity (F/m)

μ = magnetic permeability (H/m)

σ = conductivity (S/m)

ε, μ and σ describe the intrinsic properties of the material through which the electromagnetic wave propagates.

2.2 **The wave equation**

The general form of the wave equations for the electric- and magnetic field can be derived from Maxwell's equations. First the constitutive relations are used to rewrite equation (2-3) and (2-4):

$$\nabla \times \mathbf{E} = -i\omega\mu\mathbf{H} \quad (2\text{-}8)$$

$$\nabla \times \mathbf{H} = \sigma\mathbf{E} + i\omega\varepsilon\mathbf{E} \quad (2\text{-}9)$$

By using these relationships we can now reduce Maxwell's equations to only contain **E** or **H** by applying the curl to the expressions. The solution for an electromagnetic wave traveling in a uniform medium then becomes:

$$\nabla^2\mathbf{E} + k^2\mathbf{E} = 0 \quad (2\text{-}10)$$

$$\nabla^2\mathbf{H} + k^2\mathbf{H} = 0 \quad (2\text{-}11)$$

These equations are also known as Helmholtz equations. The complex wave number, *k*, in the equations is defined as:

$$k = \left(\mu\varepsilon\omega^2 - i\mu\sigma\omega\right)^{1/2} \quad (2\text{-}12)$$

For frequencies in the VLF band (and some in the LF band) and in typical earth materials the assumption $\varepsilon\omega \ll \sigma$ can be made. The wave number can then be simplified (Persson, 2001):

$$k = \left(-i\mu\sigma\omega\right)^{1/2} \tag{2-13}$$

2.2.1 **Plane waves**

If a wave is travelling in the x-direction and has no y or z dependence, it is called a plane wave. This means that the electric and magnetic fields are perpendicular to the direction of propagation. These type of waves appear when waves traveling over long distances. The plane-wave solutions when the wave number, *k*, is complex becomes:

$$\mathbf{E}(x,t) = \mathbf{E}_0 e^{-kx} e^{i(kx-\omega t)} \tag{2-14}$$

$$\mathbf{B}(x,t) = \mathbf{B}_0 e^{-kx} e^{i(kz-\omega t)} \tag{2-15}$$

where $\mathbf{E}_0$ and $\mathbf{B}_0$ are the amplitude of the electric- and magnetic field, respectively. The imaginary part of *k* results in an attenuation of the wave, i.e. decreasing amplitude with increasing x.

2.3 **Primary and secondary field**

The electromagnetic field from a transmitter can be considered as an oscillating vertical electrical dipole. The radio signals far from the transmitter can be considered being a plane wave propagating in all directions. If the wave propagates in the x direction the electromagnetic field of this wave has a vertical electrical field component, E_z, and a horizontal magnetic field component, H_y. At very large distances from the transmitter this primary field may be considered uniform.

According to the electromagnetic theory (Faraday's principle of electromagnetic induction), the magnetic field from the transmitter, i.e. the radio wave, will induce a current in the Earth. Those eddy currents will in turn create a secondary magnetic field.

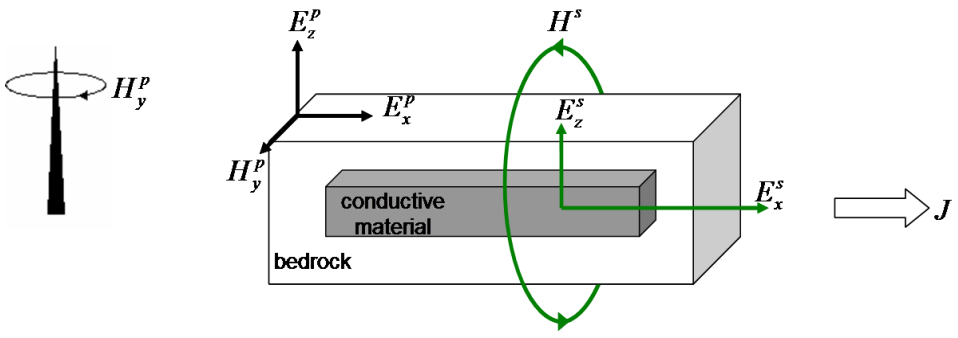

Figure 2.1 Induction due to the conductive ground. The magnetic field from the transmitter creates a current, J, in the Earth. Due to this current a small electric field is produced with electrical field components E_x^s and E_z^s.

In Figure 2.1 the induction due to the conductive ground is created by the horizontal magnetic field H_y. This creates the secondary field, with electric field components E_x and E_z. The E_z component can however be neglected in the ground. This secondary field can be phase shifted and oriented in another direction depending on the conductivity contrast and shape of the conductor.

2.4 **The 1-D model**

The simplest model of describing the earth is a homogenous half space where the conductivity is constant along the axes.

2.4.1 **Skin depth**

Equations (2-14) and (2-15) showed that there is an attenuation of the wave caused by the imaginary part of *k*. The distance it takes to reduce the amplitude by a factor of 1/e is called the skin depth and is a measure of how far the wave penetrates into the ground. Equation (2-14) can be solved for the amplitude at the surface, *z=0*, given that the complex wave number is:

$$k = \left(-i\mu\sigma\omega\right)^{1/2} = \alpha(1-i) \tag{2-16}$$

where α is a real quantity defined by:

$$\alpha = \left(\frac{\omega\mu\sigma}{2}\right)^{1/2} \tag{2-17}$$

Putting that solution into equation (2-14) for an arbitrary depth and solving for z gives the skin depth:

$$\delta = \left(\frac{2}{\omega\mu\sigma}\right)^{1/2} \approx 503\left(\frac{1}{f\sigma}\right)^{1/2} = 503\left(\frac{\rho}{f}\right)^{1/2} \tag{2-18}$$

If the resistivity is 10 kΩm the skin depth for a frequency of 15 kHz is about 410 meters while for a frequency of 300 kHz with the same resistivity the skin depth is about 90 meters. Generally this means that if the resistivity is high and the frequency low the wave will penetrate deeper into the ground.

2.4.2 **Phase**

For a distant radio transmitter with the EM-wave propagating in the x-direction the components of the wave consist of a vertical electric component, E_z, and a horizontal magnetic component, H_y. If the ground is conductive the induction due to H_y creates a horizontal electrical field component, E_x, as could be seen in section 2.3.

From the wave equation (2-9) and equation (2-11) it can be shown that into a homogenous ground the fields will diffuse as an exponentially damped wave with E_x 45° ahead of H_y (Persson, 2001).

If the ground is non-homogenous, the phase difference between E_x and H_y depend on the resistivity of the horizontally layered earth. If the top layer has higher resistivity than the lower the phase will be bigger than 45°. If it is the opposite with the lower resistivity on top the phase will be less than 45°.

2.4.3 **Impedance**

The impedance for a plane wave is defined as the ratio between E_x and H_y:

$$Z = \frac{\omega\mu}{k} = \frac{E_x}{H_y} = -\frac{E_y}{H_x} \cong \left(\frac{\omega\mu}{\sigma}\right)^{1/2} e^{i\pi/4} \qquad (2\text{-}19)$$

The last step is made by the assumption that for typical earth materials at frequencies used in magnetotelluric surveys the displacement current can be neglected. This shows that the impedance is a function of frequency and that it increases as the square root of frequency. The phase of the impedance for a homogenous half space is 45° - the same phase as between E_x and H_y in a homogenous ground.

2.4.4 **Apparent resistivity**

In reality the resistivity in the ground is not constant. Therefore something called apparent resistivity is used when making a simplification of the earth as a heterogeneous half space. Per definition apparent resistivity is *an average resistivity used for a volume average of a heterogeneous half-space* and can be defined by using the relationship for the resistivity in the ground,

$$\rho = \frac{1}{\sigma} \qquad (2\text{-}20)$$

in equation (2-19) and solve for the resistivity:

$$\rho_a = \frac{1}{\omega\mu}|Z|^2 = \frac{1}{\omega\mu}\left|\frac{E_x}{H_y}\right|^2 \qquad (2\text{-}21)$$

2.5 **The 2-D model**

Most times the Earth can be approximated by a 2-D model. This means that the conductivity variation can be neglected along one direction, the so called strike direction. The coordinate axes are normally defined such that x goes in the strike direction, y is the profile direction and z is pointing downwards into the ground.

2.5.1 **TM-mode**

In the TM-mode the electric field is perpendicular to the strike and the magnetic field is in the strike direction as shown in Figure 2.2.

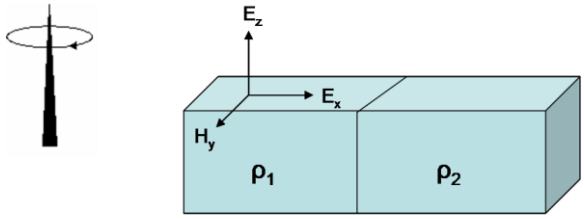

Figure 2.2. TM-mode (Transverse Magnetic mode) or H-polarization. The plane wave from the transmitter is propagating perpendicular to the strike, i.e. $H_z = 0$ (From picture by Persson, 2001).

Since the magnetic field is parallel to the strike there will be no variation over the contact. The electrical fields, however, give rise to discontinuities close to the boundary. If $\rho_1 > \rho_2$ in the model seen in Figure 2, then the apparent resistivity will decrease rapidly while the phase difference will have a peak over the boundary.

2.5.2 **TE-mode**

In the TE-mode the electrical field is in the strike direction (Figure 2.3). Since it is parallel to the boundary there will be no induced charges. Instead the electric field will vary continuously across the interface. The magnetic field will on the other hand change over the boundary since the conductivity increases in a conductor. This will magnify the currents and this change is reflected in the vertical component. The resultant magnetic field is elliptically polarized.

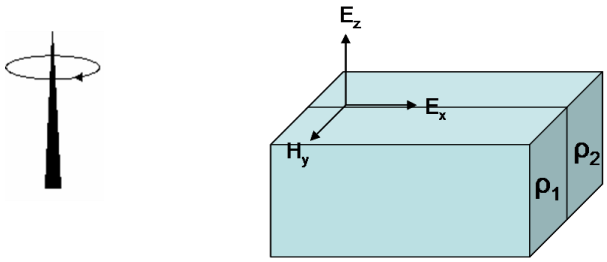

Figure 2.3. TE-mode (Transverse Electrical mode) or E-polarization. The plane wave from the transmitter is propagating parallel to the strike, i.e. $E_z = 0$ (From picture by Persson, 2001).

For an electrical field in TE-mode the apparent resistivity shows a continuous decay over the boundary. This decay is dependent on the frequency. If the frequency increases the decay will become more rapid. The phase difference over the boundary will look the reversed compared to the TM-mode.

2.5.3 **Impedance and tipper vector**

The impedance and tipper are quantities that are used when interpreting the measured magnetotelluric data. For a plane wave there exists a linear relationship between the electric field components (Ex,Ey) and the two horizontal magnetic field components (Hx,Hy) and the vertical magnetic field component (Hz), for a general conductivity distribution. From these relationships the impedance and tipper can be expressed.

Impedance

The horizontal components of the electromagnetic field are related through the impedance tensor as:

$$\begin{bmatrix} E_x \\ E_y \end{bmatrix} = Z \begin{bmatrix} H_x \\ H_y \end{bmatrix} \tag{2-22}$$

The complex impedance tensor is given by:

$$Z = \begin{bmatrix} Z_{xx} & Z_{xy} \\ Z_{yx} & Z_{yy} \end{bmatrix} \tag{2-23}$$

If the coordinate system is defined with x in the strike-direction, the impedance tensor has a simple structure. From the TE- and TM modes the 2-D impedance vector can then be defined as:

$$Z = \begin{bmatrix} 0 & Z_{xy} \\ -Z_{yx} & 0 \end{bmatrix} \tag{2-24}$$

where $|Z_{xy}| \neq |Z_{yx}|$.

When measuring, the strike angle, φ, must be known. The determinant of Z is called the effective impedance and is an average of the impedance in all current directions. It is defined as:

$$Z_{DET} = \sqrt{Z_{xx}Z_{yy} - Z_{xy}Z_{yx}} \tag{2-25}$$

It is however useful in such way that it makes the impedance tensor independent of the strike direction. According to equation (2-24) Z_{xy} corresponds to the TE-mode while Z_{yx} correspond to the TM-mode. The effective impedance can therefore be considered being the mean of the

mode data and no mode identification is required. The effective impedance thereby represents an average that can be inverted to provide robust 1D and 2D models (Oskooi, 2004).

Tipper

The geomagnetic transfer function called tipper describes the connection between the horizontal and the vertical magnetic field components:

$$H_z = AH_x + BH_y \quad (2\text{-}26)$$

The tipper vector *(A,B)* can thereby be defined just by measuring the vertical components of the magnetic field. It is independent of the actual source current and thereby only dependent on the internal conductivity.

For a homogenous or a layered earth (1-D) the tipper quantity does not exist, i.e. $A = B = 0$. However, most of the times, the Earth can be approximated by a 2D model. If the TE- and TM-mode is used in the coordinate system for the strike, as for the impedance, the 2-D tipper can be found. With the x-axis is in the strike direction *A* becomes zero and we get:

$$H_z = BH_y \quad (2\text{-}27)$$

The tipper will therefore vary along the measured profile. The strongest variation of the tipper is close to a resistivity contrast. For a tipper in 3-D structure both $A \neq 0$ and $B \neq 0$ and equation (2-26) are used for the calculations.

The interpretation of the tipper can be done either by mapping or modelling. In the mapping procedure the tipper values are transformed into the apparent resistivity and phase based on the method developed by Becken and Pedersen (2003) creates electrical resistivity maps. The modelling is done with least square inversion and image the electrical resistivity depth sections.

Real and imaginary part of the tipper in TE-mode

Except for the apparent resistivity and phase difference for a field in TE-mode the variations of the real and imaginary component of the tipper can also be investigated.

The real part of the tipper always point away from the conductor. This means that for a given frequency the real part change sign when crossing a conductor. The imaginary part is more complex since it is dependent of the depth of the conductor. Usually, if there is a conductor at a given depth, the imaginary part change sign from positive to negative with decreasing frequency (Pedersen et al., 2005).

The reason why the imaginary part of the tipper vector is more complex is that it contains the response from two wavelengths with two different polarizations. The first has a short-

wavelength response with same polarity as the real component. The second has a long-wavelength response with opposite polarity compared to the real component. This makes the imaginary component dependent of depth. If the depth increases the short wavelength response will disappear. This will leave only the long-wavelength response left with the reversed polarity. For small resistivity variations near the surface this can be seen as anomalies with same polarity for both the real and the imaginary component. If there instead is a conductive target or deep low-resistive structures this is seen as anomalies with reversed polarity in the imaginary part (Persson, 2001).

2.5.4 **Scalar and tensor transfer functions**

In the VLF and RMT methods the signal from radio transmitters with nearly distinct frequencies are used to estimate the earth electromagnetic transfer functions, namely impedance and tipper vector. There are several techniques to estimate the transfer function. Bastani (2001) introduces scalar and tensor transfer functions which are described here.

Estimation of scalar tipper

The scalar transfer function is calculated with respect to either the transmitter coordinate system or the strike direction. This means that the y-axis is perpendicular to the transmitter-receiver direction or the strike direction. The significance of the scalar tipper is different depending on if the measurement is done with two or three magnetic components. This difference has been discussed by Pedersen and Oskooi (2004):

Calculation of scalar tipper with two magnetic components

If one horizontal (H_y) and one vertical component (H_z) of the magnetic field are measured, as in standard VLF measurements, and if the strike direction is in the x-direction, then the derived scalar transfer function $B^{scalar} = H_z / H_y$ is identical to the unique tipper component B and the component A is equal to zero. If the strike direction, however, is in another direction other than the x-axis, then it is no longer possible to compensate for the rotation by some correction factor. This means that the true transfer function can not be recovered from the measured scalar transfer function, B^{scalar}.

Calculation of scalar tipper with three magnetic components

If the measurement instead is done using three orthogonal magnetic sensors, then a 2-D structure having a strike angle, θ, with respect to the x-axis can be modelled. The horizontal components of the magnetic field can then be used to calculate the field in an arbitrary direction. In this case, as can be seen later, equation (2-37) can be used to calculate the scalar transfer function. This would be identical to the true 2-D tipper along a profile perpendicular to the strike.

Tensor measurement

If three magnetic field components from two transmitters with slightly different frequencies and a nearly orthogonal direction are measured simultaneously, then for each transmitter the total field is given by:

$$T = \left(|H_x|^2 + |H_y|^2 + |H_z|^2 \right)^{1/2} \quad (2\text{-}28)$$

Map of T contains some useful information about the conductivity structure in a study area. For example the maximums in T describe the conductive structures, especially those with the strike direction parallel to the transmitter. By measuring from two transmitters simultaneously two linear equations can be obtained. From these the tipper vector can be calculated for each measuring point. This method gives a response that is independent of the transmitter direction in addition to the scalar transfer function.

2.5.5 **Rotation of coordinate system**

In practice, measuring is often done in another coordinate system than the strike coordinate system (principal coordinate system). For measurements with radio magnetotelluric (RMT) methods the coordinate system for the transmitter is used instead (Figure 2.4), which is better in some situations, for example when calculating the scalar tipper.

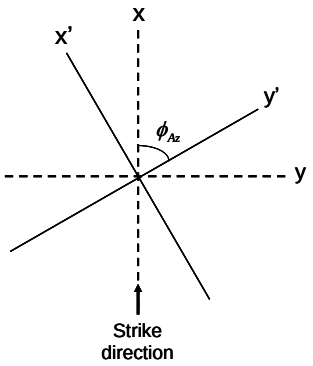

Figure 2.4. The measured coordinate system (x',y',z) compared to the principal coordinate system (x,y,z).

As mentioned earlier, the primary signal from transmitter induces a secondary current in the Earth. This gives rise to an electric field along the transmitter direction and also a horizontal magnetic field. The magnetic fie ld is rotated by 90 degrees with respect to the electric field and is usually less distorted by lateral conductivity changes. It can therefore be used to estimate the direction to the radio transmitters. This is done by rotating the coordinate system such that the power of magnetic field in the transmitter direction is minimized. The azimuths, ϕ_{Az} , are measured from the magnetic north towards the east (Figure 2.5).

$$\phi_{Az} = \frac{k\pi}{2} + 0.5 \cdot \tan^{-1}\left[\frac{2 \cdot \mathrm{Re}\left(H_x^* H_y\right)}{\left(|H_x|^2 - |H_y|^2 \right)} \right], \quad k = 0, 1 \quad (2\text{-}29)$$

Equation 2-29 yields a minimum and a maximum in horizontal magnetic field. To find the angle of minimum power the second derivative of the H_x power in the rotated coordinate system is calculated:

$$2\left(\left|H_y\right|^2-\left|H_x\right|^2\right)\cdot\cos\left(2\phi_{Az}\right)-4\left[\mathrm{Re}\left(H_x^*H_y\right)\cdot\sin\left(2\phi_{Az}\right)\right] \qquad (2\text{-}30)$$

The angle with a positive second derivative is the answer.

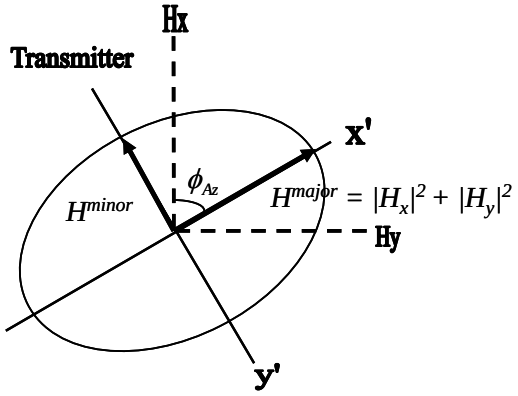

Figure 2.5. Rotation of the coordinate system. The azimuths are measured from the magnetic north towards the east. Here is the rotated H_y component equal to the H^{major}-axis, i.e. $|H_x|^2 + |H_y|^2$. The direction to the transmitter and H^{major} are always perpendicular to each other. The H_z component (out of the paper) is the same after the rotation.

The relationship between the measured and principle electromagnetic field components is:

$$\begin{bmatrix} E'_x \\ E'_y \end{bmatrix} = R^T \begin{bmatrix} E_x \\ E_y \end{bmatrix} \qquad (2\text{-}31)$$

$$\begin{bmatrix} H'_x \\ H'_y \end{bmatrix} = R^T \begin{bmatrix} H_x \\ H_y \end{bmatrix} \qquad (2\text{-}32)$$

where the components with a prime are the measured electromagnetic field components and R is the rotation matrix defined by:

$$R = \begin{bmatrix} \cos\phi_{Az} & -\sin\phi_{Az} \\ \sin\phi_{Az} & \cos\phi_{Az} \end{bmatrix} \qquad (2\text{-}33)$$

The tipper vector can now be rewritten with the rotated coordinates:

$$H'_z = B' \cdot H'_y \tag{2-34}$$

B' is the same as B^{scalar} and since there is no rotation in z-direction $H'_z = H_z$. The tipper can thereby be written as:

$$H_z = B^{scalar} \cdot H'_y \tag{2-35}$$

Finally, if H'_y is defined from equation (2-32), the expression for B^{scalar} can be written as

$$B^{scalar} = \frac{H_z}{-H_x \sin\phi_{Az} + H_y \cos\phi_{Az}} \tag{2-36}$$

2.5.6 **Degree of polarization**

The degree of polarization is an important quantity since it gives a correlation between the orthogonal components of the electromagnetic field. For a planar wave this can be described in terms of the 2×2 coherence matrix. The spectral matrix elements are defined as:

$$S_{ij} = H_i^* H_j \tag{2-37}$$

where i,j = x,y,z. The coherence matrix in 2-D can then be written as:

$$\phi = \begin{bmatrix} S_{xx} & S_{xy} \\ S_{yx} & S_{yy} \end{bmatrix} \tag{2-38}$$

The coherence matrix can be uniquely decomposed into a sum of two matrices. The first one corresponds to fully polarized and the second to fully non-polarized wave. The degree of polarization can then be expressed as the ratio of the intensity (or trace) of the polarized part to the total intensity of the field (Setälä et al., 2002).

For a 2-D field the degree of polarization can be expressed as:

$$P = \left(1 - \frac{4 \det(\phi)}{[trace(\phi)]^2} \right)^{1/2} \quad (2\text{-}39)$$

The degree of polarization is useful in that sense that for one particular transmitter the polarization is the same. Generally, if time dependence ($e^{i\omega t}$) is used, the real and imaginary parts are of opposite polarity. In most cases the real part dominates over the imaginary part (Oskooi and Pedersen, 2006).

2.5.7 **Estimation of random errors of the transfer function**

Pedersen (1982) have a discussion about error estimation of the transfer function and the difference between random and systematic (bias) error. The random error is rather insensitive to noise in the magnetic field but the error increases with increasing S/N ratio in the electric field. For the bias error it is opposite – it increases with increasing S/N ratio in the magnetic field.

To decide whether the noise in the measured data are small or not it is necessary to distinguish between the input and output channel (Müller, 2000). This is done by assuming that the input channel is "noise-free". The output channel, however, can be estimated by adding Gaussian noise to the output data. The data fit can then be calculated as the coherence between the predicted and the measured output data. If this coherence is close to one (i.e. unity) then the data fit between the measured and the predicted data is good. This means that the error is small and thus there is little noise in the data. If the coherence however is much smaller than one, then the noise is large.

There is a difference in the estimate of the error depending on whether the noise is in the output or input channel. If the noise is in the output channel, then the estimation is correct. If the noise however is in the input channel then the error is biased (systematic) and the calculated estimation can not be used. Since the estimation of the error is based on the fact that the amount of possible bias depends on the coherence, there are no difference which one of the channels that are in- or output if the coherence is close to one (the bias is small).

The general equation for coherence between two input channels (where i,j = x,y,z) can be written as:

$$\gamma_{ij}^2 = \frac{\sum_{k=1}^{n} \left| S_{ij}^k \right|^2}{\sum_{k=1}^{n} S_{ii}^k \sum_{k=1}^{n} S_{jj}^k} \quad (2\text{-}40)$$

The coherence between the input and output channels, *m*, is:

$$\gamma_{mij}^2 = \frac{\sum_{k=1}^{n} \left(S_{mm}^{(p)}\right)^k}{\sum_{k=1}^{n} S_{mm}^k} \qquad (2\text{-}41)$$

$\left(S_{mm}^{(p)}\right)^i$ is the auto-power of channel *m* as predicted from the horizontal magnetic field. As an example these two expressions can be used for estimating the variance of the impedance Z_{xx} where the two input channels are (H_x, H_y). The result then becomes:

$$\sigma_{Z_{xx}}^2 = \frac{1}{N-4} \frac{1-\gamma_{412}^2}{1-\gamma_{12}^2} \frac{\sum_{i=1}^{n} S_{44}^i}{\sum_{i=1}^{n} S_{11}^i} \qquad (2\text{-}42)$$

where $N = 2n*N_s$ is the number of degrees of freedom and N_s is the number of stacks (Bastani, 2001).

RADIO MAGNETOTELLURIC

3. Radio Magnetotelluric

In many areas of the world a large number of radio transmitters including VLF transmitters can be used for geophysical purposes. For example, in 1998 a total number of 36 and 40 remote transmitters covering the band 14 kHz to 250 kHz could be received in Sweden and the Netherlands, respectively. These transmitters provide excellent far-field signal to noise conditions and thus provide potential sources for estimating the plane wave transfer functions: the impedance tensor and the tipper vector. These sources have routinely been utilized in the traditional VLF technique (McNeill and Labson, 1989; Mc Neill, 1991; Guerin and Benderitter, 1995) and the new RMT technique (Turberg et al, 1994, Tezkan et al, 1996) as fast and simple ways to get scalar estimates of Earth response functions.

3.1 **Far-field radio transmitter**

As one could see in Figure 1, the number of RMT transmitters located in Europe is considerably higher than for VLF transmitters.

Figure shows an example of amplitude spectra from a measurement done by the EnviroMT instrument in Colledoom, Netherlands (Bastani, 2001), where the transmitters and the different frequency bands are shown.

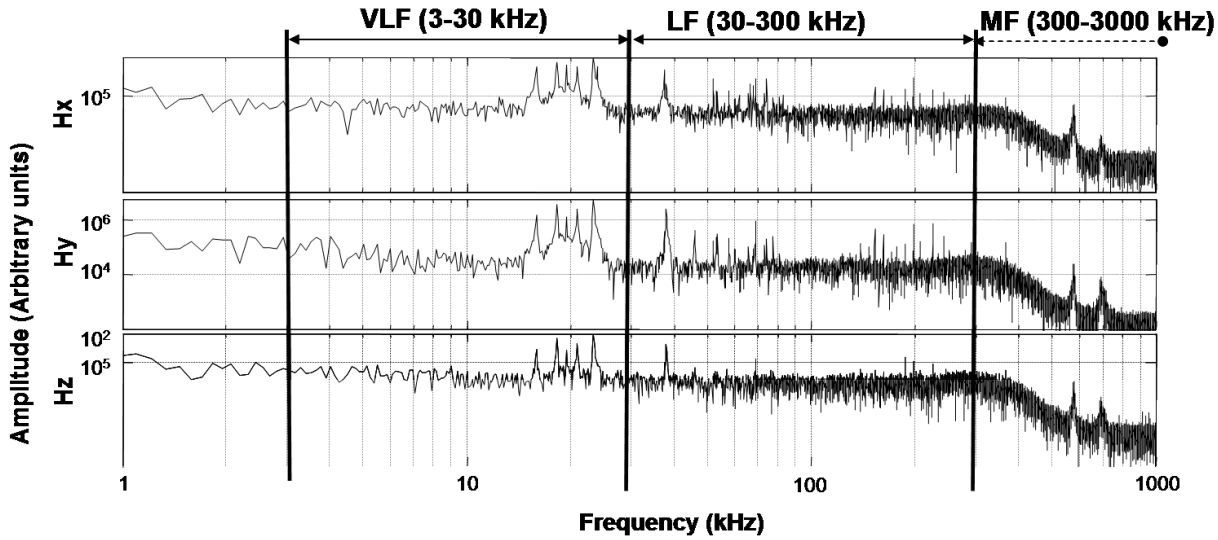

Figure 3.1. Example of an electromagnetic amplitude spectra (arbitrary units) from Collendoorn, The Netherlands, November 1998. (Bastani, 2001)

3.2 **Near-field sources**

The field far away from a transmitting antenna can be considered being plane. Near the antenna the field is more complex. The near-field sources can be of different origin such as

electronic noise of instrumentation, unbalanced power consumption or cables. When performing measurements the result can therefore include a combination of both near- and far-field sources. Since normal equations are no longer valid another type of equations has to be used. One way to overcome this problem is to separate the far-field sources from those nearby. This can be done by looking at the tipper data. Generally the real part of the tipper vector points away from a conductor in the far-field. For near-field sources the tipper will point towards the source instead (Pedersen et al., 2005). This means that for far-field transmitters the real and imaginary parts of the tipper vector are changing smoothly since they are a function of conductivity structure below the measuring profile. For the near-field sources, the tipper will instead point almost towards a fix location, namely the source location. The near-field frequencies can therefore easily be detected by calculating the scalar tipper along the measuring line. To remove these frequencies a digital notch filter can be used prior to the main transfer function calculation. Another method to find the near field sources is to use the tensor tippers and then calculate the prediction error for each individual index in the band of interest. Those indices having a prediction error greater than a certain value can be rejected.

3.3 **RMT processing overview**

The measured signals from the radio transmitters are saved as raw time series. To convert these raw time series to electromagnetic transfer function several processing steps must be performed.

3.3.1 **Fast Fourier Transform (FFT) and spectral matrix**

The Fast Fourier Transform (FFT) reduces the number of calculations for N data points to a raw spectrum with N/2 frequency indicies. Therefore are the relations between the input and output channels much simpler in the frequency domain then in the time domain. If the raw time series are divided into a number of time segments, then the FFT can be used for each segment to find the complex spectrum of that channel. Since the frequency range for RMT signals are between 10 and 350 kHz only the spectrum in the band of interest is analyzed.

One problem that can occur is that some signals are not in complete phase stability over the total measurement interval. The solution is that the spectra are converted into auto and cross powers which are the product of the field components and their complex conjugates. These are stored in a three dimensional spectral matrix, **S**, which contains the contribution from all the segments (real and imaginary parts of the auto and cross powers) for each frequency index.

3.3.2 **Transmitter picking**

The radio transmitters are located all over the world. Depending on their location and transmitting power they appear in spectrum with different S/N ratios.

3.3.2.1 **Finding the Signal-to-noise ratio**

The Signal-to-Noise ratio (S/N or SNR) is a measure of the signal strength relative to the background noise and is a function of transmitter strength, distance to the transmitter as well as the bandwidth used. Normally the aim is to increase the S/N ratio. This can be done partly by applying some noise reducing filters or signal amplification if necessary.

In the processing used in this study, the S/R is defined as the ratio between the total horizontal magnetic field energy and the background energy. The background noise is defined as the median filtered total horizontal field, a method of making a reference curve for the background noise where the width of the filter affects the estimated noise level (Figure 3.2).

Usually is the magnetic field less noisy than the electric field and the transmitting power is more or less stable in a survey area. Therefore, by choosing a threshold for the S/N ratio, radio transmitters can be detected automatically and only data with S/N ratio above this threshold will be saved to the spectra file.

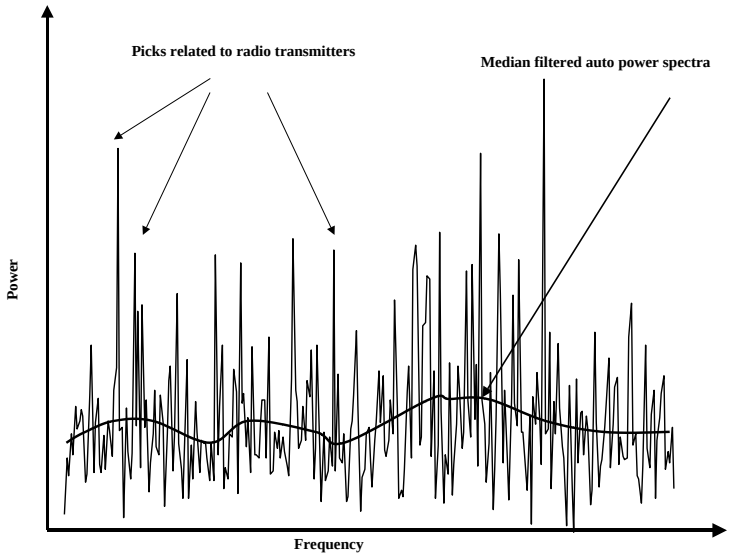

Figure 3.2. A synthetic example of an auto-power spectrum and its median filtered spectrum. The noise level is found from the median spectrum. (Bastani, 2001)

3.3.2.2 **Automatic determination of directions to radio transmitters**

As mentioned in chapter 3.5.5 a secondary current is induced in the Earth that generates a small electric field along the transmitter direction and a horizontal magnetic field rotated by 90 degrees with respect to the electric field. Since the magnetic field is less distorted by lateral conductivity changes the direction to the transmitter can hence be found. The transmitter azimuths are obtained from equation (2-29):

$$\phi_{Az} = \frac{k\pi}{2} + 0.5 \cdot \tan^{-1}\left[\frac{2 \cdot \mathrm{Re}(S_{12})}{(S_{11} - S_{22})}\right], \qquad k = 0, 1 \tag{3-1}$$

where the S_{ij}'s are the auto and cross powers of channel *i* and *j*. Here is channel 1 corresponding to the magnetic north and channel 2 to the magnetic east.

3.3.2.3 **Removal of strong local sources**

Local/near field sources often have high S/N ratios. One simple way to remove these is to use a digital notch filter. It acts on the S/N ratio before the transmitter selection. If the central frequency and bandwidth of the filter can be specified, it forces the measured values to zero for the central frequency and frequencies within half a bandwidth around it. For the EnviroMT (Bastani, 2001) the system can handle three different specified frequencies and their associated third and fifth harmonics.

3.3.3 **Locked estimating**

When measuring a lot of frequencies is saved, but only a few of these are detected transmitters and needed to estimate the transfer functions. Therefore a new spectral matrix is formed containing only the selected frequencies. The subsequent stacking is then *locked* to this new spectral matrix in order to speed up the processing. The transfer functions and their standard error can then be estimated after some procedures.

3.4. **Band splitting and averaging**

The idea behind the band splitting used here is based on that transfer functions for naturally sources in magnetotelluric are estimated in narrow bands of either one half or one octave. One octave is by definition the interval between two points where the frequency at the second point is twice the frequency of the first. Figure 3.3 shows the band splitting to provide two sets of transfer functions: the main band is split into 10 narrower sub-bands with a bandwidth of half an octave and 9 overlapping sub-bands with a bandwidth of one octave. The geometric mean of the minimum and maximum frequencies in each sub-band is defined as the nominal target frequency.

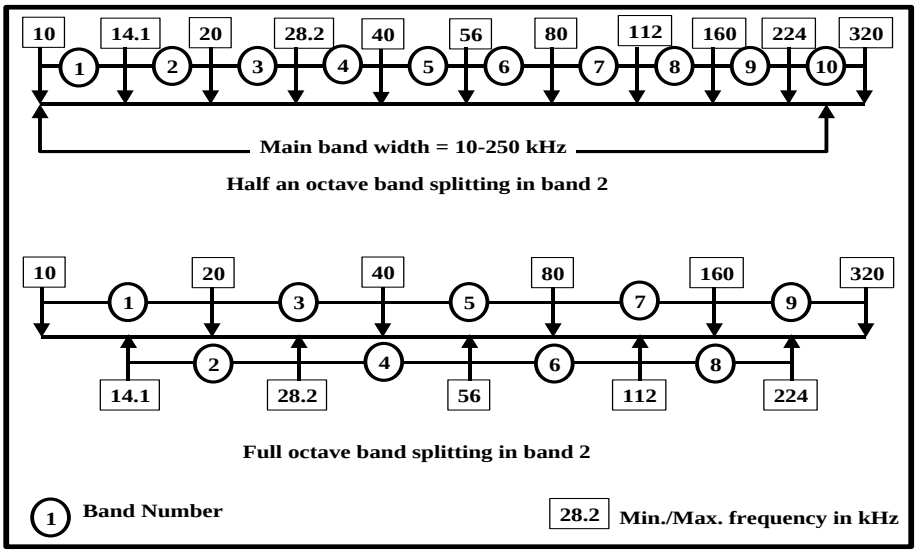

Figure 3.3. An example of band splitting in RMT processing for band 2. The first full octave sub-band starts at 10 kHz and ends at 20 kHz. The nominal frequency is then about 14 kHz. (Bastani, 2001)

In the calculation for a natural magnetotelluric source the transfer functions in each sub-band are assumed to be constant, independent of the frequency. In practice the input channel, composed of the horizontal magnetic field component, is noise free. Therefore can all frequencies belonging to a narrow sub-band be solved for transfer functions by using the least squares method. This approach is called the *band averaging technique* and is a well-known processing method. It minimizes the total prediction error energy of each output channel over the entire sub-band. For the RMT method are transmitter frequencies belonging to a sub-band selected. If there are two or more independent transmitters then there are sufficient equations to determine the unknown transfer functions (Bastani, 2001). As an example, the transfer function of the electric field in x-direction becomes:

$$\hat{Z}_{xx}(\omega_t) = \frac{\sum_{i=1}^{n} S_{22}^{i} \times \sum_{i=1}^{n} S_{14}^{i} - \sum_{i=1}^{n} S_{12}^{i} \times \sum_{i=1}^{n} S_{24}^{i}}{\sum_{i=1}^{n} S_{11}^{i} \times \sum_{i=1}^{n} S_{22}^{i} - \sum_{i=1}^{n} S_{21}^{i} \times \sum_{i=1}^{n} S_{12}^{i}}$$

$$\hat{Z}_{xy}(\omega_t) = \frac{\sum_{i=1}^{n} S_{11}^{i} \times \sum_{i=1}^{n} S_{24}^{i} - \sum_{i=1}^{n} S_{21}^{i} \times \sum_{i=1}^{n} S_{14}^{i}}{\sum_{i=1}^{n} S_{11}^{i} \times \sum_{i=1}^{n} S_{22}^{i} - \sum_{i=1}^{n} S_{21}^{i} \times \sum_{i=1}^{n} S_{12}^{i}} \qquad (3\text{-}2)$$

ω_t is the target frequency defined as the geometrical mean of the n transmitter frequencies in the sub-band and S_{ij}'s are the spectral matrix elements defined as

$$S_{ij} = C_i^{*} C_j . \qquad (3\text{-}3)$$

C_i stands for one of the measured electric or magnetic field components numbered from 1 to 5 corresponding to H_x, H_y, H_z, E_x, and E_y respectively (Bastani, 2001). The asterix denotes complex conjugation.

3.5 **RMT field layout**

In the RMT method the electric and magnetic field components from the radio transmitters are measured at the Earth surface. The RMT field layout is schematically shown in Figure 3.4. At each station the analogue filter box (AF box, No. 1) is placed at the center. The horizontal electric field components are measured in two well-defined directions, usually N-S and E-W, by the use of two pairs of steel electrodes (No. 2). The electrodes are set symmetrically with respect to the central box and the electrode separations are the same in both directions. The electrodes are connected to the buffer amplifiers (No. 4) for signal conditioning and to the AF box via special cables (No. 3). The three magnetic sensors, mounted as a fixed set on a tripod (No. 5), measure the magnetic field components. The two horizontal sensors are oriented parallel to the electric field sensors and the third sensor points vertically downwards. The easily portable tripod is placed close to the AF box and is connected to the box by a multi-wire cable (No. 6). A cable that is connected to a grounded steel electrode is plugged into the center of AF box to maintain a zero voltage reference (No. 7). After analogue filtering in the AF box the analogue signals from the five channels are transferred to the central unit (No. 8) for subsequent A/D-conversion and processing. A multi-wire cable of ten meters length connects the two units (No. 9).

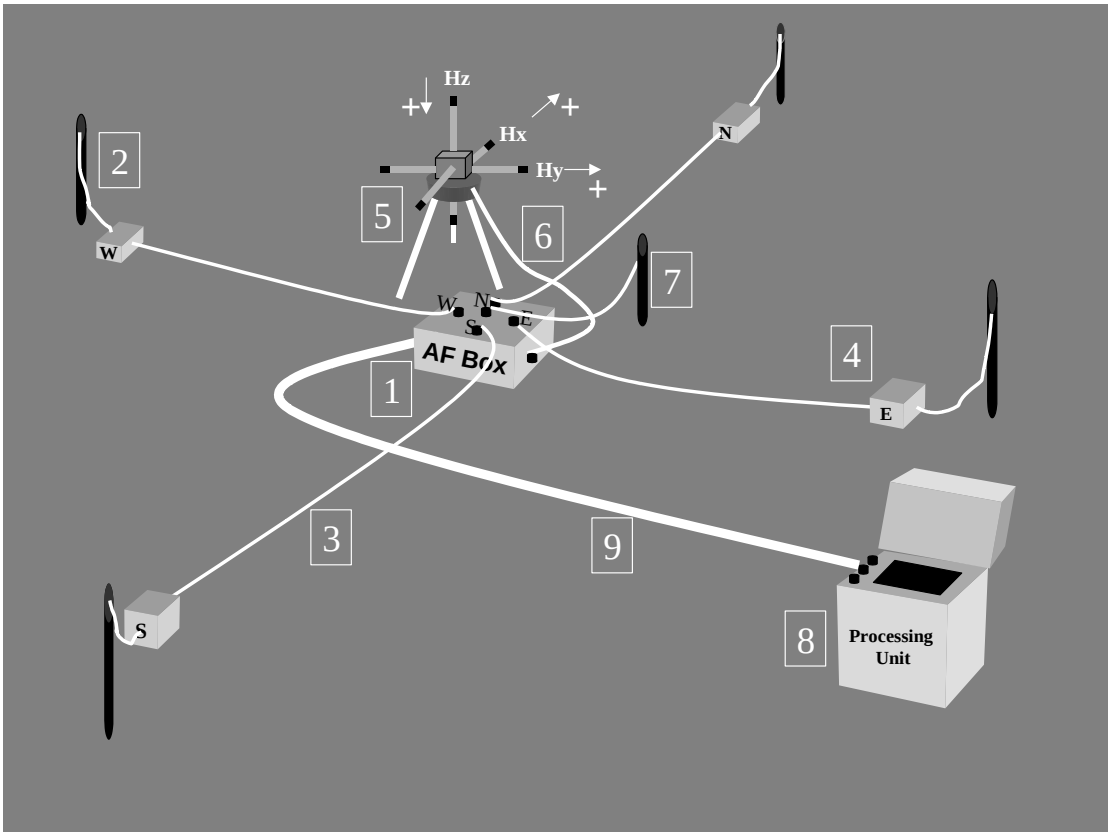

Figure 3.4 : Schematic of the RMT measurements field layout.

THE MFR INSTRUMENT
HARDWARE

4. **The MFR instrument hardware**

The instrument used by the Geological Survey of Sweden (SGU) today is called Wadi by ABEM AB and is only measuring signals from one transmitter. As mentioned before the response from e.g. a fracture zone is dependent on the strike direction. Since there are so few VLF transmitters this sometimes give rise to problems finding a transmitter in the right direction. The Wadi instrument is mainly used for investigations of the quality and featuring of the bedrock. The depth resolution is very poor since the frequency band is just 16 – 30 kHz and in a few surveys the transmitter signal has been too weak to resolve any structures at all.

The concept behind the EnviroMT instrument developed by Uppsala University (Bastani, 2001) was to improve the measurements by using the RMT method instead of VLF. Unlike the Wadi instrument it measures the signals from many transmitters and chooses those with a S/N ratio above a certain threshold. Since the RMT method uses the frequency band 15 – 250 kHz there is not only more transmitters to chose between, the depth resolutions is also better. The measurements are independent of the direction to the transmitter since it measures all three magnetic components. The drawback with EnviroMT compared to Wadi is the measuring time at every point and the size of the equipment itself. The Wadi instrument has a measuring time of 5 sec and the equipment is easy to carry around since it is light and user-friendly. The EnviroMT instrument on the other hand, is heavy (ca 25 kg) and bulky. Therefore it must be handled by at least two persons. The measuring time is as long as 2 min.

The new MFR instrument is based on the concepts used in the EnviroMT system but it is simpler and more user friendly. It is also easier to operate the instrument in the field so that it can be used by just one person (see Figure 4.1 for comparison of physical dimensions).

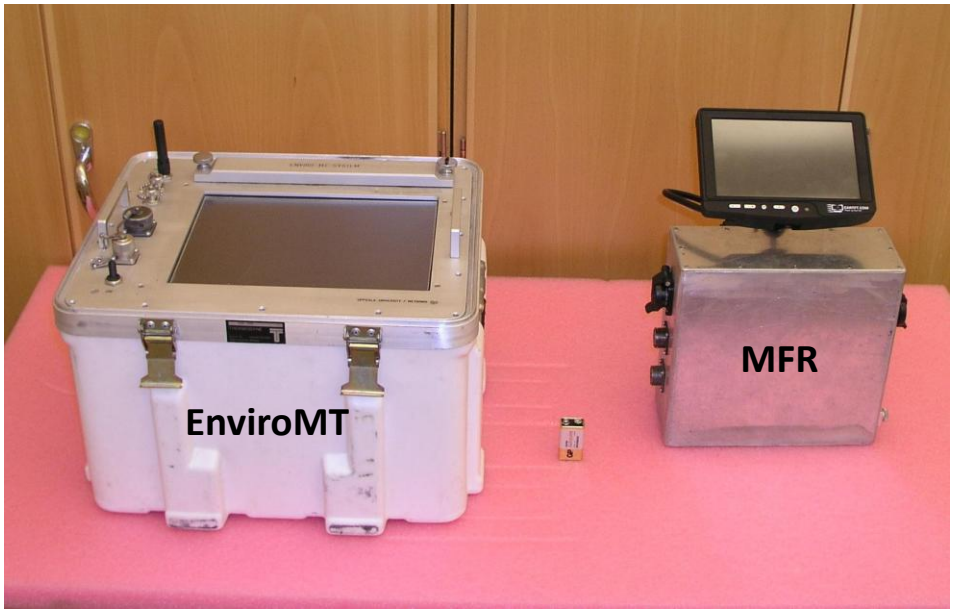

Figure 4.1 : A comparison between the size of EnviroMT and MFR instrument.

Figure 4.2 shows a block-diagram of the hardware configuration in the MFR instrument.

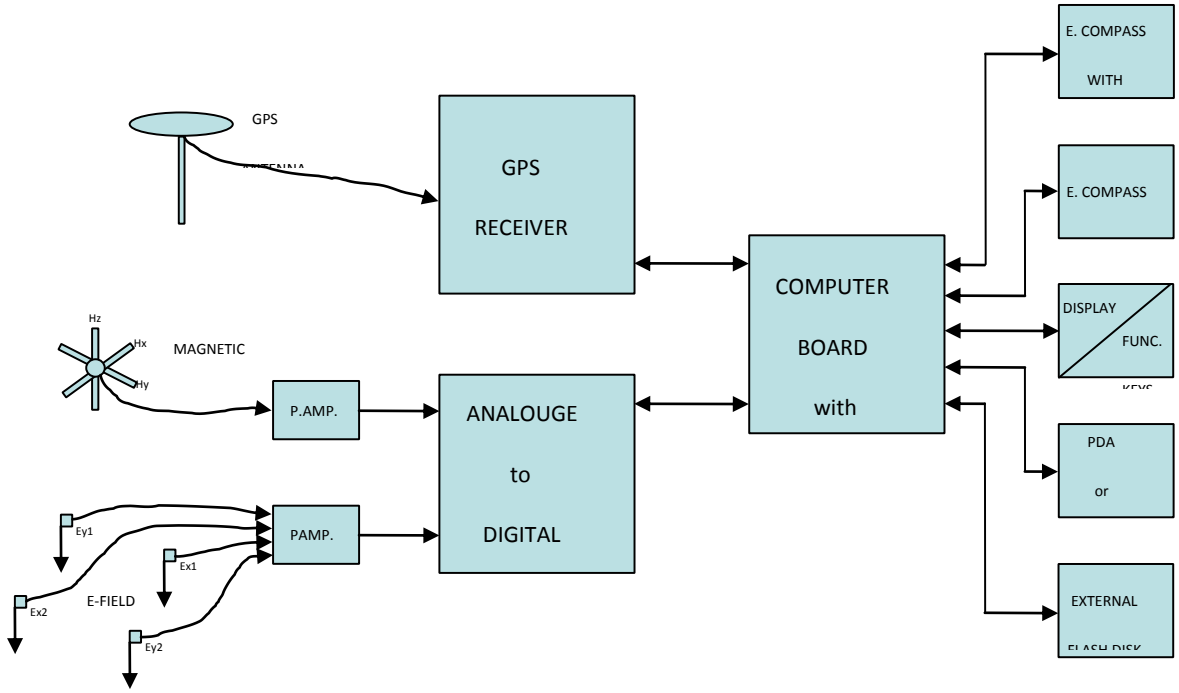

Figure 4.2. Block diagram of the multi-frequency receiver.

4.1 **Hardware**

In this part I have used the information found in the diploma thesis by Michael Schishcke (2009). The new instrument is based on PC/104 embedded x86 board with a GNU/Linux operating system (Figure 4.3). This allows us to do the software development directly on the target system while taking advantage of the wealth of free open-source software. The processor (IntelR Pentium M) is powerful enough to do real-time signal processing without the need of a dedicated DSP. One internal 8GB Compact Flash Solid State Disk and a slot for a removable Compact Flash Card for data storage are installed (Figure 4.4a) . There are two sensors, a Magnetometer for magnetic field measurements (Figure 4.4 b,c) and an Electrode Rig for electric field measurements. A post-amplifier provides a programmable gain to match the amplitude of the signal to the input range of the A/D converter. The A/D Converter board is connected to the processing unit via the PCI bus. Furthermore, a powerful GPS receiver and an electronic compass with built-in tilt meter are connected on the RS-232 ports (see Figure 4.5). The main unit with touch-screen and battery pack is enclosed in a custom ruggedized aluminum case. The external ports include USB 2.0, Fast-Ethernet and e-SATA.

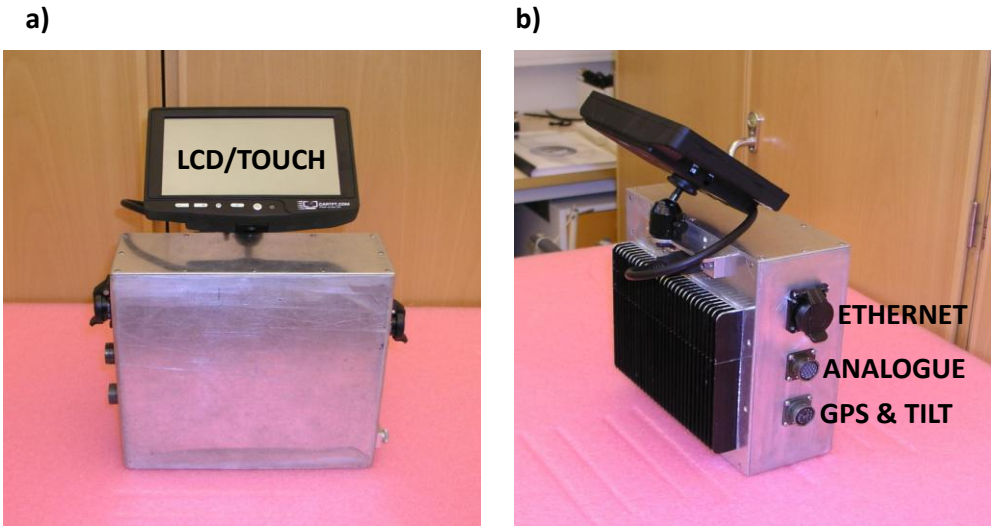

Figure 4.3. a) Front view of the instrument, b) Left view showing the Ethernet, Analogue and GPS-TILT contacts

4.1.1 **Magnetometer**

The magnetometer is a sensor for the magnetic field measurements. It consists of three ferrite rods with windings of copper wire that are arranged in an orthogonal three-axis-configuration. The magnetic sensor is an orthogonal three component coil magnetometer with a sensor length of 15 cm (Figure 4.4b). Being an inductive sensor, it measures alternating fields. It has integrated pre-amplifiers (Figure 4.4c) and an analog high-pass-filters to amplify the very low sensor voltage, attenuate the ever-present 50Hz field that is generated by power lines and to drive the signal cable.

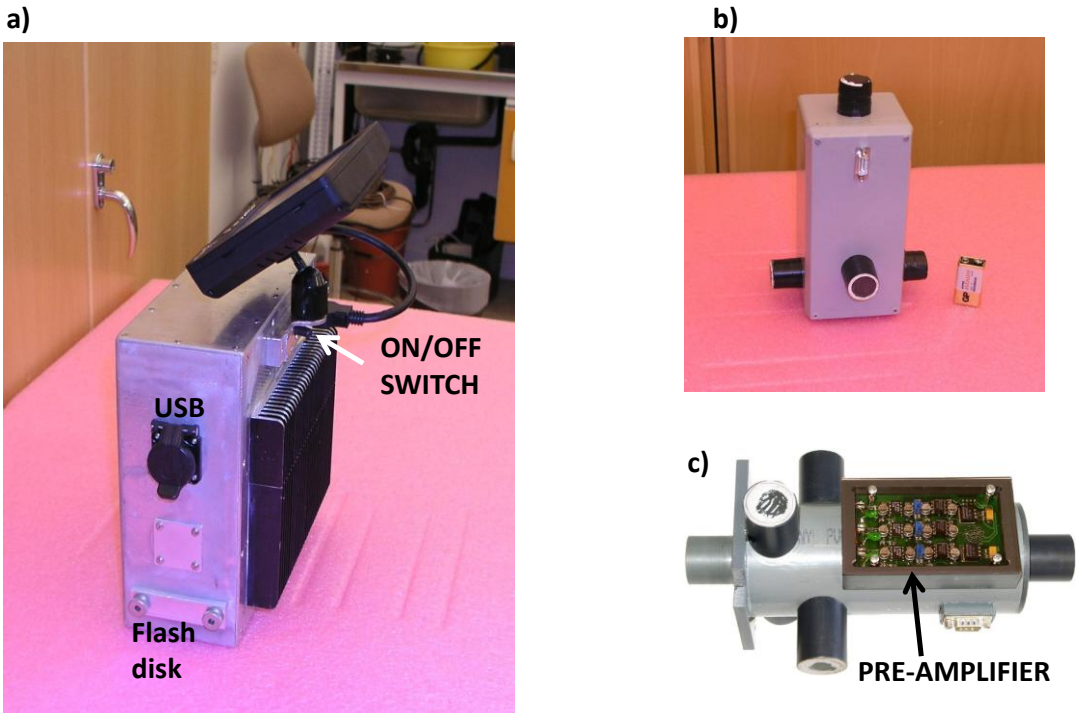

Figure 4.4. a) The USB connection and Compact Flash Disk drive. b) Three component magnetic field sensor in the case for the airborne measurement configuration. c) The magnetic sensor in the final shape and its pre-amplifier configuration.

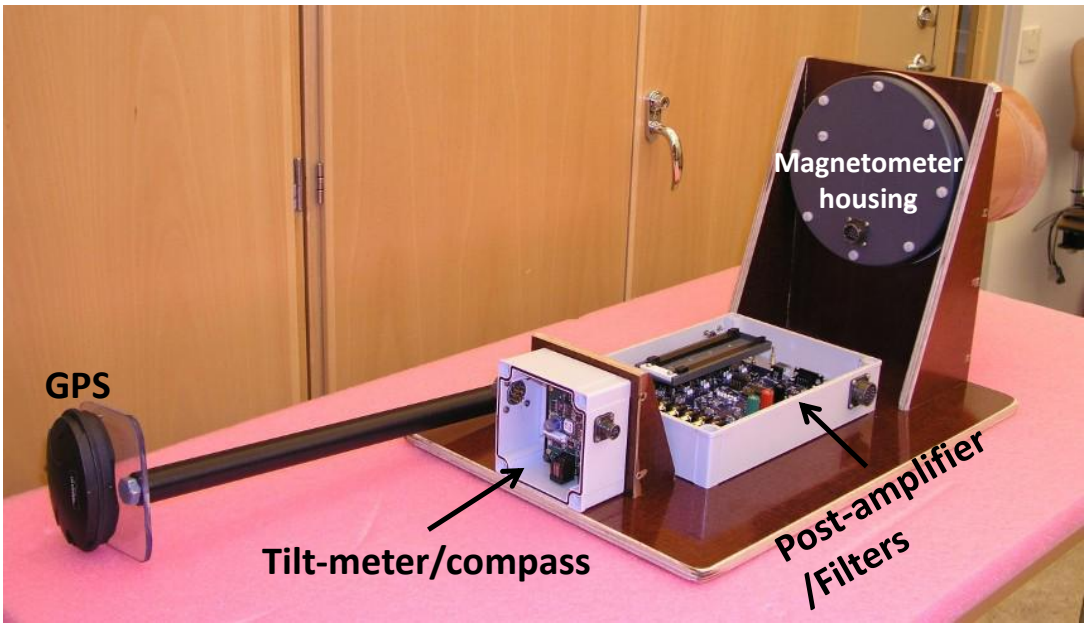

Figure 4.5. Parts of hardware used in the MFR instrument to be carried by the operator in a back-pack.

4.1.2 **Hardware in the Back-pack**

Some of the components are mounted on the back of the observer. The back pack unit is shown in Figure 4.6. The GPS receiver, the Electronic Compass, the Post-Amplifier and filters are marked in the figure. The GPS receiver is a “Seres”, made by “csi wireless”. It has a RS-232 interface and supports the NMEA 0183 standard. Its noteworthy features are the high update rate of 5Hz and relatively high precision thanks to a differential GPS mode (EGNOS/WAAS). The electronic compass is a “Revolution Compass”, made by “True North”. It contains a 3-Axis-Magnetometer to measure the Earth magnetic field and a fluid tilt-meter. Like the GPS unit it talks a NMEA 0183 dialect which tells its heading angle, as well as pitch and roll angles with an update rate of up to 15Hz. The magnetic sensor is in the cylindrical enclosure on the right. The main unit with the touch screen is carried in front but also mechanically attached to the "back pack" to unload the arms. The battery is plugged in a slot on the main unit. Figure 4.6 shows the receiver box together with the back-pack that is prepared for the measurements.

4.1.3 **Electrode Rig**

The electrode rig is an electric field sensor (figure 4.7). Two pairs of steel rods are attached to the ground, one pair in NS and the other in EW direction. Electric fields in the ground cause a potential difference between the two electrodes. Like in with the magnetometer, this signal has to be amplified and filtered. This sensor is used when the operator plans to carry out a full tensor RMT measurement (see the chapter on software). It is a foldable sensor and the operator can carry it easily between the stations.

The instrument is mainly a data acquisition instrument where the measured data is processed and displayed for each station along a profile. After the measurement is completed the data can be transferred to an external computer for further processing.

Figure 4.6. The MFR equipment for ground tipper measurements.

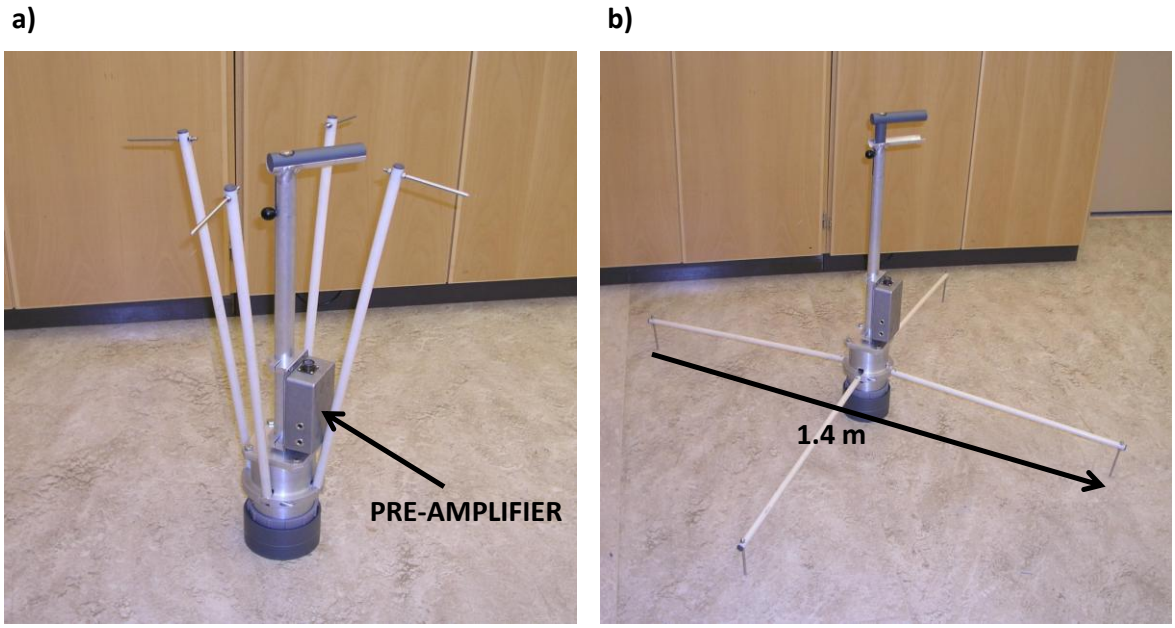

Figure 4.7: The electrode rig, a) in closed or transport position and b) open or measurement position

THE MFR INSTRUMENT SOFTWARE

The MFR Instrument Software

The MFR software is composed of a set of programs to

- Control the hardware
- Communicate with the operator (User Interface)
- Process the data online
- Visualize the data in field
- Store the data in a database

The program that controls the hardware is designed by several people and among them are Lars Dynesius (UU), Michael Schieschke (UU) and Mehrdad Bastani (SGU). Michael Schieschke (2009) provides details about the hardware control program.

The Graphical User Interface software was first designed by Mehrdad Bastani (SGU) and Lars Dynesius (UU) and then implemented by Michael Schieschke (UU) as his diploma project. In the following the original design of the User Interface is presented and the basic concepts are briefly explained.

5.1 **Basic about GUI parameters**

The multi-frequency receiver (MFR) is a new state-of-the-art instrument that makes use of the Electromagnetic (EM) signal from the VLF and radio transmitters in the frequency band 15-350 kHz. A GPS and a digital tilt-meter are also attached to MFR for positioning information. The analogue data (three or five channels depending on the measuring mode) are first digitized by the data acquisition program with a sampling frequency of 600 kHz and a number of samples equal to 16, 32, 64, 128 and 256 k. The data are stored in a shared memory area and then used by the data processing program. The data acquisition and processing programs communicate via IPC (Inter Process Communication) that are built in the Linux operating system. IPC is also used to configure and to receive information from the GPS (the co-ordinates) and the tilt-meter (Sensor orientation).

Measuring modes: MFR has four measuring modes: Continuous Time Series, Continuous Tipper (CT), Discrete Tipper (DT) and Radio Magnetotelluric (RMT). In all three modes the three components of the signal's magnetic field are registered.

Data Processing: The MFR band is subdivided into 10 sub-bands each having one octave width. These transfer functions are calculated at certain frequencies called target frequency. Each target frequency is centred logarithmically in the middle of sub-band.

Transmitter selection: In the old system called EnviroMT in order to detect the radio transmitters automatically an adjustable total magnetic S/N threshold was defined. As the transmitting power is more or less stable, the threshold could be determined by making a preliminary test just once for the whole survey area. In the MFR and specially in the CT mode automatic knowledge about the number of available radio transmitters is vital. Therefore one needs to have an update of the list after a certain number of measurements. The noise level is defined by a running median that has a certain width.

Median filter for noise level: In the MFR the median filter can have three different types, full band, linear and logarithmic. The full band filter uses all the data in 15-350 kHz band. This is a time consuming procedure and most accurate method. The linear technique selects a certain number of indexes (Based on the median length) that have a gap in a linear frequency distribution. For example if the gap is 10 and the median length is 6, the selected indexes are: 0,10,20,30, 40 and 50. The median value is then estimated (as the average value of index 3 and 4 in the sorted array) and the noise level of the first 10 indexes is set to this average. The filter is then moved 10 indexes, namely to 10,20,30,40,50 and 60 and the same procedure is repeated for second to indexes. In the logarithmic case the same procedure is carried out in a logarithmic sense meaning that the indexes are equal-spaced logarithmically. In each sub-band at least two transmitters are needed for the tensor calculation of the transfer functions and they are selected by the S/N threshold.

S/N ratios used to select the transmitters: Every time the frequency list is updated, the median filter runs to reject an old out of work transmitter from the list or add a new in line transmitter to the list. The selection is done by maintaining a S/N ratio threshold. The operator carries out a set of preliminary tests to evaluate the noise level and correspondingly applies the proper level. Those indexes that have a S/N ratio above the level are chosen as a frequency representing a radio transmitter.

Result and info delivery: The spectrums of the selected frequencies are then used to estimate EM transfer functions in each sub-band. The information about the radio transmitters and the transfer functions are then sent to the user interface program for display and database storage.

The MFR instrument has three measuring modes all having some common and each having their specific data acquisition parameters. The meaning and use of these parameters are explained briefly in the following.

5.1.1 **Data acquisition parameters**

- Line no.: The line number shows the present line number. This parameter can be just one in the case we use CT method.
- GPS: In some case where the GPS signal is weak or the device is malfunctioning, one may use the local co-ordinate system for the measurements. If the radio button is checked then the GPS is activated and a co-ordinate system is then selected.
- The local co-ordinate edit boxes are activated when the GPS is not used. They show the starting co-ordinates of the measuring profile. This system might most probably used when one of the DT or RMT methods are employed and the operator is well aware of the distance between the stations.
- Station number (just in DT & RMT): This parameter can be adjusted in case some of the measurements are to be repeated or skipped.

5.1.2 **Data processing parameters**

- Median length (in number of samples): The length of median filter given in the number of samples to calculate the signal to noise ratio (S/N) of the total magnetic field to use to select the available radio transmitters that lie over a certain threshold. The S/N threshold is given in dB units. The length is a function of sampling frequency and number of samples.

- Signal to noise (S/N) in dB: This level can be automatic by checking the radio button.
- Median type: Full length, linear or logarithmic.
- Digital notch: Three digital filters can be used to filter the local noise (e. g., near field transmitters). The number of visible check boxes depends on the number of filters needed. The drop down list shows the number of filters. The first column of the boxes shows the central frequency of the filter in kHz and the second shows the filter width in kHz. If the radio button is not checked the boxes are invisible.
- No. of samples, N: This parameter can get 16, 32, 64, 128, and 256 K samples depending on the resolution needed in the measurements. ($\Delta f = f_s/N$, for a given sampling frequency)
- Sampling frequency, f_s (just in CT & DT): A longer sampling time may be needed to achieve longer integration time to overcome a noisy situation. This also increases the frequency resolution. ($\Delta f = f_s/N$, for a given number of samples, N)
- Median update rate (just in CT): The parameter determines the number of measurements to carry out to update the transmitter list using the median filter.
- No. of stacks (just in DT & RMT): In DT and RMT measuring modes a certain number measurements at each station are carried out and the measured data are stacked in the frequency domain. This is the number of stacks. Each individual data in the stack will most probably be stored for post processing purposes.
- Electrode spacing (just in RMT): This is the distance between the electric field sensors (or electrodes) in the unit of meters. The measured horizontal electric field is an average taken in this interval (E = V/d, V is the potential difference, and d is the electrode spacing).

5.2 **Preliminary GUI of MFR**

The interface for the MFR instrument is mainly used to

- Deliver the project information and measuring parameters to the server (MFR instrument)
- Communicate with the measuring processes, e. g., data acquisition module (DAM), data processing Program (DPP).
- Display the results on the screen in different measuring modes.

Startup window: Using the MFR icon the operator starts the application for creating a new project or continuing an existing one. Figure 5.1 shows the main menu when a new project starts. The 1st button to use at the beginning of a new project is the PROJECT SETUP that leads you to a new window to specify the project specifications. Note that the other buttons except EXIT are passive.

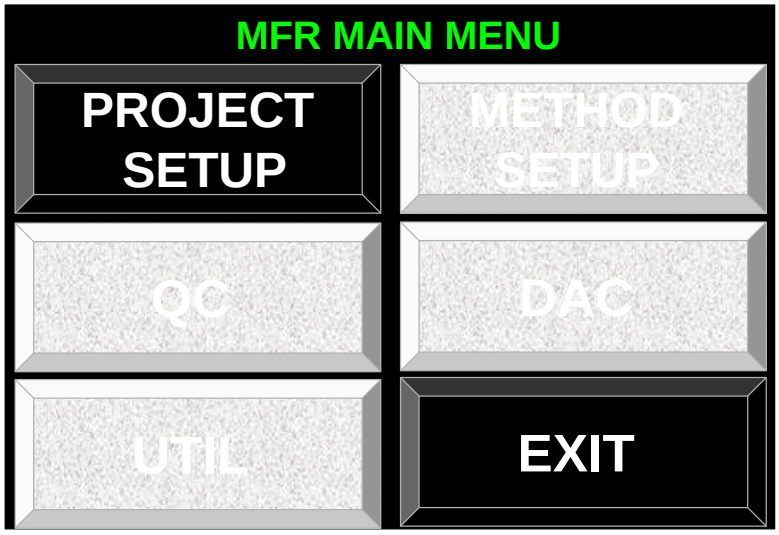

Figure 5.1

Starting a new project: A project contains the measurements in a certain location, a date and by using a particular method. The information about the client and operator must also be attached to the project. These are information needed to build up a database for later data manipulation and interpretation. Figure 5.2 is a picture of project setup window. Three edit boxes are used to hold the

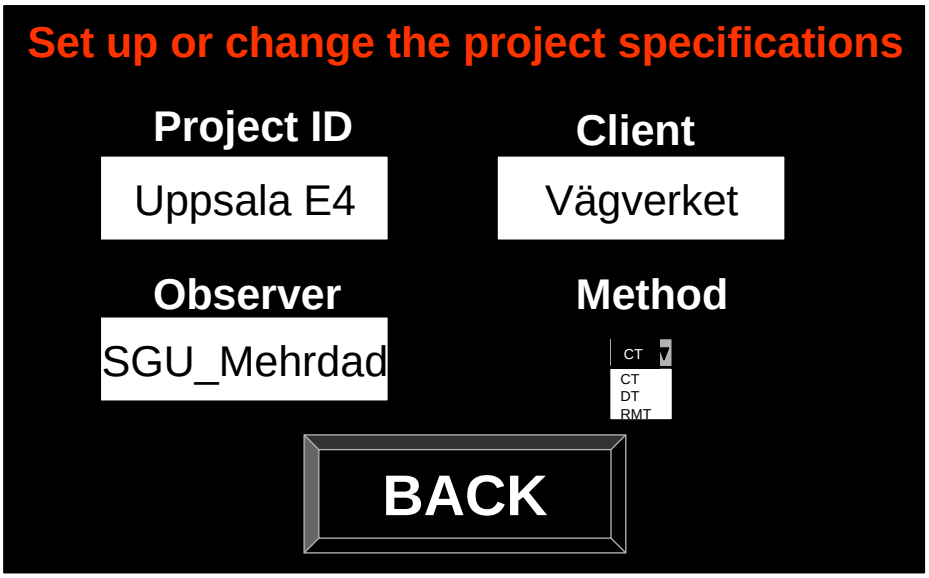

Figure 5.2

Project ID, Client and observer's name. Using a drop down list the operator can select the planned measuring method. The MAIN MENU button is used to return to the main menu window.

Method setup: The measuring method is one of Continuous Tipper (CT), Discrete tipper or Radio Magnetotelluric (RMT). In the main menu using the Method setup button (that is activated at this stage) leads to the window shown in figure 5.3 to the right. The text in the red box shows the action to take to proceed. Each method has a set of parameters to adjust. The use of parameter is described in a separate document.

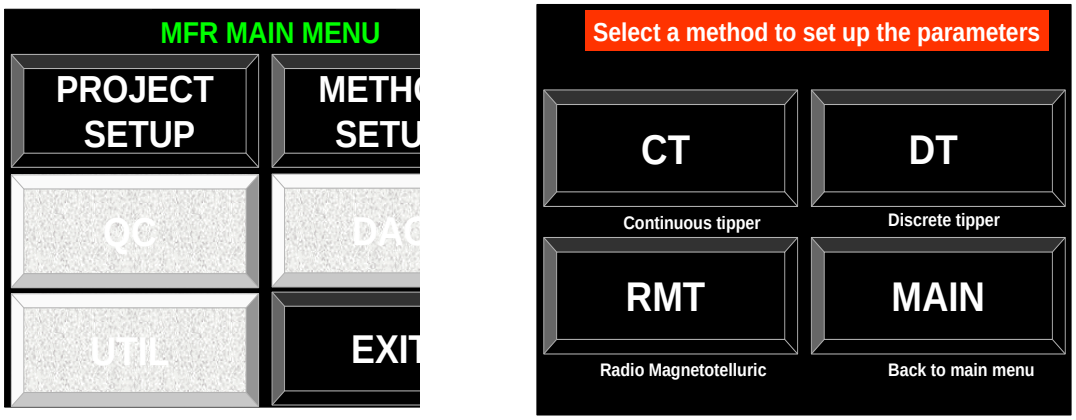

Figure 5.3

CT method: Continuous tipper method (mode) measures continuously three components of the magnetic field. This means that the data acquisition proceeds without any interruption.

This mode is used both on the ground and airborne measurements. The parameters to set are shown in figure 5.4.

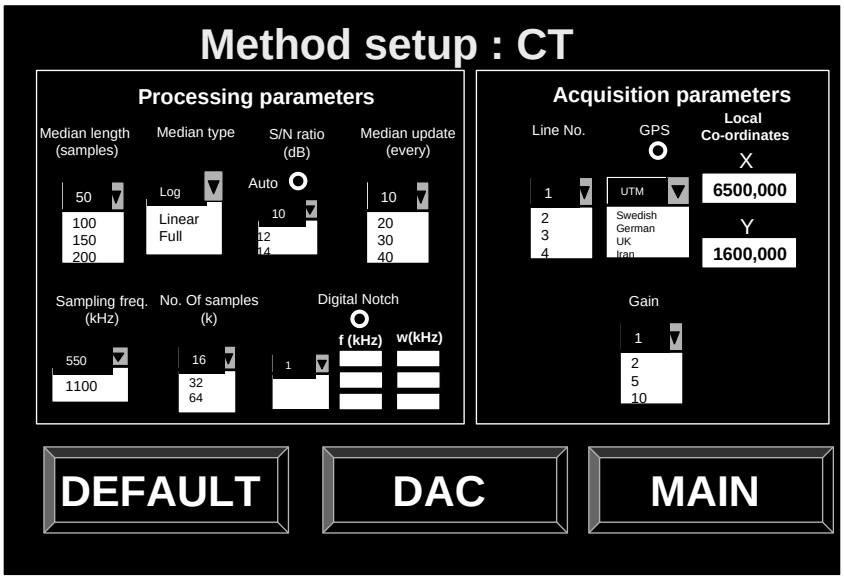

Figure 5.4

Two types of parameters have to be set, namely processing and Acquisition. The processing and data acquisition programs use the former after. The latter determine the geometry of the data acquisition, namely which line and where on the Earth. Since the measuring parameters can be set or changed either at the starting or in the middle of a measuring phase, two buttons are designed to fulfil different tasks. In this example we assume a case there a new project is being built. The "DEFAULT" button loads the default parameters that are kept in a default_parameters file. The DAC (Data Acquisition) and MAIN buttons lead to data acquisition and MAIN windows.

DT method: Continuous tipper method (mode) measures three components of the magnetic field at a certain distance or location. In this case the data acquisition is initiated by the operator and stops after a set of number of measurements (No. of Stacks) are carried out. The number of parameters is almost the same with DT and CT methods but there are a few parameters more to set in the CT mode (see figure 5.5). In the DT mode, since the measuring parameters can be set or changed either at the starting or in the middle of a measuring phase, two buttons are designed to fulfil different tasks. One can also use the default parameters by clicking on the "Use defaults" button.

RMT method: RMT method is used mainly with discrete ground studies. In this method three components of the magnetic field as well as two components of the electric field are measured simultaneously. Figure 5.6 shows the input parameters for the RMT method. This method has the most number of parameters. Electrode spacing is a unique parameter that reflects the electric field measurements. Assume that one of the methods above is selected and the parameters are set. Using the MAIN button operator turns back to the MFR MAIN MENU window. Note that use of MAIN button in all case leads to MAIN MENU window and all the buttons are activated (figure 5.7).

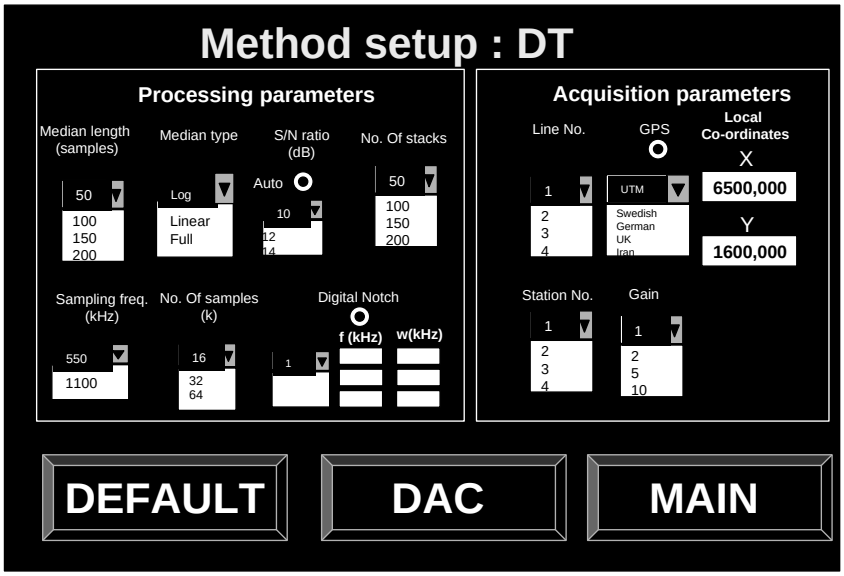

Figure 5.5

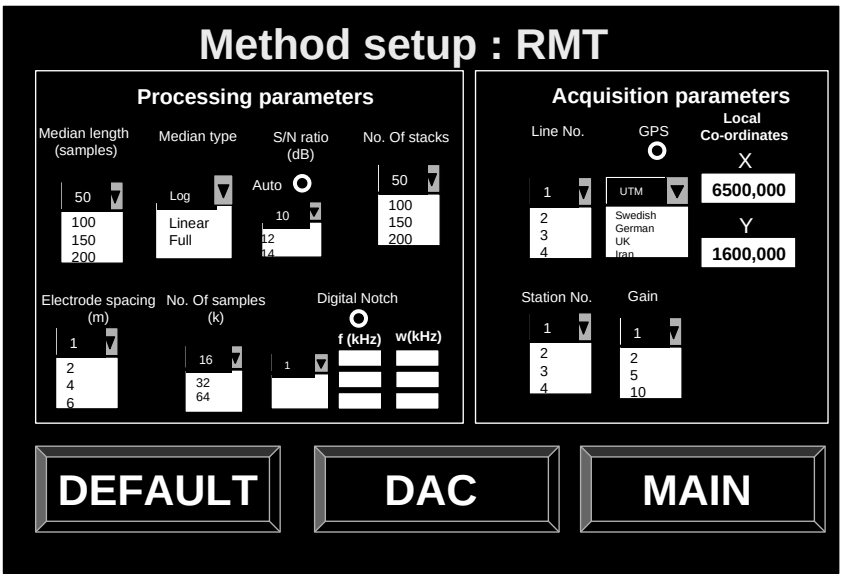

Figure 5.6

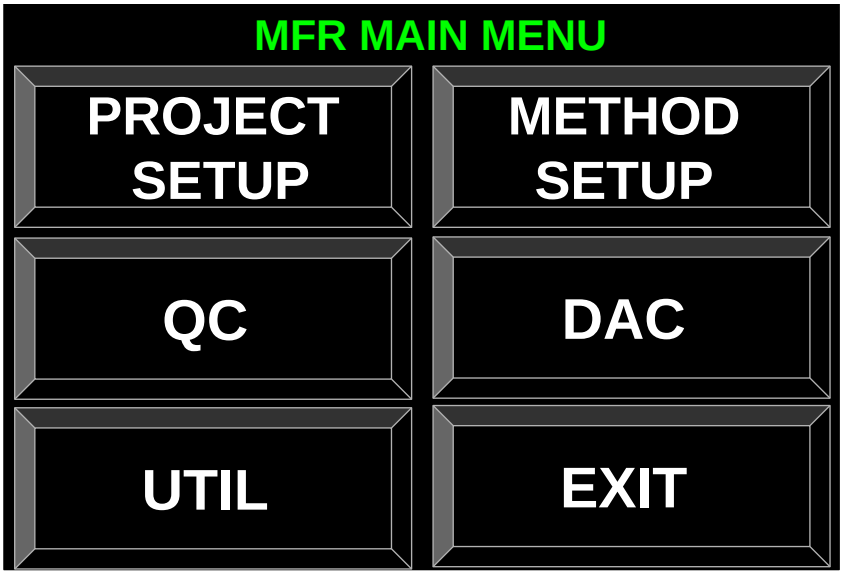

Figure 5.7

Data quality control: At the very early stage of a project a test has to be carried out to evaluate the S/N level and also the signal content. Pushing the QC button in figure 5.1 leads to the window shown in figure 5.8

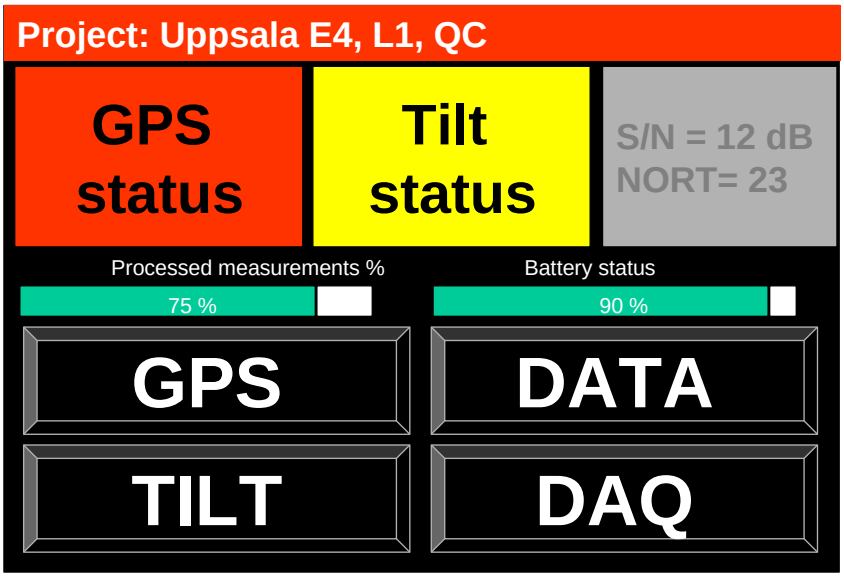

Figure 5.8

The red bar at the top shows the project information. Three boxes below the red bar from left to right display the GPS, Tilt and transmitters status, respectively. The color in the first two boxes shows a relative status. This means that: a red color shows that the device is not functioning properly, yellow a low functioning status and green a full functioning status. The two green bars show the processed measurements and battery status. The former is 0% when the project starts. Four buttons are designed to test: GPS, TILT-meter, DATA quality and to go to DAQ data acquisition window.

GPS test: Testing the GPS provides the information about the number of available satellites,

their signal strength and distribution. This can be achieved by using GPS button in the test facilities window. Figure 5.9 shows the information in the GPS test window. The position (distribution) of the detected satellites, the number of them and also their strength compared to the standard signal (the colored vertical bar) strength are shown in this window. One may change the position in the field and study signal strength of the GPS. Depending on the measuring status, four buttons offer different possibilities to proceed.

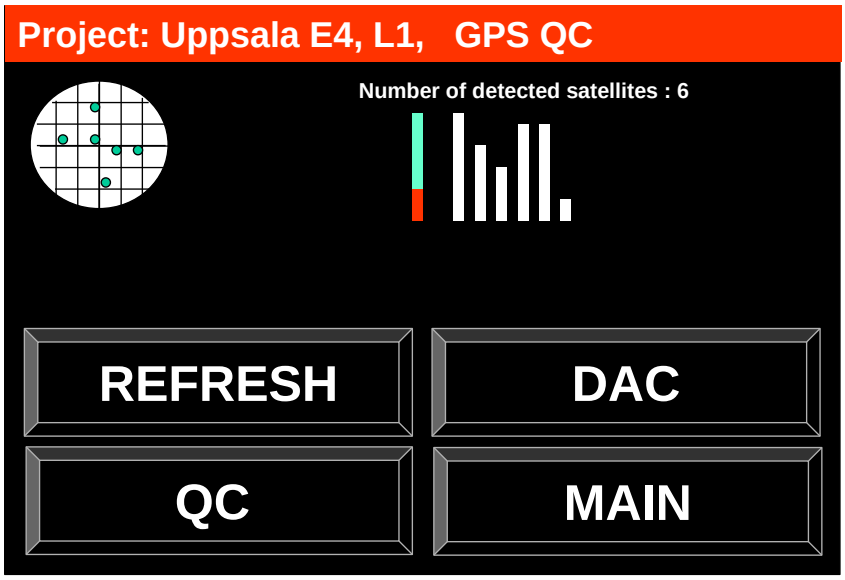

Figure 5.9

TILT-meter test: The tilt-meter is a digital device that measures and delivers the orientation of the three magnetic sensors that measure the three components of the EM signal. Three angles so-called heading, pitch and roll are used to rotate the measuring co-ordinate system into the EM co-ordinate system (+X→ north, +Y→East, +Z → downwards). The TILT button is used to check the tilt-meter's functionality. Figure 5.10 shows the tilt-meter test window.

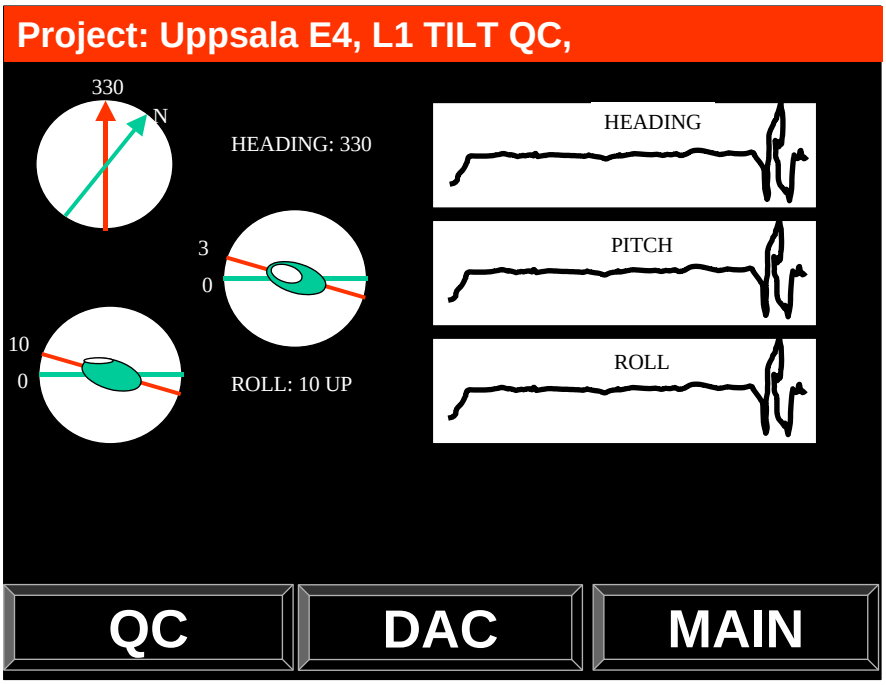

Figure 5.10

Pushing the REFRESH button show the last measurements of the three angles in the left side of the window using three circles and appropriate symbols. To the right recent measurements of the angles (maximum of 100) is shown.

Data quality test: The number of acceptable transmitters is strongly dependent on the noise level as well as the S/N threshold. In order to make the optimal use of the signal, a quality control test must be conducted. In the test main window (figure 5.8) the DATA button leads to the data quality control window as shown in figure 5.11. The processing parameters are those described in the appendix B. The RUN button starts the DAP and DPP. The No. of stacks shows the number of data acquisition sequences. The QC button leads to the MAIN QC window. The DAQ and MAIN switch the program to DATA ACQUISITION and MAIN MENU window respectively. These buttons are designed to fast access the desired window and to skip undesired extra clicking buttons.

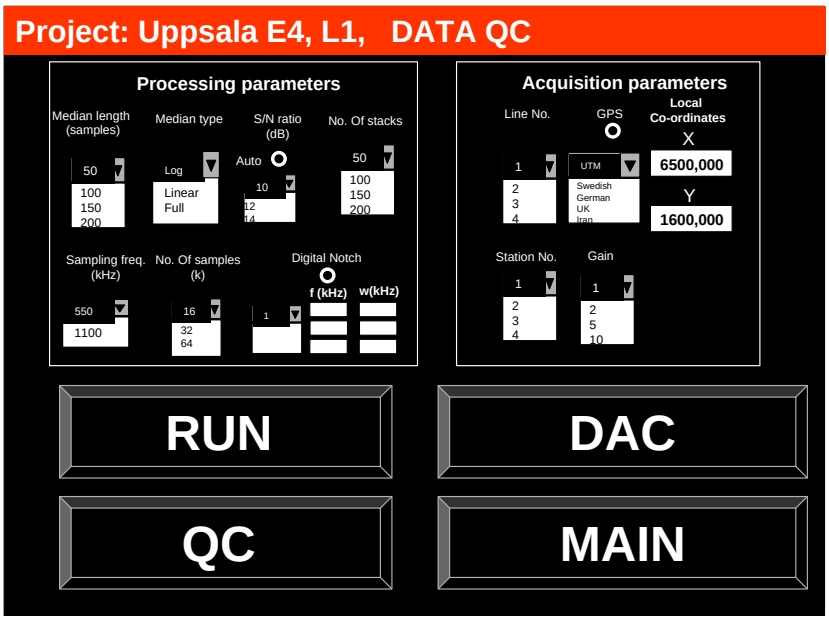

Figure 5.11

The results are shown in the new window shown in figure 5.12 after each run.

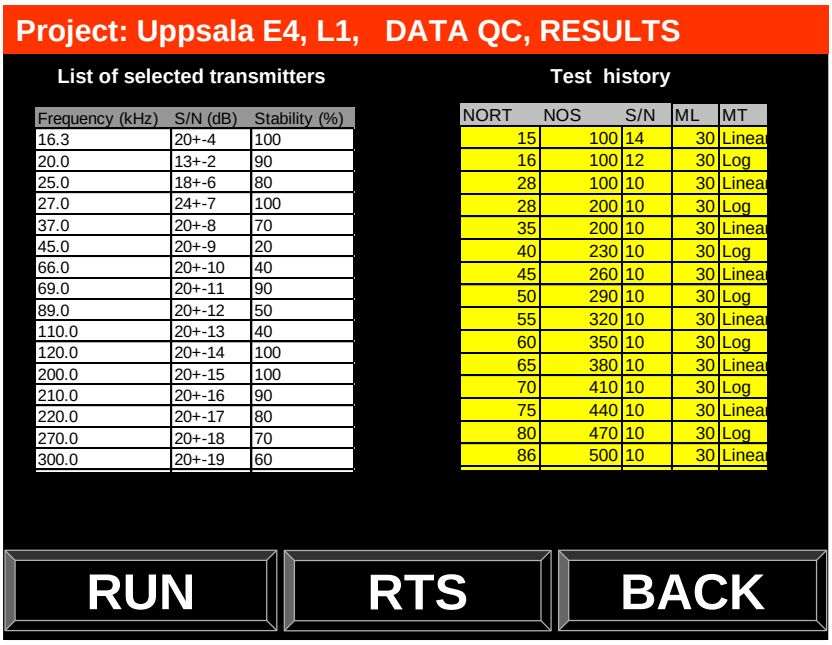

Frequency (kHz)	S/N (dB)	Stability (%)
16.3	20+-4	100
20.0	13+-2	90
25.0	18+-6	80
27.0	24+-7	100
37.0	20+-8	70
45.0	20+-9	20
66.0	20+-10	40
69.0	20+-11	90
89.0	20+-12	50
110.0	20+-13	40
120.0	20+-14	100
200.0	20+-15	100
210.0	20+-16	90
220.0	20+-17	80
270.0	20+-18	70
300.0	20+-19	60

NORT	NOS	S/N	ML	MT
15	100	14	30	Linea
16	100	12	30	Log
28	100	10	30	Linea
28	200	10	30	Log
35	200	10	30	Linea
40	230	10	30	Log
45	260	10	30	Linea
50	290	10	30	Log
55	320	10	30	Linea
60	350	10	30	Log
65	380	10	30	Linea
70	410	10	30	Log
75	440	10	30	Linea
80	470	10	30	Log
86	500	10	30	Linea

Figure 5.12

In this page the results of the current measurement are shown in the white table and if several test are conducted the last 10 are shown in the yellow window for comparison. The information is about the transmitters stability, S/N and frequency at the peak. NORT is the Number Of Radio Transmitters in the yellow table and shows the effect of changes in various parameters. NOS, S/N, ML, MT stand for Number of Stacks, Signal to Noise Ratio, Median Length, and Median Type, respectively. Using RTS button enables the user to see the measured Raw Time Series (RTS) in a new window (figure 5.13).

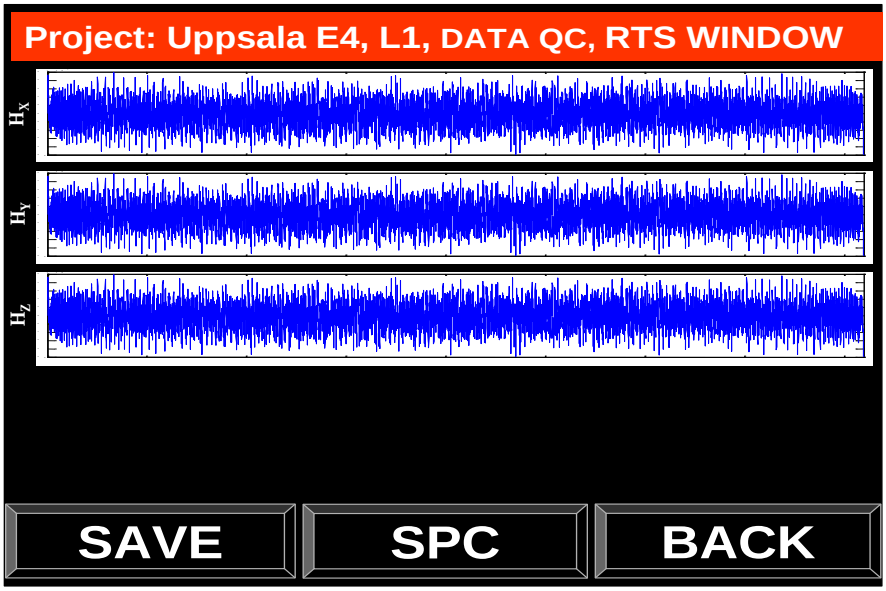

Figure 5.13

Depending on the acquisition method number of channels can be different. The RTS can be saved using SAVE, the spectrum can be shown using SPC and to go back to the previous window (QC WINDOW) using BACK. Use of SPC in figure 5.13 leads to the window shown in figure 5.14. A Fast Fourier Transform (FFT) of the RTS calculates the amplitude and phase of the EM signal in a certain frequency range. Showing the variation of amplitude versus frequency is an effective way of checking the data quality. The window shown in figure 5.13 is a real example of the measurements carried out in Uppsala in 2006 in the laboratory. The strong signal from a nearby strong source dominates the spectrum. Even in this case the noise level can be easily recognized and S/N ratio for the observed peaks can roughly be estimated.

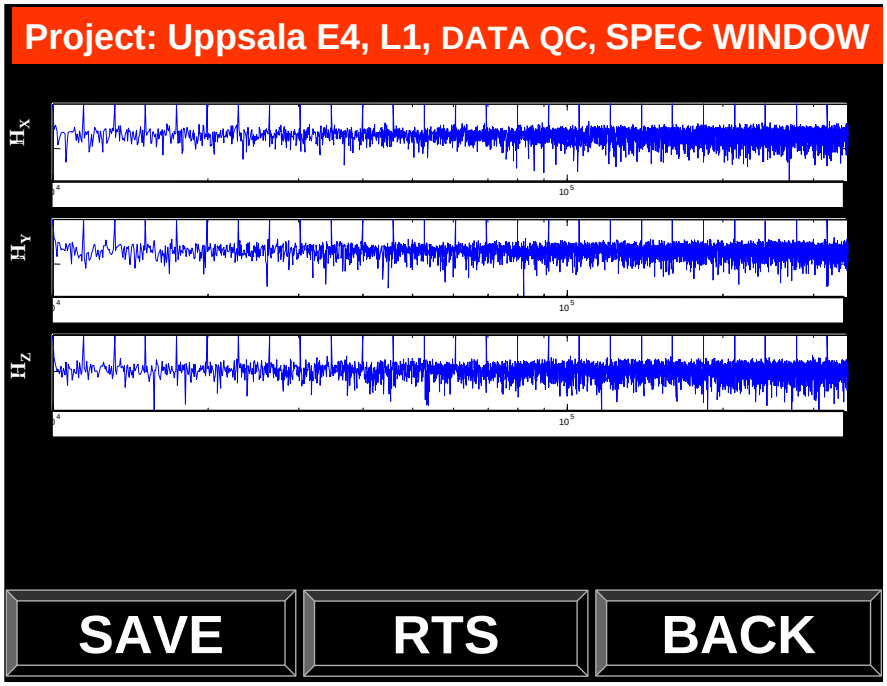

Figure 5.14

Performing data acquisition: After the preliminary QC and DAQ parameter setting, the

system is ready for data acquisition. CT, DT and RMT are the DAQ modes that are described in the following.

CT mode: Using DAQ button in the CT mode leads to the window shown in figure 5.15. The GPS and tilt-meter status are shown in boxes with appropriate colors, and to the right the selected S/N and the latest number of selected transmitters are presented in a gray box. Pushing RUN initiates DAQ and switches the display to window shown in figure 5.16.

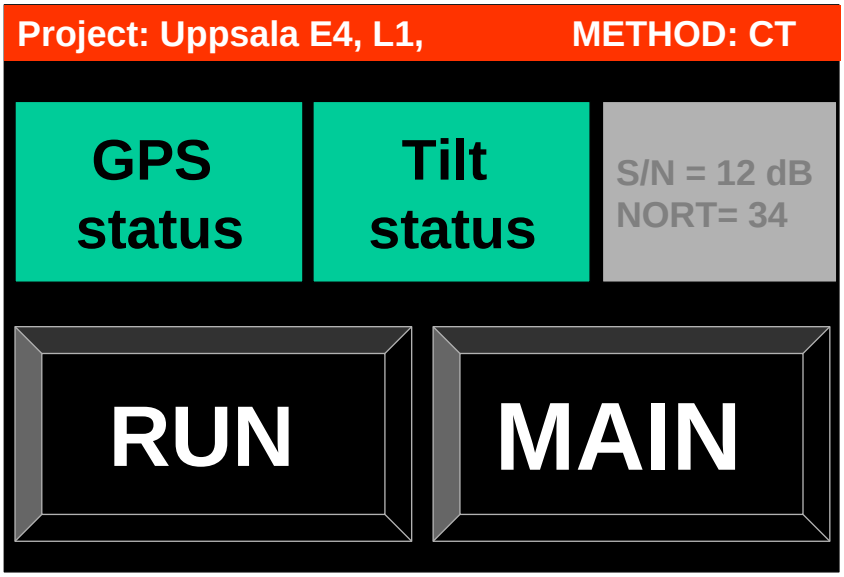

Figure 5.15

Since the measurements are continuous the operator can just halt the DAQ using STOP button. If there is something wrong with data acquisition the gray box will turn to red showing the proper message about the problem. The same is valid with GPS and Tilt-meter.

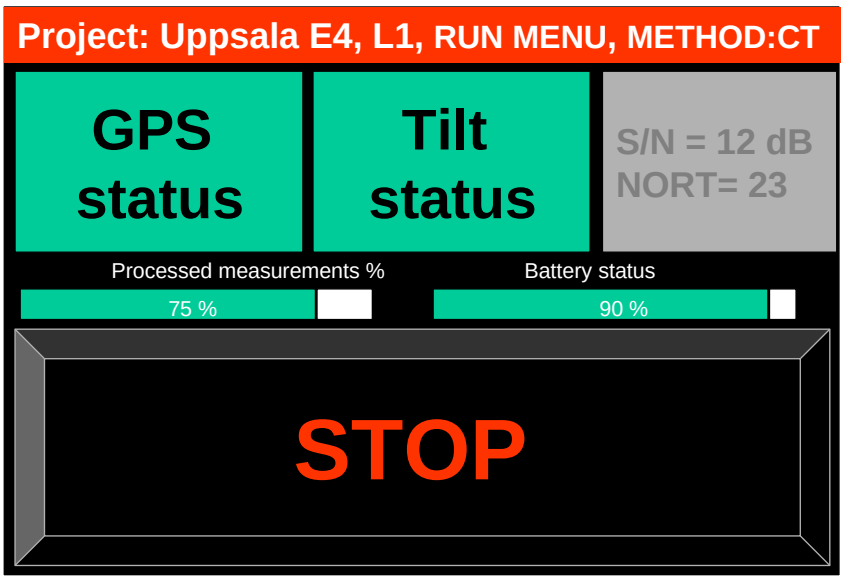

Figure 5.16

If the operator halts the DAQ for any reason the RUN MENU window turn to STOP MENU shown in figure 5.17. At this stage two toolbars show the status of processed measurements

and Battery. If the power is below 50% the bar turn to yellow and if below 25% turns to red. RUN leads to RUN MENU (figure 5.16), MAIN to main menu (figure 5.1), QC to QUALITY CONTROL (see figure 5.8). DISPLAY is a unique button that is explained under a separate section below.

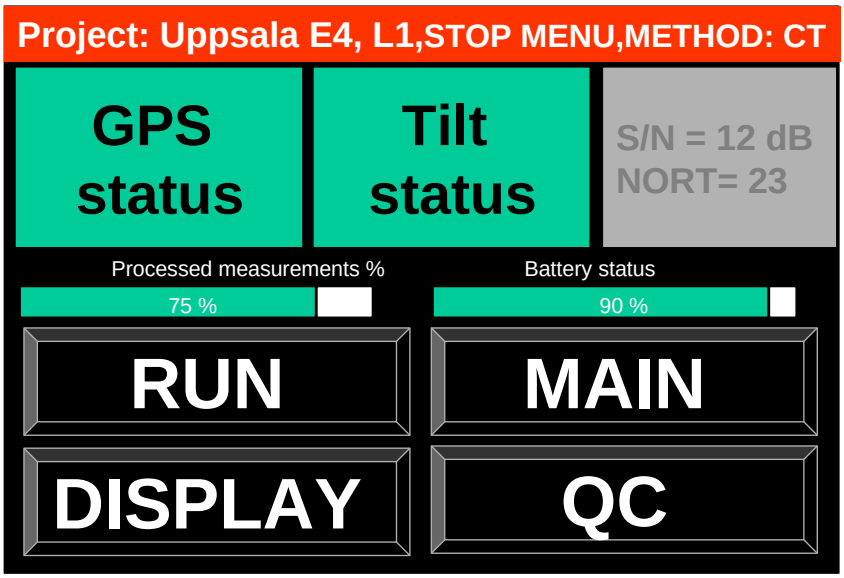

Figure 5.17

Display mode in CT: In order to show the measurements along a path, DISPLAY button is used. Figure 5.18 shows a typical layout of the display window in CT mode. In the MFR the EM transfer functions are estimated in 0 sub-bands with a one-octave bandwidth (see appendix A). The lowest mid-band frequency is ca 14 kHz and the highest is ca 320 kHz. Three frequencies from low, mid and high band are selected to display the data. This includes 20, 100, and 300 kHz. The real and imaginary parts of tipper components (A, B) are shown with different colors for each selected frequency.

Each single tipper component can be zoomed and checked (figure 5.19). The display will have scroll bars to navigate through the measurements. The horizontal axis is distance along the profile in meters extracted from the GPS information (The distance gone not the distance between the starting and present locations). The vertical axis shows either the real part or the imaginary part of the tipper components. The vertical scale is between –1 and +1. The BACK button takes the one step back to the previous window. Since in the CT mode a lot of data is collected at a very short period of time 2D visualization of the data is vital. Using 2D button a new window pops up that contains the 2D plots. Figure 5.20 is a sample of such. Like 1D plots the user is capable of zooming on a single tipper component.

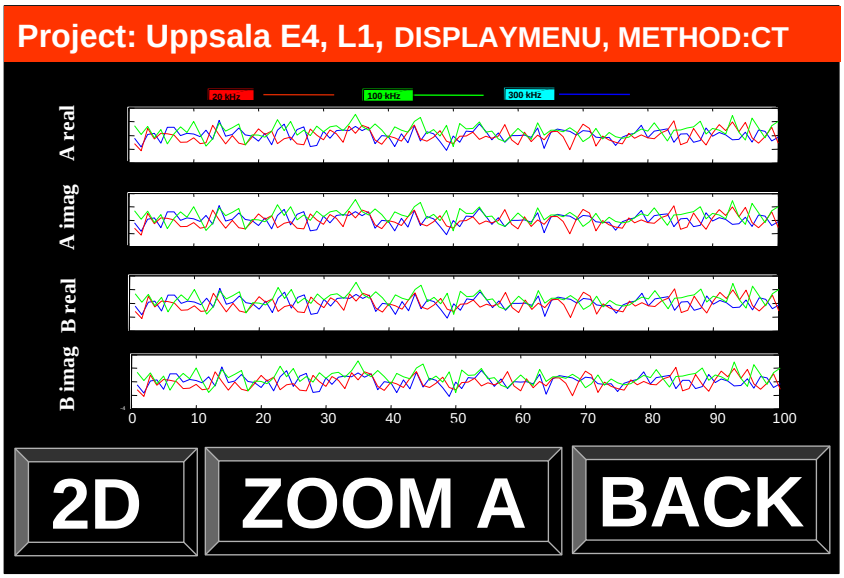

Figure 5.18

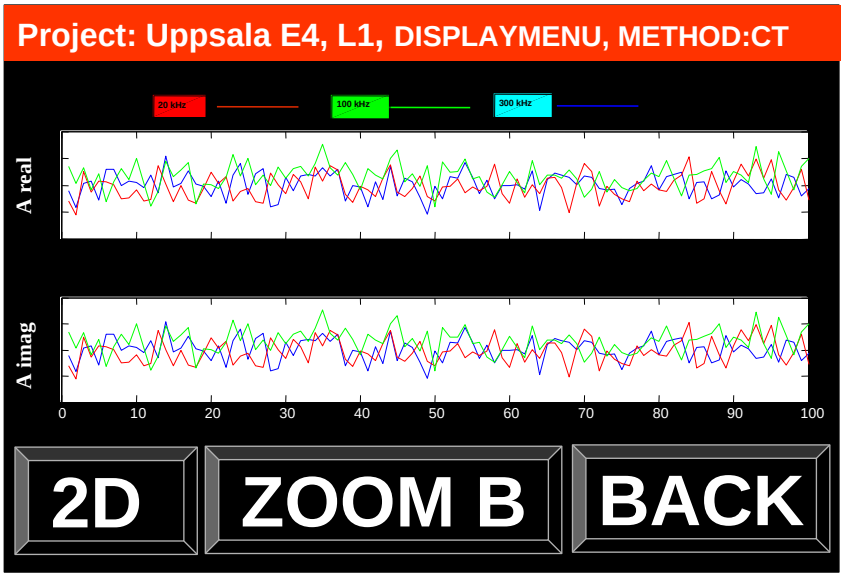

Figure 5.19

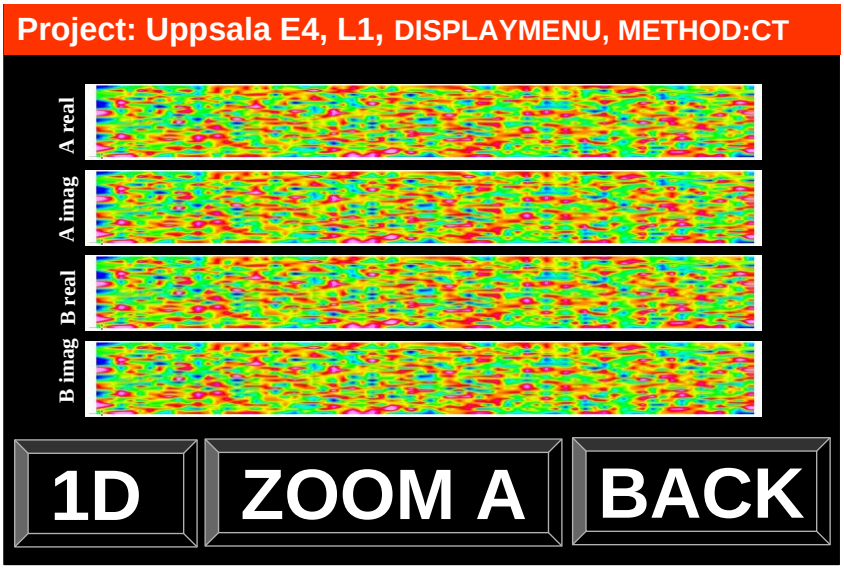

Figure 5.20

DT mode: Using DAQ button in the DT mode leads to the window shown in figure 5.21. The GPS and tilt-meter status are shown in boxes with appropriate colors, and to the right the selected S/N and the latest number of selected transmitters are presented in a gray box. In this window the QC button takes the operator to the window shown in figure 5.8. Pushing RUN initiates DAQ and switches the display to window shown in figure 5.22 that has exactly the same feature as in figure 5.16. The difference between CT and DT is the event after pushing the STOP button. If the user interrupts the measurements in DT mode the system turns to the window in figure 5.21 so that either QC or the MAIN menus can be accessed to check the problem. Note that after the maintained number of stacks reached, the estimated transfer functions are shown versus frequency (see figure 5.23). These are real and imaginary components of Tipper A and B. In figure 5.23 a picture from the EnviroMT system is shown in a real case. In the EnviroMT the transfer functions in 9 sub-bands, starting from14 kHz (mid-band frequency) and ending with 230 kHz, were estimated. In the MFR the upper limit will be extended to 330 kHz.

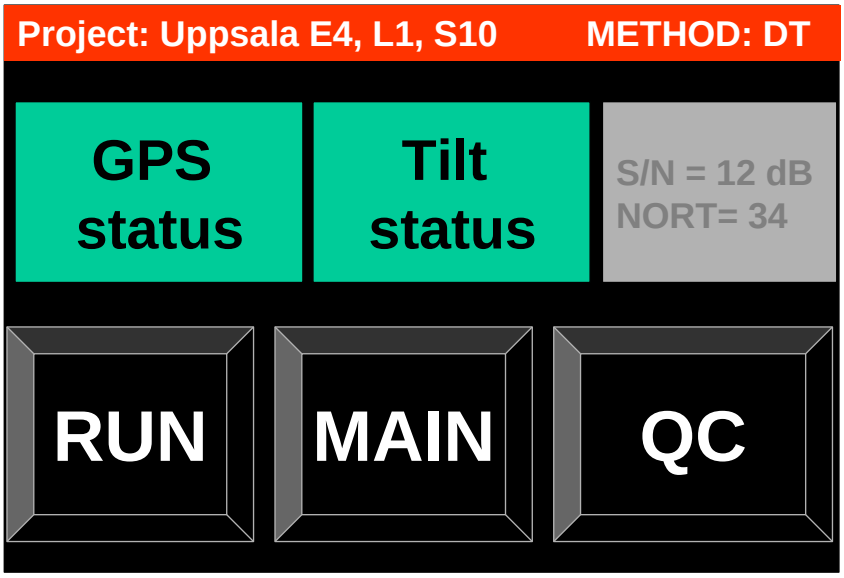

Figure 5.21

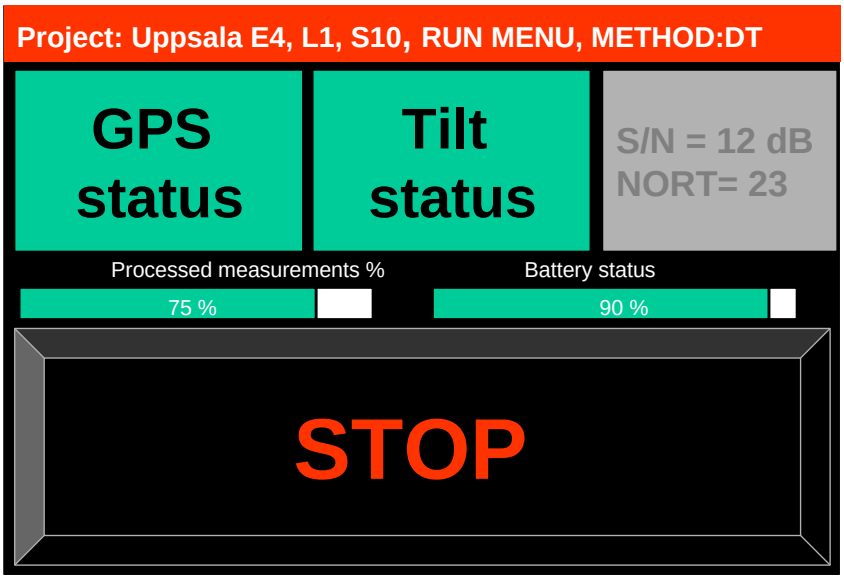

Figure 5.22

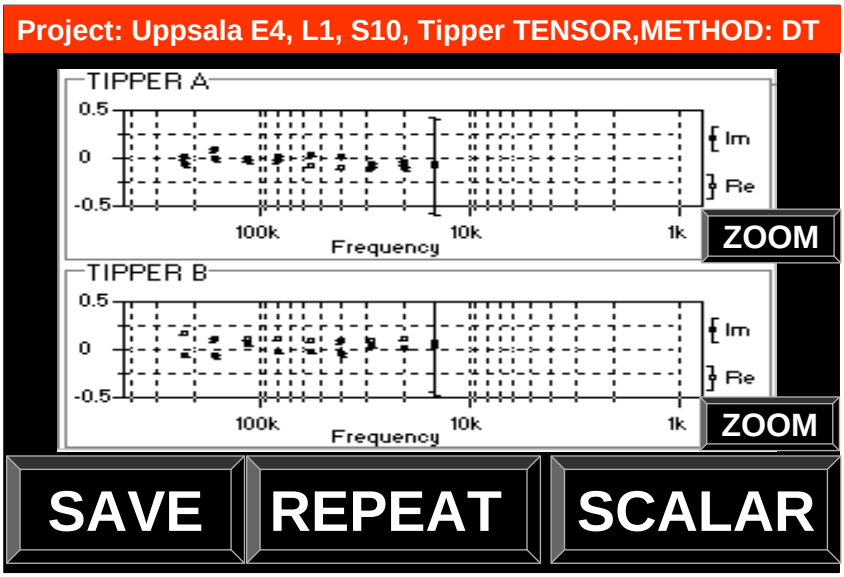

Figure 5.23

Using any of the ZOOM buttons in figure 5.23 helps the user to have a closer look to the selected component. Figure 5.24 is an example of zoom on the Tipper A. The FULL button steps back the display to figure 5.23. If the data are reasonable the user can save them by SAVE button otherwise the REPEAT steps back to figure 5.21 to either repeat of make a QC. The SAVE and REPEAT button lead to figure 5.21. The difference is that the info about the station number can change (SAVE) or stay the same (REPEAT).

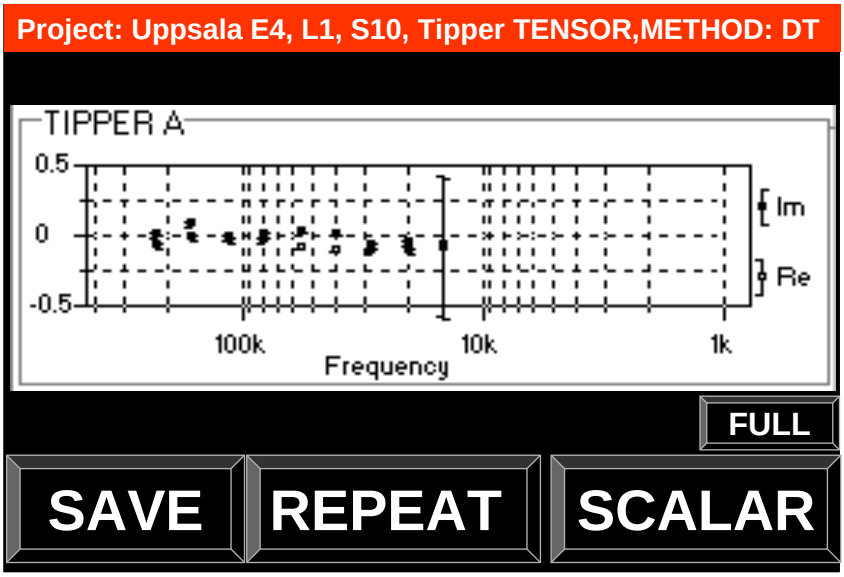

Figure 5.24

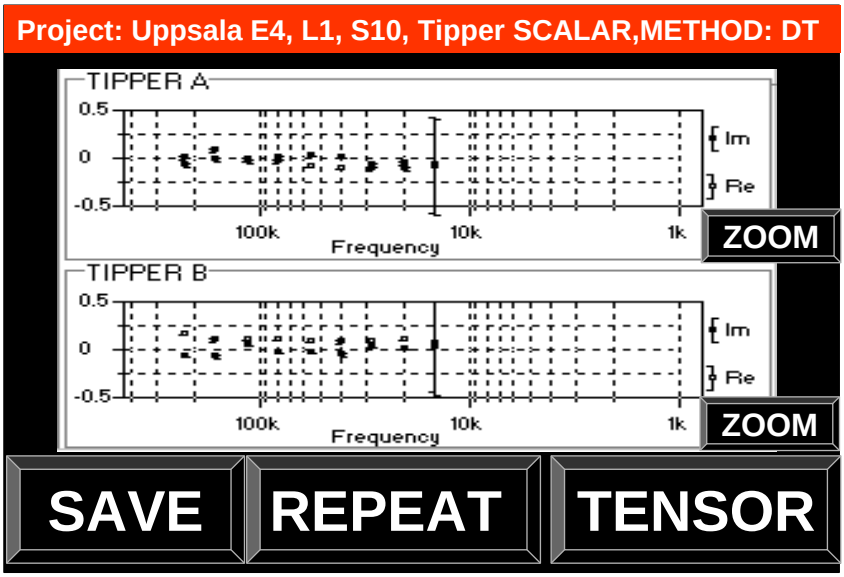

Figure 5.25

Since the data can be displayed as a tensor as well as scalar, use of SCALAR button in figure 23 leads to figure 5.25 were the scalar results are shown (Not in this example). Note that the info tab and also buttons are changed accordingly. The same is valid in the window shown in figure 24 (the resulting action is not shown as a figure).

RMT mode: Using DAQ button in the RMT mode leads to the window shown in figure 26. All the procedures in the DT mode are valid in the RMT mode (see figures 5.26 to 5.31). The main difference is where the results are presented. In the RMT mode four quantities are presented. Apparent resistivity, phase, Tipper A and Tipper B in the tensor mode are the default plots (figure 5.28). User can select either AP (Apparent resistivity-Phase) or Tipper plots in both tensor (figure 5.29 & 5.31) and scalar modes (figure 5.30).

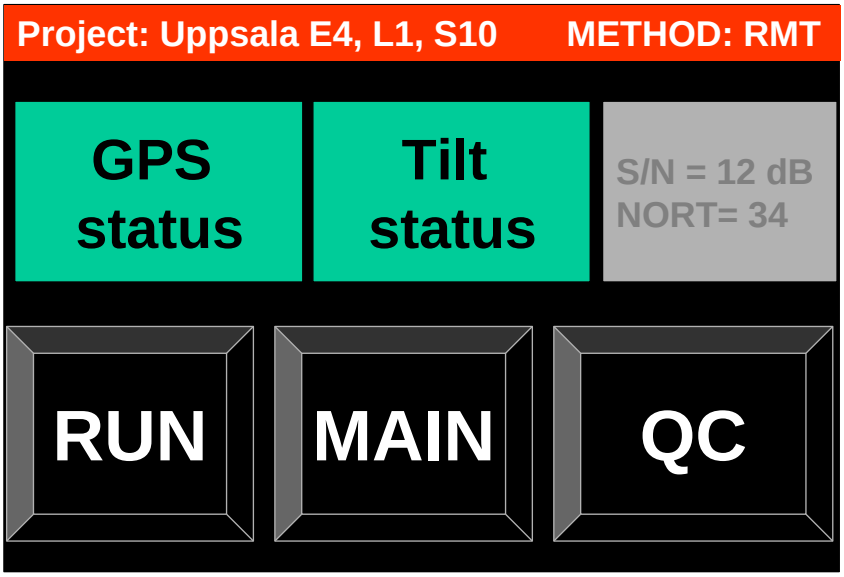

Figure 5.26

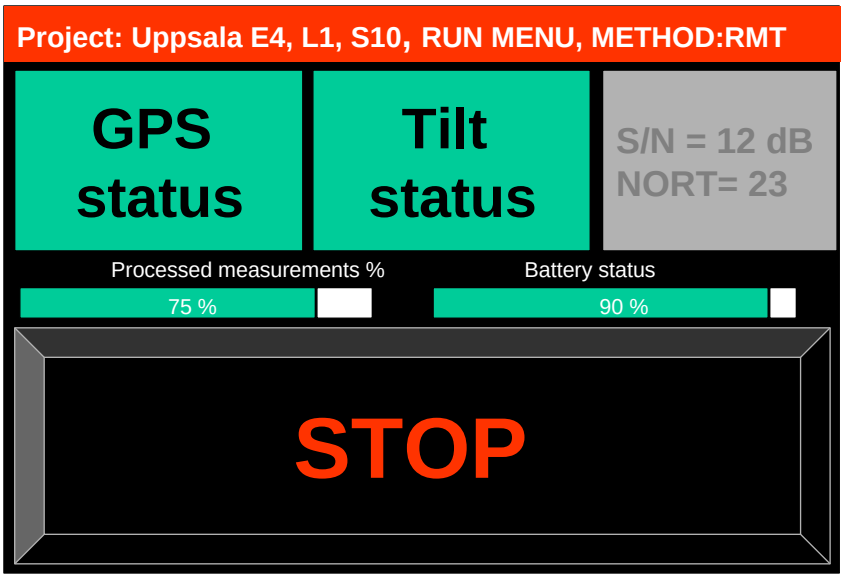

Figure 5.27

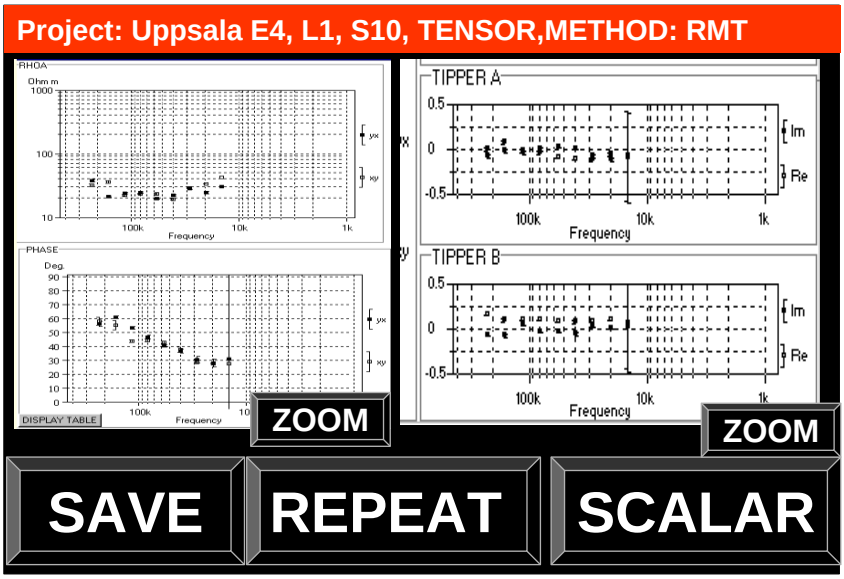

Figure 5.28

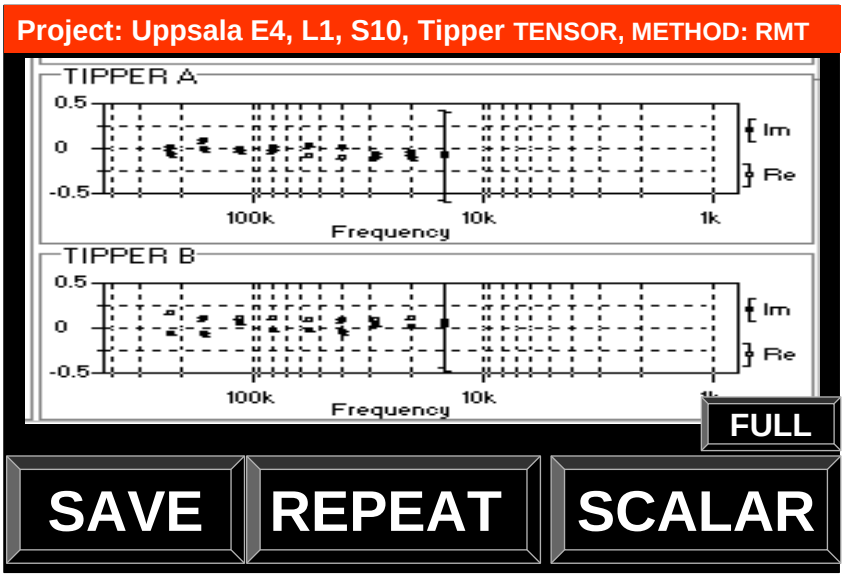

Figure 5.29

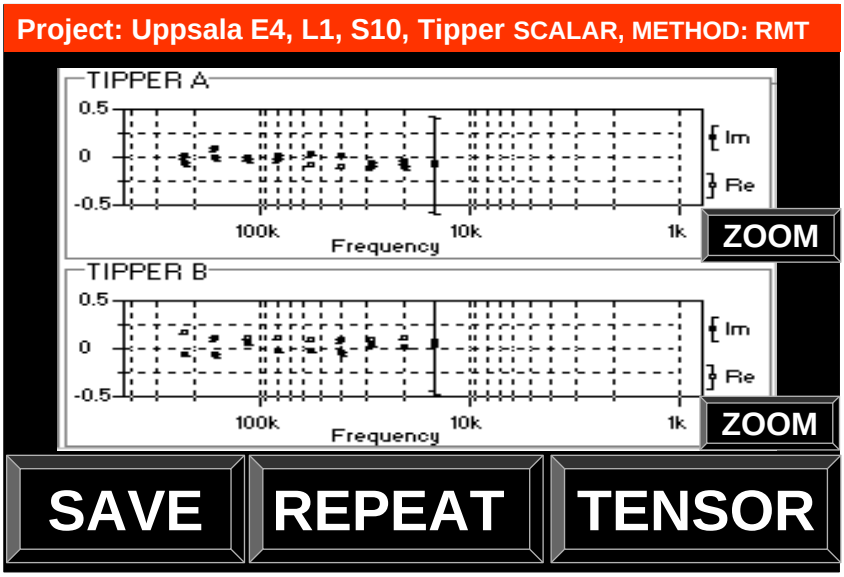

Figure 5.30

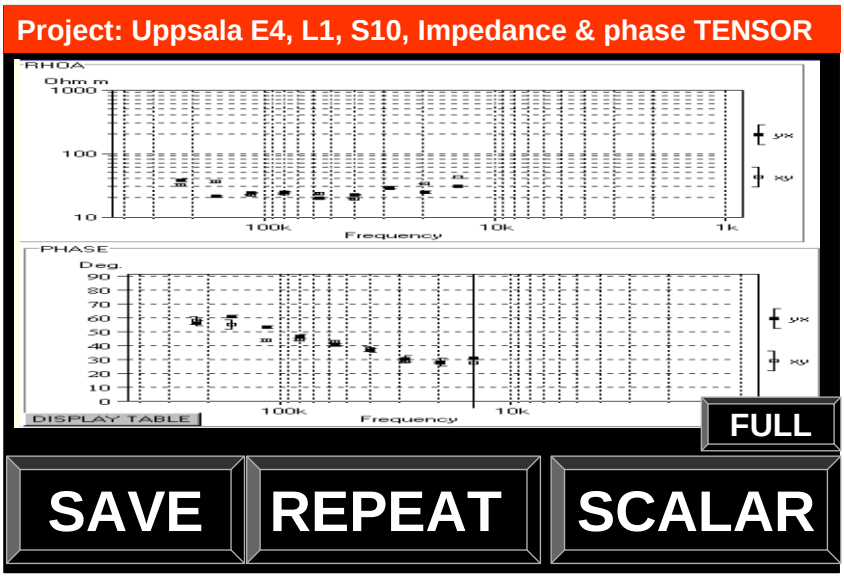

Figure 5.31

5.3 **Final GUI of MFR**

It was chosen to use the libraries GTK+ and glade to build the user interface because this nicely integrates with the rest of the code that is written in C. The GUI runs on a screen resolution of 800x600 pixels in full-screen mode. GTK+ allows fully scalable user-interfaces that make optimal use of the available screen size by, for example, growing buttons to use all the available space. It was decided to create the GUI layout with the graphical GUI designer that comes with Glade. The layout is stored as a XML file which is parsed at runtime and converted into data structures for the widgets. Since there is no keyboard available on the instrument but text entry is necessary in some dialogs a software solution had to be found. The package \matchbox-keyboard" provides an on-screen keyboard that was embedded 1 seamlessly into the GUI. It can be enabled in all configuration dialogs that require text entry - the rest of the user interface shrinks accordingly.

5.3.1 **Workflow (GUI Dialogs)**

The application is started by running the application controller. A window pops up full screen that offers a selector for the project root directory and the buttons “Preferences”, “Quality Control”, “Data Acquisition”, “Utilities” and “Quit”. Each button leads to a new full-screen window for the respective actions. When controller is first started in an empty directory, the buttons “Quality Control” and “Data Acquisition” are inactive. When clicking “Preferences” the user will be prompted to enter some project information, such as a project name. Then he will come to the “Preferences” which contains buttons that lead to separate sub-dialogs for Data Acquisition, Processing and Expert parameters. After the desired settings are made, he comes back to the main screen, where the “Quality Control” Button is clicked to make a test measurement. If the results are not acceptable, the user will go back to “Preferences” and adjust settings until he is happy with the results. To start collecting actual data, “Data Acquisition” is clicked. The Line Number and Station Number can be set before the measurement is started. In both Data Acquisition and Quality Control the status of various components (GPS, Compass, ADC, mfr1st and System) is available by clicking the respective buttons in the status list. In Figure 5.33 a graph of all dialogs with the possible transitions is shown.
Detailed specifications were given in the previous section. Actual screen shots of the finished software are shown in this section instead. If this document is printed on A4 paper, the screenshots will have approximately the same size that they would on the actual display (7 inch, 16:10 aspect ratio). See Figures 5.34 to 5.47.

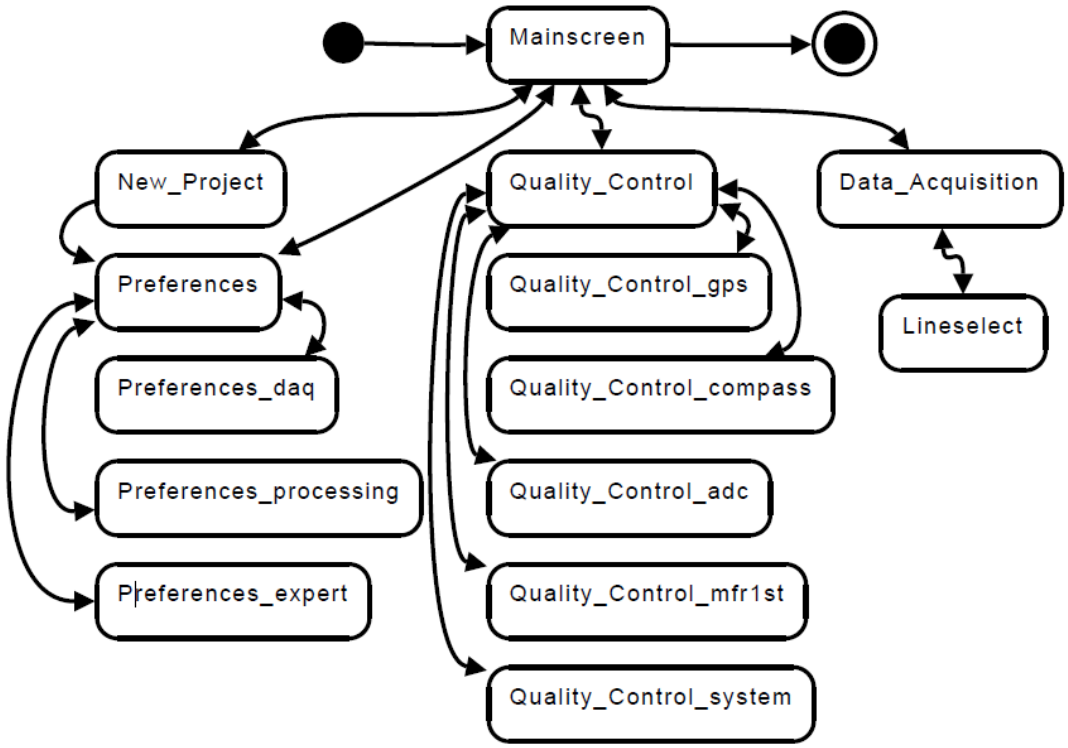

Figure 5.33

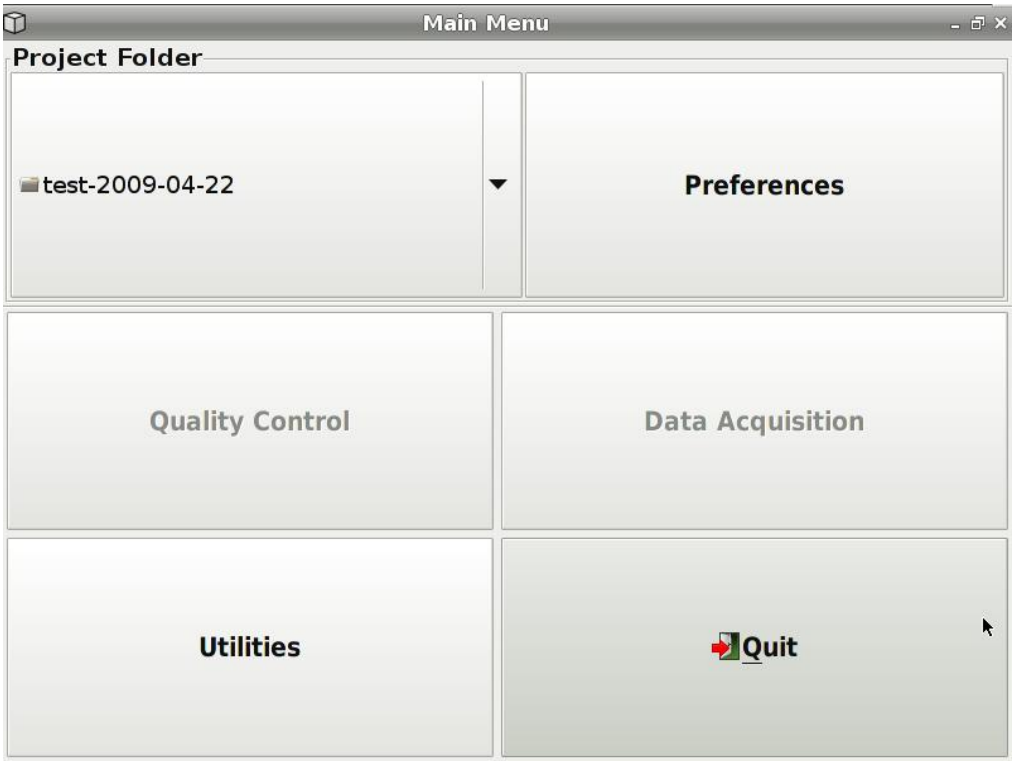

Figure 5.34

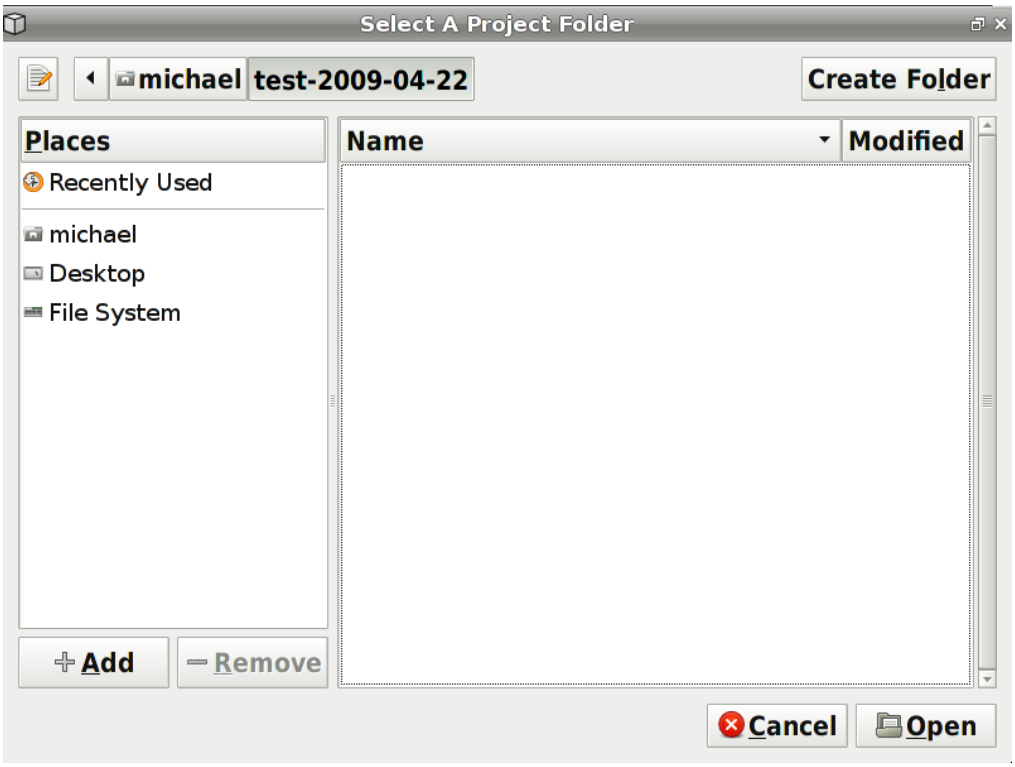

Figure 5.35

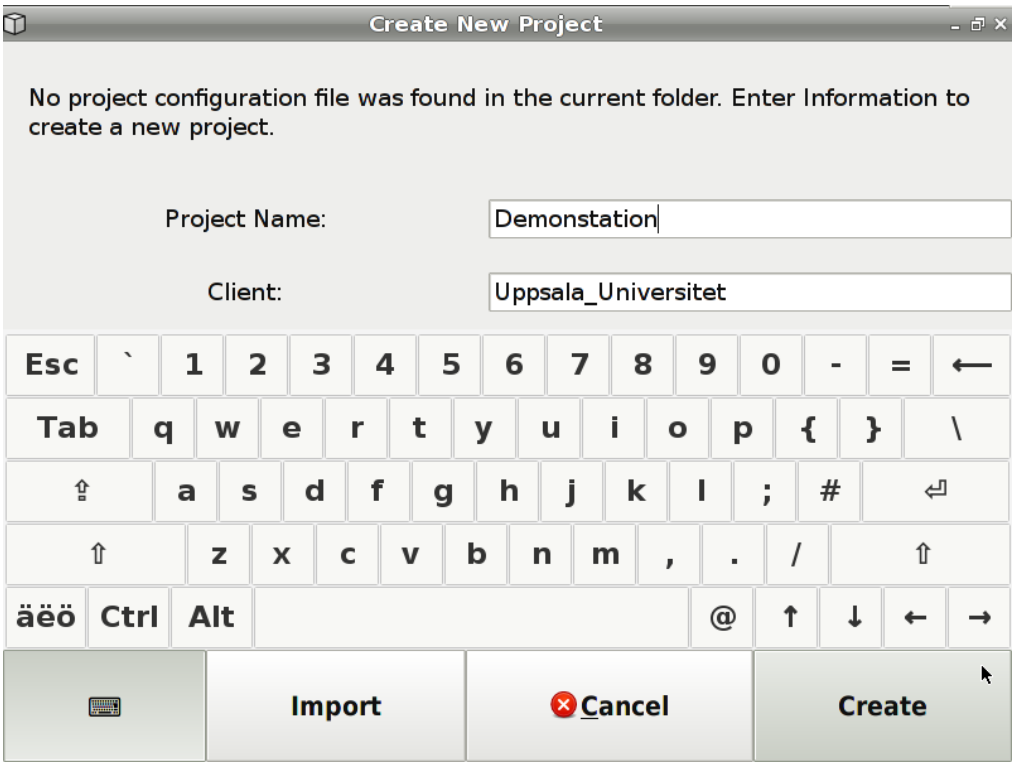

Figure 5.36

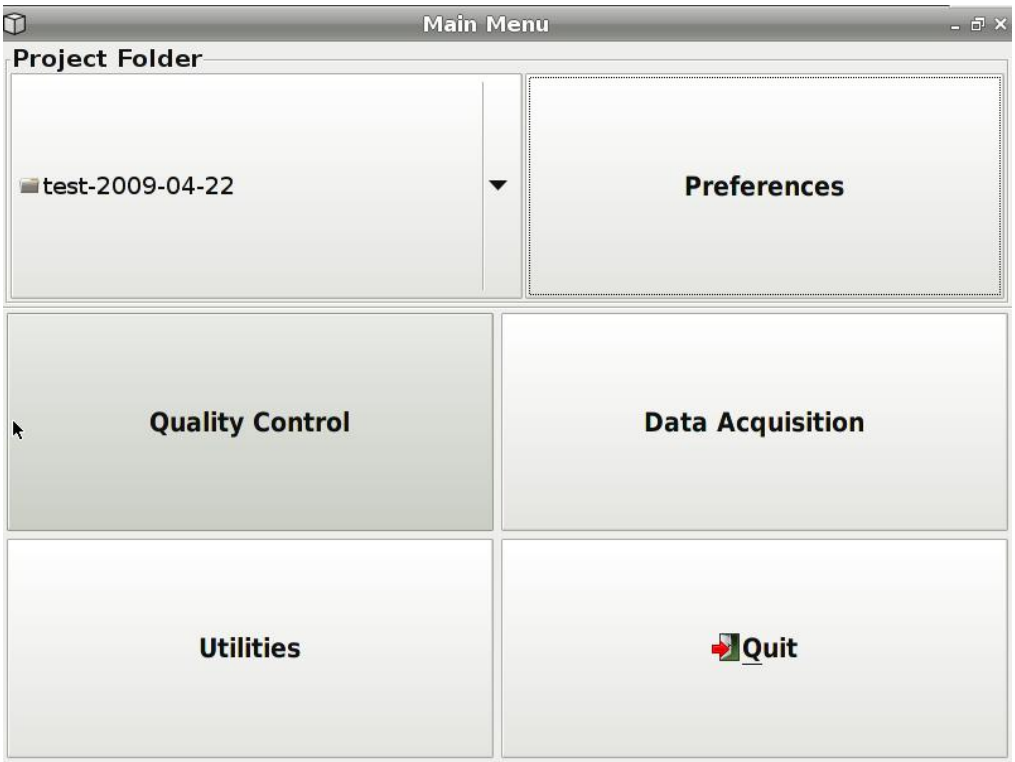

Figure 5.37

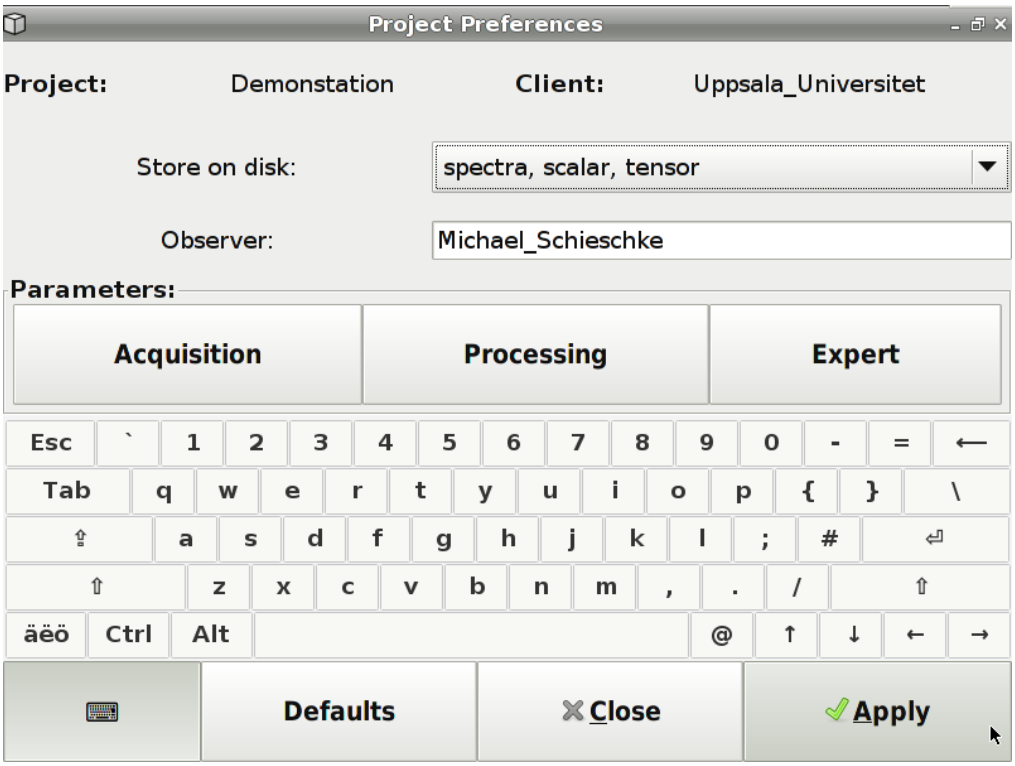

Figure 5.38

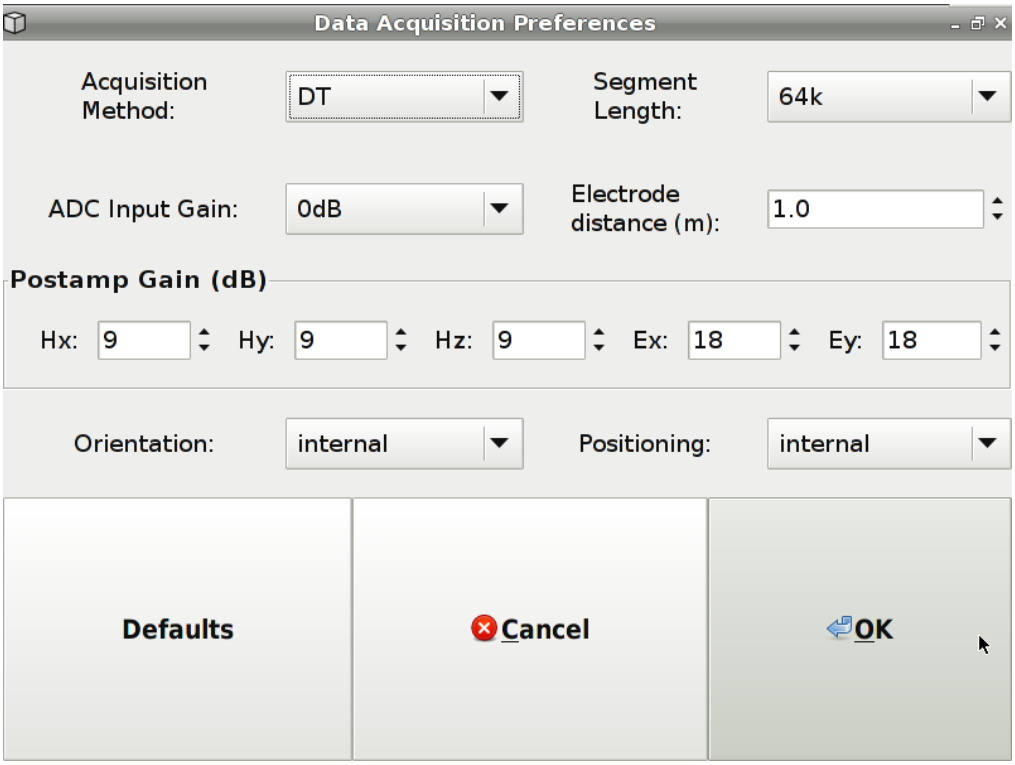

Figure 5.39

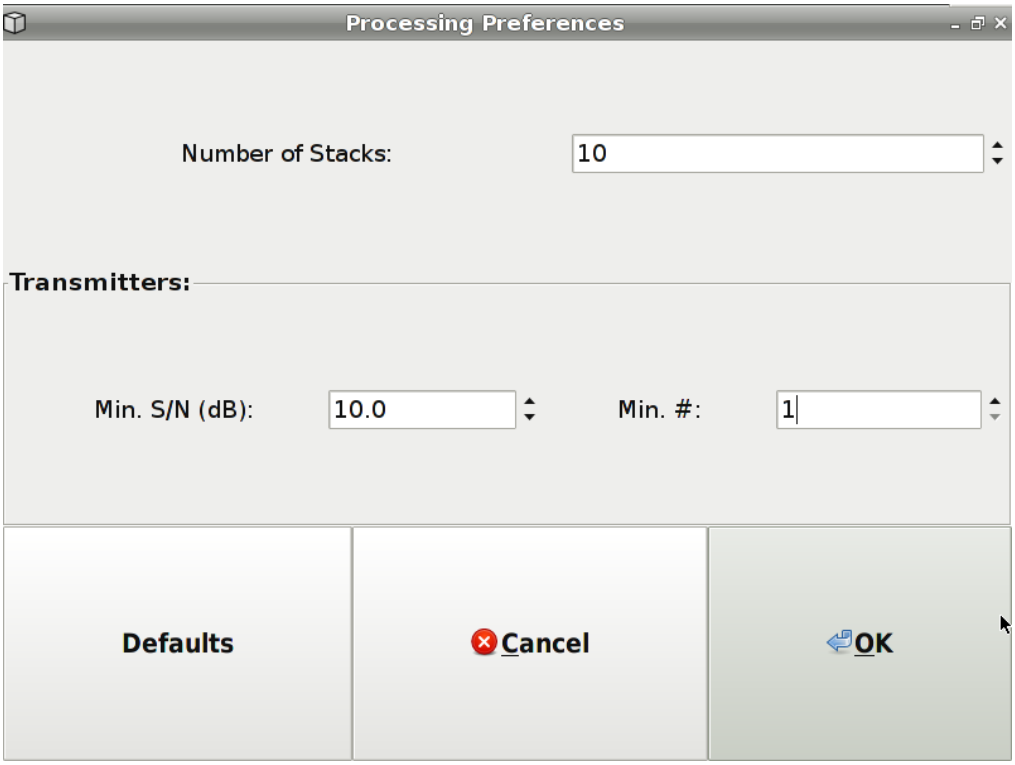

Figure 5.40

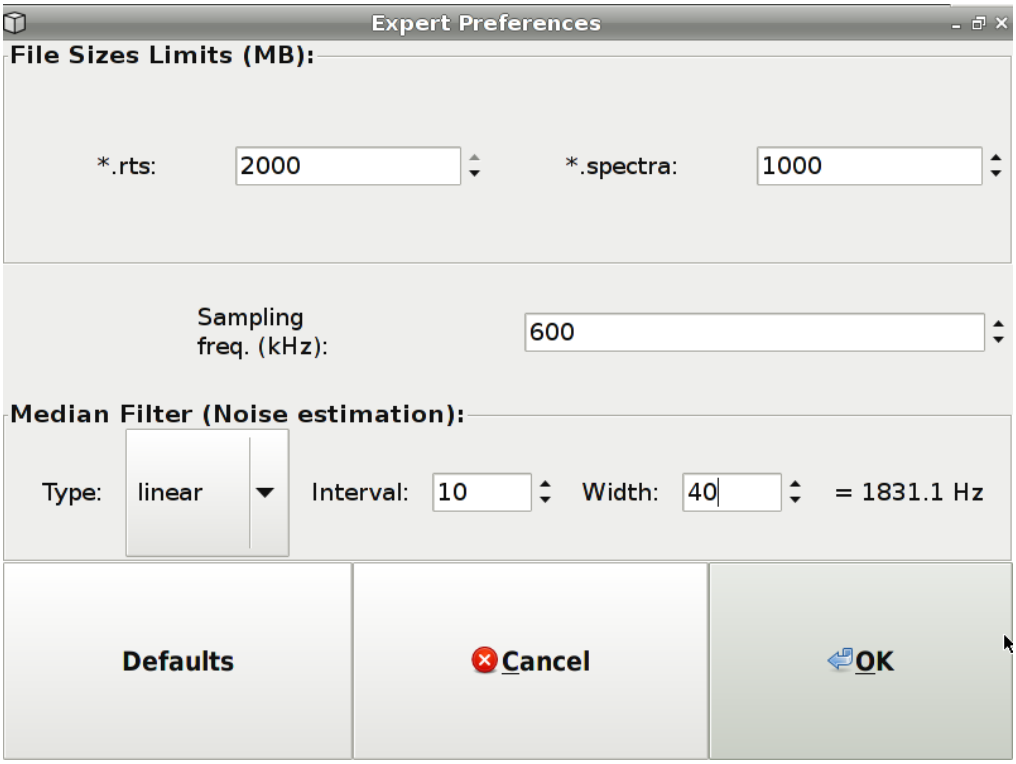

Figure 5.41

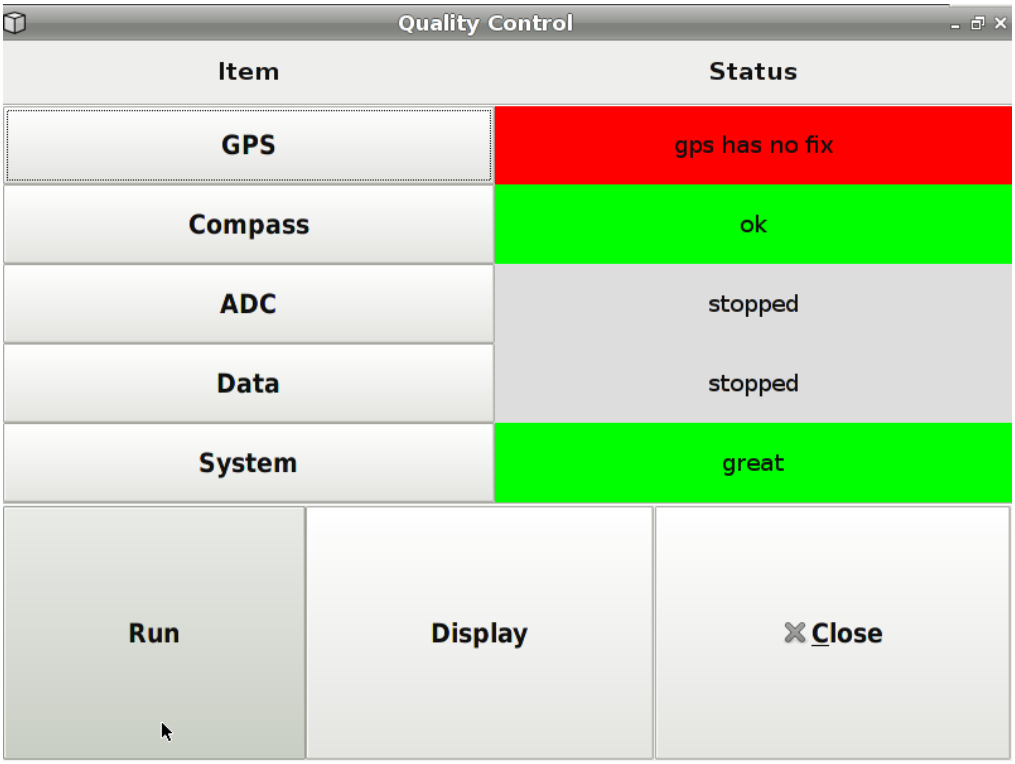

Figure 5.42

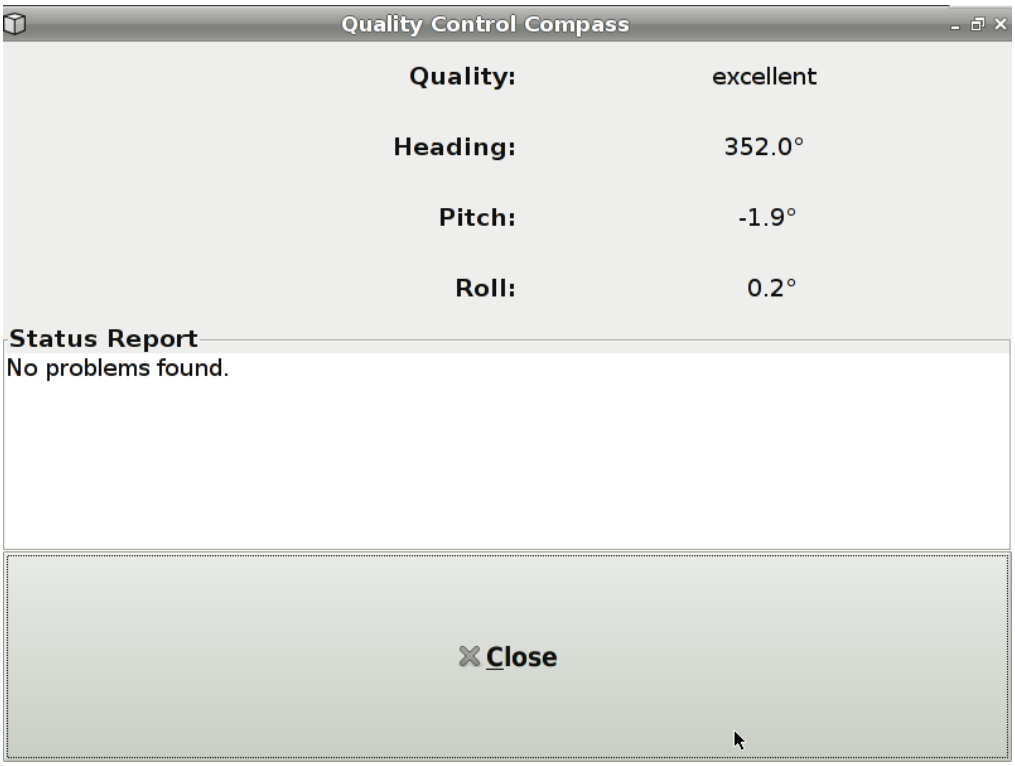

Figure 5.43

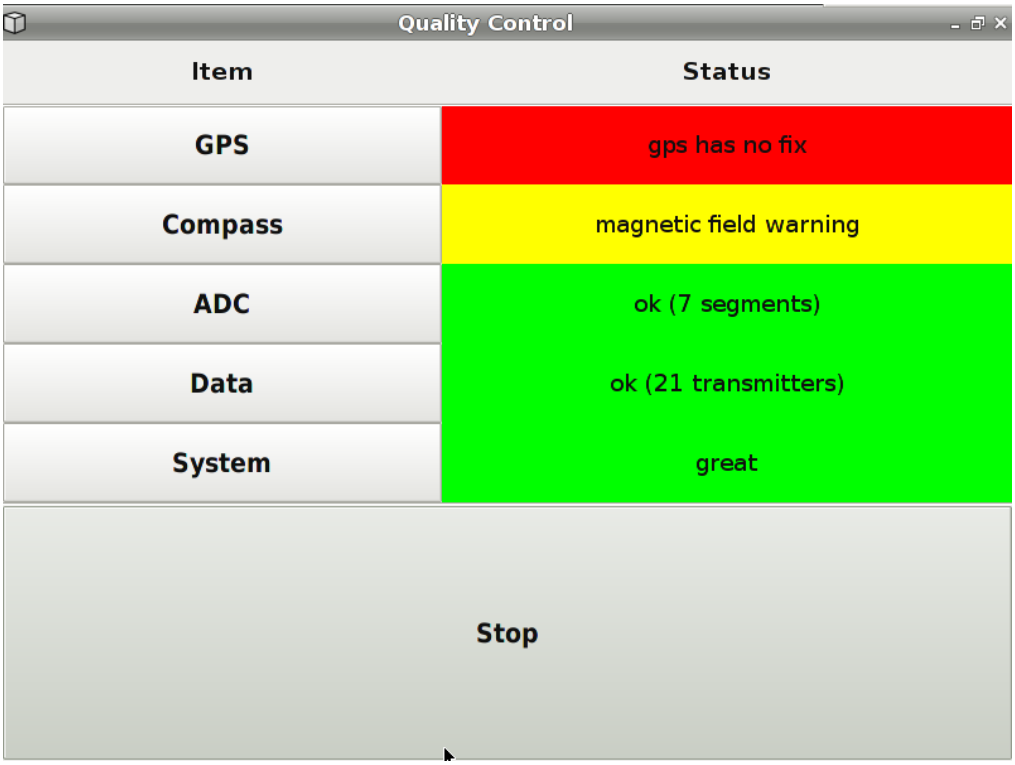

Figure 5.44

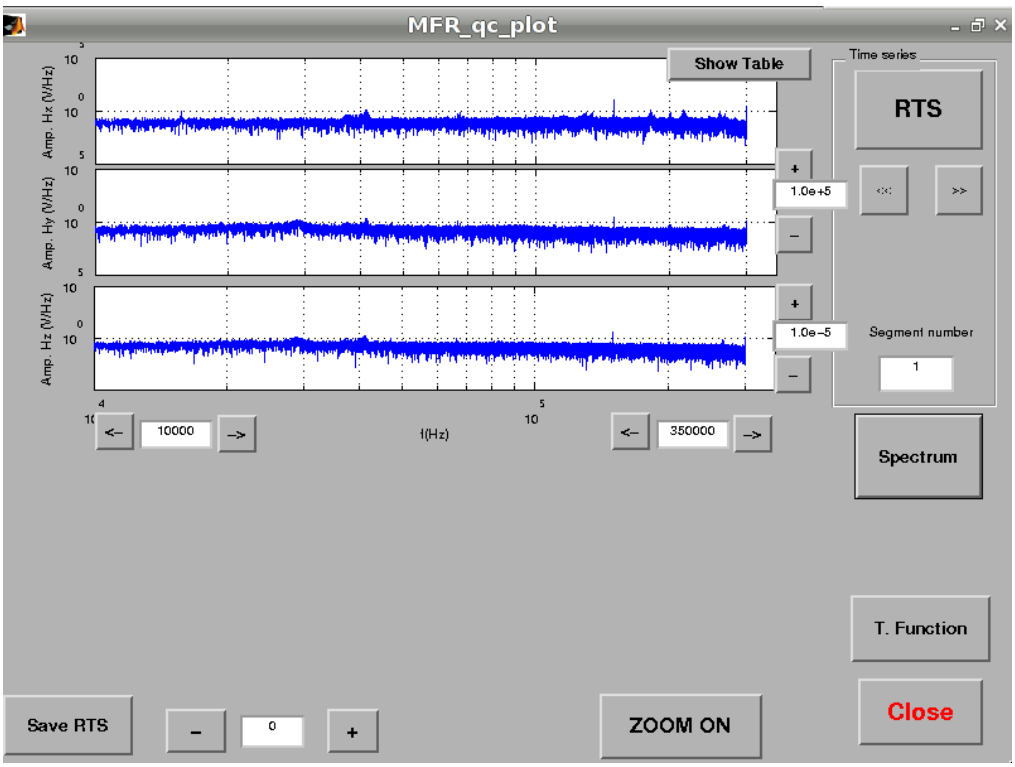

Figure 5.45

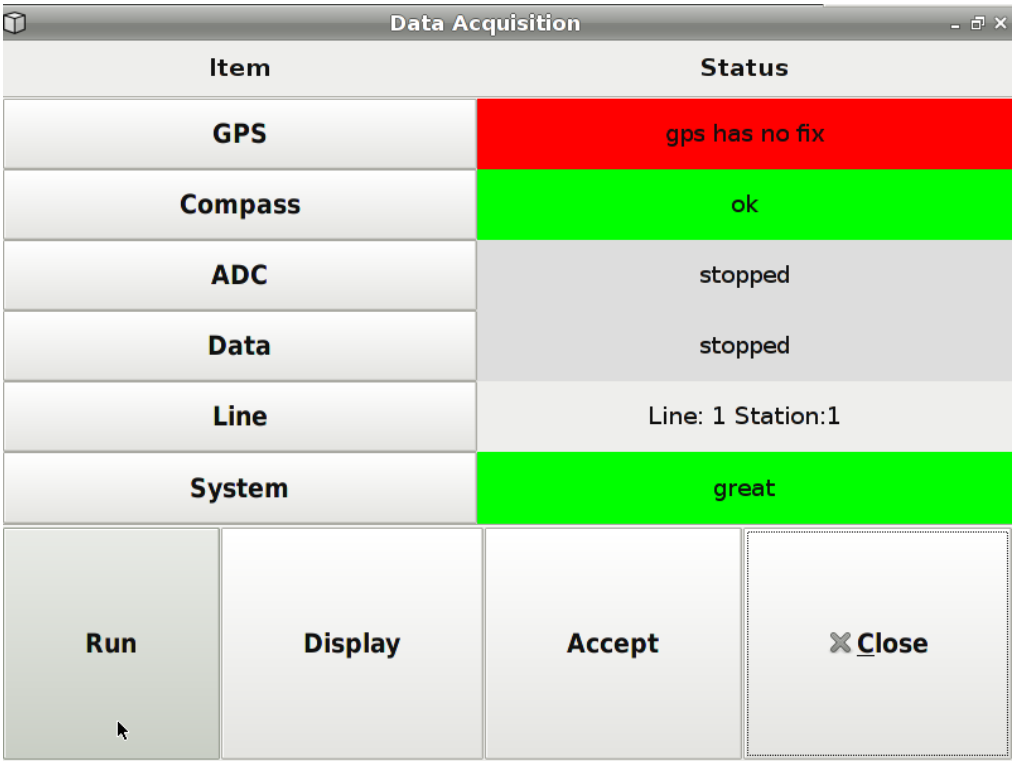

Figure 5.46

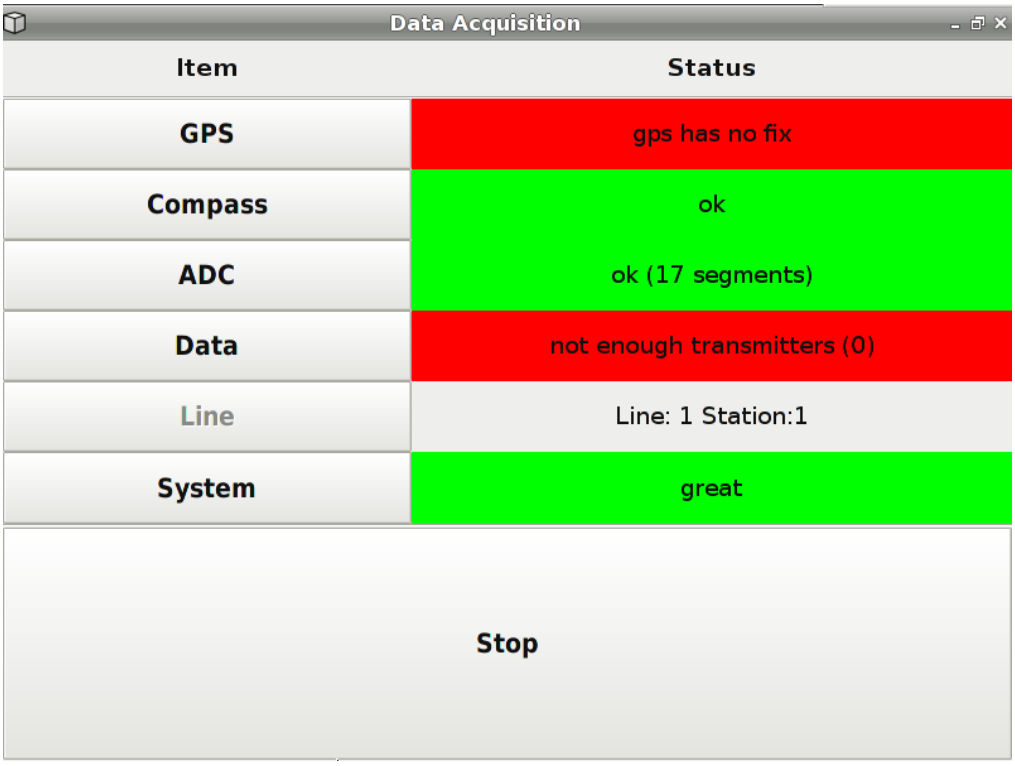

Figure 5.47

The field-data-plotting software (Figure 5.45) is written in MATLAB programming language by Mehrdad Bastani (SGU). The program is then complied as a MATLAB executable file that can be controlled by the GUI software.

CALIBRATION OF MFR

Calibration of MFR

6.1 Introduction

This report is about a calibration program written in MATLAB for a radio magnetotelluric (RMT) instrument, called Multi Frequency Receiver (MFR), which is used for measurements of the electromagnetic field components in the frequency range of 10-350kHz. The instrument is a further development of the EnviroMT instrument (Bastani, 2001) that was developed by Uppsala University. Calibration is necessary for any measuring instrument to remove the effect of the system response from the raw data. This program estimates the system response of the MFR instrument. Using the estimated system response function this effect can be eliminated or at least reduced.
In this report first a short measurement field layout description is given, and then the fundamentals behind the estimation of the response function are discussed. The functions in the calibration program are presented in detail and the results of a system response function, using a real data set, are shown.

6.2 Field layout

The MFR instrument consists of three magnetic coils (each 15 cm long) placed orthogonal to each other, the two horizontal are parallel to the electric sensors and the third is vertical in the middle (Figure 6.1). There are also five electrodes, one used for grounding, and the other four measure the electric field in two horizontal directions, usually in east-west and north-south. The pairs of electrodes with equal separation are contacted to the ground in directions parallel to the two horizontal magnetic field sensors. Both sets of sensors are connected to an amplifier/filter box that is attached to the main processing unit. The analogue signal is then digitized by an A/D-converter and processed.

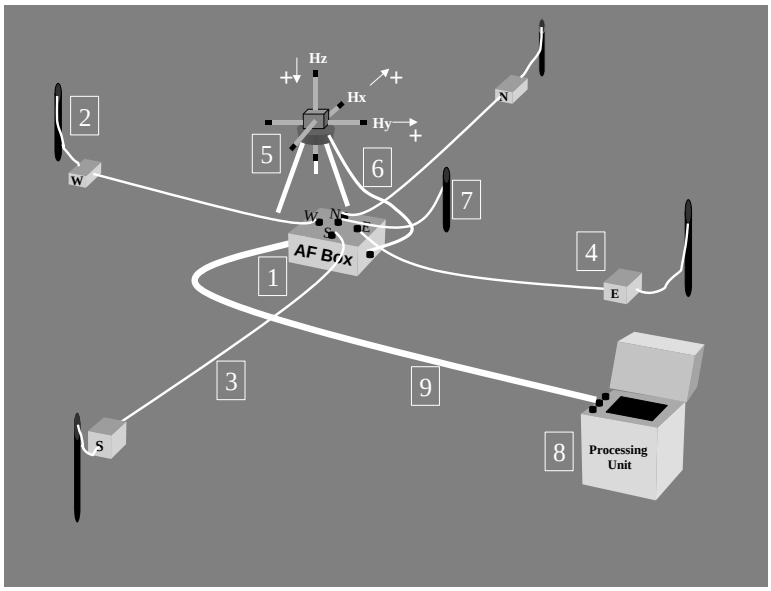

Figure 6.1 : Schematic of the RMT measurements field layout. (From Bastani, 2001).

6.3 **Calibration**

Before final estimation of the magneto-telluric transfer function, a correction of the data has to be done. The actual measured data is influenced (modified) by the instrument setup. The output data are linearly related to the input data by the system response.

The calibration process can be defined as removing the effect of the system response that is convolved with the signal (in the time domain). In the frequency domain this is equivalent to a multiplication. This can be written as an equation:

$$\widetilde{g(t) * s(t)} = \widetilde{r(t)} = G(f) \times S(f)$$

where r(t), g(t) and s(t) are the measured signal, real signal and system response functions in the time domain, respectively. * stands for convolution operator and tilde is the Fourier transformation. G(*f*) and S(*f*) are the Fourier transforms of g(t) and s(t). This means that in the Fourier domain by a simple division of measured signal by the system response we can calibrate our measurement to get the real signal.

6.3.1 **Magnetic sensor calibration**

Figure 6.2 displays the circuitry layout used during the calibration of the magnetic sensors. A signal source generates a field measured by the sensor being calibrated and recorded simultaneously at the reference channel. A sweep signal containing sinusoids with logarithmically distributed frequencies is generated as the input signal to the reference channel and registered as the voltage that is measured across a known resistor R. The current flows in the Helmholtz coils and generates a magnetic field at the center of the coil and is measured by the senor being calibrated (Figure 6.3). The geometry of the coils is well determined and the magnetic field is extremely stable and homogeneous at the center.

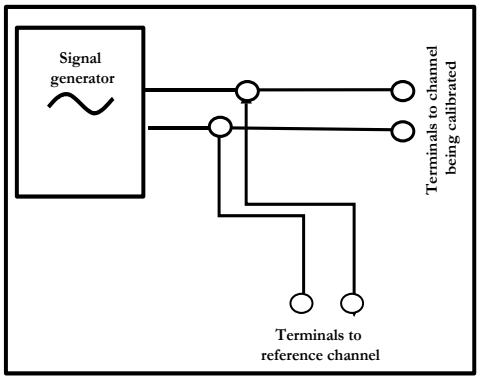

Figure 6.2. Schematics of the calibration circuitry. (From Bastani, 2001).

Our experience shows that because of the geometry and construction of the magnetic sensor used in the MFR system the induced magnetic field in the sensor at the center induces magnetic field in the other two directions. This effect is known as "cross-talk" and has a considerable effect on the estimation of the RMT transfer functions. Therefore, the signals in all the magnetic channels are measured at the same time to make an estimate of the cross-talk as well. The magnetic field data are saved in an output matrix **O.** The measured voltage across the resistor at the reference channel is stored in matrix **I**. These two vectors are related to each other via the calibration matrix, **D** as **O = DI**. The matrices can be written in a more extended form for the target frequency *f* as

$$\mathbf{O}=\begin{bmatrix} V_1^1(f) & V_1^2(f) & V_1^3(f) \\ V_2^1(f) & V_2^2(f) & V_2^3(f) \\ V_3^1(f) & V_3^2(f) & V_3^3(f) \end{bmatrix} = \begin{bmatrix} D_{16}^1(f) & D_{16}^2(f) & D_{16}^3(f) \\ D_{26}^1(f) & D_{26}^2(f) & D_{26}^3(f) \\ D_{36}^1(f) & D_{36}^2(f) & D_{36}^3(f) \end{bmatrix} \begin{bmatrix} V_6^1(f) & 0 & 0 \\ 0 & V_6^2(f) & 0 \\ 0 & 0 & V_6^3(f) \end{bmatrix} \tag{1}$$

where V_j^i is the measured voltage at channel *j* while calibrating channel *i*. D_{j6}^i is the calibration transfer value for the channel *j* while calibration channel *I* when using channel 6 as the reference. The matrices are all complex and have a real and imaginary part at each target frequency. The reference signal is always measured at channel number 6. In practice the calibration has to be carried out for one channel at a time. For example the first column of matrix D contains the calibration values for (H_x)that are estimated as the following

$$\begin{aligned} D_{16}^1(f) &= \frac{V_1^1(f)}{V_6^1(f)} = \frac{V_6^1(f)^* V_1^1(f)}{V_6^1(f)^* V_6^1(f)}; \\ D_{26}^1(f) &= \frac{V_2^1(f)}{V_6^1(f)} = \frac{V_6^1(f)^* V_2^1(f)}{V_6^1(f)^* V_6^1(f)}; \\ D_{36}^1(f) &= \frac{V_3^1(f)}{V_6^1(f)} = \frac{V_6^1(f)^* V_{31}^1(f)}{V_6^1(f)^* V_6^1(f)} \end{aligned} \tag{2}$$

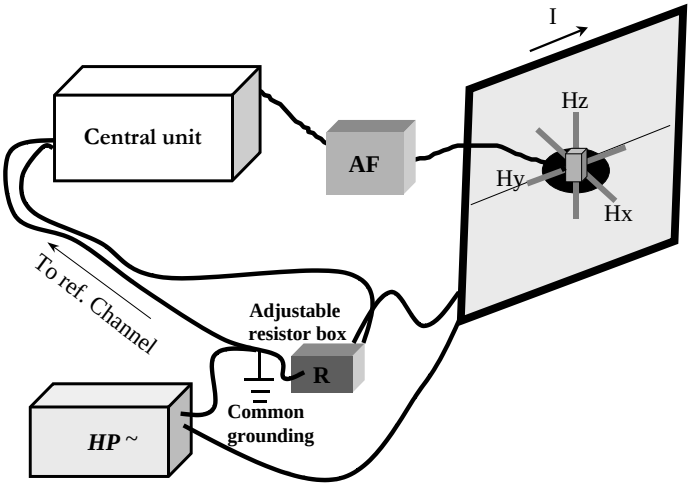

Figure 6.3. Schematic of calibration setup for the MFR magnetic sensor. (From Bastani, 2001).

The measured data in the field are calibrated prior to the estimation of the RMT transfer functions using matrix **D**. For example equation below shows the relationship between the measured field components and RMT transfer function elements, namely impedance tensor.

$$E_x(f) = Z_{xx}(f) * H_x(f) + Z_{yy}(f) * H_y(f) \quad (3)$$

For the simplest case where there is no cross-talk **D** matrix is diagonal. For the simplicity of our equations the diagonal elements of D are replaced by T_1, T_2 and T_3 that represent the calibration values for H_x, H_y and H_z. The field components in (3) are then replaced by their corresponding measured voltages and calibration values as

$$E_x(f) = V_4(f)/T_4(f);\ H_x(f) = V_1(f)/T_1(f);\ H_y(f) = V_2(f)/T_2(f); \quad (4)$$

T_is are the transfer coefficients (system response) between the "real field" to the "voltage" we register at that channel in question. These coefficients are composed of two parts. The first one that is a real number and independent of frequency, we call it "form factor" *F*, and the other one is a complex number, $T_{i6}(f)$, that is frequency dependent. $V_i(f)$ is the Fourier transformation of measured signal at channel i, and H(*f*) is the Fourier transformation of the real magnetic field signal.
With

$$T_i = \frac{V_i(f)}{H(f)} = \frac{T_{i6}(f)R}{G};\ i=1,2,3 \quad (5)$$

we find the form factor equal to R/G for the magnetic channel. The current in the Helmhotlz coil can be found by

$$V_6(f) = R \times I(f) \quad (6)$$

The voltage is measured across the resistor R and is registered at the reference channel. The measured current generates a magnetic field at the centre of the loop that is proportional to the current via the G factor. It is possible to use a special geometry for the Helmholtz coil. Here we show three possibilities. The magnetic field at the center of a circular loop with radius a is given by:

$$H = I/2a = IG_c \quad (7)$$

and for a rectangular loop with width of 2a and length of 2b H is:

$$H = \cos[\tan^{-1}(b/a)]/a + \cos[\tan^{-1}(a/b)]/b * I = IG_r \quad (8)$$

and for a square loop with a = b is

$$H = \sqrt{2} * I/(\pi * b) = IG_s \quad (9)$$

where H is the magnetic field, I is the current, and G_i is the geometrical factor determined by the coil geometry.

We substitute the magnetic field in (5) by IG and get

$$T_i(f)=\frac{V_i(f)}{H(f)}=\frac{V_i(f)}{I(f)G};\ i=1,2,3 \tag{10}$$

Substituting for I(*f*) from (6) into (10) and introducing $T_{i6}= V_i/V_6$ we get

$$T_i(f)=\frac{V_i(f)}{\frac{V_6(f)}{R}G}=T_{i6}\frac{R}{G}=FT_{i6};\ i=1,2,3 \tag{11}$$

F has the units of ohm-m. In case of i=1 the magnetic field $H_x(f)$ in (4) has a unit of volts/(ohm-m)=A/m that is correct.
The MFR calibration data for each channel are calculated as columns of complex matrix **D** and stored for each frequency. The measured data are then calibrated using the inverse of matrix **D**. Assume that the measured magnetic field components at the target frequency f_t are $V_x(f_t)$, $V_y(f_t)$, and $V_z(f_t)$ are stored in complex vector $\mathbf{V}(f_t)$. The complex vector $\mathbf{H}(f_t)$ contains the real magnetic field components, $H_x(f_t)$, $H_y(f_t)$, and $H_z(f_t)$ that are calculated by

$$\mathbf{H}(f_t)=\mathbf{D}^{-1}(f_t)\mathbf{V}(f_t) \tag{12}$$

6.4 **MFR calibration procedure**

Figure 6.4 shows a picture from the calibration measurements of the magnetic sensor carried out in Uppsala, August 2009. As mentioned before MFR instrument has six input channels. The first five channels are used to measure the five components of the EM fields and sixth channel is used for the calibration measurements. The calibration data are measured continuously in five channels and stored on a disk. The first three channels are the three components of the magnetic field. Channel number 4 is for the trigger signal and number 6 for the reference signal. The measurements are carried out for a certain time that can be tuned by the operator. With the maximum segment length of 256 K and a sampling frequency of 600 kHz a very fine frequency resolution of about 2.3 Hz is achieved. The recording time for each segment is 436.9 ms. In order to get a better estimation of the calibration transfer function we need to reduce the noise effect by stacking the auto and cross powers of the calibration and reference channels. The measuring time can then be adjusted by targeting a proper stacking height N. A value of 1000 is a proper choice to have an effective noise reduction. A logarithmic sweep signal was generated that covers the RMT frequency band ± 10%. The sweep is triggered by a signal and in order to perform a constructive stacking we need to have a good knowledge about the starting time of the sweep. This is done by storing the trigger signal in a separate channel (4).. It is important to set proper sweep parameters. Figure 6.5 is an example of a logarithmic sweep. The parameters used to generate this sweep are shown in Figure 6.6. The selected sweep has a frequency content that can be analyzed using a Fourier transformation. Figure 6.7 is the Fourier transformation of the signal in Figure 6.5.

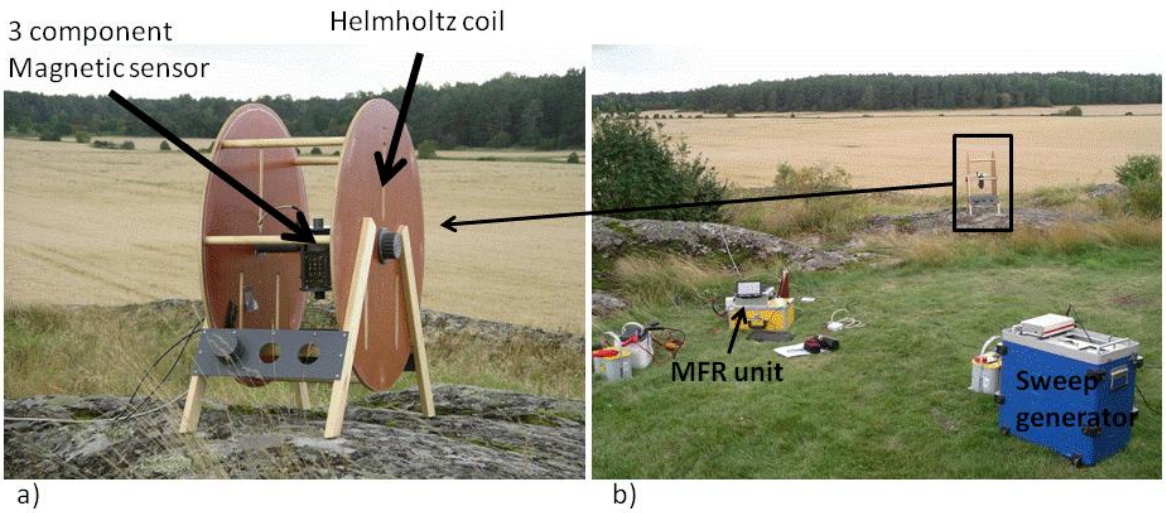

Figure 6.4. The calibration setup for the measurements in Uppsala August 2009. a) The Helmholtz coil with the magnetic senor at the centre. b) The entire setup showing the calibration coil, MFR unit used for the data storage and processing and the HP sweep generator.

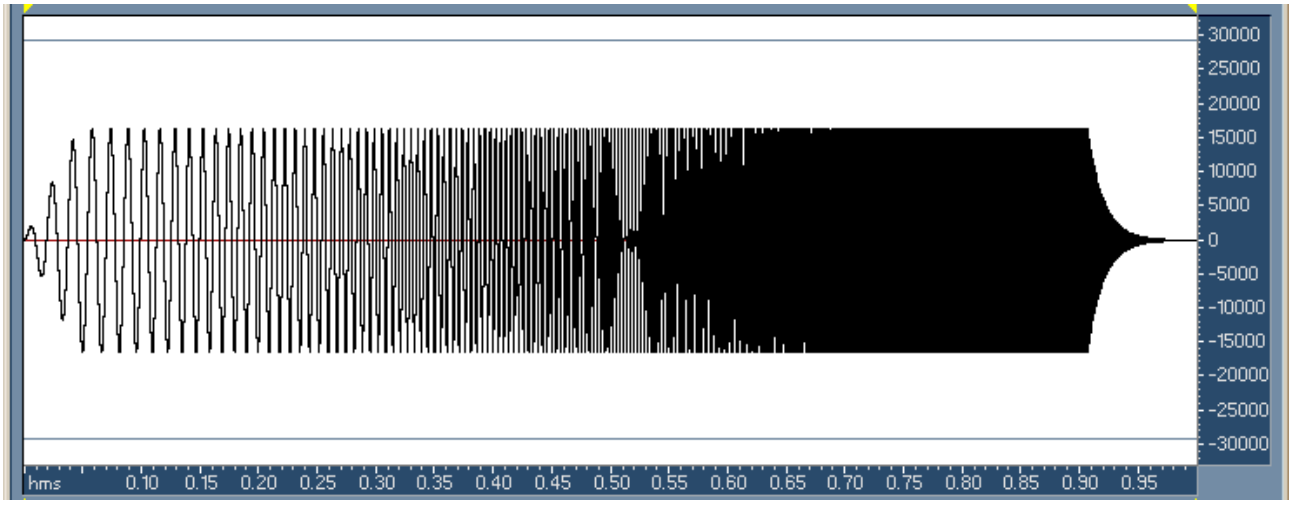

Figure 6.5. An example of a logarithmic sweep generated with an HP signal generator.

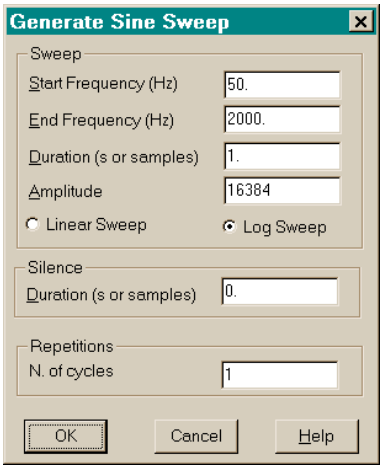

Figure 6.6. Sweep parameters for the signal shown in Figure 5.

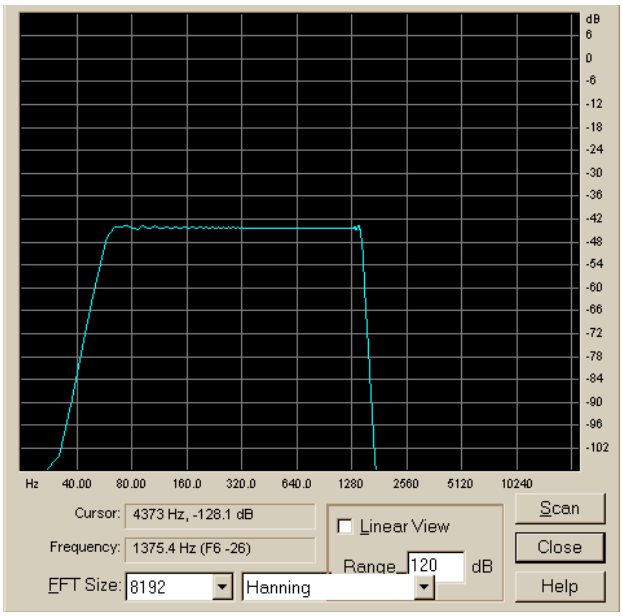

Figure 6.7. The amplitude spectrum of the sweep signal in the frequency domain.

The trigger time (ΔT) has to be longer than the sweep time (ΔS) to cover all the frequencies in the band of interest. In the MFR calibration a trigger time and sweep time of 500 ms and 430 ms was used, respectively. Using these parameters together with a 1000 stacking height the measurement time for each channel is 500 seconds. Figure 6.8 shows the concept used for generating the proper sweep and trigger signals to reach a constructive stacking.

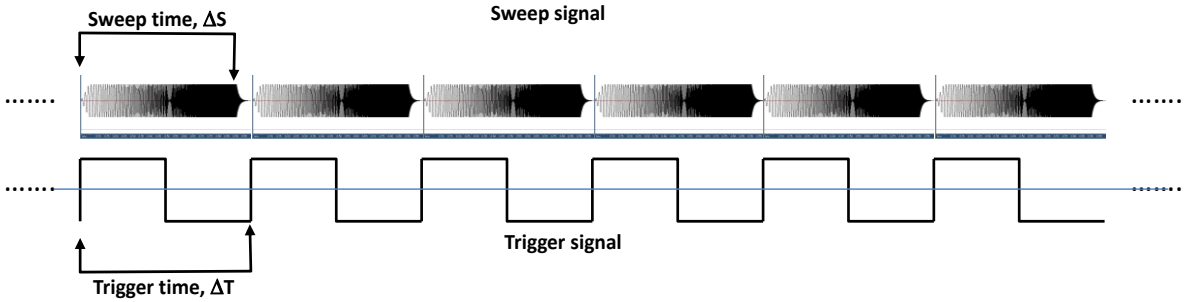

Figure 6.8. Sweep and trigger signals to maintain a stable phase for constructive stacking.

The data for each channel are stored in separate files (five files for each magnetic channel). In the calibration program the trigger file is read in and the starting indexes of the trigger are determined. This is done by using the derivative of trigger signal and searching for maximum variations for a given number of triggers. As shown in table 6.1 at the sample length between the starting points is nearly constant 300033 samples.

By displaying the time series from the starting point for the length of the trigger, it was proved that the starting trigger points where determined correctly. Figure 6.9 is an example of the measured magnetic field data together with the reference signal.

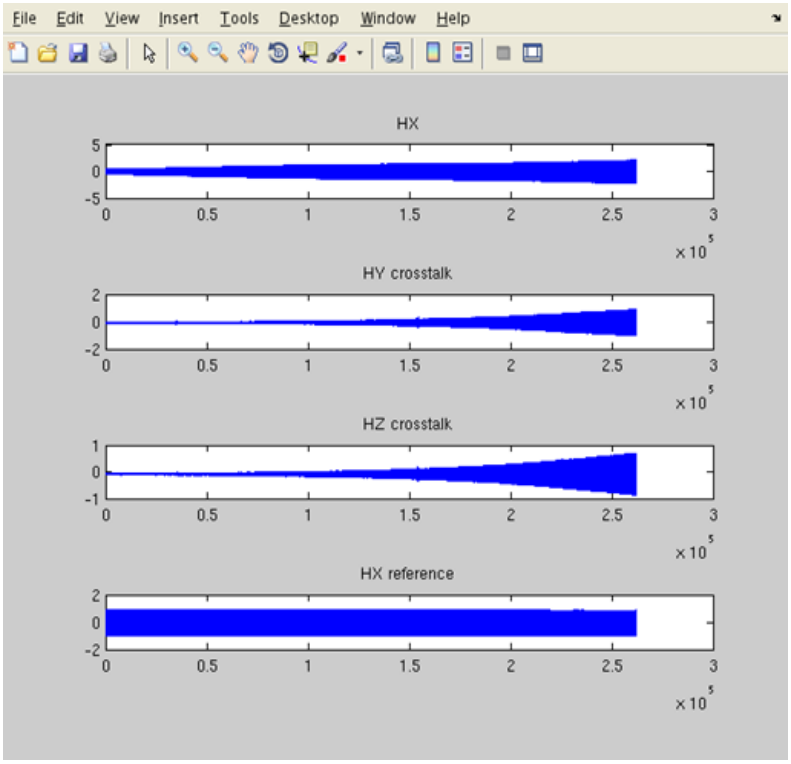

Figure 6.9. Time series of Hx, Hy,Hz and reference channel.

The longest segment for the processing in the MFR instrument is 256 K samples (262144) that provides a frequency resolution of 2.3 Hz (using a 600 kHz sampling frequency). The calibration data for the shorter segment lengths can be then easily extracted from the longest segment calibration data. Using the starting points' indexes, from each file (equal to one segment) are read in and stored in a matrix. Each column of the matrix has the time segment of one channel. These data segments are tapered with a 5% edge cosine filter in the time domain, so that when each block is transformed in the frequency domain by a Fast Fourier Transformation (FFT), the variance of one frequency does not influence another frequency during the FFT. The FFT is done on each column of the matrix and then the auto and cross powers (in the frequency domain) are stacked in a new matrix. For each stacking the frequencies of auto and cross power are added to this matrix.
Before estimating the transfer function the number of stacks and the pregain is removed. With these stacked data the calibration transfer function is then estimated as shown above.

The Program also estimates the standard deviation of the response function. The transfer functions are estimated in the frequency band 10 to 250 kHz and median filtered to suppress noise which is higher at high frequencies.

The standard deviation is estimated by:

$$\sigma^2_{T_{ij}} = \frac{1}{N-4}.(1-\Gamma^2_{ij}).\frac{S_{ii}}{S_{jj}}, \text{ where } \Gamma^2_{ij} = \frac{|S_{ij}|^2}{S_{ii}S_{jj}} \quad (13)$$

where Sij is defined as $V_i^* V_j$ and the star stands for the complex conjugate operation.

6.5 **Description of the GUI**

With this program it is possible to calibrate the instrument in two different modes. In the first mode the user can calibrate single magnetic and electric channels one at a time, whereas in the second mode the user is lead through the calibration of all channels by the program. If a magnetic channel is calibrated, all magnetic channels are recorded together with the trigger and the reference channel. We need all magnetic channels to estimate the crosstalk between the magnetic sensors in three directions. Calibrating the electric channel only the target, reference and trigger channel are recorded. After each calibration the transfer function is saved in an output file.

The GUI changes during the calibration process and in this part the change and different GUI options are explained as well as the functionality of the different buttons.

The first GUI window (Figure 6.10) shows edit windows and a drop down menu. In the edit windows the user can change the default values of voltage (mV), resistance (Ohm), coil windings (n = 2),the pregain and the start and stop frequencies for the band filter. Furthermore the coil type and measuring parameters used in the calibration instrument (circular, rectangular or square) are specified. The default value for the coil size is set to circular with a radius of 40 cm

- *Single channel calibration*
If the check box with single calibration mode (DO SINGLE CALIBRATION) is activated, then after pressing the "OK" - button the interface changes for calibration mode for single channel. The default values should be corrected, if necessary, before pressing the OK button.

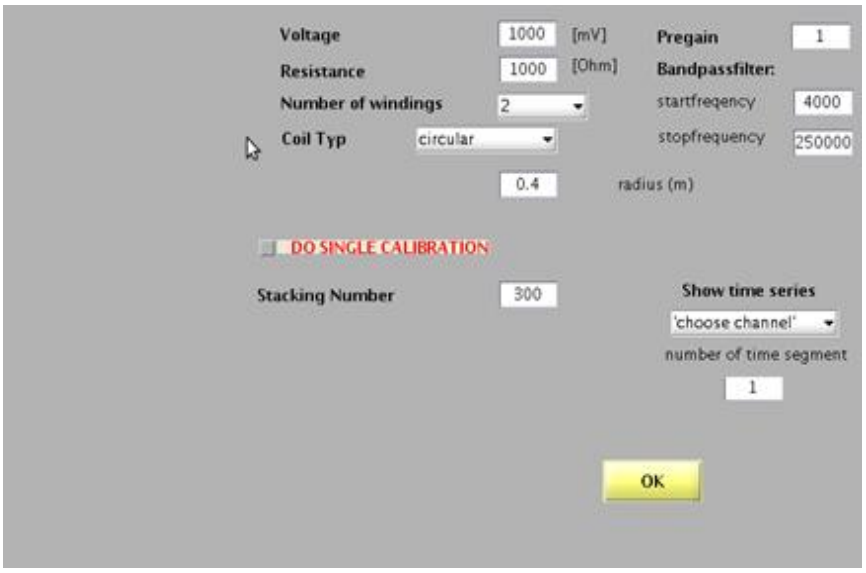

Figure 6.10. The first GUI window where the default values are shown and can be changed.

Then a dropdown menu that contains a list of calibration channels becomes visible (Figure 6.11).

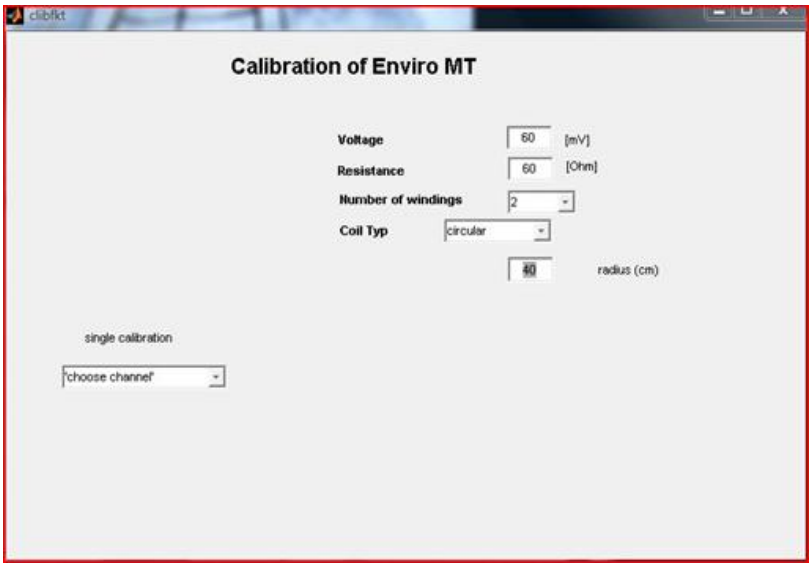

Figure 6.10. The window for the single calibration. User can select the calibration channel using the dropdown list "single calibration".

After selecting one of these channels, the corresponding data are read in and the transfer function is estimated (Figure 6.12). The user has to select the right data file in a directory window which will appear. If the target-, reference-, and trigger- data are not stored in the same directory an error window is shown, warning the user to correct and try again. The prefixes and extension of the file names are predefined in the MATLAB code, so either the file names or the code has to be changed if the names do not correspond.
After selection of a channel, the interface displays trigger frequency, sampling frequency, number of samples in each segment and stacking number (Figure 6.13).

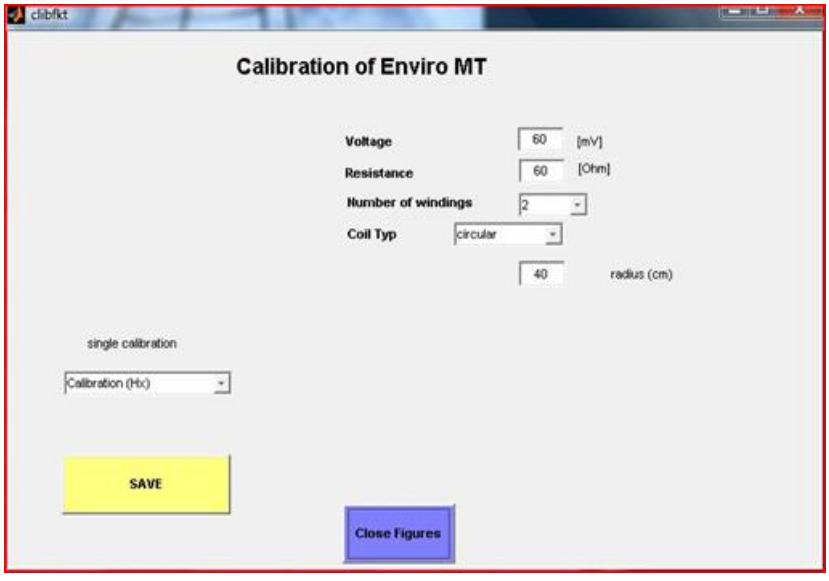

Figure 6.12. Calibration window after selection of single channel.

With the "save" -button the calibration function is saved in file with a proper name. Additionally the figures showing the imaginary part, real part, and the standard deviation (error) pop up. The real and imaginary parts of crosstalk (only for magnetic channels) in a different colour are also plotted. These windows can be closed by the "Close Figures" button.

It is possible to show the time series of the recorded channels by selecting a channel under "show time series" → " choose channel" and a segment number (see Figure 6.10).

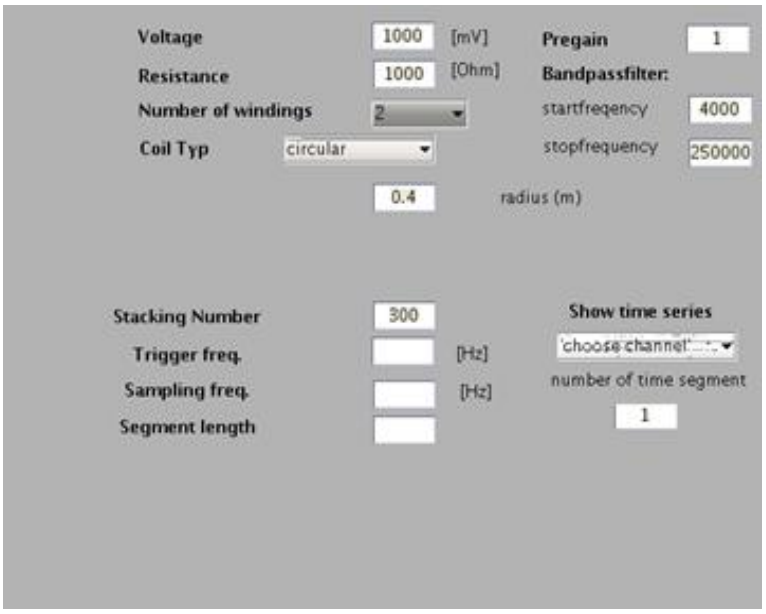

Figure 6.13. The selected parameters for the calibration.

- *Multi-channel calibration*
If the check box is not activated the interface changes to the second mode. First a "Delect Data" -button appears (Figure 6.14). By pressing it all data headers are read in if all files are stored together in a directory, otherwise an error is displayed. The interface now displays again the trigger-, sampling-frequency, stacking number, and the number of samples in each segment (Figure 6.15).

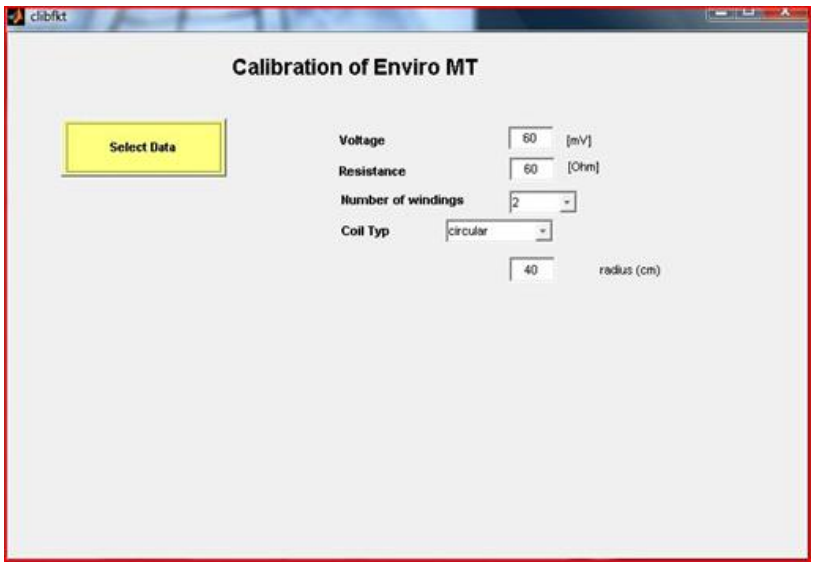

Figure 6.14. The GUI interface for the multi-channel calibration.

The multi-channel calibration process starts and the text for the button changes to “Calibration (H_x)” and the figure with the transfer function pops up, a “close”- button and “save”-button appears as in the first mode. The operator can also repeat the processing and then save them. By saving the H_x results the next channel, H_y, is then calibrated and the same procedure repeats until all the channels are calibrated.

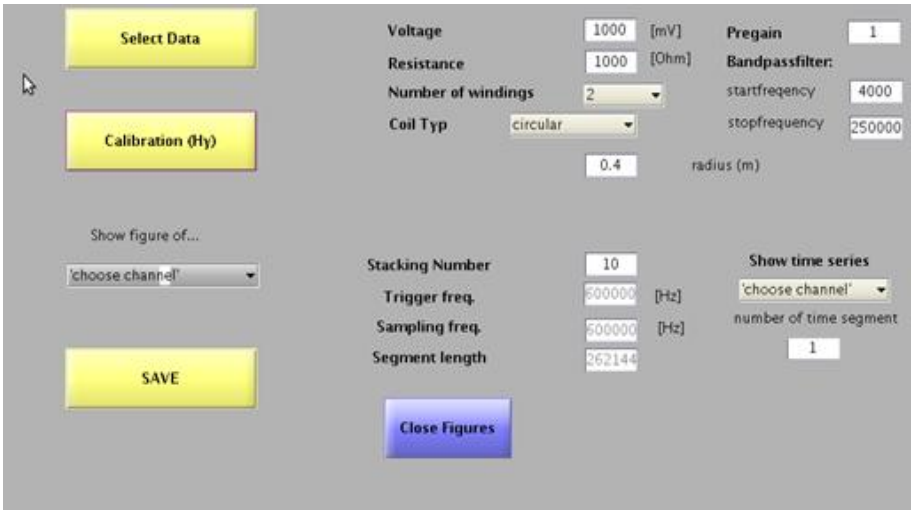

Figure 6.15. The GUI window after saving the first calibration results in multi-channel mode.

The text of calibration button also changes to “Calibration (Hy)”. Furthermore a drop down menu is displayed where it is possible to select a single channel and display the results of the calibration function (Figure 6.15).

6.6 **Results**

A set of calibration measurements was carried out in Uppsala, May 2009. Two measuring systems were calibrated, MFR from Uppsala University/SGU and ADU07 from Metronix GmbH in Germany. The latter was used in an airborne data acquisition campaign in Falun area, in Sweden. In this report the results for the calibration of MFR magnetic channels are presented. In Figures 6.16, 6.17, and 6.18 the amplitude and phase of the transfer function for each H_x, H_y and H_z channels are shown, respectively. The data are very noisy, especially at frequencies higher than 150 kHz.

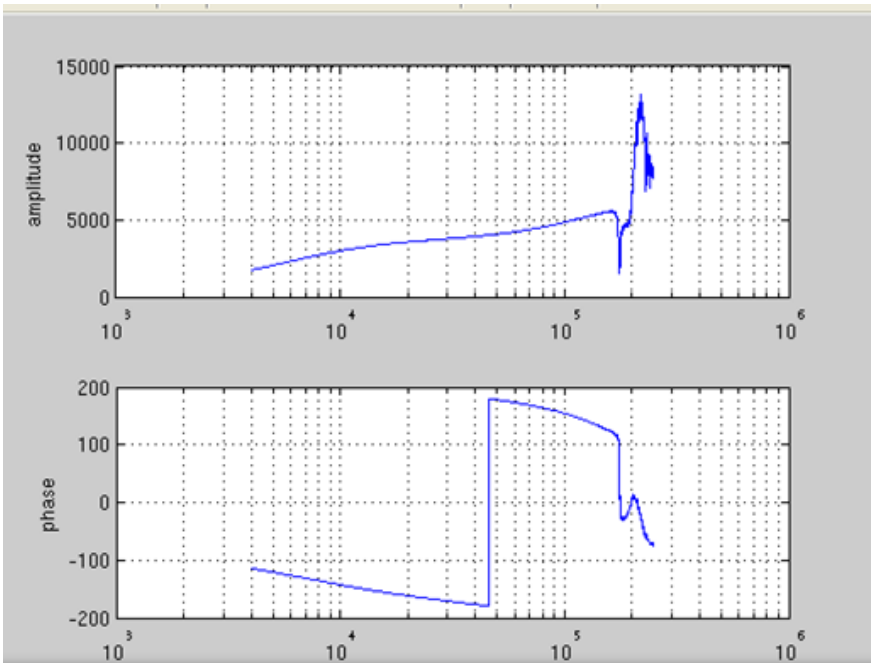

Figure 6.16. Amplitude and phase of H_x transfer function

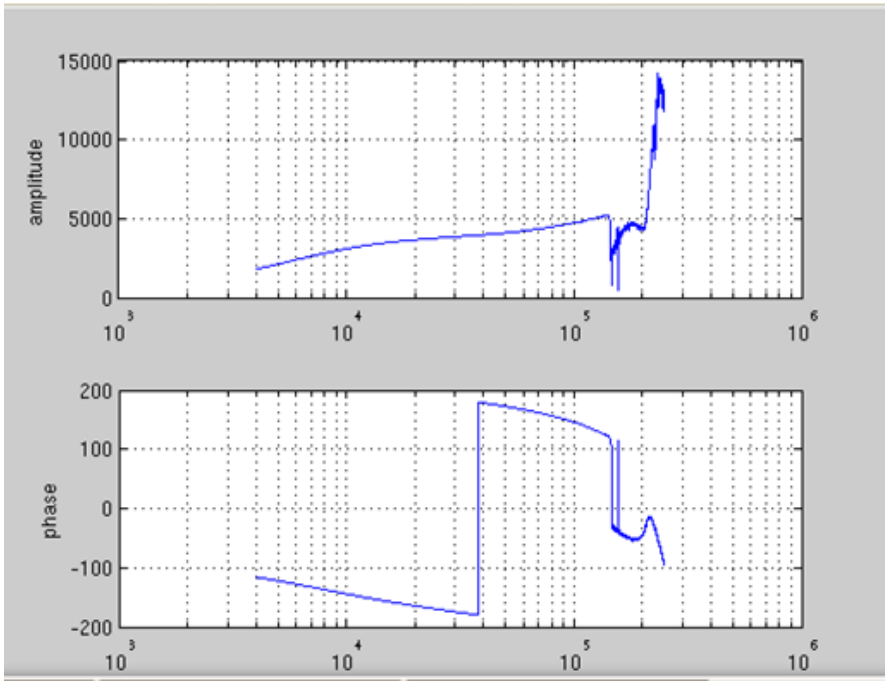

Figure 6.17. Amplitude and phase of H_y transfer function

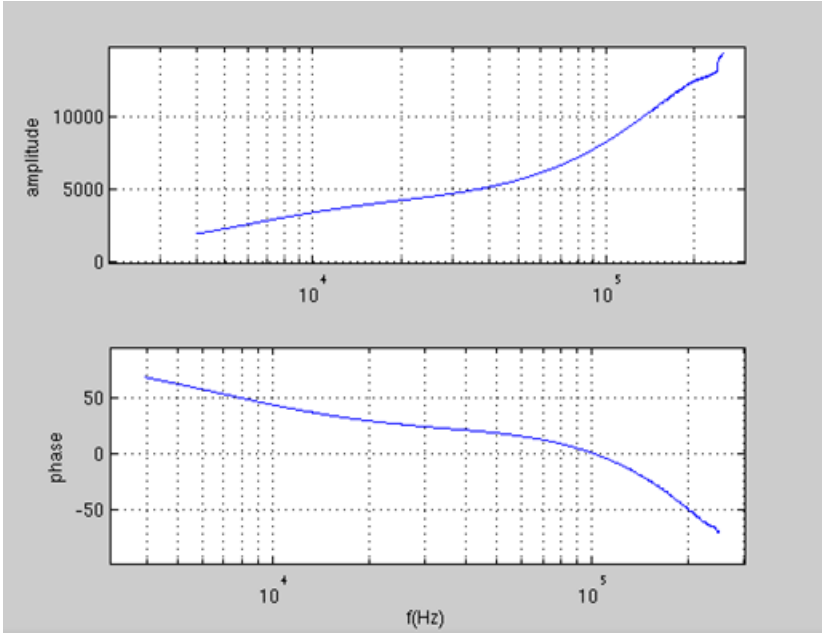

Figure 6.18. Amplitude and phase of H_z transfer function

To decrease the noise the data are median-filtered with a median width of 200 samples. The results shown are based on a set of wrong sweep parameters so that the higher frequency signal was cut from the data. This gives reason to the strange behaviour of the transfer functions at higher frequencies.
Figure 6.19 shows the error and the real and imaginary part of the H_z transfer function in blue. Red is the crosstalk in the H_x and yellow is the crosstalk in the H_y coil. The crosstalk is also frequency dependent as it increases with higher frequencies.

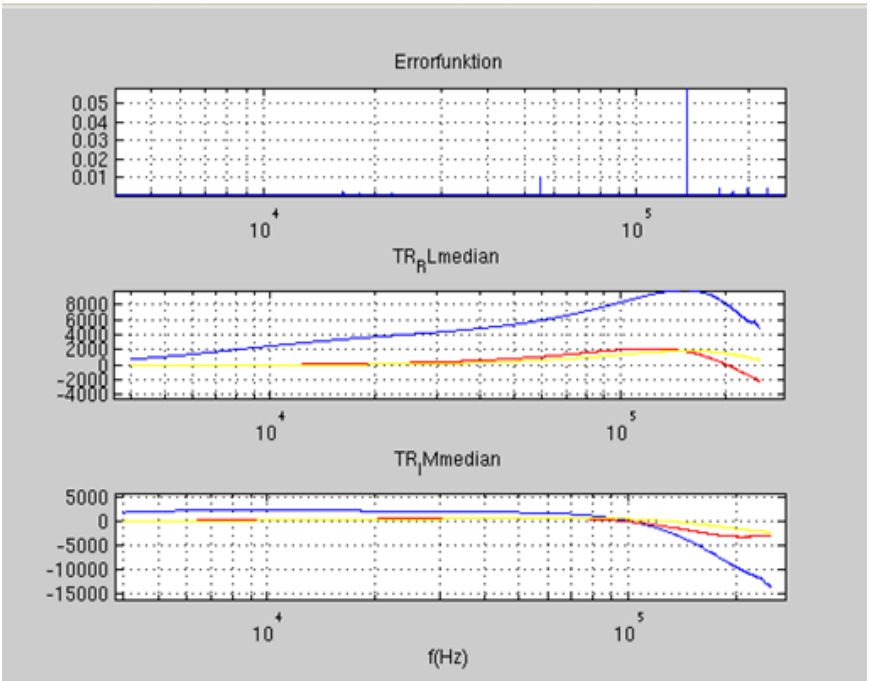

Figure 6.19. Error function and real/ imaginary part of transfer function (crosstalk in red and yellow)

The program shows fairly good results. But due to the non linear behaviour of the transfer

functions at higher frequencies the calibration measurement has to be repeated to get better results.

Table 6.1. Number of samples between indexes of the trigger starting points

287888	300032	300033
300032	300033	300032
300033	300033	300033
300033	300033	300033
300032	300032	300033
300033	300033	300032
300033	300033	300033
300032	300032	300033
300033	300033	300032
300033	300033	300033
300033	300032	300033
300032	300033	300033
300033	300033	300033
300033	300032	300032
300032	300033	300033
300033	300033	300033
300033	300033	300032
300032	300032	300033
300033	300033	300033
300033	300033	300033
300032	300033	300033
300033	300033	300032
300033	300032	300033
600065	300033	300033
300033	300033	300032
300033	300032	300033
300032	300033	300033
300033	300033	300033
300033	300032	
300032	300033	
300033	300033	
300033	600065	
300032	300033	
300033	300033	
300033	300033	
300033	300032	
300032	300033	
300033	300033	
300033	300032	
300032	300033	
300033	300033	
300033	300033	
300032	300032	
300033	300033	
300033	300033	

MFR DATABASE SOFTWARE

7. **MFR database software**

The MFR database program has been made to store the acquired data for data quality control, data visualization, post-processing and modeling. The main structure of the program is based on the EnviroMT database program. Lars Dynesius (UU) and Mehrdad Bastani (SGU) have planned the preliminary concepts of the database. In order to implement the program it was announced as a student Master Project. In this part of the report I have mainly used the material from the thesis written by David Alfonso Grande that was supervised by Mehrdad Bastani (SGU) and Lars Dynesius (UU).

The aim of this project is the development of a tool to manipulate the information stored in the database created by the MFR system. One of the requirements was that the tool should be a cross platform application, so it should run both in Linux and Windows. For that reason, after some discussions, the programming language chosen was Java.
Java is an object oriented programming language which is used in a lot of applications. This is because in this time it is a common requisite for programmers that their programs have to run in different operating systems. An application programmed in Java can be executed in Windows, Linux, Mac Os, Solaris..., if the user has installed in his computer the Java Virtual Machine.
As we commented, the program must be able to connect to a database. Here we have another advantage with Java, because it has a lot of native drivers to connect with several database management systems. Another benefit using Java is that we have a lot of Integrated Development Environments (IDE's) , such as the famous Eclipse. As the program is a Graphical User Interface, we decided to search an IDE with some extension that allows building interfaces easily. Finally we used JBuilder, which is a program based in Eclipse and provides some features that let us build graphical interfaces just by Drag & Drop.
Once the program is connected to the database, some operations can be performed by the user to read and manipulate the data. Some of these features are:

- Plot XY graphs of data for the stations.
- Plot cross section graphs for entire line or group of stations along a line.
- Perform 1D and 2D inversion of the data at one station, a group of stations, or a line and plot the results.
- Save the results of the inversion.
- See the relevant data in a table view.
- Modify data in a table view.
- Image viewer, where saved images can be seen along with some relevant information.
- Reprocessing of the data, by changing some processing parameter e.g., number of stacks and signal-to-noise-ratio (S/N) threshold.
- Another feature of the program is that it can manage several versions of the same project. The different versions can be of the whole project or just of some lines. These revisions can be selected when selecting a line.

7.1 **Description of the database**

The database used in the project is MySql. This is a relational database management system, multithread and multi-user . It runs as a server providing access to the different databases. The databases can be accessed from the local machine where the server is installed and also from another computer connected to the server. MySql is platform independent, so it can run in Linux and Windows, so it fulfills this important requirement in the project.

Another important feature of MySql is that there is a native driver for Java so the program communicates very easy with the database. Figure 7.1 illustrates a small schema of the tables in the database:

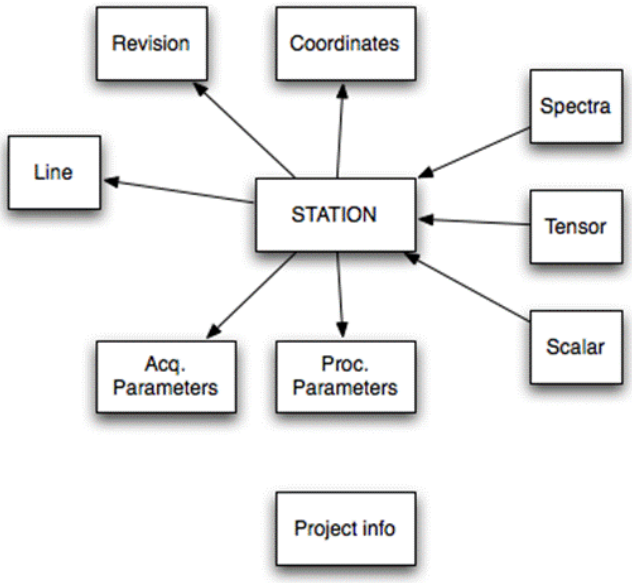

Figure 7.1. Schematic showing the concept of tables in the MFR database

7.2 Use of the GUI

The Graphical User Interface, as we said before, is used to read and manipulate data from the database. In the next subsections the different features of the application are described.

7.2.1 Data visualization

When the program is opened, the main screen of the program is shown. We can see it in the Figure 7.2. In the upper half of the frame we can see the Select Data panel, which is divided in 6 more panels: Select Project, Method, Data Type, Quantity, Selection Set and Line/Station. To select the data we have to follow the next steps:

- Select a project: In the select project panel there is a list with all the projects in the database. If we want to add a new project, just we have to press the button Add Project, and a new program will be executed to add the new project. Once we have selected the project, the program will set the methods that are available for the project.
- Select a method: Select the radio button from the methods that are available in the project. When a method is selected, the data type panel is set for this method.
- Select a data type: Select the radio button from which we want to retrieve the information.
- Select quantity: From the Quantity panel, we have to select at least one element. There is the possibility to select up to four items in this panel.
- Select a set: Select from the Selection Set panel the option that we want (Station, Group or Line).
- Select Line/Station: Depending on the selection made in the Selection Set panel, there are different options in this panel.

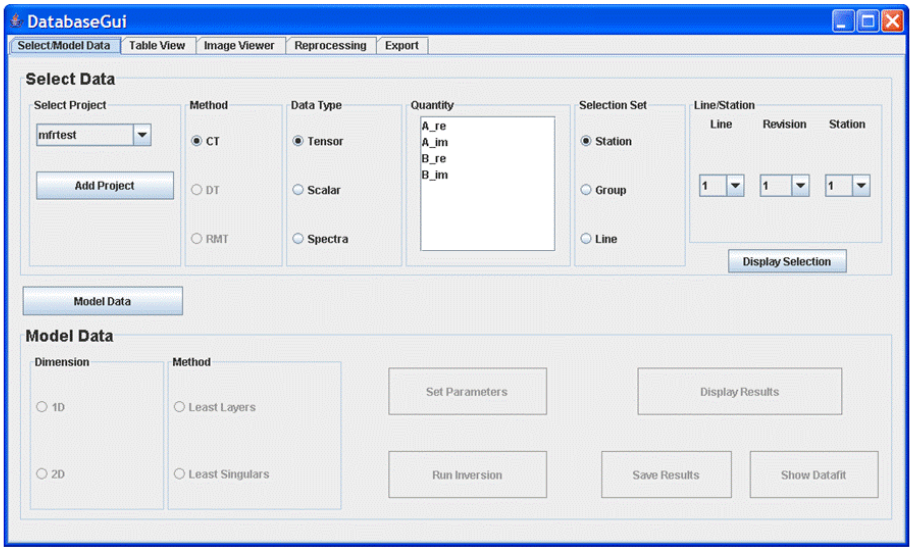

Figure 7.2. The main tab in the MFR GUI.

Line: Select which line we want and which revision of the line.
Station: Select which line, revision and station we want.
Group: Select the line, revision and the group of station from which we want the information.

After selecting the different parameters, we just have to press the button Display Selection and we will have a chart with the information we wanted

7.2.1.1 **Station plot**

The information from a station will appear, as an XY plot (see Figure 7.3) using the Display selection button. In this window the title, station number and the line number are shown. We also have the axes labels and the plot with error bars. One can navigate though the different stations just by pressing the "previous" and "next" arrows in the lowest part of the XY-plot window. We can also change the line and station. Another feature is that we can save the image to a _le using the menu File of the menu bar and then select Save as. Then a save dialog is displayed and the file is given a proper name and directory.

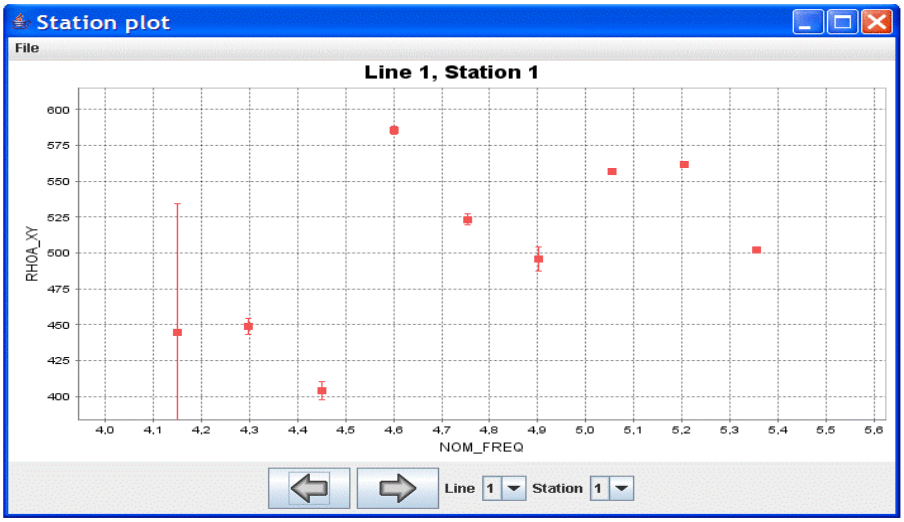

Figure 7.3. An example of XY plots at a single station. Note that the line and station numbers can be set so that the data are displayed very quickly.

7.2.1.2 **Group/Line plot**

To see the information of a whole line or group of stations, a cross section plot is needed. That plot is obtained by pressing the display button (see Figure 7.4).
The line number and the name of the axes are shown in the panel. Also a color scale is placed on the bottom of the window. The option to save the image in the same way than in the XY Plot is also available here.

Another functionality is the possibility to change the range in the color scale. It can be done from the Set button in the menu bar. A new panel will appear where the minimum and the maximum values for the color scale can be changed.
As we told before, in the Quantity panel we can select up to four items. When we make a plot of this selection, a window appears with all the graphs in it (see Figure 7.5). This window works in the same way for one graph or more.

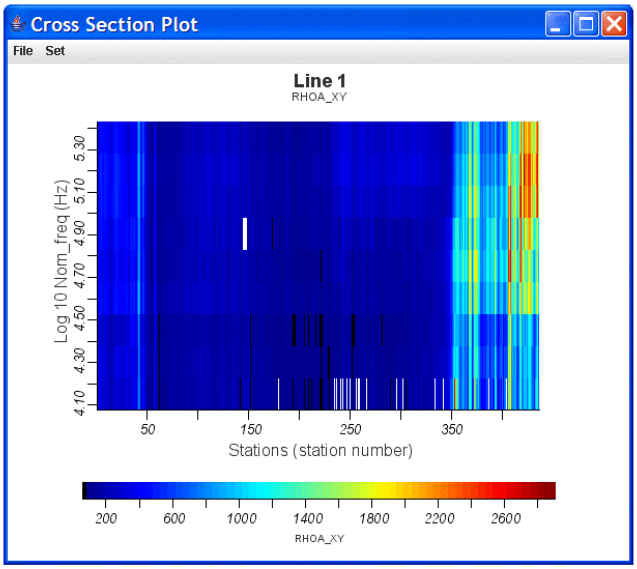

Figure 7.4. The cross section plot along a line and a group of stations.

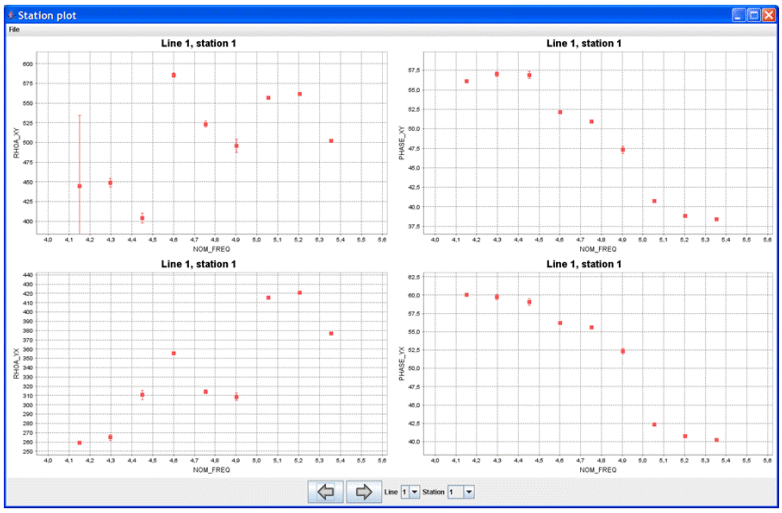

Figure 7.5. Multiple XY plots of different results at a single station.

7.2.1.3 **Data modeling**

We can see in the lower part of the Figure 7.2 the selection panels for the data modeling. When the button Model Data is pressed, these panels are activated, so we can make our selection and run the inversion programs.

7.2.1.4 **1D Inversion**

The next steps have to be taken to visualize the data modeled:
- Select 1D in the Dimension panel.
- Choose method in the Method panel. We can choose between Least Singulars or Least Layers.
- Set parameters: When pressing the button Set Parameters, a new panel will be displayed with all the parameters that we can set (Figure 7.6). Once we have modified the parameters, just pressing the Set button, a file will be created with the parameters ready to be used by the inversion program. There is also created the input file for the inversion program selecting from the database the data that we want to invert.
Instead of modifying the parameters in the panel, it is possible to load a file with a configuration previously used. For that reason we are able to save our configurations to a text file.
Once we have set the parameters, the Run Inversion button is enabled.

- Run inversion: The inversion program corresponding to the method selection will be executed. When the inversion programs have finished the execution, the Display Results button becomes enabled.
- Display Results: After pressing this button, the program reads a result file of the inversion program and creates a cross section plot of the inverted data.
This plot has the same characteristics than the cross section plot of the data visualization.

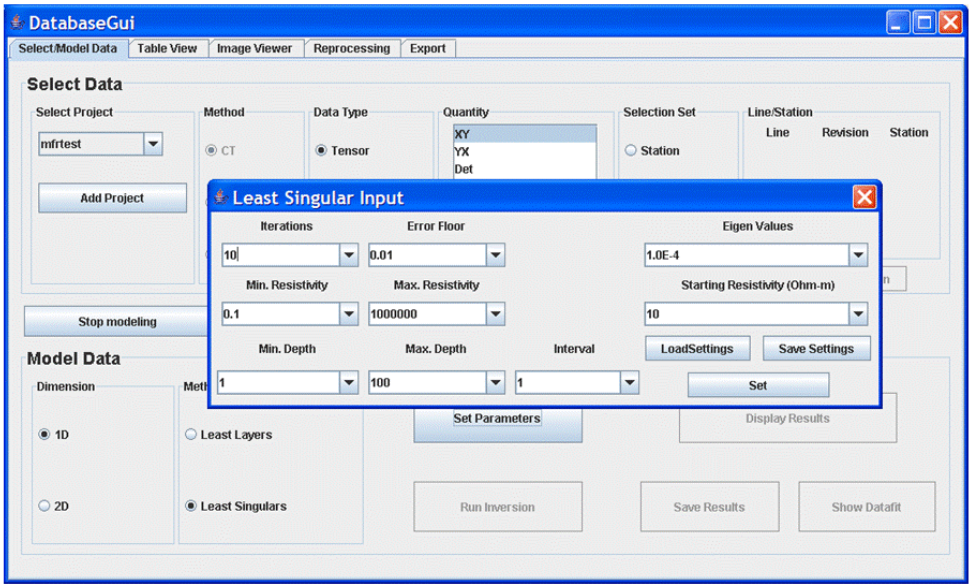

Figure 7.6. An example of 1D inversion parameter setting panel. The plot shows the Least Singular Inversion input parameters.

7.2.1.5 **2D Inversion**

The steps to take to visualize the data modeled are (see Figure 7.7):
- Select 2D in the Dimension panel.
- Choose the method in the Method panel. We can choose between Rebocc and Occam.
- Create data file: For the Rebocc method, when pressing this button, a save panel will be displayed. Here we have to put the name and select a destination folder for the data file. In this file the program will write the data that we selected for modeling.
- Run inversion: For Rebocc, a Matlab program is executed. This program will take as an argument the file created previously and the user have to set more parameters to run the inversion.

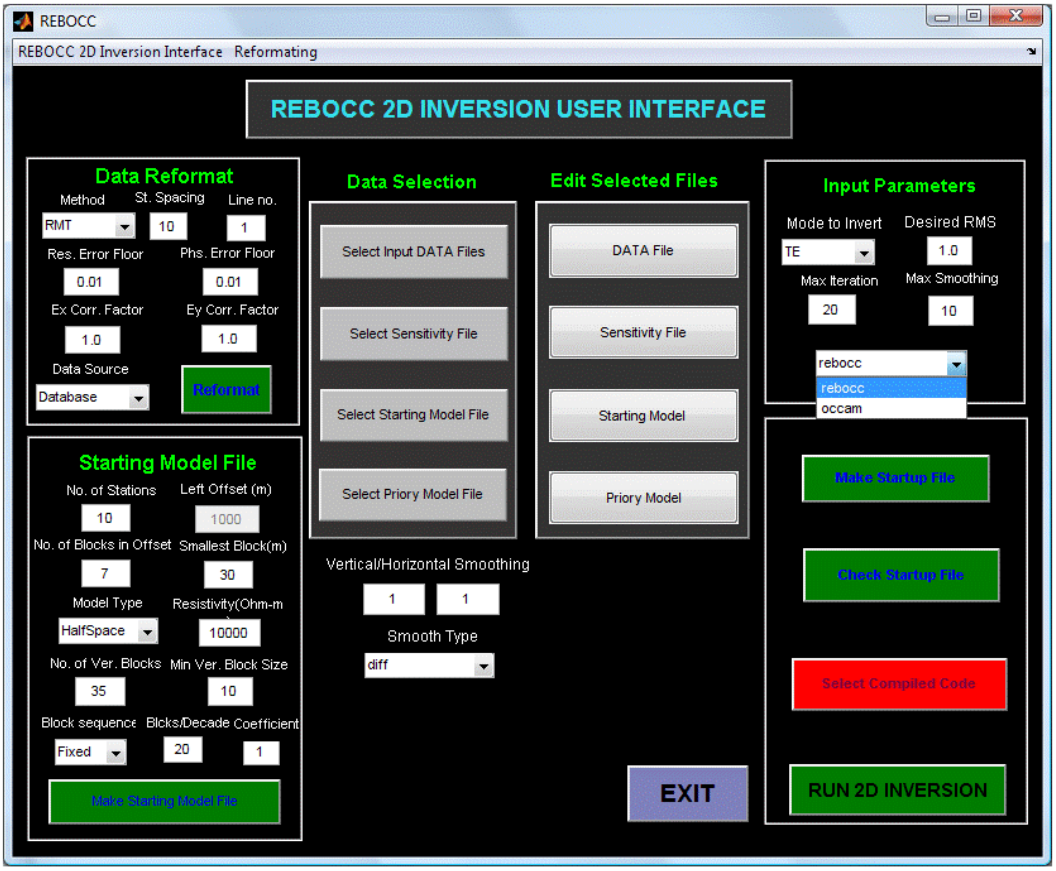

Figure 7.7. Interface to 2D inversion program. Two inversion techniques (REBOCC and OCCAM) can be selected to model the data.

7.3 **Data manipulation**

Usually, after looking the plots, we can realize that there are some values out of range. To remove these outliers, we need a utility able to show us the data in an intuitive way, and also where we can modify it. As the database for the application is divided in several tables and

the information is distributed in these tables, we need the possibility to take the data from different tables and show it all together. The best way to do so is in a table view (Figure 7.8). To show the data, the user needs to select the line, method, revision and data to be shown. Once the selection is done, pressing the Show button will display a table with the information requested.
A feature of this utility is the possibility to edit the data. If the user wants to edit a value, he has to press the Edit button and a panel asking for a password will appear (the password is 'uppsala'). Then we can edit the values and these changes will be updated to the database. Note that there are some values, as the line or station number that cannot be edited. If we make a mistake changing the data, pressing the Undo button will return the table to the previous state.
Observe also that in the bottom of the window there is another table showing the processing parameters for the data selected.

7.4 **Results visualization**

When we were describing the data visualization utility, we mentioned that the images generated could be saved to the file system. In this tab, we can see these images saved.
As we can see in the Figure 7.9, on the left part of the window we have a tree view of the file system. Here we can select the image that we want to observe, and this picture will be displayed in the central panel. To have more information, when we select an image and is displayed, some text appears on the text panel situated on the right side of the window. If the image corresponds to a station or line plot, the information shown is about the acquisition parameters and the processing parameters. But if the image was saved after performing an inversion operation, we also have information about the parameters that we set before running the inversion program.

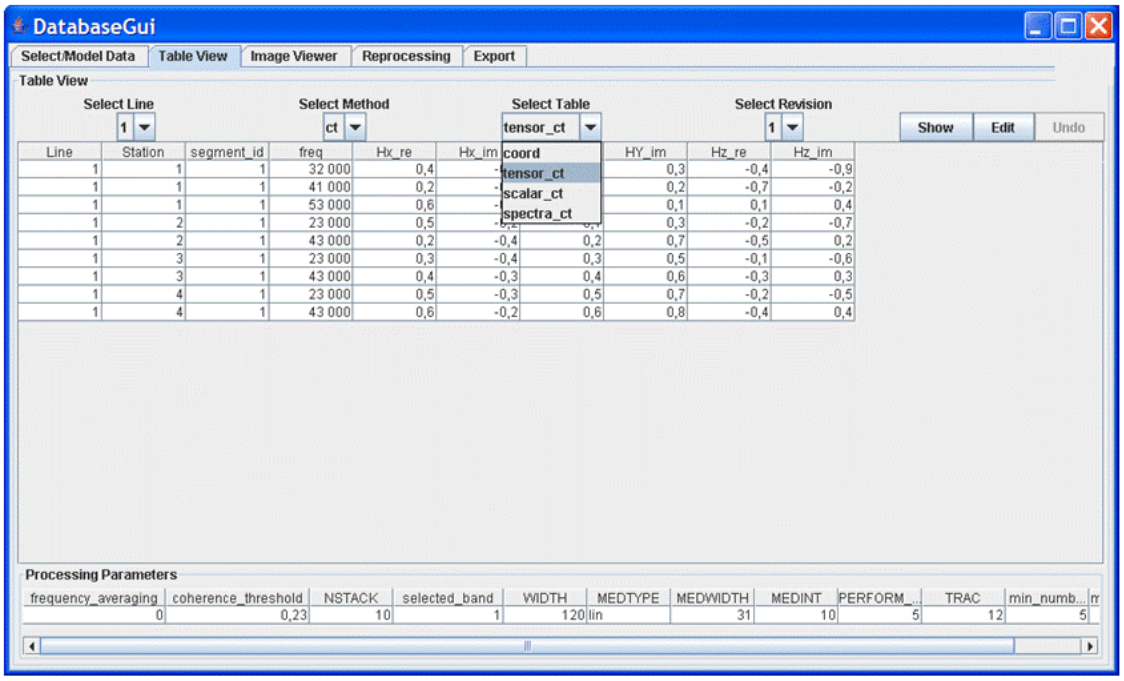

Figure 7.8. Table view tab. The data from various measuring modes can be checked in a table form.

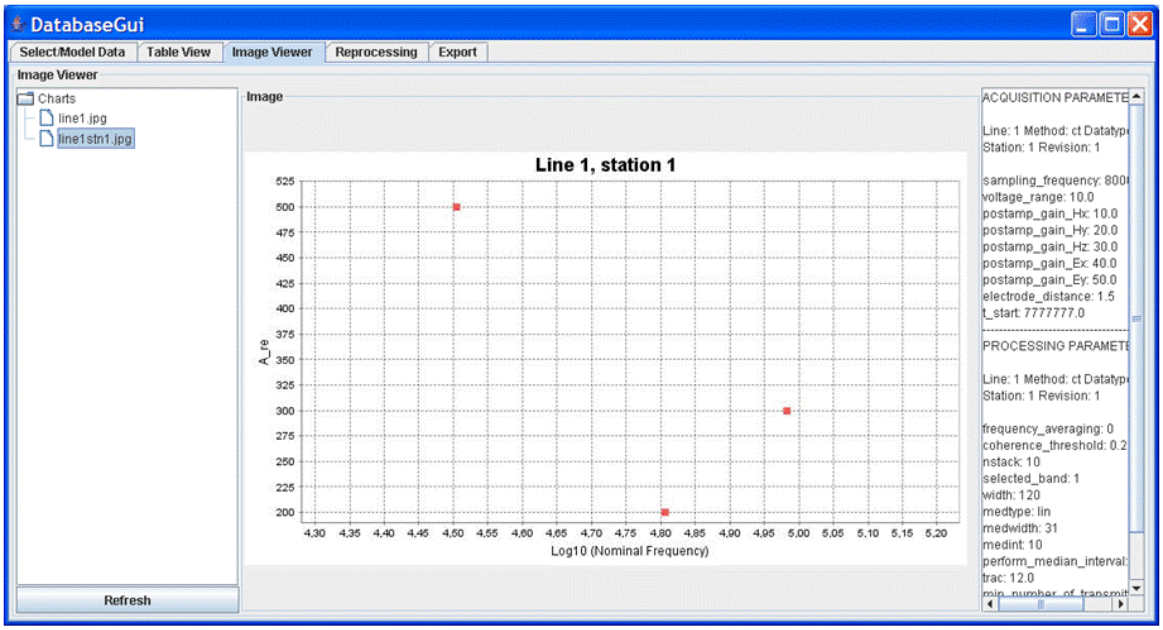

Figure 7.9. Image viewer in plot and processing parameter forms.

7.5 **Reprocessing data**

One important feature of this system is that we can manage several versions of the same project. Away to obtain a new version of the project (or just a part of the project) is to reprocess the data (Figure 7.10). The steps that a user has to follow to perform the reprocessing are the next:
- Select the line to be reprocessed.
- Select the method of the line to be reprocessed.
- Select the revision of the line to be reprocessed.
- Choose if the reprocessing will be of the whole line, of a group of stations of just of a station.
- In case that the reprocessing will be of a station or a group, select them.
- Set the parameters for the reprocessing. These parameters are the number of stacks and the signal/noise threshold.

There is also the option to create a notch list of frequencies. This feature is situated on the bottom of the window and is activated selecting the checkbox Notch Frequencies. The frequencies that the user wants to add to the list can be selected from the table. There is also possible to select Harmonics, checking the corresponding checkbox , and modify the bandwidth, changing the value of the number of index.
Once that the frequency is selected it is added to the list pressing the Add button.
A frequency can be removed from the list using the Remove button.
When the user has finished with the selection and settings, he has to press the
Run button. If the notch frequencies option is enabled, the program will create a text file with the information about the frequencies, harmonics and bandwidth, and then it will make a call to the reprocessing program.

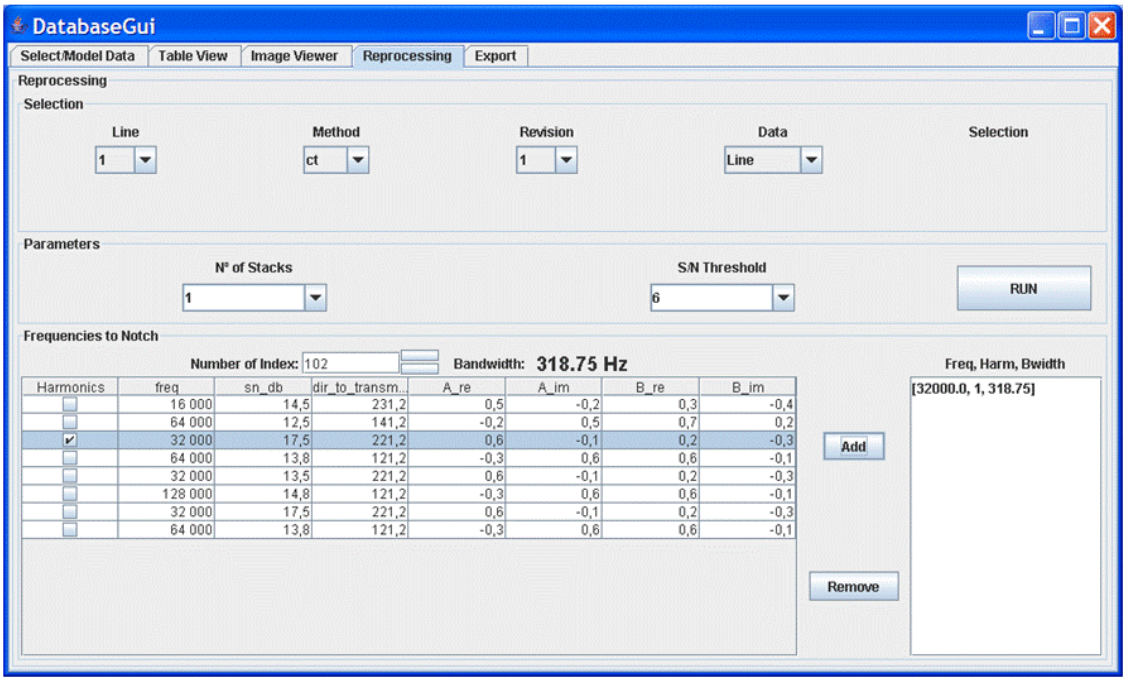

Figure 7.10. Data reprocessing tab. It is possible to reprocess the data in different modes with different processing techniques and parameters.

7.6 **Export data**

Usually, after view, analyze and manipulate the data, the user may want to save some of this data to text files in order to use them with another application. The export of the data consists in two parts (Figure 7.11).
Firstly, the data to be exported have to be selected. For this reason, the user must choose from which line, method and revision the data has to be taken.
In the second place, the user has to select which data he wants to be represented in the text file. The elements that are available to choose are the following:
- Line number.
- Station number.
- Coordinates: WGS84, local or both.
- Tensor data.
- Scalar data.
- Spectra data.

Only one of the three data elements (Tensor, Scalar, Spectra) can be selected at the same time. When the selection is ready and the user press the Export button, a save dialog will appear. Here the name of the file must be set and the destination folder must be chosen.

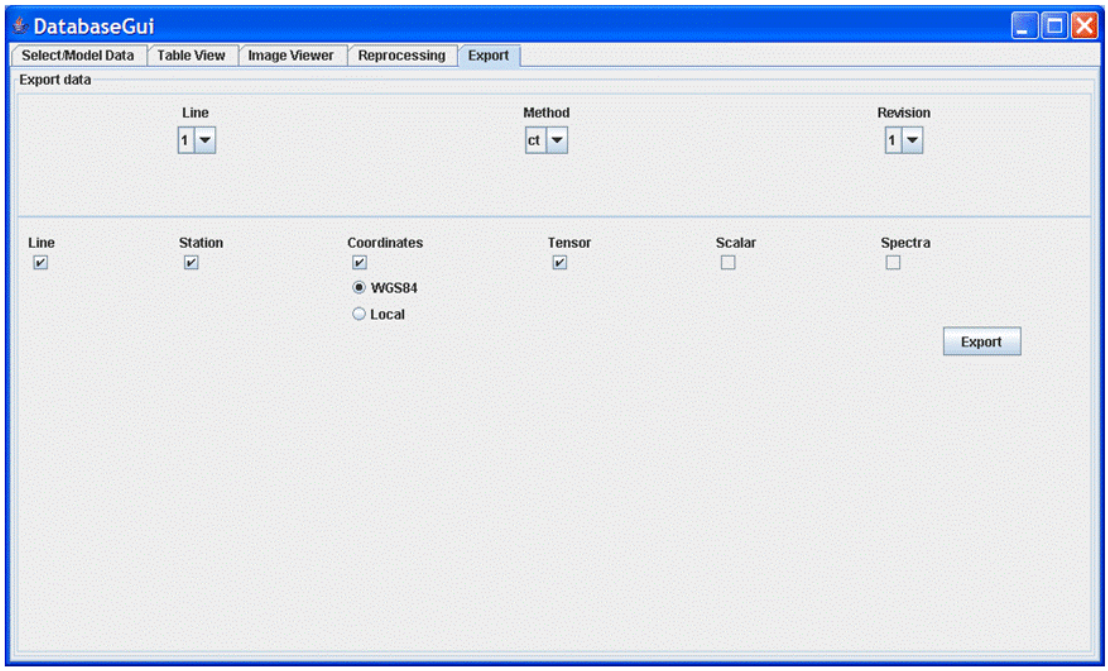

Figure 7.11. Export data tab that enables the user to select different data and information to export as an xyz text file.

7.7 **Work to do**

- In the main tab, the button Add Project still doesn't have any functionality.
Ultimately, it will call to a program made by another student that creates a new database.
- In the Model Data panel, the functionality of the buttons Save Results and
Show Datafit must be completed.
- In the reprocessing tab, when the user presses the Run button, the program only creates the notch list if required. It also will have to call the reprocessing application with the correct parameters when it is finished.

MFR TEST MEASUREMENTS

8. MFR test measurements

The MFR instrument was tested once in an airborne measurement and once on the ground. In both tests only the magnetic field components were measured. This is due to the problems we faced when testing the instrument with five channels. The main cause was the choice of A/D converter that could not handle the 5 channels with the sampling frequency used. Schieschke (2009) addresses such problems in details. After several correspondences with the producer and receiving new drivers for the A/D board and a lot programming (done by Michael Schieschke) the problem was handled. At the moment we are planning to calibrate the system with five channels for making the measurements with five channels that provide a full tensor EM measurement. In the following we just mention the references that are digitally attached to the digital version of this report and are the results of two airborne data acquisition campaigns. The first data acquisition was carried out using the MFR receiver together with the MFR magnetic sensor in November 2007 in Falun area. Anna Gustavsson (2008) delivers a detailed report about the measurements and the results found (appendix A). We have also carried out an airborne measurement in 2008 with another receiver box called ADU07 that belong to Metronix GmbH in Germany. We used our own three component magnetic sensor (Uppsala design and Metronix construction) and also developed all the data acquisition and data processing software. The results are presented in details by Miguel Ángel Alfonzo Carmona (2009) in his Master thesis that is attached to this report as appendix B.

Appendix A. Master thesis: Post processing of airborne data from Multi Frequency Receiver system. Anna Gustavsson. September 2008.

Appendix B. Master thesis: Post-processing of Airborne data using the Broadband Frequency Receiver instrument ADU07. Miguel Ángel Alfonzo Carmona, June 2009

ACKNOWLEDGMENTS

9. Acknowledgements

I would like to thank the Geological Survey of Sweden (SGU) for financing this research under the internal R&D project number 35100. I learned a lot from the collaboration I had with the people at the Geophysics Department in Geocentrum, Uppsala University. Among those I thank Professor Laust B. Pedersen, Senior Research Engineer Lars Dynesius, Dr. Thomas Kalscheuer, Dr. Maxim Smirnov, and Mr. Sören Karlsson.
The support from the airborne group at SGU is highly appreciated. Mr. Sören Byström and Mr. Mats Wedmark supported this project both scientifically and technically.
Mr. Uli Matzander from Metronix GmbH in Germany provided valuable technical supports and sent us ADU07 for two airborne measurements. He also made the three component magnetic sensor for Uppsala University.
Special thanks go to Michael Schieschke who has carried out an excellent job on programming the A/D converter and making the GUI for the field measurements. His assistance in acquiring the airborne data in three airborne measurements in Sweden is appreciated.

9.1 **Student projects and publications**

The complexity of the MFR project demanded a very detailed investigation and pedagogical breakthrough of many effects and parameters. In this context we announced a 5 exam projects that were taken by Master students at Uppsala University. This was a teaching and learning procedure. I had the opportunity to be the first supervisor in four and second supervisor in one the thesis that are listed below:

- **Anna Gustavsson**. September 2008. Post processing of airborne data from Multi Frequency Receiver system. (Supervisors, Mehrdad Bastani, Laust B. Pedersen)
- **David Alfonso Grande**, June 2008. Database Graphical User Interface for MFR System. (Supervisors, Mehrdad Bastani, Lars Dynesius)
- **Miguel Ángel Alfonzo Carmona**, June 2009. Post-processing of Airborne data using the Broadband Frequency Receiver instrument ADU07. (Supervisors, Mehrdad Bastani, Laust B. Pedersen)
- **Barbara Hachmöller**, 2009 under revision. Calibration of Multi Frequency Receiver System. (Supervisors, Mehrdad Bastani, Laust B. Pedersen)
- **Michael Schieschke**, August 2009. Development of Software for a Data Acquisition System for Geophysical Electromagnetic Measurements. (Supervisors, Lars Dynesius, Mehrdad Bastani)

REFERENCES

Bastani, M. (2001). EnviroMT - A New Controlled Source/Radio Magnetotelluric System. *Uppsala Dissertations from the Faculty of Science and Technology* 32. Uppsala University.

Becken, M. and Pedersen, L. B. (2003). Transformation of VLF anomaly maps into apparent resistivity and phase. *Geophysics*, 68 (2): 497-505.

Dynesius, L., Smirnov, M. and Pedersen, L. B. (2004). Multifrequency VLF/LF receiver. A new tool for fast and detailed mapping of near surface geology. *Report for the Geological Survey of Sweden, March 31, 2004*. Uppsala University.

Goldstein, M. A. and Strangway, D. W., 1975. Audio-frequency magnetotellurics with grounded electric dipole source: *Geophysics*, Vol. **40**, 669-689.

Guerin, R. And Benderitter, Y., 1995. Shallow karst exploration using MT-VLF and DC resistivity methods: *Geophys. Prosp.*, Vol. **43**, 635-653.

Larsen, J. C., Mackie, R. L., Manzella, A., Fiordelisi A., and Rieven, S., 1996. Robust smooth magnetotelluric transfer functions: *Geophys. J. Internat.*, Vol. **124**, 801-819.

McNeill, J.D. and Labson, V.F., 1989. Geological mapping using VLF radio fields. In: *Electromagnetic methods in applied geophysics*, Vol. **2**, part B (ed. M.M. Nabighian), Ch. 7, SEG, Tulsa.

McNeill, J.D., 1991. Advances in electromagnetic methods for groundwater studies: *Geoexploration*, Vol. **27**, 65-80.

Müller, A. (2000). A new method to compensate for bias in Magnetotellurics. *Geophysical Journal International*, 142: 257-269.

Oskooi, B. (2004). A broad view on the Interpretation of Electromagnetic Data (VLF, RMT, MT, CSTMT). *Uppsala Dissertations from the Faculty of Science and Technology* 959. Uppsala University.

Oskooi, B. and Pedersen, L. B. (2006). Resolution of airborne VLF data. *Journal of Applied Geophysics* 58: 158-175.

Paal, G., 1965. Ore prospecting based on VLF-radio signals: *Geoexploration*, Vol. **3**, 139-147.

Pedersen, L.B. (1982). The magnetotelluric impedance tensor – Its random and bias errors. *Geophysical Prospecting* 30: 188–210.

Pedersen, L.B., Qian, W., Dynesius, L., and Zhang, P., 1994. An airborne tensor VLF system. From concept to realisation: *Geophys. Prosp.*, Vol. **42**, 863-883.

Pedersen, L. B. and Oskooi, B. (2004). Airborne VLF measurements and variations of ground conductivity: A tutorial. *Surveys in Geophysics* 25: 151-181.

Pedersen, L. B., Bastani, M. and Dynesius, L. (2005). Groundwater exploration using combined controlled-source and radiomagnetotelluric techniques. *Geophysics*, 70 (1): G8-G15.

Pedersen, L. B. and Dynesius, L. (2008). Final report on the Multi Frequency VLF/LF receiver (MFR) project, September 2008. Uppsala University.

Persson, L. (2001). Plane Wave Electromagnetic Measurements for Imaging Fracture Zones. *Uppsala Dissertations from the Faculty of Science and Technology 30*. Uppsala University.

Reynolds, J. M., 1997. An Introduction to Applied and Environmental Geophysics: *Chichester, John Wiley & Sons, Inc.*

Setälä, T., A. Shevchenko and M. Kaivola / Degree of polarization for optical near fields, *Physical Review E* **66** (2002), pp. 016615: 1-7

Schieschke, M., 2009. Development of Software for a Data Acquisition System for Geophysical Electromagnetic Measurements. Master Thesis.

Tezkan, B., Goldman, M., Greinwald, S., Hordt, A., Muller, I., Neubauer, F.M., Zacher, G.A., 1996. Joint application of radiomagnetotellurics and transient electromagnetics to the investigation of a waste deposit in Cologne(Germany): *J. Appl. Geophys.*, Vol. **34**, 199-212.

Turberg, P., Muller, I., and Flury, F., 1994. Hydrogeological investigation of porous environments by Radio magnetotelluric-Resistivity (RMT-R 12-240 kHz): *J. Appl. Geophys.*, Vol. **31**, 133-143.

Vozoff, K., 1991. The magnetotelluric method: *Electromagnetic methods in applied geophysics*, Vol. **2**, No. 3, Nabighian, M. N., Ed., SEG Investigations in geophysics, 641-711.

Zonge, K. L., and Hughes, L. J., 1991. Controlled Source Audio-Frequency Magnetotellurics: *Electromagnetic methods in applied geophysics*, Vol. **2**, No. 3, Nabighian, M. N., Ed., SEG Investigations in geophysics, 713-809.

APPENDIX A

Post processing of airborne data from Multi Frequency Receiver system

Anna Gustavsson

Department of Earth Sciences - Geophysics
Uppsala University

Department of Physics
Umeå University

Examiner: Krister Wiklund, Umeå University
Supervisors: Mehrdad Bastani, Geological Survey of Sweden
Laust B. Pedersen, Uppsala University

Keywords: MFR, VLF, RMT, EnviroMT, Tipper, Scalar

The Master Thesis Work is performed at the Department of Earth Sciences – Geophysics, at Uppsala University.

Acknowledgements

There is always a special feeling to end a project – especially an interesting and instructive one like this. My initial intention with this project was to provide results that could be useful in the future process in the development of the MFR instrument. But real life project is not as fixed experiments in school. You do not now what the data looks like and the outcome is not always the expected. But as Thomas Edison once said: "*I have not failed. I've just found 10,000 ways that won't work*". I have still learned a lot – perhaps more than if everything worked correctly from the beginning.

I specially would like to thank my supervisor Mehrdad Bastani for his invaluable time he spent on me and all advices he gave me – especially that I had to learn patience when it looked as worst. I also want to thank Laust B. Pedersen for giving me the opportunity to make this master thesis project at the Geophysics department at Uppsala. Many thanks to Lars Dynesius for putting up with my sometimes stupid technical questions and Majid Beiki for giving me help with the software Oasis Montaj. I also want to thank everyone on the Geophysical department in Uppsala for giving me a good time and I wish you all the best in the future.

Last but not least I would like to thank my grandparents and my family for all things you have done for me during my studies. There is a lot more persons that I like to thanks. I do not mention any of you since I hope you know that you are all special to me anyway and that your support has done my education a lot easier.

It leaves some kind of sadness to not be involved in the final solving of the problems. I really hope that the next measurement provides better data so that the problems that occurred during this processing can be solved. Good luck with the future work with the project.

"Rivers know this: There is no hurry, we shall get there some day"
Winnie the Pooh

Anna Gustavsson

Uppsala, 2008-06-14

Abstract

In November 2007 an airborne measurement was carried out by the Geological Survey of Sweden (SGU) to test a new instrument called MFR, for airborne VLF+LF surveys. The instrument is developed by Uppsala University (UU) together with SGU. The aim with this new instrument is to extend the so-called Tensor VLF technique that is used today by SGU for geophysical prospecting and also producing different anomaly maps to a broader frequency range. The new developed instrument MFR (Multi Frequency Receiver) uses the electromagnetic signals from the distant radio transmitters in the frequency band 10 – 350 kHz and measures all three magnetic components of the primary and secondary signals. The latter arises due to the induction in the ground. The main ideas behind the concepts originate from another instrument developed by UU - the EnviroMT instrument (Bastani, 2001).

The airborne data acquisition was carried out continuously with a sampling frequency of about 800 kHz. The preliminary results show that there are some near-field sources of noise in the airplane that contaminate the data and highly affect the transfer functions estimated from the signal from the radio transmitters. Some of these near-field sources are known since an earlier test with the EnviroMT (2001) and originate from other SGU's measuring systems onboard the airplane. The main aim was to firstly find a method that identifies the near-field sources and then find a proper method to filter them out. Finally, new reliable electromagnetic transfer functions (tipper vectors) are calculated that can be used to obtain the resistivity structure of the ground.

Due to some technical problems during the measurement like high amplitude noise (around 120 Hz) coming from the airplane's engines and lack of a proper high pass filter a very low amplification gave rise to clipping phenomena in the registered time-series. Therefore the data were recorded with lowest amplification. This gave a very low signal to noise ratio (S/N) that led to poor data processing. Another source of noise was the other equipment used for routine airborne measurements by SGU. It seems the strongest source has a fundamental frequency of about 27.4 kHz and we could see it's even and odd harmonics up to 320 kHz. The noise was clearly seen in all three channels. Firstly an automatic technique to identify the ambient noise in the airplane was found. The technique worked as long as the noise level was low but in the air it failed. The filtering therefore had to be done by arranging a preferred frequency list that could be identified as noise. The final transfer functions were then calculated. They did not show the expected results from the SGU's previous measurements. The major problem was some striping generated in the map of the transfer functions. The artifacts were most probably due to some technical problems or error in the data processing program. The weak S/N-ratio is also an important factor so that a lower threshold had to be applied. This resulted in a lot more noise disturbing the calculations. This could be seen in the imaginary part of the tipper that did not show any fluctuations. On the other hand the estimated real part of the tippers (A,B) were rather stable and to some extent matched the variation seen in the SGU data.

Even if the results were not as expected they showed weaknesses in the system that had to be improved. Two controlling parameters that could give a considerable improvements in the processing are: Firstly to add a new high-pass filter to lower the noise from the airplane's engine and secondly to use a higher dynamic range (24 bits) to tolerate a larger difference in the signal to noise ratio in the band of interest. A new measurement will take place with a somewhat different hardware in august 2008. Hopefully this measurement will give better data quality and therefore a more realistic tipper vector estimation.

Sammanfattning

I november 2007 gjordes en flygmätning av Sveriges Geologiska Undersökning (SGU) i syfte att testa ett nytt instrument, MFR, för flygburna VLF+LF mätningar. Instrumentet är utvecklat av Uppsala Universitet (UU) tillsammans med SGU som ett forskningsprojekt. Målet med det nya instrumentet är att förbättra den så kallade Tensor-VLF teknik som SGU använder sig av idag för geofysisk prospektering och därmed kunna producera förbättrade anomalikartor med hjälp av ett bredare frekvensband. Detta nyutvecklade instrument, MFR (Multi Frequency Receiver) använder sig av elektromagnetiska signaler från radiosändare i frekvensbandet 10 – 350 kHz och mäter alla tre magnetiska komponenter för de primära och sekundära signalerna, där den senare uppkommer pga. induktion i marken. Grundidéerna bakom konceptet baseras på ett annat instrument, EnviroMT, som utvecklats av UU (Bastani, 2001).

Datainsamlingen under mätningen utfördes kontinuerligt med en samplingsfrekvens på ca 800 kHz. Det preliminära resultatet visar dock att det finns vissa störningar från närfälts källor i flygplanet som kontaminerar signalerna från radiosändarna och påverkar beräkningen av överföringsfunktionen. Några av dessa närfälts källor är kända sedan tidigare tester med EnviroMT (2001) och härstammar från olika mätsystem som finns i flygplanet. Målet med detta examensarbete är att först och främst att hitta en metod som kan identifiera och filtrera bort dessa störningskällor. När detta är gjort kan man beräkna nya tillförlitliga överföringsfunktioner (tipper vectors) som kan användas för att skapa kartor över resistiviteten i undersökningsområdet.

På grund av flygplanets motorer och brist på ett korrekt hög-pass filter under mätningen blev nivån på bakgrundsbruset väldigt hög. Detta medförde en låg förstärkning som gav upphov till distorsion i den registrerade tidsserien. Därför fick man ett svagt signalbrus (S/N) förhållande som gav sämre förutsättningar under själva databehandlingen. En annan källa för störningar kom från utrustning som används rutinmässigt av SGU under flygmätningar. Det verkar som den starkaste störningen har en fundamental frekvens av ca 27,4 kHz och dess udda och jämna multipler kan ses ända upp till 320 kHz. Bruset ses tydligt i alla tre kanaler.

Först försökte vi hitta en teknik för att filtrera störningsfrekvenserna automatiskt. Denna metod fungerade när nivån på bakgrundsbruset var lågt men inte för flygmätningarna. Filtreringen fick därför ske genom att göra en lista för de frekvenser som tydligt kunde identifieras som störningar och ta bort dessa. Den slutliga överföringsfunktionen kunde sen beräknas. Den överrensstämde dock inte med SGU:s tidigare resultat för området. Det största problemet var systematiska ränder i kartan för överföringsfunktionen. Detta problem beror med största sannolikhet på något tekniskt problem eller fel i databehandlingsprogrammet. Det svaga signalbrus förhållandet är också en viktig faktor eftersom man får använda ett lägre tröskelvärde som resulterar i fler störningar som påverkar beräkningarna. Detta kunde ses i den imaginära delen av tippern som inte visade några fluktuationer. Den reella delen av tippern (A,B) var däremot ganska stabil och överensstämde i viss utsträckning med variationer i SGU:s data.

Även om slutresultatet inte blev det förväntade visar de på saker att förbättra. Två kontrollparametrar som kan ge en avsevärd förbättring är: Ett nytt hårdvarufilter för att sänka nivån på bakgrundsbruset och att använda ett större dynamiskt område (24 bits) för att tolerera en större skillnad i signalbrusförhållandet. En ny mätning med något annorlunda hårdvara kommer att ske i augusti 2008. Förhoppningsvis kommer denna mätning att ge bättre datakvalité och därmed även mer realistiska tipper beräkningar.

Contents

Chapter 1

Introduction

In November 2007 an airborne measurement was done near Torsby, Sweden. The purpose was to test a new instrument called MFR, for airborne VLF+LF surveys developed by Uppsala University (UU) together with the Geological Survey of Sweden (SGU). The aim with this new instrument is to extend the so-called Tensor VLF technique that is used today by SGU for geophysical prospecting.

The MFR instrument is based on a method called Radio Magnetotelluric (RMT) that uses electromagnetic signals from distant radio transmitters in the frequency range 10 – 350 kHz (VLF+LF) to model the electrical resistivity of the earth. The model together with field observations can then be used to map or resolve structures in the survey area. The RMT method is an extension of the VLF technique.

SGU once started measuring signals from one VLF (10 – 30 kHz) transmitter. The drawback with the VLF method is that response from e.g. a fracture zone is dependent on the strike direction. That means that structures perpendicular to the strike are not imaged at all. Furthermore there are very few VLF transmitters to use today and this sometimes gives rise to either problems finding a transmitter in the right direction or very weak signals. Today measurements are done from two transmitters instead as an attempt to avoid directional dependency problem. On the other hand the VLF band is very narrow and the vertical resolution of the method is rather poor.

In order to overcome the poor resolution problem some developments to construct a new instrument called MFR (Multi Frequency Receiver) were suggested by Uppsala University (UU) in the form of a joint research project with SGU. The ideas originate from the main thoughts behind the concepts used in another instrument developed by UU, namely the EnviroMT instrument (Bastani, 2001). The concept is to improve the measurements by extending the measuring band to 350 kHz and also to make a more user-friendly instrument that a person can operate in the field to carry out RMT measurements. The instrument can be even used in the airborne measurements to extend the traditional VLF measurement band (10-30 kHz) to a much wider band like the one used in the EnviroMT. Since the RMT method uses the frequency band 10 – 350 kHz there is not only more transmitters to choose, the depth resolutions is also better and allows for quantitative inverse modelling in two and three dimensions (Oskooi and Pedersen, 2005). The instrument measures signals from multiple transmitters and chooses to save data from those transmitter that have a high signal-to-noise ratio.

The airborne measurements for this new system were carried out continuously with a sampling frequency of about 800 kHz. The preliminary results, however, show that there are some near-field sources of noise in the airplane that contaminate the signal from the radio transmitters and affect the calculated transfer functions. Some of these near-field sources are known since an earlier test with the EnviroMT (2001) and originate from other measuring

systems onboard the SGU's airplane. Most of these were measuring systems running in parallel with the MFR.

The main aim of this work is to find a method that identifies the near-field sources and a method to filter them out. After these have been filtered new reliable transfer functions can be obtained representing the resistivity structure of the survey area.

Chapter 2

Magnetotelluric

Magnetotelluric (MT) is an electromagnetic method used to image the electrical resistivity of the earth's structure from depths of a few 10 meters to several 100 kilometers. If an electromagnetic wave is generated, naturally or artificially, it can penetrate the Earth's interior. It will then decay with a rate depending on the wavelengths of the wave and also the electrical resistivity of the ground. Low frequency signals in a more resistive medium travel further down than signals with high frequencies in a less resistive medium.

By measuring the electric and magnetic components of the EM fields at the surface the electrical resistivity of the earth can be estimated. This is because different rocks give rise to different resistivities. In general, rocks containing fluids will have low resistivity while dry and cold rocks will have high resistivities. The model can then, together with field observations, be used in bedrock mapping or resolving boundaries in an area. Today electromagnetic data are mainly used in bedrock mapping, hydrogeology and mineral exploration purposes.

2.1 VLF method

The Very Low Frequency (VLF) method is a quick tool for mapping near surface structures. It was first used during the 1960's after discovering that the VLF signal can be used for geophysical exploration other than just to communicate with submarines. The first field tests in Sweden were made by SGU in Lappland and the tests showed that the method was very useful for mineral exploration and detecting other conductive structures.

Per definition, VLF uses the frequency band from 3 – 30 KHz and can be divided into two methods based on which parameters that are measured (Oskooi and Pedersen, 2005). The first method measures only the component of the elliptically polarized magnetic field. The other method measures one horizontal magnetic and one horizontal electric component. Normally, the electric component is measured perpendicular to the profile, parallel to the strike. The best response for e.g. a fracture zone is obtained for a transmitter located in the strike direction. Structures perpendicular to the strike are not imaged at all. If the measurement is done with data from only one transmitter this sometimes becomes a problem since the transmitter has to be in the right direction compared to the direction of the anomaly (Oskooi and Pedersen, 2006). Since 1995, however, most of SGU's VLF instruments are based on a technique developed by Pedersen et. al (1994) which uses information from two transmitters to overcome this problem.

Standard VLF-instrument measures the total field obtained from three orthogonal components of the magnetic field. But since the VLF data have a very narrow bandwidth, the signal received can be too weak in some situations to resolve structures in detail. The VLF method can still be good for getting an overview of the lateral extent of the conductors and of their depth distribution (Oskooi and Pedersen, 2005)

2.2 RMT method

The VLF methods use the frequency band from 3 – 30 KHz but during the recent years it has been extended to also involve frequencies in the so called Low Frequency (LF) band (30 – 300 kHz). The method that uses both the VLF- and LF band is called radio magnetotelluric (RMT) and is similar to the VLF method. Since RMT has a broader frequency range it resolves the upper as well as the lower parts of the structure better than VLF. This method is therefore very useful in investigations of shallow depth with high lateral and/or vertical resolution.

The source for VLF measurements is transmitters used for submarine communication while the source for LF is radio transmitters used for e.g. aircraft communication. During the last years some of the active VLF transmitters have been shut down and are not in use anymore. In Sweden and in Europe as a whole there are no more than 30 transmitters lying in the VLF frequency band 15 – 30 kHz. For transmitters that are using VLF and LF-frequencies, 15 – 250 kHz, there are a few hundreds of transmitters in Europe. The location for these transmitters can be seen in Figure 1.

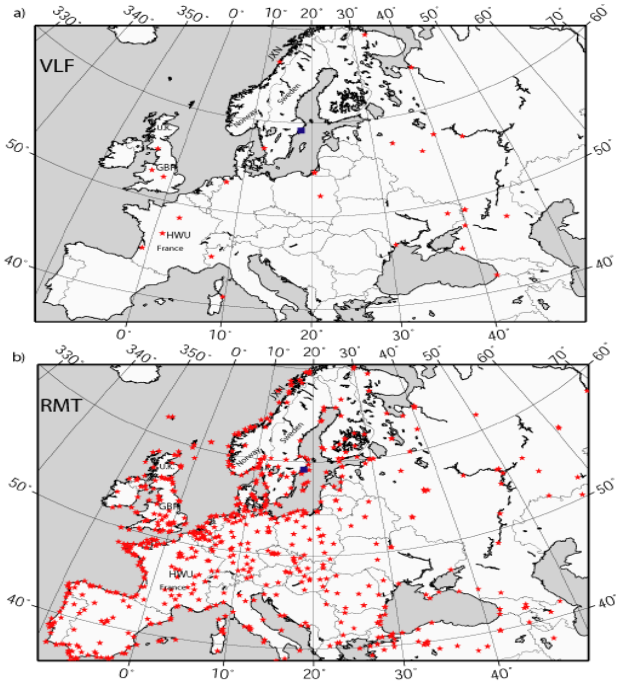

Figure 1. The location of a) VLF (15-30 kHz) and b) RMT (30-300 kHz) transmitters in Europe.

Chapter 3

Theory

In order to be able to describe the concepts behind magnetotelluric methods we have to start by looking at the fundamentals of the electromagnetic theory.

3.1 Maxwell's equations

There are four equations that summarize the theoretical content of electrodynamics. These are called Maxwell's equations. Assuming a time dependence as $e^{i\omega t}$ in the frequency domain they can be described as:

$$\nabla \cdot \mathbf{D} = \rho \qquad \textit{Gauss's law} \qquad (3\text{-}1)$$

$$\nabla \cdot \mathbf{B} = 0 \qquad \textit{no name} \qquad (3\text{-}2)$$

$$\nabla \times \mathbf{E} = -i\omega\mathbf{B} \qquad \textit{Faraday's law} \qquad (3\text{-}3)$$

$$\nabla \times \mathbf{H} = J + i\omega\mathbf{D} \qquad \textit{Ampere's law with Maxwell's correction} \qquad (3\text{-}4)$$

where in the SI system

E = electrical field intensity (V/m)
D = dielectric displacement (C/m^2)
B = magnetic flux density (T)
H = magnetic field intensity (A/m)
J = electric current density (A/m^2)
$\omega = 2\pi f$ = angular frequency (Hz)
ρ = electric charge density (C/m^3)

The vectorial magnitudes in Maxwell's equation for a linear, isotropic medium can be related through their constitutive relationships:

$$\mathbf{D} = \varepsilon\mathbf{E} \qquad (3\text{-}5)$$

$$\mathbf{B} = \mu\mathbf{H} \qquad (3\text{-}6)$$

$$\mathbf{J} = \sigma\mathbf{E} \qquad (3\text{-}7)$$

where

ε = electric permittivity (F/m)
μ = magnetic permeability (H/m)
σ = conductivity (S/m)

ε, μ and σ describe the intrinsic properties of the material through which the electromagnetic wave propagates.

3.2 The wave equation

The general form of the wave equations for the electric- and magnetic field can be derived from Maxwell's equations. First the constitutive relations are used to rewrite equation (3-3) and (3-4):

$$\nabla \times \mathbf{E} = -i\omega\mu\mathbf{H} \tag{3-8}$$

$$\nabla \times \mathbf{H} = \sigma\mathbf{E} + i\omega\varepsilon\mathbf{E} \tag{3-9}$$

By using these relationships we can now reduce Maxwell's equations to only contain **E** or **H** by applying the curl to the expressions. The solution for an electromagnetic wave traveling in a uniform medium then becomes:

$$\nabla^2\mathbf{E} + k^2\mathbf{E} = 0 \tag{3-10}$$

$$\nabla^2\mathbf{H} + k^2\mathbf{H} = 0 \tag{3-11}$$

These equations are also known as Helmholtz equations. The complex wave number, *k*, in the equations is defined as:

$$k = \left(\mu\varepsilon\omega^2 - i\mu\sigma\omega\right)^{1/2} \tag{3-12}$$

For frequencies in the VLF band (and some in the LF band) and in typical earth materials the assumption $\varepsilon\omega \ll \sigma$ can be made. The wave number can then be simplified (Persson, 2001):

$$k = \left(-i\mu\sigma\omega\right)^{1/2} \tag{3-13}$$

3.2.1 Plane waves

If a wave is traveling in the x-direction and has no y or z dependence, it is called a plane wave. This means that the electric and magnetic fields are perpendicular to the direction of propagation. These type of waves appear when waves traveling over long distances. The plane-wave solutions when the wave number, *k*, is complex becomes:

$$\mathbf{E}(x,t) = \mathbf{E}_0 e^{-kx} e^{i(kx-\omega t)} \tag{3-14}$$

$$\mathbf{B}(x,t) = \mathbf{B}_0 e^{-kx} e^{i(kz-\omega t)} \tag{3-15}$$

where $\mathbf{E}_0$ and $\mathbf{B}_0$ are the amplitude of the electric- and magnetic field, respectively. The imaginary part of *k* results in an attenuation of the wave, i.e. decreasing amplitude with increasing x.

3.3 Primary and secondary field

The electromagnetic field from a transmitter can be considered as an oscillating vertical electrical dipole. The radio signals far from the transmitter can be considered being a plane wave propagating in all directions. If the wave propagates in the x direction the electromagnetic field of this wave has a vertical electrical field component, E_z, and a horizontal magnetic field component, H_y. At very large distances from the transmitter this primary field may be considered uniform.

According to the electromagnetic theory (Faraday's principle of electromagnetic induction), the magnetic field from the transmitter, i.e. the radio wave, will induce a current in the Earth. Those eddy currents will in turn create a secondary magnetic field.

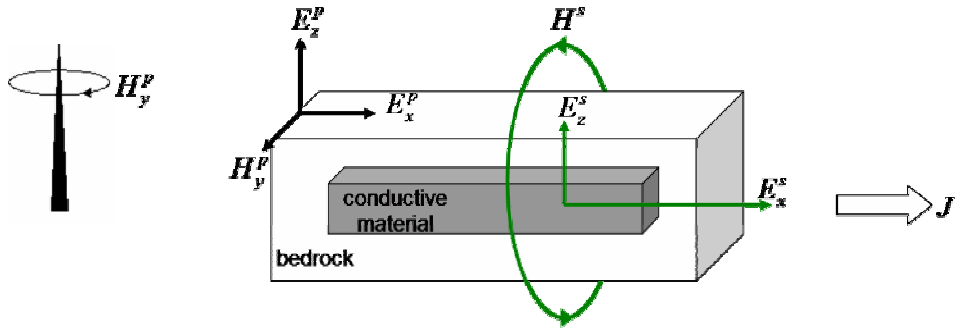

Figure 2. Induction due to the conductive ground. The magnetic field from the transmitter creates a current, J, in the Earth. Due to this current a small electric field is produced with electrical field components E_x^s and E_z^s.

In Figure 2 the induction due to the conductive ground is created by the horizontal magnetic field H_y. This creates the secondary field, with electric field components E_x and E_z. The E_z component can however be neglected in the ground. This secondary field can be phase shifted and oriented in another direction depending on the conductivity contrast and shape of the conductor.

3.4 The 1-D model

The simplest model of describing the earth is a homogenous half space where the conductivity is constant along the axes.

3.4.1 Skin depth

Equations (3-14) and (3-15) showed that there is an attenuation of the wave caused by the imaginary part of *k*. The distance it takes to reduce the amplitude by a factor of 1/e is called the skin depth and is a measure of how far the wave penetrates into the ground. Equation (3-14) can be solved for the amplitude at the surface, *z=0*, given that the complex wave number is:

$$k = \left(-i\mu\sigma\omega\right)^{1/2} = \alpha(1-i) \qquad (3\text{-}16)$$

where α is a real quantity defined by:

$$\alpha = \left(\frac{\omega\mu\sigma}{2} \right)^{1/2} \tag{3-17}$$

Putting that solution into equation (3-14) for an arbitrary depth and solving for z gives the skin depth:

$$\delta = \left(\frac{2}{\omega\mu\sigma} \right)^{1/2} \approx 503 \left(\frac{1}{f\sigma} \right)^{1/2} = 503 \left(\frac{\rho}{f} \right)^{1/2} \tag{3-18}$$

If the resistivity is 10 kΩm the skin depth for a frequency of 15 kHz is about 410 meters while for a frequency of 300 kHz with the same resistivity the skin depth is about 90 meters. Generally this means that if the resistivity is high and the frequency low the wave will penetrate deeper into the ground.

3.4.2 Phase

For a distant radio transmitter with the EM-wave propagating in the x-direction the components of the wave consist of a vertical electric component, E_z, and a horizontal magnetic component, H_y. If the ground is conductive the induction due to H_y creates a horizontal electrical field component, E_x, as could be seen in section 3.3.

From the wave equation (3-9) and equation (3-11) it can be shown that into a homogenous ground the fields will diffuse as an exponentially damped wave with E_x 45° ahead of H_y (Persson, 2001).

If the ground is non-homogenous, the phase difference between E_x and H_y depend on the resistivity of the horizontally layered earth. If the top layer has higher resistivity than the lower the phase will be bigger than 45°. If it is the opposite with the lower resistivity on top the phase will be less than 45°.

3.4.3 Impedance

The impedance for a plane wave is defined as the ratio between E_x and H_y:

$$Z = \frac{\omega\mu}{k} = \frac{E_x}{H_y} = -\frac{E_y}{H_x} \cong \left(\frac{\omega\mu}{\sigma} \right)^{1/2} e^{i\pi/4} \tag{3-19}$$

The last step is made by the assumption that for typical earth materials at frequencies used in magnetotelluric surveys the displacement current can be neglected. This shows that the impedance is a function of frequency and that it increases as the square root of frequency. The phase of the impedance for a homogenous half space is 45° - the same phase as between E_x and H_y in a homogenous ground.

3.4.4 Apparent resistivity

In reality the resistivity in the ground is not constant. Therefore something called apparent resistivity is used when making a simplification of the earth as a heterogeneous half space. Per definition apparent resistivity is *an average resistivity used for a volume average of a*

heterogeneous half-space and can be defined by using the relationship for the resistivity in the ground,

$$\rho = \frac{1}{\sigma} \tag{3-20}$$

in equation (3-19) and solve for the resistivity:

$$\rho_a = \frac{1}{\omega\mu}|Z|^2 = \frac{1}{\omega\mu}\left|\frac{E_x}{H_y}\right|^2 \tag{3-21}$$

3.5 The 2-D model

Most times the Earth can be approximated by a 2-D model. This means that the conductivity variation can be neglected along one direction, the so called strike direction. The coordinate axes are normally defined such that x goes in the strike direction, y is the profile direction and z is pointing downwards into the ground.

3.5.1 TM-mode

In the TM-mode the electric field is perpendicular to the strike and the magnetic field is in the strike direction as shown in Figure 3.

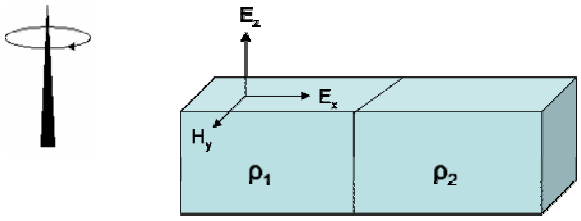

Figure 3. TM-mode (Transverse Magnetic mode) or H-polarization. The plane wave from the transmitter is propagating perpendicular to the strike, i.e. $H_z = 0$ (From picture by Persson, 2001).

Since the magnetic field is parallel to the strike there will be no variation over the contact. The electrical fields, however, give rise to discontinuities close to the boundary. If $\rho_1 > \rho_2$ in the model seen in Figure 3, then the apparent resistivity will decrease rapidly while the phase difference will have a peak over the boundary.

3.5.2 TE-mode

In the TE-mode the electrical field is in the strike direction. Since it is parallel to the boundary there will be no induced charges. Instead the electric field will vary continuously across the interface. The magnetic field will on the other hand change over the boundary since the conductivity increases in a conductor. This will magnify the currents and this change is reflected in the vertical component. The resultant magnetic field is elliptically polarized.

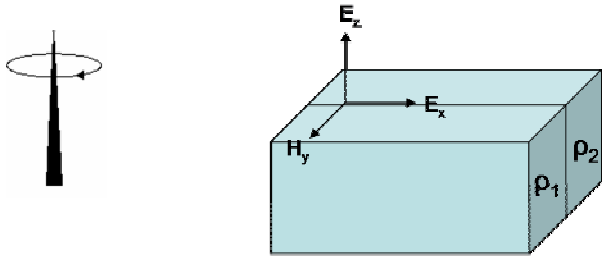

Figure 4. TE-mode (Transverse Electrical mode) or E-polarization. The plane wave from the transmitter is propagating parallel to the strike, i.e. $E_z = 0$ (From picture by Persson, 2001).

For an electrical field in TE-mode the apparent resistivity shows a continuous decay over the boundary. This decay is dependent on the frequency. If the frequency increases the decay will become more rapid. The phase difference over the boundary will look the reversed compared to the TM-mode.

3.5.3 Impedance and tipper vector

The impedance and tipper are quantities that are used when interpreting the measured magnetotelluric data. For a plane wave there exists a linear relationship between the electric field components (Ex,Ey) and the two horizontal magnetic field components (Hx,Hy) and the vertical magnetic field component (Hz), for a general conductivity distribution. From these relationships the impedance and tipper can be expressed.

Impedance

The horizontal components of the electromagnetic field are related through the impedance tensor as:

$$\begin{bmatrix} E_x \\ E_y \end{bmatrix} = Z \begin{bmatrix} H_x \\ H_y \end{bmatrix} \tag{3-22}$$

The complex impedance tensor is given by:

$$Z = \begin{bmatrix} Z_{xx} & Z_{xy} \\ Z_{yx} & Z_{yy} \end{bmatrix} \tag{3-23}$$

If the coordinate system is defined with x in the strike-direction, the impedance tensor has a simple structure. From the TE- and TM modes the 2-D impedance vector can then be defined as:

$$Z = \begin{bmatrix} 0 & Z_{xy} \\ -Z_{yx} & 0 \end{bmatrix} \tag{3-24}$$

where $|Z_{xy}| \neq |Z_{yx}|$.

When measuring, the strike angle, φ, must be known. The determinant of Z is called the effective impedance and is an average of the impedance in all current directions. It is defined as:

$$Z_{DET} = \sqrt{Z_{xx}Z_{yy} - Z_{xy}Z_{yx}} \quad (3\text{-}25)$$

It is however useful in such way that it makes the impedance tensor independent of the strike direction. According to equation (3-24) Z_{xy} corresponds to the TE-mode while Z_{yx} correspond to the TM-mode. The effective impedance can therefore be considered being the mean of the mode data and no mode identification is required. The effective impedance thereby represents an average that can be inverted to provide robust 1D and 2D models (Oskooi, 2004).

Tipper

The geomagnetic transfer function called tipper describes the connection between the horizontal and the vertical magnetic field components:

$$H_z = AH_x + BH_y \quad (3\text{-}26)$$

The tipper vector *(A,B)* can thereby be defined just by measuring the vertical components of the magnetic field. It is independent of the actual source current and thereby only dependent on the internal conductivity.

For a homogenous or a layered earth (1-D) the tipper quantity does not exist, i.e. $A = B = 0$. However, most of the times the Earth can be approximated by a 2-D model. If the TE- and TM-mode is used in the coordinate system for the strike, as for the impedance, the 2-D tipper can be found. With the x-axis is in the strike direction *A* becomes zero and we get:

$$H_z = BH_y \quad (3\text{-}27)$$

The tipper will therefore vary along the measured profile. The strongest variation of the tipper is close to a resistivity contrast. For a tipper in 3-D structure both $A \neq 0$ and $B \neq 0$ and equation (3-26) are used for the calculations.

The interpretation of the tipper can be done either by mapping or modelling. In the mapping procedure the tipper values are transformed into the apparent resistivity and phase based on the method developed by Becken and Pedersen (2003) creates electrical resistivity maps. The modelling is done with least square inversion and image the electrical resistivity depth sections.

Real and imaginary part of the tipper in TE-mode

Except for the apparent resistivity and phase difference for a field in TE-mode the variations of the real and imaginary component of the tipper can also be investigated.

The real part of the tipper always point away from the conductor. This means that for a given frequency the real part change sign when crossing a conductor. The imaginary part is more complex since it is dependent of the depth of the conductor. Usually, if there is a conductor at a given depth, the imaginary part change sign from positive to negative with decreasing frequency (Pedersen et al., 2005).

The reason why the imaginary part of the tipper vector is more complex is that it contains the response from two wavelengths with two different polarizations. The first has a short-wavelength response with same polarity as the real component. The second has a long-wavelength response with opposite polarity compared to the real component. This makes the imaginary component dependent of depth. If the depth increases the short wavelength response will disappear. This will leave only the long-wavelength response left with the reversed polarity. For small resistivity variations near the surface this can be seen as anomalies with same polarity for both the real and the imaginary component. If there instead is a conductive target or deep low-resistive structures this is seen as anomalies with reversed polarity in the imaginary part (Persson, 2001).

3.5.4 Scalar and tensor transfer functions

In the VLF and RMT methods the signal from radio transmitters with nearly distinct frequencies are used to estimate the earth electromagnetic transfer functions, namely impedance and tipper vector. There are several techniques to estimate the transfer function. Bastani (2001) introduces scalar and tensor transfer functions which are described here.

Estimation of scalar tipper

The scalar transfer function is calculated with respect to either the transmitter coordinate system or the strike direction. This means that the y-axis is perpendicular to the transmitter-receiver direction or the strike direction. The significance of the scalar tipper is different depending on if the measurement is done with two or three magnetic components. This difference has been discussed by Pedersen and Oskooi (2004):

Calculation of scalar tipper with two magnetic components

If one horizontal (H_y) and one vertical component (H_z) of the magnetic field are measured, as in standard VLF measurements, and if the strike direction is in the x-direction, then the derived scalar transfer function $B^{scalar} = H_z / H_y$ is identical to the unique tipper component B and the component A is equal to zero. If the strike direction, however, is in another direction other than the x-axis, then it is no longer possible to compensate for the rotation by some correction factor. This means that the true transfer function can not be recovered from the measured scalar transfer function, B^{scalar}.

Calculation of scalar tipper with three magnetic components

If the measurement instead is done using three orthogonal magnetic sensors, then a 2-D structure having a strike angle, θ, with respect to the x-axis can be modelled. The horizontal components of the magnetic field can then be used to calculate the field in an arbitrary direction. In this case, as can be seen later, equation (3-37) can be used to calculate the scalar transfer function. This would be identical to the true 2-D tipper along a profile perpendicular to the strike.

Tensor measurement

If three magnetic field components from two transmitters with slightly different frequencies and a nearly orthogonal direction are measured simultaneously, then for each transmitter the total field is given by:

$$T = \left(|H_x|^2 + |H_y|^2 + |H_z|^2 \right)^{1/2} \qquad (3\text{-}28)$$

Map of T contains some useful information about the conductivity structure in a study area. For example the maximums in T describe the conductive structures, especially those with the strike direction parallel to the transmitter. By measuring from two transmitters simultaneously two linear equations can be obtained. From these the tipper vector can be calculated for each measuring point. This method gives a response that is independent of the transmitter direction in addition to the scalar transfer function.

3.5.5 Rotation of coordinate system

In practice, measuring is often done in another coordinate system than the strike coordinate system (principal coordinate system). For measurements with radio magnetotelluric (RMT) methods the coordinate system for the transmitter is used instead, which is better in some situations, for example when calculating the scalar tipper.

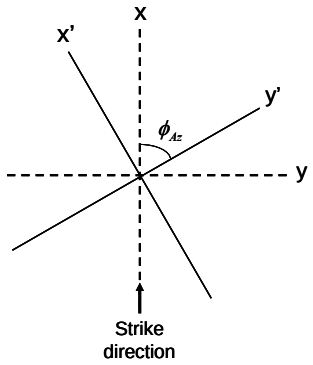

Figure 5. The measured coordinate system (x',y',z) compared to the principal coordinate system (x,y,z).

As mentioned earlier, the primary signal from transmitter induces a secondary current in the Earth. This gives rise to an electric field along the transmitter direction and also a horizontal magnetic field. The magnetic field is rotated by 90 degrees with respect to the electric field and is usually less distorted by lateral conductivity changes. It can therefore be used to estimate the direction to the radio transmitters. This is done by rotating the coordinate system such that the power of magnetic field in the transmitter direction is minimized. The azimuths, ϕ_{Az}, are measured from the magnetic north towards the east.

$$\phi_{Az} = \frac{k\pi}{2} + 0.5 \cdot \tan^{-1}\left[\frac{2 \cdot \mathrm{Re}\left(H_x^* H_y\right)}{\left(|H_x|^2 - |H_y|^2 \right)} \right], \quad k = 0, 1 \qquad (3\text{-}29)$$

Equation 3-29 yields a minimum and a maximum in horizontal magnetic field. To find the angle of minimum power the second derivative of the H_x power in the rotated coordinate system is calculated:

$$2\left(|H_y|^2 - |H_x|^2 \right) \cdot \cos(2\phi_{Az}) - 4\left[\mathrm{Re}\left(H_x^* H_y\right) \cdot \sin(2\phi_{Az}) \right] \qquad (3\text{-}30)$$

The angle with a positive second derivative is the answer.

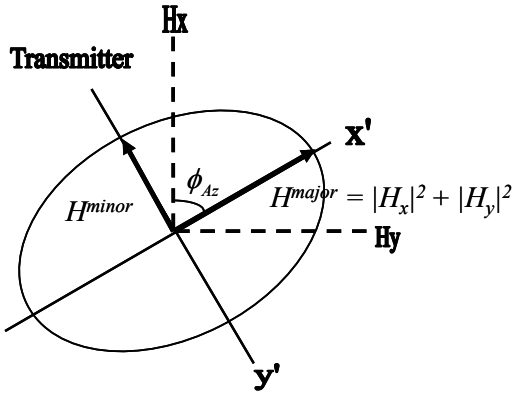

Figure 6. Rotation of the coordinate system. The azimuths are measured from the magnetic north towards the east. Here is the rotated H_y component equal to the H^{major}-axis, i.e. $|H_x|^2 + |H_y|^2$. The direction to the transmitter and H^{major} are always perpendicular to each other. The H_z component (out of the paper) is the same after the rotation.

The relationship between the measured and principle electromagnetic field components is:

$$\begin{bmatrix} E'_x \\ E'_y \end{bmatrix} = R^T \begin{bmatrix} E_x \\ E_y \end{bmatrix} \tag{3-31}$$

$$\begin{bmatrix} H'_x \\ H'_y \end{bmatrix} = R^T \begin{bmatrix} H_x \\ H_y \end{bmatrix} \tag{3-32}$$

where the components with a prime are the measured electromagnetic field components and R is the rotation matrix defined by:

$$R = \begin{bmatrix} \cos\phi_{Az} & -\sin\phi_{Az} \\ \sin\phi_{Az} & \cos\phi_{Az} \end{bmatrix} \tag{3-33}$$

The tipper vector can now be rewritten with the rotated coordinates:

$$H'_z = B' \cdot H'_y \tag{3-34}$$

B' is the same as B^{scalar} and since there is no rotation in z-direction $H'_z = H_z$. The tipper can thereby be written as:

$$H_z = B^{scalar} \cdot H'_y \tag{3-35}$$

Finally, if H'_y is defined from equation (3-32), the expression for B^{scalar} can be written as

$$B^{scalar} = \frac{H_z}{-H_x \sin\phi_{Az} + H_y \cos\phi_{Az}} \tag{3-36}$$

3.5.6 Degree of polarization

The degree of polarization is an important quantity since it gives a correlation between the orthogonal components of the electromagnetic field. For a planar wave this can be described in terms of the 2×2 coherence matrix.

The spectral matrix elements can be defined as:

$$S_{ij} = H_i^* H_j \tag{3-37}$$

where i,j = x,y,z. The coherence matrix in 2-D can then be written as:

$$\phi = \begin{bmatrix} S_{xx} & S_{xy} \\ S_{yx} & S_{yy} \end{bmatrix} \tag{3-38}$$

The coherence matrix can be uniquely decomposed into a sum of two matrices. The first one corresponds to fully polarized and the second to fully non-polarized wave. The degree of polarization can then be expressed as the ratio of the intensity (or trace) of the polarized part to the total intensity of the field (Setälä et al., 2002).

For a 2-D field the degree of polarization can be expressed as:

$$P = \left(1 - \frac{4 \det(\phi)}{[trace(\phi)]^2} \right)^{1/2} \tag{3-39}$$

The degree of polarization is useful in that sense that for one particular transmitter the polarization is the same. Generally, if time dependence ($e^{i\omega t}$) is used, the real and imaginary parts are of opposite polarity. In most cases the real part dominates over the imaginary part (Oskooi and Pedersen, 2006).

3.5.7 Estimation of random errors of the transfer function

Pedersen (1982) have a discussion about error estimation of the transfer function and the difference between random and systematic (bias) error. The random error is rather insensitive to noise in the magnetic field but the error increases with increasing S/N ratio in the electric field. For the bias error it is opposite – it increases with increasing S/N ratio in the magnetic field.

To decide whether the noise in the measured data are small or not it is necessary to distinguish between the input and output channel (Müller, 2000). This is done by assuming that the input channel is “noise-free”. The output channel, however, can be estimated by adding Gaussian noise to the output data. The data fit can then be calculated as the coherence between the predicted and the measured output data. If this coherence is close to one (i.e. unity) then the data fit between the measured and the predicted data is good. This means that the error is small and thus there is little noise in the data. If the coherence however is much smaller than one, then the noise is large.

There is a difference in the estimate of the error depending on whether the noise is in the output or input channel. If the noise is in the output channel, then the estimation is correct. If

the noise however is in the input channel then the error is biased (systematic) and the calculated estimation can not be used. Since the estimation of the error is based on the fact that the amount of possible bias depends on the coherence, there are no difference which one of the channels that are in- or output if the coherence is close to one (the bias is small).

The general equation for coherence between two input channels (where i,j = x,y,z) can be written as:

$$\gamma_{ij}^2 = \frac{\sum_{k=1}^{n} \left| S_{ij}^k \right|^2}{\sum_{k=1}^{n} S_{ii}^k \sum_{k=1}^{n} S_{jj}^k} \tag{3-40}$$

The coherence between the input and output channels, *m*, is:

$$\gamma_{mij}^2 = \frac{\sum_{k=1}^{n} \left(S_{mm}^{(p)} \right)^k}{\sum_{k=1}^{n} S_{mm}^k} \tag{3-41}$$

$\left(S_{mm}^{(p)} \right)^i$ is the auto-power of channel *m* as predicted from the horizontal magnetic field. As an example these two expressions can be used for estimating the variance of the impedance Z_{xx} where the two input channels are (H_x, H_y). The result then becomes:

$$\sigma_{Z_{xx}}^2 = \frac{1}{N-4} \frac{1-\gamma_{412}^2}{1-\gamma_{12}^2} \frac{\sum_{i=1}^{n} S_{44}^i}{\sum_{i=1}^{n} S_{11}^i} \tag{3-42}$$

where $N = 2n*N_s$ is the number of degrees of freedom and N_s is the number of stacks (Bastani, 2001).

Chapter 4

Radio Magnetotelluric

4.1 Far-field radio transmitters

As one could see in Figure 1, the number of RMT transmitters located in Europe is considerably higher than for VLF transmitters.

Figure 7 shows an example of amplitude spectra from a measurement done by the EnviroMT instrument in Colledoom, Netherlands (Bastani, 2001), where the transmitters and the different frequency bands are shown.

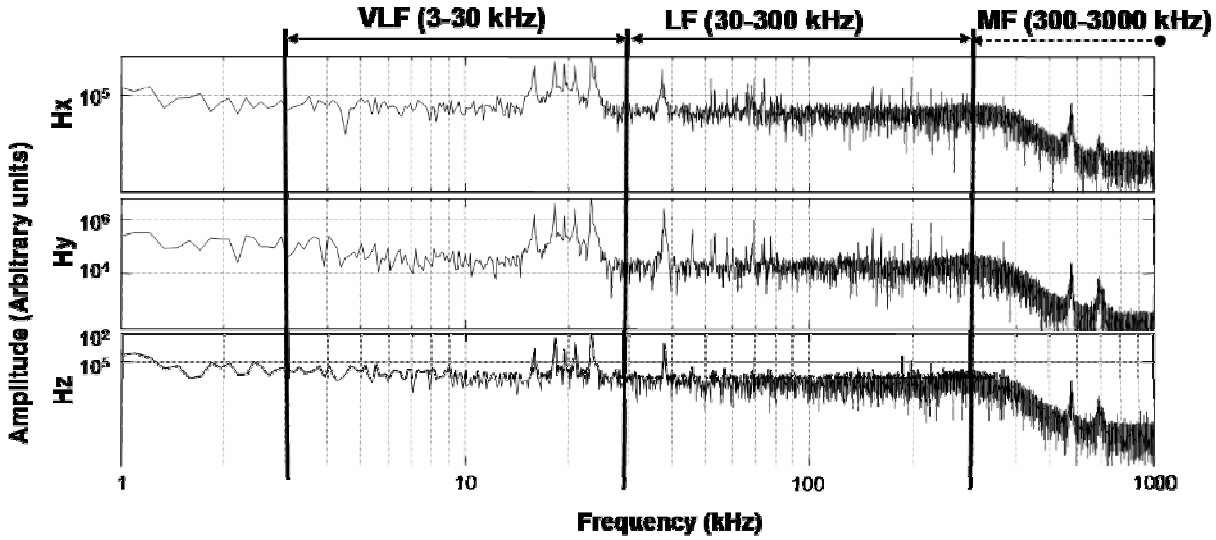

Figure 7. Example of an electromagnetic amplitude spectra (arbitrary units) from Collendoorn, The Netherlands, November 1998. (Bastani, 2001)

4.2 Near-field sources

The field far away from a transmitting antenna can be considered being plane. Near the antenna the field is more complex. The near-field sources can be of different origin such as electronic noise of instrumentation, unbalanced power consumption or cables. When performing measurements the result can therefore include a combination of both near- and far-field sources.

Since normal equations are no longer valid another type of equations has to be used. One way to overcome this problem is to separate the far-field sources from those nearby. This can be done by looking at the tipper data.

Generally the real part of the tipper vector points away from a conductor in the far-field. For

near-field sources the tipper will point towards the source instead (Pedersen et al., 2005). This means that for far-field transmitters the real and imaginary parts of the tipper vector are changing smoothly since they are a function of conductivity structure below the measuring profile. For the near-field sources, the tipper will instead point almost towards a fix location, namely the source location. The near-field frequencies can therefore easily be detected by calculating the scalar tipper along the measuring line.

To remove these frequencies a digital notch filter can be used prior to the main transfer function calculation. Another method to find the near field sources is to use the tensor tippers and then calculate the prediction error for each individual index in the band of interest. Those indices having a prediction error greater than a certain value can be rejected.

4.3 RMT processing overview

The measured signals from the radio transmitters are saved as raw time series. To convert these raw time series to electromagnetic transfer function several processing steps must be performed.

4.3.1 Fast Fourier Transform (FFT) and spectral matrix

The Fast Fourier Transform (FFT) reduces the number of calculations for N data points to a raw spectrum with N/2 frequency indicies. Therefore are the relations between the input and output channels much simpler in the frequency domain then in the time domain. If the raw time series are divided into a number of time segments, then the FFT can be used for each segment to find the complex spectrum of that channel. Since the frequency range for RMT signals are between 10 and 350 kHz only the spectrum in the band of interest is analyzed.

One problem that can occur is that some signals are not in complete phase stability over the total measurement interval. The solution is that the spectra are converted into auto and cross powers which are the product of the field components and their complex conjugates. These are stored in a three dimensional spectral matrix, **S**, which contains the contribution from all the segments (real and imaginary parts of the auto and cross powers) for each frequency index.

4.3.2 Transmitter picking

The radio transmitters are located all over the world. Depending on their location and transmitting power they appear in spectrum with different S/N ratios.

Finding the Signal-to-noise ratio

The Signal-to-Noise ratio (S/N or SNR) is a measure of the signal strength relative to the background noise and is a function of transmitter strength, distance to the transmitter as well as the bandwidth used. Normally the aim is to increase the S/N ratio. This can be done partly by applying some noise reducing filters or signal amplification if necessary.

In the processing used in this study, the S/R is defined as the ratio between the total horizontal magnetic field energy and the background energy. The background noise is defined as the median filtered total horizontal field, a method of making a reference curve for the background noise where the width of the filter affects the estimated noise level (Figure 8).

Usually is the magnetic field less noisy than the electric field and the transmitting power is more or less stable in a survey area. Therefore, by choosing a threshold for the S/N ratio, radio transmitters can be detected automatically and only data with S/N ratio above this threshold will be saved to the spectra file.

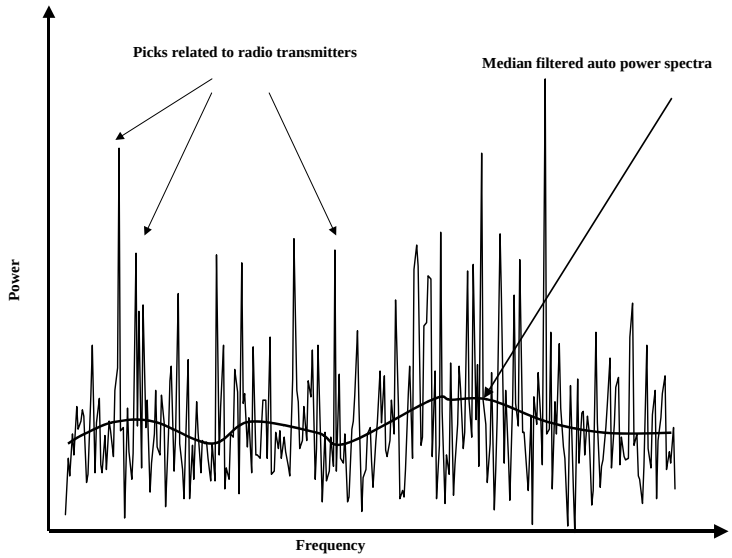

Figure 8. A synthetic example of an auto-power spectrum and its median filtered spectrum. The noise level is found from the median spectrum. (Bastani, 2001)

Automatic determination of directions to radio transmitters

As mentioned in chapter 3.5.5 a secondary current is induced in the Earth that generates a small electric field along the transmitter direction and a horizontal magnetic field rotated by 90 degrees with respect to the electric field. Since the magnetic field is less distorted by lateral conductivity changes the direction to the transmitter can hence be found. The transmitter azimuths are obtained from equation (3-29):

$$\phi_{Az} = \frac{k\pi}{2} + 0.5 \cdot \tan^{-1}\left[\frac{2 \cdot \mathrm{Re}(S_{12})}{(S_{11} - S_{22})}\right], \qquad k = 0, 1 \qquad (4\text{-}1)$$

where the S_{ij}'s are the auto and cross powers of channel i and j. Here is channel 1 corresponding to the magnetic north and channel 2 to the magnetic east.

Removal of strong local sources

Local/near field sources often have high S/N ratios. One simple way to remove these is to use a digital notch filter. It acts on the S/N ratio before the transmitter selection. If the central frequency and bandwidth of the filter can be specified, it forces the measured values to zero for the central frequency and frequencies within half a bandwidth around it. For the EnviroMT (Bastani, 2001) the system can handle three different specified frequencies and their aassociated third and fifth harmonics.

4.3.3 Locked estimating

When measuring a lot of frequencies is saved, but only a few of these are detected transmitters and needed to estimate the transfer functions. Therefore a new spectral matrix is formed containing only the selected frequencies. The subsequent stacking is then *locked* to this new spectral matrix in order to speed up the processing. The transfer functions and their standard error can then be estimated after some procedures.

Band splitting and averaging

The idea behind the band splitting used here is based on that transfer functions for naturally sources in magnetotelluric are estimated in narrow bands of either one half or one octave. One octave is by definition the interval between two points where the frequency at the second point is twice the frequency of the first. Figure 9 shows the band splitting to provide two sets of transfer functions: the main band is split into 10 narrower sub-bands with a bandwidth of half an octave and 9 overlapping sub-bands with a bandwidth of one octave. The geometric mean of the minimum and maximum frequencies in each sub-band is defined as the nominal target frequency.

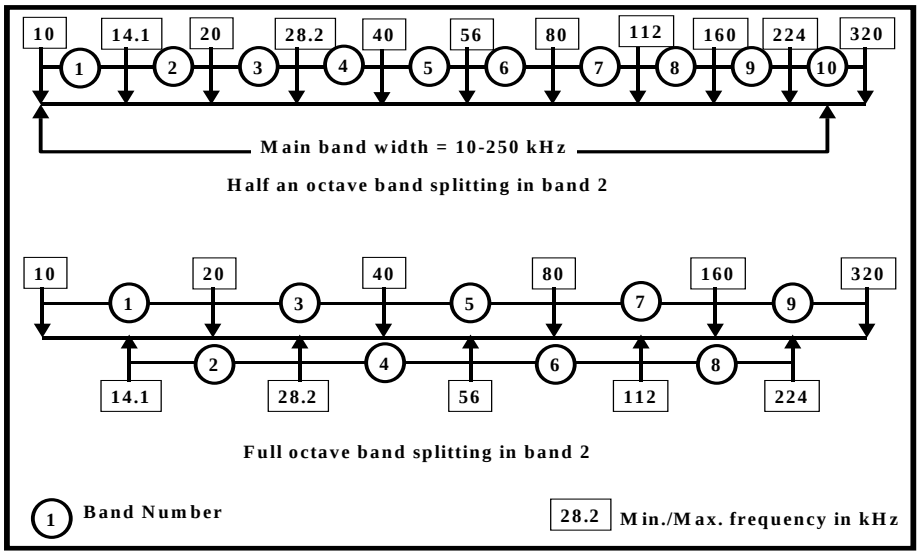

Figure 9. An example of band splitting in RMT processing for band 2. The first full octave sub-band starts at 10 kHz and ends at 20 kHz. The nominal frequency is then about 14 kHz. (Bastani, 2001)

In the calculation for a natural magnetotelluric source the transfer functions in each sub-band are assumed to be constant, independent of the frequency. In practice the input channel, composed of the horizontal magnetic field component, is noise free. Therefore can all frequencies belonging to a narrow sub-band be solved for transfer functions by using the least squares method. This approach is called the *band averaging technique* and is a well-known processing method. It minimizes the total prediction error energy of each output channel over the entire sub-band. For the RMT method are transmitter frequencies belonging to a sub-band selected. If there are two or more independent transmitters then there are sufficient equations to determine the unknown transfer functions (Bastani, 2001). As an example, the transfer function of the electric field in x-direction becomes:

$$\hat{Z}_{xx}(\omega_t) = \frac{\sum_{i=1}^{n} S_{22}^i \times \sum_{i=1}^{n} S_{14}^i - \sum_{i=1}^{n} S_{12}^i \times \sum_{i=1}^{n} S_{24}^i}{\sum_{i=1}^{n} S_{11}^i \times \sum_{i=1}^{n} S_{22}^i - \sum_{i=1}^{n} S_{21}^i \times \sum_{i=1}^{n} S_{12}^i}$$

$$\hat{Z}_{xy}(\omega_t) = \frac{\sum_{i=1}^{n} S_{11}^i \times \sum_{i=1}^{n} S_{24}^i - \sum_{i=1}^{n} S_{21}^i \times \sum_{i=1}^{n} S_{14}^i}{\sum_{i=1}^{n} S_{11}^i \times \sum_{i=1}^{n} S_{22}^i - \sum_{i=1}^{n} S_{21}^i \times \sum_{i=1}^{n} S_{12}^i} \qquad (4\text{-}2)$$

ω_t is the target frequency defined as the geometrical mean of the n transmitter frequencies in the sub-band and S_{ij}'s are the spectral matrix elements defined as

$$S_{ij} = C_i^* C_j . \qquad (4\text{-}3)$$

C_i stands for one of the measured electric or magnetic field components numbered from 1 to 5 corresponding to H_x, H_y, H_z, E_x, and E_y respectively (Bastani, 2001). The asterix denotes complex conjugation.

Estimation of random errors of transfer functions

After the transfer functions have been calculated the random error can be estimated as shown in chapter 3.5.7.

Chapter 5

The MFR instrument

The instrument used by the Geological Survey of Sweden (SGU) today is called Wadi by ABEM AB and is only measuring signals from one transmitter. As mentioned before the response from e.g. a fracture zone is dependent on the strike direction. Since there are so few VLF transmitters this sometimes give rise to problems finding a transmitter in the right direction. The Wadi instrument is mainly used for investigations of the quality and featuring of the bedrock. The depth resolution is very poor since the frequency band is just 16 – 30 kHz and in a few surveys the transmitter signal has been too weak to resolve any structures at all.

The concept behind the EnviroMT instrument developed by Uppsala University (Bastani, 2001) was to improve the measurements by using the RMT method instead of VLF. Unlike the Wadi instrument it measures the signals from many transmitters and chooses those with a S/N ratio above a certain threshold. Since the RMT method uses the frequency band 15 – 250 kHz there is not only more transmitters to chose between, the depth resolutions is also better. The measurements are independent of the direction to the transmitter since it measures all three magnetic components. The drawback with EnviroMT compared to Wadi is the measuring time at every point and the size of the equipment itself. The Wadi instrument has a measuring time of 5 sec and the equipment is easy to carry around since it is light and user-friendly. The EnviroMT instrument on the other hand, is heavy (ca 25 kg) and bulky. Therefore it must be handled by at least two persons. The measuring time is as long as 2 min.

The new MFR instrument is based on the concepts used in the EnviroMT system but it should be simple and user friendly as the Wadi instrument. At the end the thought is that it will become so easy that it can be handled by just one person in field.

5.1 The instrument

The principal for the MFR instrument is described by Bastani et al. (2004). It can be operated in two data acquisition modes: automatic or manual. In the automatic mode the measurement is done continuously when moving the instrument. In the manual mode the measurement is done at discrete equidistant points along a profile manually by the operator. The positioning data is stored together with the result and is governed by a differential GPS receiver.

The magnetic sensor is an orthogonal three component coil magnetometer with a sensor length of 15 cm. The orientation of the magnetometer (roll, tilt and heading), and the electrode rig will also be measured and stored. The magnetometer will operate in the frequency band 14-350 kHz and can be used for ground measurements as well as in an airplane. The approximately weight of the rig for ground measurements (Figure 10) are about 8 kg.

Figure 10. The MFR equipment for ground measurements. (Picture by M. Bastani)

The instrument is mainly a data acquisition instrument where the measured data is processed and displayed for each station along a profile. After the measurement is completed the data can be transferred to an external computer for further processing.

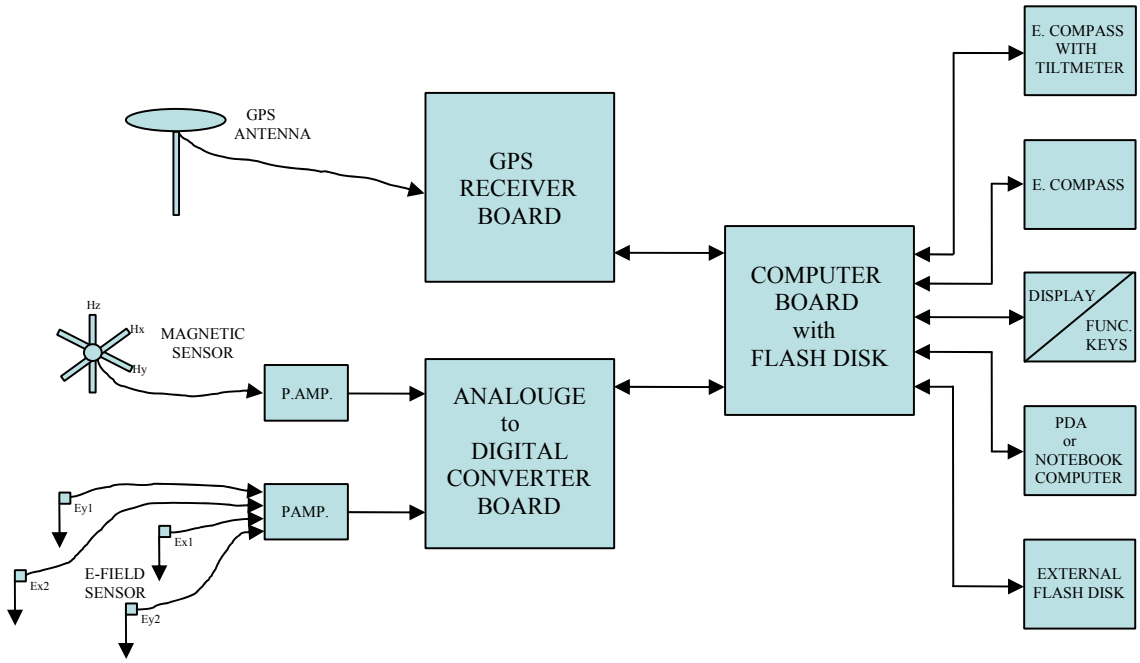

Figure 11. Block diagram of the multi-frequency receiver.

5.2 MFR airborne data processing overview and interpretation

The airborne data acquisition time series are recorded continuously for just three magnetic field components on a disk and GPS information are in parallel saved in another file. This is due to the fact that measuring the horizontal electric field of a vertical electric dipole in the air is almost impossible. The MFR airborne data processing is partly different than the traditional data processing and is described in the next section.

5.2.1 Time series

The transfer functions are estimated from processing of the measured data. The raw time series (RTS) recorded from the measurements are in this case divided into a number of time segments with a tuneable length. This gives a lot more freedom to control the quality of the estimated transfer functions. The longest number of samples, N, is 2^{18} (256 k) and the sampling frequency, F_s, 800 kHz. Using the longest segment a frequency resolution, $\Delta f = F_s/N$, of about 3 Hz is achieved. Compared to the EnviroMT data with a segment length of 16 k samples and sampling frequency of 2 MHz (frequency resolution of 122.2 Hz) , the MFR has 40 times accuracy in resolving the peaks from the radio transmitters. The long segment also provides a good control on the S/N ratio since the transfer functions are calculated in the frequency domain.

5.2.2 Conversion to the frequency domain and spectra files

The recorded time series are then processed on the ground to estimate the tipper components. For each time segment the measured magnetic fields are converted from time to the frequency domain using Fourier Transformation (FFT). This will create a raw spectrum with N/2 frequency indices. The transmitters are then selected based on the method described in section 4.3.2. The raw data contain three magnetic field components that were processed in advance and saved in spectra files containing index, frequency, S/N ratio and the real and imaginary parts of the magnetic field components. The spectra files also include headers containing timestamp, number of transmitters and the position of the plane among other things (see Appendix B for details). For processing of the raw data a width of 200 samples was used in the median filtering and the chosen S/N threshold was put to 6 dB. The raw spectra files were used for processing of the data within the extent of this thesis work.

5.2.3 The filtering process

SGU carried out some test measurements with the EnviroMT instrument from Uppsala University in 2001. The project aimed at studying the possibilities to replace SGU's old dual VLF system with the multi-frequency RMT system. Due to some limitations on the SGU's receiver antenna the results were not satisfactory. The test measurements also showed that there are some artifacts (local noise sources) coming from the other equipment on board the airplane. The frequency content of these noise sources was well known and studied. Therefore these frequencies could be filtered before calculating the transfer functions. This can be done manually or automatically. The filtered data are then saved in a new spectra file for further processing. To decide whether a frequency could be identified as noise or not was to primary look at the S/N ratio data, the tipper data and the direction for some kind of correlation.

The peaks for the S/N-data were considered to be some kind of transmitter. The first step was to plot these peaks for the horizontal S/N ratio for the unfiltered data and try to see whether some noise could be identified or not. The plot showed very clearly a harmonic noise frequency of 27.4 kHz. This could be seen even more clearly when plotting the normalized magnetic amplitude (H_{xyz}). The amplitudes for these frequencies were 4-10 times bigger than for the rest of the frequencies. These could therefore easily be removed by picking a threshold, but to avoid that the chosen threshold also takes away desired data it preferably has to be combined with some other method. The harmonic frequency was used as a reference when investigating other methods.

According to the theory, the tipper from a near-field source that moves with the source, i.e. the airplane located 60 meters above the ground, should be a rather constant function compared to the tipper for the far-field transmitters. The main idea behind whether a frequency could be identified as noise is therefore that the tipper should have an extraordinary response with a small imaginary part. The noise should also have a more or less fixed frequency in all three components. Therefore, by looking at the scalar tipper for every single frequency, it should be possible to easily detect the near field frequencies and remove them from the list of radio transmitters preferably by a digital notch filter (Figure 12). The plotted tipper was however not stable enough for the peak (scalar) values of the data. Therefore an average value from a vector around each peak was calculated as an attempt to get a better result in combination with a rotation of the system. This new tipper showed some improvement but was not good enough for identifying any noise frequencies.

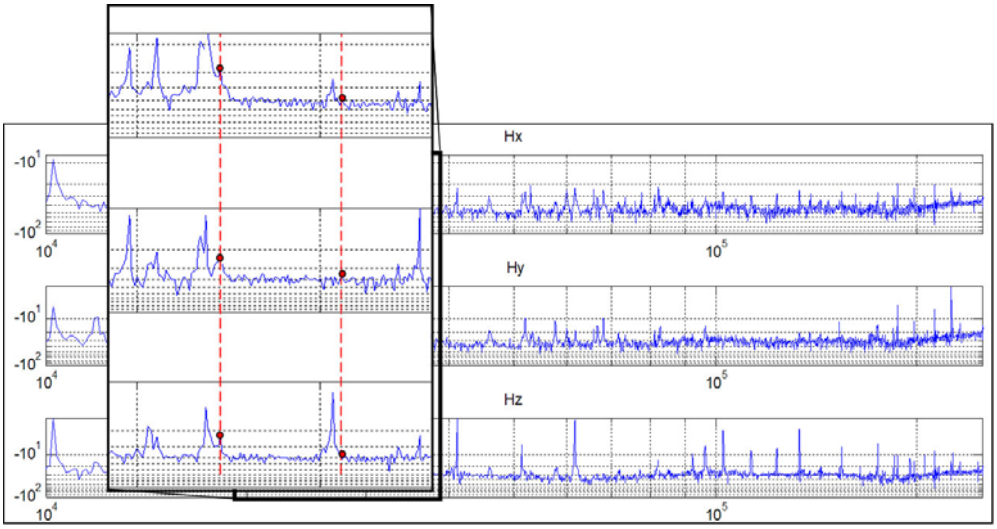

Figure 12. Example of frequency spectra for the components, H_x, H_y and H_z where the dashed lines show the noise frequencies that will be removed by a digital notch filter.

Another method that was investigated was to compare with the degree of polarization. This is because one transmitter should have the same polarization. Surprisingly, this method did not show the expected result. Therefore this method was not reliable enough to use as a secondary method for picking out the noise.

Automatically filtering

One way to proceed with the filtering was to not just look at the horizontal S/N ratio but also the cross S/N ratio. The cross S/N ratio was calculated for each frequency at every station. Those with a value above the mean value + 1 standard deviation (std) were saved and counted in a special occurrence list. Finally were the frequencies with an occurrence above a chosen

threshold considered being noise and removed from the spectra file together with a specified bandwidth around them similarly to a notch-filter. As for a notch filter the choice of the bandwidth influences the effect of eliminating the noise frequency. This bandwidth may therefore be needed to be experimented with. This method worked in such way that is also removed the harmonic noise frequency found.

Unfortunately there was no obvious correlation between either of the methods that were investigated. This could be an affect of the weak signal but also, as it was shown later, an error in the calculations. The only satisfying method to remove the data automatically was therefore to use the cross S/N ratio.

Manually filtering

Since this automatically filtering method perhaps removes more frequencies than wanted the final filtering of the data was done by removing the harmonic noise frequency manually and then assuming that the rest of the peak frequencies were transmitters. The frequencies for these peaks were then used to calculate the tipper in the next processing step.

Those frequencies that were chosen as noise frequencies were the found noise frequency of 27.4 kHz and its harmonics. These frequencies were put in a text-file that the program could read. When the program reads these frequencies it removes them from the spectra file together with a specified bandwidth similar as for the automatic filtering process. The choice of bandwidth is also here an ad hoc, trial-and-error method to get the best effect of eliminating the noise frequencies.

Interpretation of the filtering process in Matlab

The filtering was done in a Matlab-function called *FilterAirData*. Depending if you choose manual or automatic filtration the program uses different sub-functions.

The manual part of the program *FilterAirData* starts by asking after a text file containing the identified noise frequencies and the bandwidth of frequencies that should be removed around these. The bandwidth was here chosen to be 300Hz. The program then calls for another function called *RunSpectra* that read the spectra files and remove the noise by the sub-function *RemoveIndicies*. These new data are then saved as filtered spectra files.

If the automatic filtering process is chosen instead the program first use a sub-function called *PickNoise.* This sub-function calculates the cross S/N ratio in the function *Addtable* and compare against the value of the calculated mean + 1 standard deviation (std). Those values that are above this mean+1std are then saved in an occurrence list. The results of the occurrence are then plotted and on the basis from this a threshold can be chosen. In our test this threshold was set to 50%. After this is done the function *RunSpectra* takes this occurrence list and pick those frequencies that are above the threshold. The frequencies are then removed in *RemoveNoise* that also allows choosing a bandwidth for frequencies to be removed around the picked noise-frequency. As for the manually filtering the new data are saved as filtered spectra files.

The function *RunSpectra* also reuse the function *Addtable* for new calculations of the cross S/N ratio after the filtration just as a check.

5.2.4 Change of sign according to the flight direction

The measurement of the magnetic components is dependent of the flight direction. This means that if the airplane is flying in N-S direction, the H_x and H_y components have to change sign when the plain is flying to the south (Figure 13).

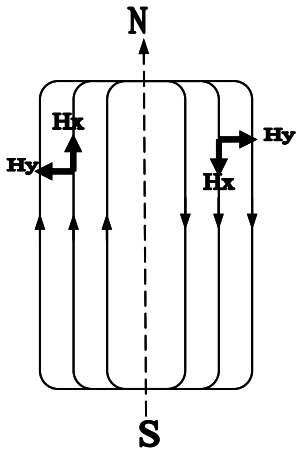

Figure 13. Flight for the airplane is in N-S direction. To the north H_x and H_y is positive. In the south direction these two components have to change sign. (H_z is pointing up from the paper and is independent of flight direction.)

Therefore a method to find when the plane change direction has to be developed. This could be done easily by looking at the derivative of the coordinates for the plane. Another method is to find the maximum and minimum values for the plotted profile of the x-coordinate for the plane (Figure 14). If the plane is travel in N-S direction this means that the maximum values are in north and the minimum values in the south. For every line between a maximum and a minimum value there has to be a sign change to compensate for the change in direction.

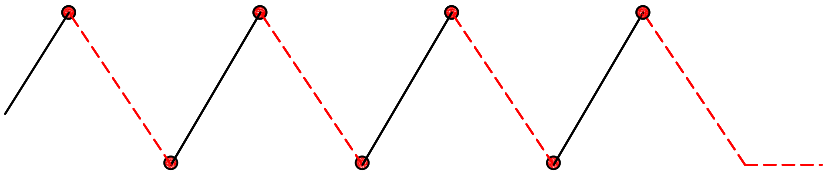

Figure 14. Simplification for a part of the plotted profile of the x-coordinate for the plane. Red circles show the peak-values. The black lines are the flight direction to north and the red lines are the south direction with sign change.

The derivative-method was used at the beginning but since there was problem with the data giving rise to stripes this method was abandoned when testing the other method. It was later shown that the striping had nothing to do with the choice of method to change sign. Instead there were other causes giving rise to these stripes as can be seen later.

The change of flight direction was done directly in the filtered data files with the Matlab function *ChangeSign*.

5.2.5 Estimation of transfer functions

The transfer functions can are then calculated based on the method explained in Section 4.3.3. The processing of the data so far was done in Matlab. The stacking of the filtered spectra and the calculation of the transfer functions (i.e. the tippers A and B) together with their errors is done in a program called *mfr2nd* with source code written in C by Bastani (2007).This program is a modification of RMT code written by Bastani for the EnviroMT instrument. This code is well proven and works well without errors.

The program creates separate output files (tensor and scalar) with calculated transfer functions, spectral matrix data and transmitter information. The data is stored together with synchronized positioning information.

5.2.6 Data visualisation

The instrument is mainly a data acquisition instrument. Therefore another external program has to be used for processing the data like 1D or 2D inversion of complete profiles and for data visualisation including pseudo sections of apparent resistivity, phase, tippers and results from the inversions. For visualisation of the data a software called Oasis Montaj was used. To import the data to Oasis Montaj the tensor and spectra files from the step before has to be pre-processed by a program called *RunTensor* in Matlab that store the information for each stacked frequency and save it as separate files. These files can then easily be imported to Oasis Montaj for visualisation.

Chapter 6

Airborne measurements with MFR

6.1 Airborne measurements at SGU

The Geological Survey of Sweden (SGU) has carried out airborne magnetic measurements since 1960. From the beginning the main purpose was to explore for iron ore but today it is to provide information about the structural featured of the bedrock. In 1972 they also started with airborne electromagnetic measurements for exploration of mineral deposits.

Normally the airplane flies in straight lines from east to west or north to south at intervals of 200 meters. Due to this the data during the post processing must be interpolated between the profiles. The flight speed is about 250 km/h. The sampling distance, i.e. the distance between the measured points along a line, thereby becomes about 16 meters. This means that according to Nyquist theorem the minimum wavelength that can be investigated is 32 meters.

The influence of flight height has been discussed by Oskooi and Pedersen (2006). They showed that for an increasing altitude of the flight the anomalies attenuate quite rapidly. Until 1994 the measurements were done at an altitude of 30 meters since this height gave better resolution. Today the most measurements are done at an altitude around 60 m since this is regarded to be the minimum safety height for the plane.

To ensure correct positioning during the measurement radar altimeters and GPS are used. The sensor (magnetometer) can be placed on a wing tip, nose stinger or a towed so-called bird.

On the ground the conduction give rise to a secondary field where the electric components can be measured. In the air there instead becomes a displacement effect that makes measurements of the electric field very difficult. This displacement effect comes from the fact that radio transmitters create very large vertical electrical components. In the air – if the plane is not flying exactly horizontally – this can create projection errors in the data against the ground. In combination with the noisy environment in the airplane and grounding difficulties this give an uncertainty in the data. The electric field can therefore not be measured properly from an airplane.

6.2 The MFR measurement at Torsby, Sweden

The survey area is located near Torsby, Sweden. This area is since before well documented by the Geological Survey of Sweden, SGU, hence the results can be compared with old maps. The measurement was done along flight lines in the N-S direction with 100 m separation, at an altitude of about 60 m. The speed of flight was approximately 200 km/h giving a sampling distance about 16 m. The sampling frequency is 800 kHz. This provide better S/N ratio and frequency resolution.

The magnetometer (Figure 15) record the field in three directions: H_x, H_y and H_z. These are then saved as raw time series together with information containing position and orientation of the airplane/magnetometer.

Figure 15. The left picture shows the mounting of the magnetometer on the plane for the measurement performed at Torsby in November 2007. The final assembly can be seen in the picture to the right. (Pictures by M. Bastani)

Chapter 7

Results

7.1 The filtering process

As mentioned before a lot sources of noise were residing on the board of SGU's airplane. Therefore the signal measured with the MFR-instrument showed a very high noise floor in the raw time data. The main source of the noise was a generator onboard the airplane. The noise from the generator is at a frequency of about 100 Hz and can be seen very clearly on the spectra. This problem can be solved by applying a proper high pass filter, e. g. a 2 pole butterworth filter with a cut-off frequency of around 3 kHz. Generally the noise floor for environments like in an airplane is higher than on the ground. Because of the high noise amplitude any amplification resulted signal clipping and therefore the gain had to be set to the lowest value meaning zero amplification. The high noise floor and no amplification affected the S/N ratio and degraded the data quality. This problem influenced all the interpretations of the data and therefore also the results.

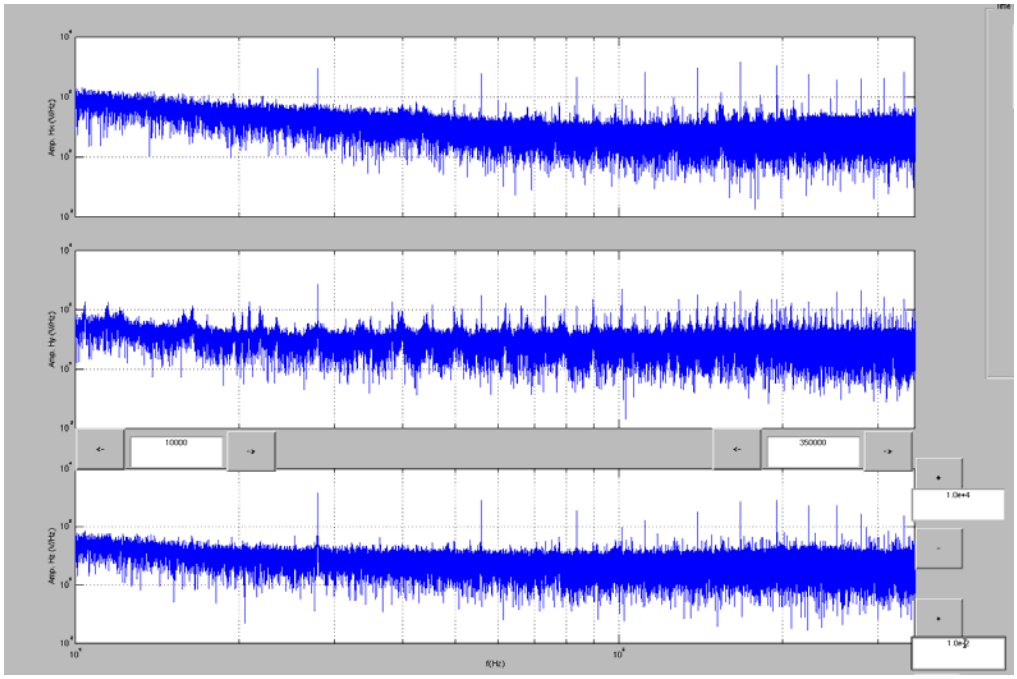

Figure 16. Raw spectra from the measurement. As can be seen the noise floor is very high. The amplitude for H_x (V/Hz) can be seen on top, the amplitude for H_y in the middle and the amplitude for H_z at the bottom. The frequencies in this picture are ranging from 10 kHz to 350 kHz.

The main aim of this work was to find a method to identify the near field noise sources and filter them out. Due to the the weak signal use of standard S/N ratio criteria was not possible to remove the noise frequencies effectively since the main part of signal could have been

filtered out. This fact is clearly seen in Figure 16 where the noise peaks (around 27.9 kHz and its harmonics) are much stronger than for example those for VLF band.

Figure 17 shows an example from the attempt to find a correlation between different methods for picking out the noise. The first two plots on top shows the tipper A and B after rotation with their real and imaginary parts for the chosen station. The third plot shows the peaks for the S/N-ratio data. These peaks were considered to be some kind of transmitters. On the bottom the calculations for the degree of polarization can be seen. This was one of the methods investigated to find a secondary method of picking out the noise. According to the theory one transmitter should have the same polarization. This method did not show the expected result and could not be used in the further process.

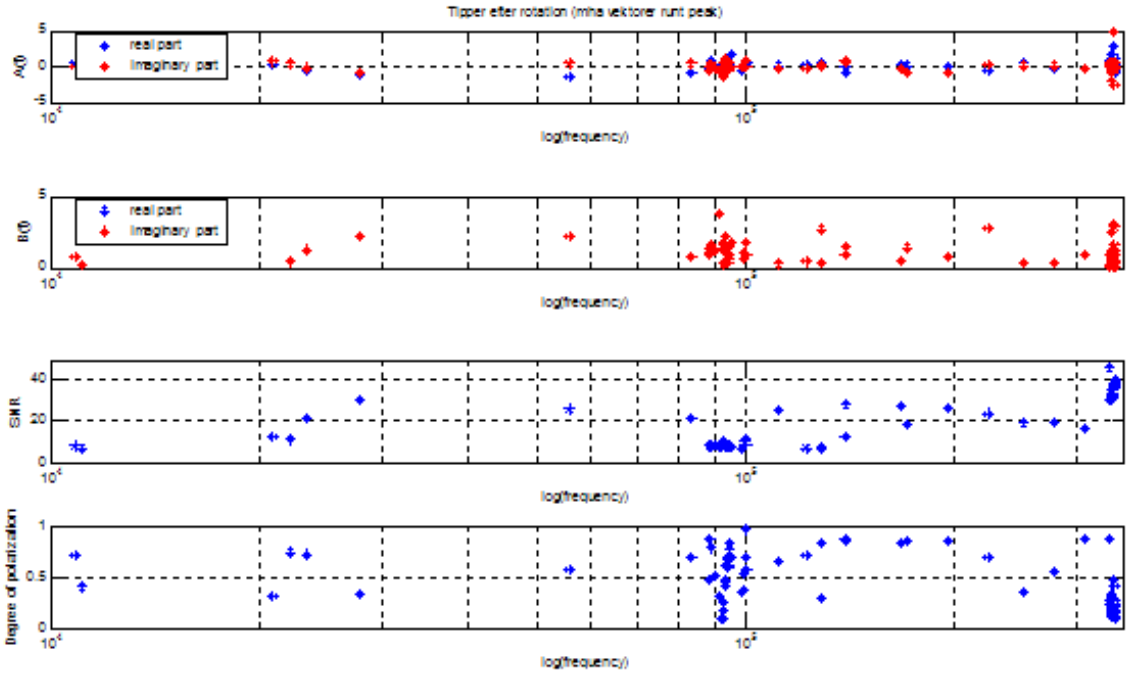

Figure 17. Different plots for noise identification for station number 10 497 (out of 27 342). The two plots on top shows the tipper A and B after rotation for this station with their real and imaginary parts. Below these plots is the S/N-ratio shown and at the bottom the calculations for the degree of polarization. All calculations are done for an average of vector values around the peaks and with rotation of the system.

The plot on top in Figure 18 shows the final solution of picking the noise frequencies for the automatic noise identification (filtering). The blue stars are the calculated mean plus one standard deviation (std). Those red stars (the S/N ratio) that are above this level are defined as the noise-frequencies for the current station. These frequencies are saved and counted every time they appear in a special occurrence list. An example of an occurrence plot for the automatic filtration can be seen in Figure 19. The frequencies that were considered being noise were those with an occurrence of above 50%. Figure 19 (bottom) shows a plot of the frequencies that remains after the processing where the noise frequencies have been removed. The decision to determine the threshold to be 50% of the occurrence is based on experiment. The threshold used in this case could therefore probably be varied to give better results.

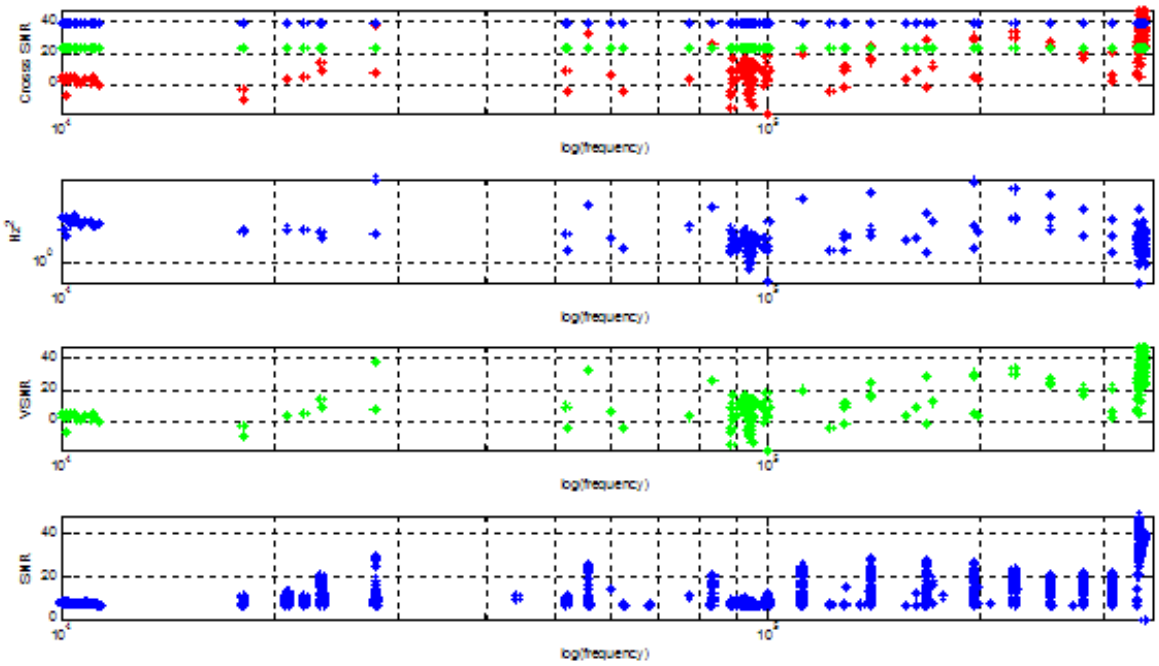

Figure 18. Different plots for noise identification for station number 10 497 (out of 27 342). The two plots on the bottom shows the horizontal (SNR) and vertical (VSNR) Signal-to-Noise ratios. The plot on top shows cross S/N ratio – the solution for the automatic filtration where the red stars are the S/N ratio, the green stars are the mean value and the blue stars the mean + 1 standard deviation.

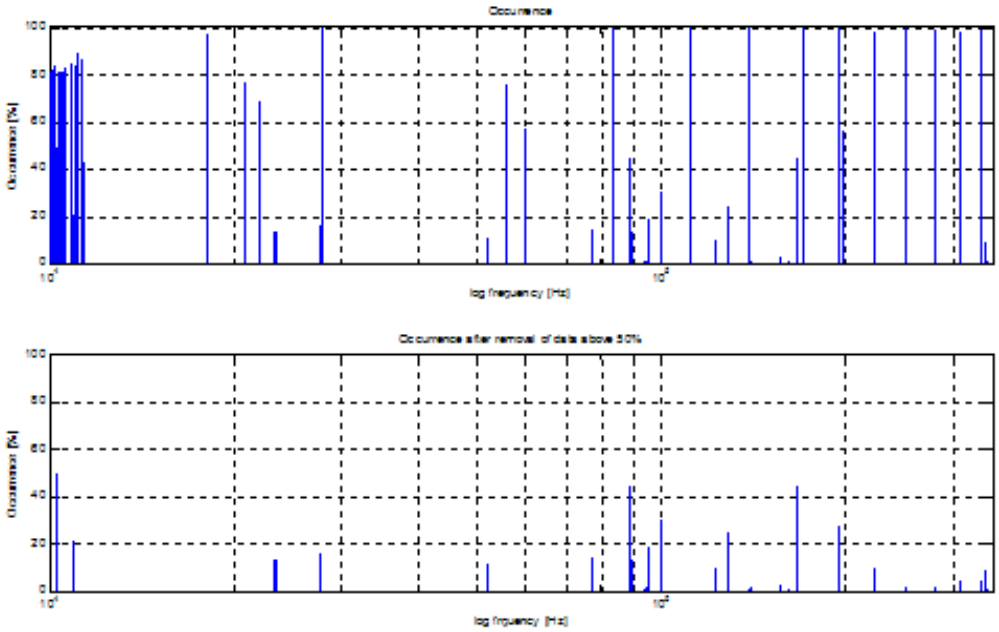

Figure 19. The plot on top shows the occurrence of cross S/N ratios above the threshold mean+1std after all stations in the spectra file number 65 (station numbers 10 282 – 10 500) are processed. The plot on the bottom shows the result when the noise frequencies (those with an occurrence above 50%) are removed**.**

The method for the automatic filtering process worked fine with data measured when the airplane was standing still at the airport. When the airplane, however, was flying in the air the noise level was raised due to the load on the engines. This raised noise level made so that possible frequencies of importance could be hidden in the noise floor. Thereby was the automatic filtering method not usable for the measured air data.

Since the near field sources could not be clearly identified by automatic method the manually filtering was done by just removing the pre-identified harmonic noise frequency of 9.14 kHz. **Fel! Ogiltig självreferens i bokmärke.** shows the calculations for the harmonics and their corresponding frequencies found in the data. Those frequencies that could be identified were later removed in the manually filtering process.

Table 1. Calculations of the harmonic frequency 9.14 kHz and the corresponding frequencies found in the data. Those that were found were added in a list for further use in the manually filtering process.

Number of harmonic	Calculated frequency [Hz]	Removed frequency in data [Hz]
1st	1*9142 = 9 142	9 142
2nd	2*9142 = 18 284	18 283
3rd	3*9142 = 27 426	27 428
4th	4*9142 = 36 568	36 570
5th	5*9142 = 45 718	45 712
6th	6*9142 = 54 852	54 848
7th	7*9142 = 63 994	63 997
8th	8*9142 = 73 136	73 140
9th	9*9142 = 82 278	82 282
10th	10*9142 = 91 420	91 425
11th	11*9142 = 100 562	100 567
12th	12*9142 = 109 704	109 720
13th	13*9142 = 118 846	*Not found*
14th	14*9142 = 127 988	*Not found*

Figure 20 and Figure 21 shows the Signal-to-Noise ratio before and after the manually and automatically filtering. The automatic filtering has removed more known transmitters than the manually filtering. This is probably an effect of hidden frequencies of importance in the high noise floor. It is also affected by the choice of bandwidth to be removed around each picked noise frequency. Depending on the bandwidth chosen there can be differences in the result either by remaining a lot of noise/unknown frequencies or removing known transmitters from the data. For the manually case in Figure 20 the bandwidth chosen to be removed is 300 Hz (around 100 indices in the spectra file). With same bandwidth in the automatic case in Figure 21 almost every frequency will disappear. The bandwidth is therefore set to 50 Hz (around 16 indices) after some experiments for the automatic filtering process.

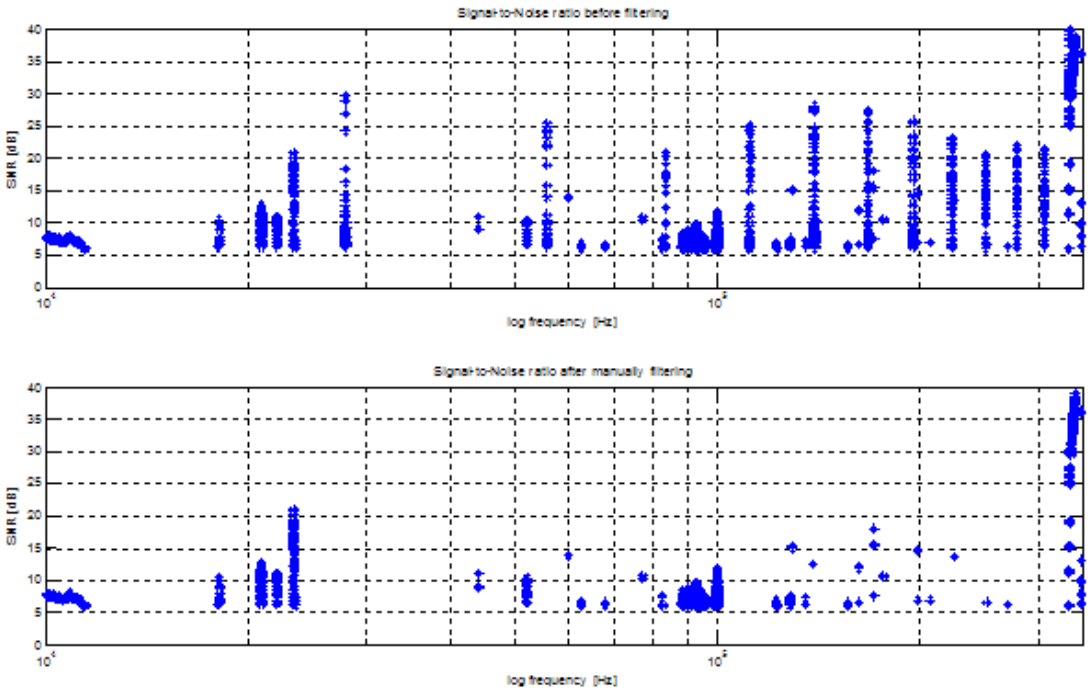

Figure 20. Signal-to-Noise ratio before and after manual filtering for station number 10 332 (out of 27 342). The removed bandwidth for each frequency is 300 Hz (approximately 100 indices in the file).

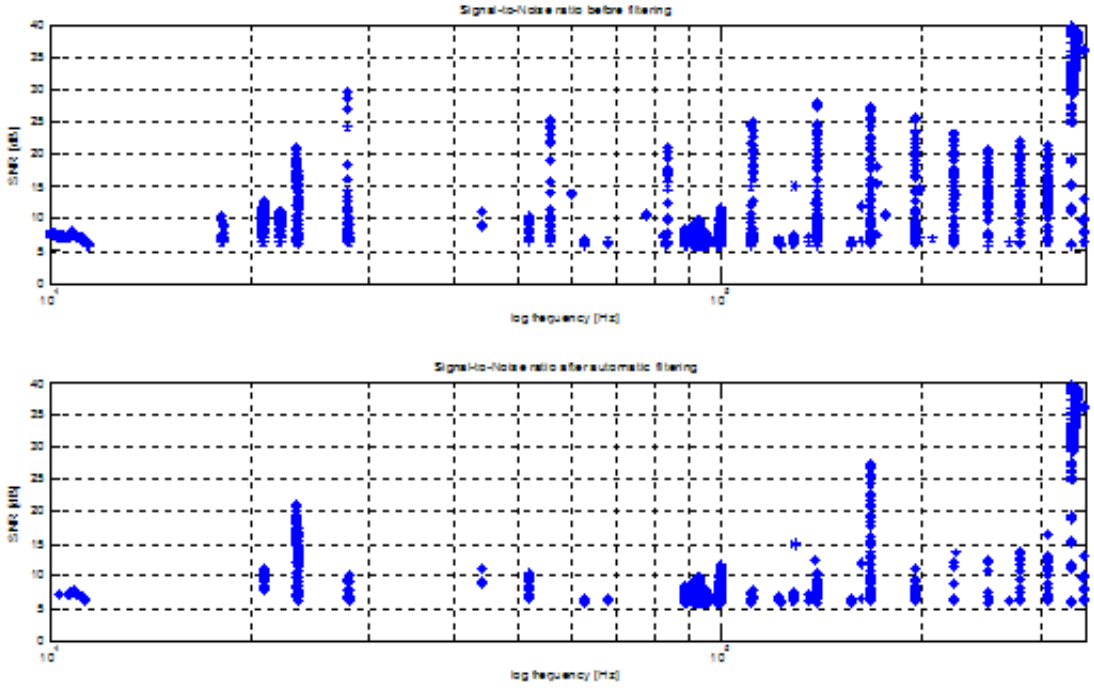

Figure 21. Signal-to-Noise ratio before and after automatic filtering for station number 10 332 (out of 27 342). The removed bandwidth for each frequency is 50 Hz (approximately 16 indices in the file). A change in bandwidth improves some frequencies but remove others. With a bandwidth as for the manually filtering removes almost every frequency.

Those frequencies that were left were compared to known transmitters from VLF surveys performed at Collendoorn, the Netherlands (1998) and by SGU at Gotland (2008), Sweden, by the EnviroMT equipment (Table A-1, Appendix A). This showed that some of the peaks in the data correspond to known transmitter frequencies or close to one. One thing to keep in mind is that the S/N ratio here is a function of distance to the transmitter and also the local noise level. By considering the fact that the environment in the airplane is much noisier than those measurements performed at Gotland and the Netherlands and also that the location of Torsby area is further to the north, the results seen in the table in appendix A are considered to be very good in that sense that some well-known transmitters (like VLF 23.4 kHz and the one in Germany DCF77 at 77.5 kHz) can be identified. Another difference between the measurements done by EnviroMT and the one here is that the EnviroMT data is from at least 10 stacks while this data is done with just one stack. The EnviroMT also has proper pre- and post-gain facilities that are not available in the measurements done here.

There are thou a lot of frequencies that differs in Table A-1 in Appendix A. Whether these are noise or some kind of transmitter has to be further investigated. There are different methods that can be useful. One is to look at the estimation of the transfer function for the peaks, where the outliers in the data could be possible noise. Another method is to look at the direction to the transmitter.

7.2 Profile for tipper

The result of the plotted tipper (tensor) from the software Oasis Montaj, used by SGU for visualization of processed data, can be seen in Figure 22. Since according to the theory we measure three magnetic components and the system is rotated the calculations are identical to a 2-D tipper. This means that one of the tipper components are zero. In this case it is the tipper component B. This can be seen in the figure where the fluctuation for tipper B is very small and about zero. The figure also shows two problems for the calculated tipper A. The first is that the real part only is positive. There should be a fluctuation around zero with both positive and negative values. The other is that the imaginary part is not changing at all. One possibility why this occur could be that the noise somehow influences the imaginary part.

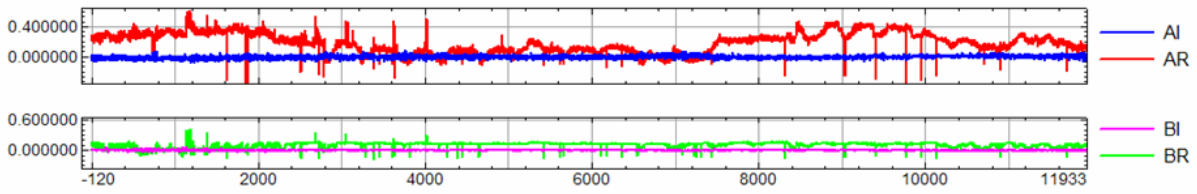

Figure 22. A part of the profile for tensor tipper A and B for the stacked frequency 113 kHz. The red line, showing the real part of tipper A, is not showing any fluctuations around zero as it should. The blue line, the imaginary part of tipper A, is not showing any variations at all. The lower picture is showing tipper B where green is the real part and pink the imaginary part. The x-axis shows the station numbers.

7.3 Map of tipper

Figure 23 shows the tipper map for the real part of A (tensor) over the measured area in Torsby compared to SGU's map over the same area for old VLF measurements. There are two major problems with the measured map. The first originates from the fact that the real component of the tipper only has positive values instead of fluctuating around zero. The other problem is the striping. Despite this the maps agree well with each other.

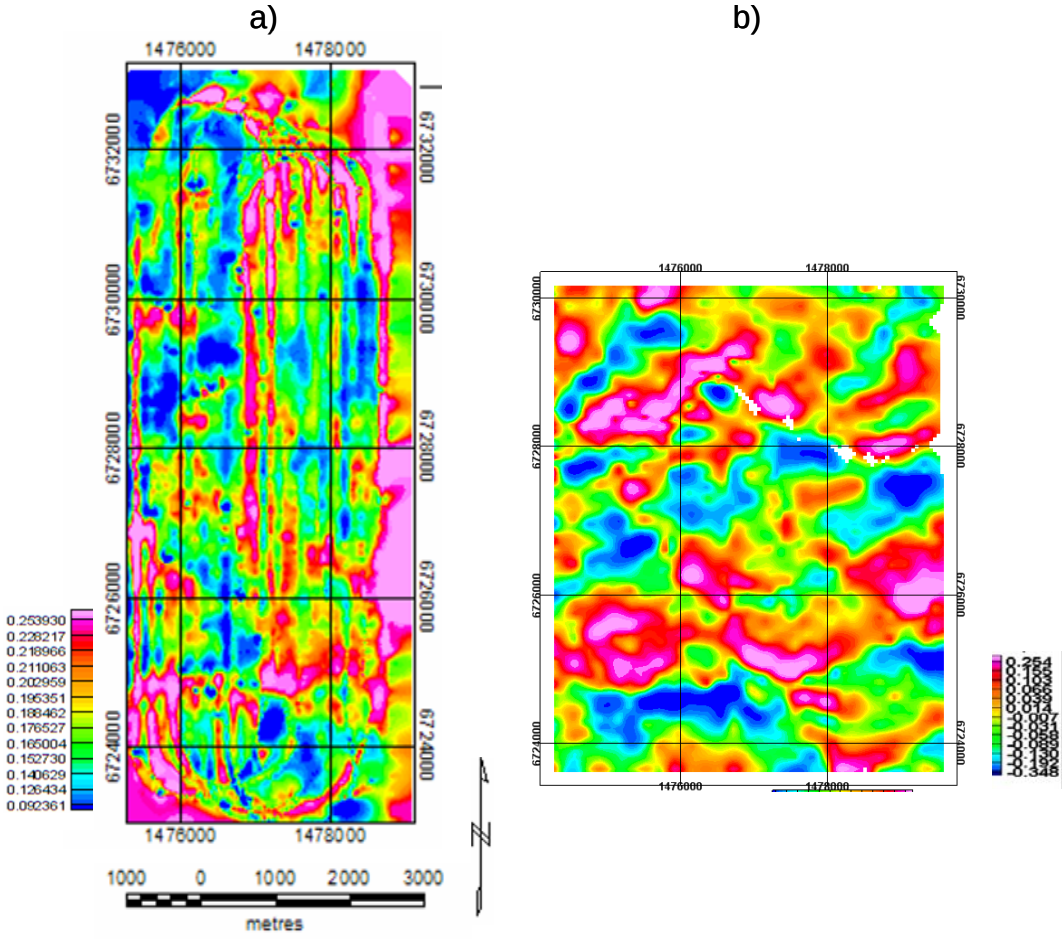

Figure 23. Map for the calculated transfer function (tipper) A for a) the measured data, b) SGU's map over the area. The measured map show stripes on every second profile. Due to this striping, information is lost for every second profile. Another problem is that there only are positive values for the tipper.

The flight path for an airplane collection data can be seen in Figure 24. For an ordinary flight path one half of the area should be directed to north (positive) and the other half to the south (negative sign). The map in Figure 23 shows some striping effects on every other profile (more or less). Right now it looks that the signs are alternating through the map. This leads to some loss of information. There were some ideas why this striping occurs that was investigated. None of them, however, solved the problem. The striping is still there.

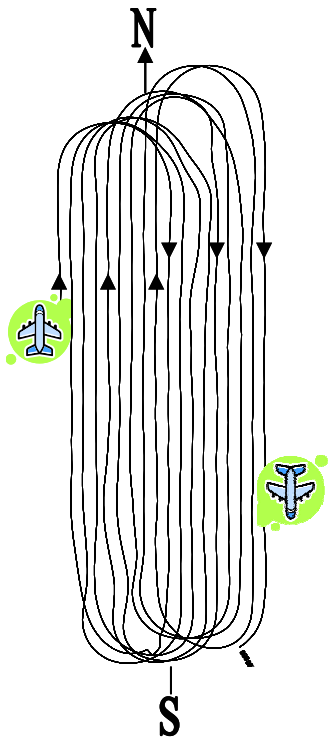

Figure 24. The flight path for airborne measurements. The flight routes are elliptical and overlap each other. The measured data when the plane is flying in S-N direction is here defined as positive and negative in the opposite direction. This means that the data for half the area should be positive and the other negative.

The first possibility was that the files were not processed in the right order. Another thing that could generate the striping was if the calculation of the direction is not correct. Here two methods were tested; the gradient method and max-min method, described in section 5.2.4, but none of them improved the data. There was also an idée that the striping could originate from some kind of technical error. One of these was if the component H_x and H_z had been changed somehow during the measurement, either by some cable or how the magnetometer was mounted. This was tested easily by changing components in the data files before any calculation. The result however did not show any improvements in resolution compared to the map without changes.

There is still some possibility that the striping can occur due to some technical problem that generates some kind of systematic error. There could also be a systematic noise, not seen in the data, which give rise to the striping effects.

Chapter 8

Discussion

In the beginning of a project a school term seems to be a long time. At the end it was not enough. Even if the noise was worse than expected the results are promising for the future development. There are thou still things that can be changed to improve the quality of the signal and the processing afterwards. A new measurement is planned to be performed during august 2008. This new survey will take into account the problems discovered during this processing and will hopefully provide better data.

New hardware
At the measurement the high amplitude noise (around 120 Hz) and no amplification due to lack of proper high-pass filter affected the S/N ratio and degraded the data quality. This problem influenced all the interpretations of the data and therefore also the results. There are therefore some main changes on the hardware that will be done before next measurement. The most important change is to prevent signal clipping when amplifying. This is done by installing a new analogue high pass filter with higher order and with a more appropriate cut-off frequency to receive a better signal. This cannot prevent the high noise floor completely since the environment in the airplane by itself generates higher noise compared with measurements performed at the ground.

Another problem is to get ride of the noise frequency of about 100 Hz coming from the generator in the plane. This can also be solved by installing a proper high-pass filter, e.g. a 2 pole butter-worth filter with a cut-off frequency of around 3 kHz.

The filtering process
The problem with the filtering process was that the noise frequencies could not be removed effectively since the signal was too weak. This could be seen in the raw spectra data where noise frequencies were much stronger than the signal itself. Due to this a lot of frequencies of interest could be hidden in the noise and removed during the filtering.

To find a reliable method of picking out the noise frequencies several methods must be combined but those investigated did not show the expected results. The problem of not finding a correlation could have explanations not thought of at the time of investigation. One possible explanation was based on the fact that the direction of the flight had not been taken into account in the calculations. This was compensated for very late in the process and was assumed to be a reason why the results for the polarization, tipper etc. were strange. This should however not influence the calculations since the only thing that happens is that there will become a change of sign in the result if the direction is opposite. Better data from the new measurement in august 2008 will perhaps find the correlations not found here.

The automatic noise detection worked well for data measured at the ground but not for

airborne data due to weak signal and high noise floor generated by the load on the engines. Therefore was this method not useable. Instead the filtering had to be done manually by removing the pre-identified harmonic frequency of 9.41 kHz. The frequencies left in the data after the filtering process looked very promising when comparing with old data measured with the EnviroMT equipment in Sweden and the Netherlands. Some of these frequencies were identified known radio transmitters. There are thou still unknown frequencies left in the filtered data. Whether these frequencies are noise or not is also of importance to know. The plan was to investigate these frequencies with respect to direction to the transmitter, coherence and also estimation of the transfer function. Unfortunately, in the timeframe of this project, there was not enough time to investigate these parameters that for sure could have been a good complement in the identification process.

The choice of bandwidth as well as the threshold of the occurrence is more or less based on trial-and-error to get the best effect of eliminating the noise frequencies. These values could probably be varied to improve the results. If there is some relation between a change of occurrence and bandwidth in the automatic filtering method has not been investigated since the final filtering was done manually.

Use information of the heading in calculations for flight direction

Something that was discovered late in the project was the dependence of flight direction for the magnetic components. This was seen for the first time when plotting the map for the tipper over the survey area and was compensated for very late in the process. The sign change has to be done on the H_x and H_y component and these are used in many of the calculations. Therefore should the sign change preferably be done early to ensure correct calculations.

The method used for finding the flight direction right now is to find the maximum and minimum values for the plotted profile of the x-coordinate for the plane. For every line between a maximum and a minimum value there has to be a sign change to compensate for the change in direction. This method is perhaps not the best. Another, and maybe better, method for calculation of the direction is to use the information of the heading (direction towards north) together with the coordinates for the plane that can be found in the header in the data files. The heading information was however not available during the measurement and could not be used in the process. The intention for the planned measurement in august is that the information for the heading is available together with the other flight parameters so that the method for sign change of the components can be done more properly next time.

Stripes in the map of the calculated transfer functions

In the map of the calculated transfer function every second profile (more or less) loses some information due to striping. The reason why this occurs is not solved yet but some things have been investigated to overcome this systematic error. One presumable cause for this behaviour could be either some error in the data processing program or a technical problem when saving the data during the measurement. Today the data is saved for every about 10 000 measurements in two separate files: one for data and another for coordinates etc. If these somehow are not connected to each other as they should they can give rise to these striping effects. The method for the technical saving of the data must therefore be examined before the next measurement in august 2008 to ensure that it work correctly. If this is not the problem then the question remains why the striping occurs and further investigation has to be done.

Peak frequencies to improve the imaginary part of the tipper
Today an S/N threshold is used to pick the far-field transmitters in the data. The frequencies for these are then saved together with *n* frequencies around each transmitter. Almost all of these transmitters has quite large signal (i.e. large S/N ratio) and have the same direction. With EnviroMT the smallest threshold used is 10dB (on ground measurements) but in our case we had an environment with a lot more noise and a threshold of just 6dB. This resulted in more noise affecting the calculations. This could be seen in the imaginary part of the tipper that did not show any fluctuations. By choosing the peak-frequencies instead, the probability that a noise frequency with lower S/N ratio should be used is lower i.e. the data is less affected by noise. A smaller test with picked peak-frequencies showed an improvement in the imaginary part of the tipper due to this.

The estimated real part of the tippers (A,B) is rather stable with only positive values. However, it matches the variations seen in old SGU data for the survey area to some extend.

Main proposal of improvements
There are two parameters that can be changed very easily and that could give a huge improvement in the processing: One of these has been mentioned earlier but is summarized here:

- Add a new high-pass filter to lower the noise from the airplane's engines.
- Use a higher dynamic range (24 bits) to tolerate a larger difference in the S/N ratio in the band of interest.

The dynamic range refers to the range of values that can be measured by the instrument.

Unanswered questions of issue
There are questions that became unanswered during this work and could be of interest to look at if the next processing is working well. The main question is how the accomplished data can become better. Other examples of questions that can be investigated are if the S/N ratio can be improved or how to find the direction and stability of the transmitters and if these transmitters are natural or artificial.

References

Bastani M. / EnviroMT – a New Controlled Source/Radio Magnetotelluric System, *Uppsala Dissertations from the Faculty of Science and Technology* **32** (2001)

Bastani, M., Pedersen, L.B., and Dynesius, L., / Multifrequency VLF/LF receiver. A new tool for fast and detailed mapping of near surface geology, *Report to the Geological Survey of Sweden*, (2004)

Becken, M. and Pedersen, L. B., / Transformation of VLF anomaly maps into apparent resistivity and phase, *Geophysics, Vol. 68, No. 2*, pp. 497-505 (2003).

Müller, A. / A new method to compensate for bias in magnetotellurics, *Geophys. J. Int.* **142**, pp. 257-269 (2000)

Oskooi, B. / A Broad View on the Interpretation of Electromagnetic Data (VLF, RMT, MT, CSTMT), *Comprehensive Summaries of Uppsala Dissertations from the Faculty of Science and Technology* **959** (2004)

Oskooi, B., Pedersen L.B., / Comparison between VLF and RMT methods. A combined tool for mapping conductivity changes in the sedimentary cover, *Journal of Applied Geophysics* **57**, pp. 227–241 (2005)

Oskooi, B., Pedersen L.B., / Resolution of airborne VLF data, *Journal of Applied Geophysics* **58**, pp. 158–175 (2006)

Pedersen, L.B. / The magnetotelluric impedance tensor – Its random and bias errors, *Geophysical Prospecting* **30**, pp. 188–210 (1982)

Pedersen, L. B., Qian, W., Dynesius, L., and Zhang, P., / An airborne tensor VLF system. From concept to realization, *Geophysical Prospecting* **42**, pp. 863-883 (1994)

Pedersen, L.B., Oskooi, B. / Airborne VLF measurements and variations of ground conductivity: A tutorial, *Surveys in Geophysics* **2**, pp. 151-181 (2004)

Pedersen, L.B., Bastani, M.,and L. Dynesius / Ground water exploration using combined controlled source and RadioMagnetoTelluric techniques, *Geophysics* **70**, pp. G8–G15 (2005)

Persson, L. / Plane Wave Electromagnetic Measurements for Imaging Fracture Zones, *Uppsala Dissertations from the Faculty of Science and Technology* **30** (2001)

Setälä, T., Shevchenko, A. and Kaivola, M. / Degree of polarization for optical near fields, *Physical Review E* **66**, pp. 016615: 1-7 (2002)

www.sgu.se/sgu/eng/produkter-tjanster/produkter/databaser/geofysik_databas_e.html (acc. 2008-05-05), Geological Survey of Sweden (SGU)

Appendix

Appendix A Comparison of found frequencies
Appendix B File information
Appendix C Flow chart over the processing
Appendix D Source-code for Matlab

Appendix A

Comparison of found frequencies from the manual and automatic filtration compared with corresponding known transmitters from EnviroMT surveys at Gotland (2008) and Netherlands (1998).

Table A-1. Comparison of found frequencies. The S/N threshold for the different areas are: Torsby 6dB, Collendoorn in Netherlands 12dB and on Gotland 10 dB. For the manual filtering 8 known transmitters are found (removed bandwith = 300 Hz) while it for the automatic filtering is found 6 known transmitter (removed bandwidth = 50Hz)

Torsby with manual filtering		**Torsby** with automatic filtering		**Gotland**	**Netherlands**	Comments
Frequency [kHz]	S/N –ratio [dB]	Frequency [kHz]	S/N –ratio [dB]	Frequency [kHz]	Frequency [kHz]	
10.0	7.98					
10.9	8.10	10.9	7.68			
					15.99	
				16.5		16.4 kHz = JXN, Norway
18.1	10.62					
					18.31	18.3 kHz = HWU, LeBlanc, France
				19.6	19.53	19.6 kHz = GBZ, Anthorn, UK
				20.1		
20.9	12.83	20.9	10.76			
22.1	10.95					
23.4	20.93	23.4	20.93	23.4	23.44	23.4 kHz = DHO38 Saterland D
				24		24 kHz = Cutler?, USA
		27.8	9.53			
				37.5	37.6	
				44.1		
					45.9	
51.9	10.20	52.0	10.38	52	52	
					57.37	
60.0	13.94			60	60.06	60 kHz = MSF, UK
62.6	6.73			62.6	62.62	
					65.8	
				67.9	67.99	
					68.85	
					71.41	
					73.36	
					74.95	75 kHz = HBG, Switzerland
77.5	10.93			77.5	77.51	77.5 kHz = DCF77 Mainflingen, Germany
				82.8		
					84.59	
					85.69	
89-99	9.79[1]	*89-99*	9.79[2]			
100.0	11.76	100.0	11.76			100 kHz = LoranC
		111.7	8.00			
				112.9	112.67	
					115.6	
122.5	6.95	122.5	6.95			
					126.83	
128.4	7.21					
129.0	15.27	129.0	15.27	129	128.91	129.1 kHz = DCF49, Germany
					131.71	
				135.5		
		139.6	10.36	139	138.79	139 kHz = DBF39 Burg, Germany

[1] Vid frekvensen 92.7
[2] Vid frekvensen 92.7

					141.44	
					144.65	
				147.4	147.34	147.3 kHz = DHH47
				153	152.95	153 kHz = DLF
156.5	6.61	156.5	6.61			
		162.0	12.27	162	161.99	
				166		
		167.3	26.91			
171.0	18.00			171	171.02	
				177	177	177 kHz = D-radio
				183	182.98	
		195.4	11.0			
				198	198	198 kHz = BBC4, UK
				207	207.03	207 kHz = DLF, Germany
					215.94	
				225	224.98	
					234.01	
					243.04	
		251.2	12.36			
		279.1	13.86			
		306.9	16.4			

Appendix B

File information

Spectra-files

Header 1: ***The first header only appears once in the beginning of the file.***

1st Segment	2nd Segment	# of channels	project name	# of line	# of station											# of transmitters

Header 2:

Counter	Timestamp	Timestamp	latitude	longitude	x	y	altitude	Position quality	heading	pitch	roll	Orientation quality	S/N-threshold	# of transmitters

Data: ***Contain lines equal to the number of transmitters from information in header 2.***

Index	Frequency	S/N	Hx_re	Hx_im	Hy_re	Hy_im	Hz_re	Hz_im

Tensor-files

Header 1: As above
Header 2: As above

Data: ***Contain only 10 lines with pre-defined (stacked) frequencies***

Frequency	Stacked Frequency	A_re	A_im	A_error	B_re	B_im	B_error

Scalar-files

Header 1: As above
Header 2: As above

Data: ***Contain lines equal to the number of transmitters from information in header 2.***

Transmitter Frequency 1	Transmitter Frequency 2	S/N	Direction to transmitter (degrees)	A_re	A_im	B_re	B_im

Appendix C

Flow chart over the processing. All functions are processed in Matlab except for the main function *mfr2nd* with source code written in C by Bastani (2007).

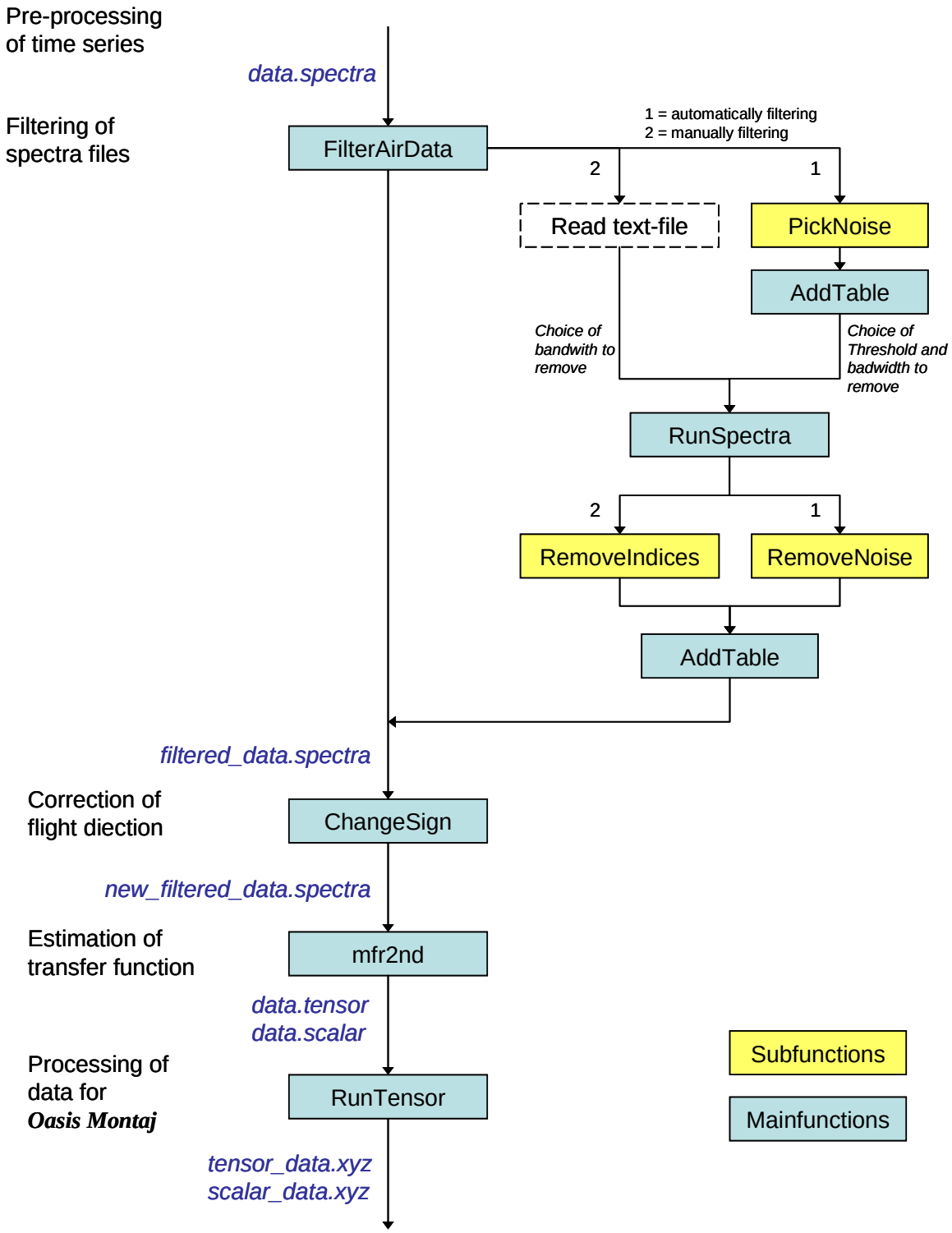

Appendix D

Source-code for Matlab

D-1 Main function: FilterAirData.m

```
function FilterAirData(X)
% ************************************************
% Reading all spectra-files in a directory, filter
% them and save the "new" filtered files in a new
% directory
%
% Input variables:
%   X = If X is set to 1 - automatic filtration
%       If X is set to 2 - Manual filtration
%
% Called functions:
%   PickNoise   (subfunction)
%   RunSpectra  (mainfunction)
%
% Comment 1:
% StaticTable contain a list of frequencies to be removed
% in the last step (function 'RunSpectra').
%
% Comment 2:
% Detailed information of the content in the spectra files
% can be found in file documentation 'files_info.doc'.
% ************************************************

% Select file for processing
datapath    = uigetdir('C:\','Select the data directory to read')
resultpath  = uigetdir('C:\','Select the results directory to write')
files = dir(datapath);
NoofFiles = size(files);

if X == 2

    % Select file
    [filename path] = uigetfile('*.txt','Select a file for frequencies to remove');
    file2 = [path filename];

    % Choosing bandwith to remove from file
    width = input('Choose bandwith to remove (in Hz): ');
    df = 800000/(2^18);
    extra.dk = round(width/df);
    fid2 = fopen(file2);

    %Reading frequencies from file and save as StaticTable
    freq_list = [];
    j = 0;
    while ~feof(fid2)
         j = j+1;
         freq_list(j) = fscanf(fid2,'%10d \n',1);
    end;
    StaticTable = freq_list;
    fclose(fid2);
end

for kk =3:NoofFiles

    if X == 1
        % Read file and pick frequencies to remove
        StaticTable = PickNoise([datapath '\' files(kk).name]);
    end

    % Read "old" file, filter and save as new (filtered) file
    RunSpectra(X,datapath,resultpath,files(kk).name,StaticTable,extra.dk);
end;
```

```
% ************************************************
% Subfunction: PickNoise
%
% Creates a list of frequencies (StaticTable) to be
% removed in a later step...
%
% Input variables:
%   filename
%
% Output variables:
%   StaticTable
%
% Called functions:
%   AddTable    (mainfunction)
% ************************************************
function StaticTable = PickNoise(file)

fid = fopen(file);

% Creating Static Table
datadf = 800000/(2.0^18); % Make the frequency resolution
lengthf = round((350000-9000)/datadf);
stind = round(9000/datadf);

StaticTable = zeros(lengthf,4);
StaticTable(:,1) = stind:1:lengthf+stind-1;
dataf = StaticTable(:,1)*datadf;

% Reading the spectra file header:
extra.first_segment = fscanf(fid,'%d',1);
extra.last_segment  = fscanf(fid,'%d',1);
extra.used_channels = fscanf(fid,'%d',1);
extra.project_name  = fscanf(fid,'%s',1);
extra.line_number   = fscanf(fid,'%d',1);
extra.station_number= fscanf(fid,'%d',1);

% Number of stations in file
N = extra.last_segment - extra.first_segment;

extra.spectra = [];
extra.num_transmitters = [];

% Reading information for the tramsmitters
for i=1:(N-1)
    if ~feof(fid)

        %Reading information header about the transmitters
        extra.segment_counter(i)   = fscanf(fid,'%f',1);
        extra.timestamp_tv_sec(i)  = fscanf(fid,'%f',1);
        extra.timestamp_tv_usec(i) = fscanf(fid,'%f',1);
        extra.latitude(i)          = fscanf(fid,'%f',1);
        extra.longitude(i)         = fscanf(fid,'%f',1);
        extra.X(i)                 = fscanf(fid,'%f',1);
        extra.Y(i)                 = fscanf(fid,'%f',1);
        extra.altitude(i)          = fscanf(fid,'%f',1);
        extra.position_quality(i)  = fscanf(fid,'%f',1);
        extra.heading(i)           = fscanf(fid,'%f',1);
        extra.pitch(i)             = fscanf(fid,'%f',1);
        extra.roll(i)              = fscanf(fid,'%f',1);
        extra.orientation_quality(i)  = fscanf(fid,'%f',1);
        extra.sn_treshold(i)       = fscanf(fid,'%f',1);
        extra.num_transmitters(i)  = fscanf(fid,'%d',1);

        %Reading information from spectra data
        slask = fscanf(fid,'%f %f %f %f %f %f %f %f %f \n',[9,extra.num_transmitters(i)]);
        extra.spectra(:,1:9) = slask';

        %Reading noise-frequencies and save as StaticTable
        Temp = Addtable(extra,i);
        StaticTable(:,2) = StaticTable(:,2)+ Temp(:,2);
        StaticTable(:,3) = StaticTable(:,3)+ Temp(:,3);

        extra.spectra =[];

    else
        fprintf('End of file reached \n');
    end
```

```
end
fclose(fid);

StaticTable(:,4) = StaticTable(:,2)./StaticTable(:,3);
disp('function: PickNoise - ready!')

% Plot frequency occurrence
figure(1)
subplot(2,1,1);
semilogx(dataf,StaticTable(:,4)*100);
axis([10000 350000 0 100]); grid on;

% Choice of threshold
extra.thresh = input('Choose threshold (in %): ');
%extra.thresh = 50;

        % **** ONLY FOR COMPARSION **********
        % Remove data over a certain threshold
        noiseindex = find(StaticTable(:,4)*100 >= extra.thresh);

        if noiseindex>0
            StaticTest = StaticTable;
            datafTest  = dataf;

            StaticTest(noiseindex,:) = NaN;
            datafTest(noiseindex) = NaN;

            %Remove any rows containing NaNs from a matrix X
            StaticTest(any(isnan(StaticTest),2),:) = [];
            datafTest(any(isnan(datafTest),2),:) = [];

            % Plot when occurance > threshold is removed
            subplot(2,1,2);
            semilogx(datafTest,StaticTest(:,4)*100);
            axis([10000 350000 0 100]); grid on;

        else
            disp(['PickNoise: No values above ', num2str(extra.thresh) ,' % can be found']);
        end;
```

D-2 Main function: AddTable.m

```
function StaticTable = Addtable(extra,i)

% ************************************************
% Make the statistical table for all the indices in the
% spectra (9000 kHz-350 kHz)
%
% Input variables:
%   extra   = struct array
%   i       = station number
%
% Output variables:
%   StaticTable
%
% Called functions:
%   lmax    (main function)
%
% ************************************************

% Identify the peaks in the SNR-data
df = 12;                            % interval
[b,a]=lmax(extra.spectra(:,3),df);

%     %Write frequecylist
%     DF = 800000/(2^18);
%     ftop = [extra.spectra(a,1) (extra.spectra(a,1)*DF)/1000 extra.spectra(a,3)];
%     fprintf('%10d %10.1f %8.1f \n',ftop');
%     length(ftop)
%     pause

% Creating Static Table
datadf = 800000/(2.0^18); % Make the frequency resolution
lengthf = round((350000-9000)/datadf);
stind = round(9000/datadf);

StaticTable = zeros(lengthf,4);
StaticTable(:,1) = stind:1:lengthf+stind-1;


% Calculations for peak data (rotated system)

% create imaginary i
icom = sqrt(-1.0);

% Define Hx, Hy och Hz as complex numbers
Hx  = extra.spectra(a,4) + icom.*extra.spectra(a,5);
Hy  = extra.spectra(a,6) + icom.*extra.spectra(a,7);
Hz  = extra.spectra(a,8) + icom.*extra.spectra(a,9);

% calculate the vertical S/N ratio (VSNR) assuming that it has
% the same noise level as the horizontal S/N ratio (HSNR)
HSNR = extra.spectra(a,3);
Vnoise = ((abs(Hx).^2 + abs(Hy).^2)./10.^(HSNR/10))/4.0; %Vertical noise
Hnoise = 10.^(HSNR/10);                                  %Horizontal noise
VSNR  = 10*log10((abs(Hz).^2./Vnoise));

% Calculation of CrossSN to be compared against threshold in a later step)
CrossN = sqrt((Vnoise.*Hnoise));
CrossSN = 10*log10(CrossN);

% Calculation of mean and standard deviation for CrossSN and VSNR
MnCross = mean(CrossSN);
%MnCross = median(CrossSN);
MnV = median(VSNR);
CrossSt = std(CrossSN);            % Old: CrossSt = mean(abs(VSNR-MnV));
CrossStV = std(VSNR);

CrossLen = length(CrossSN);
Midd = MnCross*ones(length(CrossSN));
StdMidd = (MnCross+CrossSt)*ones(1,length(CrossSN));

MiddV = MnCross*ones(length(VSNR));
StdMiddV = (MnV+CrossStV)*ones(1,length(VSNR));
```

```
limit = mean(StdMidd);
limitV =mean(StdMiddV);

% Finds values for CrossSN above limit
aboveStdMidd = find(CrossSN>=limit );
aboveStdMiddV = find(VSNR>=limitV);

listme = extra.spectra(a(aboveStdMidd),1);
listmeV = extra.spectra(a(aboveStdMiddV),1);

Len = length(listme);
if(Len)

    % Create index for frequencies with crossSN above limit
    for kk = 1:length(listme)
      staticindex(kk) = find(StaticTable(:,1)== listme(kk));
    end

    % Add to list over occurance for frequencies with crossSN
    % above threshold
    StaticTable(staticindex,2) =  StaticTable(staticindex,2)+1;
    StaticTable(:,3) = StaticTable(:,3)+1;
    StaticTable(a,4) = StaticTable(a,2)./StaticTable(a,3);

    staticindex = [];
    listme = [];
    listmeV = [];

    MF2    = abs(Hz).^2;
    MF3    = log10(abs(Hz).^2./(abs(Hx).^2 + abs(Hy).^2));

    % Plot of the results
    figure(5); clf;
      subplot(4,1,1);   % *** crossSNR etc vs. frequency
        semilogx(extra.spectra(a,2), VSNR, '*r');
        hold on
        semilogx(extra.spectra(a,2), MnV, '*g');
        semilogx(extra.spectra(a,2), StdMiddV, '*b');
        axis([10000 350000 min(VSNR) max(VSNR)]); grid on;
        xlabel('log(frequency)'); ylabel('Crosss SNR');

      subplot(4,1,2);   % *** abs(Hz)^2 vs. frequency
        loglog(extra.spectra(a,2), MF2, '*b');
        axis([10000 350000 min(MF2) max(MF2)]); grid on;
        xlabel('log(frequency)'); ylabel('Hz^2');

      subplot(4,1,3);   % *** VSNR vs. frequency
        semilogx(extra.spectra(a,2), (VSNR), '*g');
        axis([10000 350000 min((VSNR)) max((VSNR))]); grid on;
        xlabel('log(frequency)'); ylabel('VSNR');

      subplot(4,1,4);    % *** SNR vs. frequency
        semilogx(extra.spectra(:,2), extra.spectra(:,3), '*b');
        axis([10000 350000 min(extra.spectra(:,3)) max(extra.spectra(:,3))]); grid on;
        xlabel('log(frequency)'); ylabel('HSNR');

end
```

D-3 Main function: RunSpectra.m

```
function RunSpectra(X,datapath,resultpath,file,StaticTable,dk)

% ************************************************
% Reading spectra-files from a directory, filter
% them and save the "new" filtered files in a new
% directory
%
% Input variables:
%   X = If X is set to 1 - automatic filtration
%       If X is set to 2 - Manual filtration
%   datapath
%   resultatpath
%   file
%   StaticTable = list of frequencies to be removed
%   dk          = Bandwidth to remove
%
% Called functions:
%   RemoveIndicies   (subfunction)
%   RemoveNoise      (subfunction)
%   Addtable         (mainfunction)
%
% Comment:
% Detailed information of the content in the spectra files
% can be found in file documentation 'files_info.doc'.
% ************************************************

fprintf(' The data file being processed: %s \n',file)
extra.dk = dk;

% Creating Table
datadf = 800000/(2.0^18); % Make the frequency resolution
lengthf = round((350000-9000)/datadf);
stind = round(9000/datadf);

Table = zeros(lengthf,4);
Table(:,1) = stind:1:lengthf+stind-1;
dataf = Table(:,1)*datadf;

% open files
fid1 = fopen([datapath '\' file]);
out_filename = [resultpath '\' 'filtered_' file];
fid2 = fopen(out_filename, 'wt');

% Reading the spectra file header:
extra.first_segment = fscanf(fid1,'%d ',1);
extra.last_segment  = fscanf(fid1,'%d ',1);
extra.used_channels = fscanf(fid1,'%d ',1);
extra.project_name  = fscanf(fid1,'%s ',1);
extra.line_number   = fscanf(fid1,'%d ',1);
extra.station_number= fscanf(fid1,'%d ',1);

% Save the spectra file header in the new file:
fprintf(fid2,'%10d ',extra.first_segment);
fprintf(fid2,'%10d ',extra.last_segment);
fprintf(fid2,'%10d ',extra.used_channels);
fprintf(fid2,'%s ',extra.project_name);
fprintf(fid2,'%10d ',extra.line_number);
fprintf(fid2,'%10d \n',extra.station_number);

% Number of stations in file
N = extra.last_segment - extra.first_segment;

extra.spectra = [];
extra.num_transmitters = [];
add = 1;
% Reading information for the tramsmitters
for i=1:N
    if ~feof(fid1)

        %Reading information header about the transmitters
        extra.segment_counter(i)   = fscanf(fid1,'%f',1);
        extra.timestamp_tv_sec(i)  = fscanf(fid1,'%f',1);
        extra.timestamp_tv_usec(i) = fscanf(fid1,'%f',1);
```

```
        extra.latitude(i)          = fscanf(fid1,'%f',1);
        extra.longitude(i)         = fscanf(fid1,'%f',1);
        extra.X(i)                 = fscanf(fid1,'%f',1);
        extra.Y(i)                 = fscanf(fid1,'%f',1);
        extra.altitude(i)          = fscanf(fid1,'%f',1);
        extra.position_quality(i)  = fscanf(fid1,'%f',1);
        extra.heading(i)           = fscanf(fid1,'%f',1);
        extra.pitch(i)             = fscanf(fid1,'%f',1);
        extra.roll(i)              = fscanf(fid1,'%f',1);
        extra.orientation_quality(i)  = fscanf(fid1,'%f',1);
        extra.sn_treshold(i)       = fscanf(fid1,'%f',1);
        extra.num_transmitters(i)  = fscanf(fid1,'%d',1);

        %Reading information from spectra data
        slask = fscanf(fid1,'%f %f %f %f %f %f %f %f \n',[9,extra.num_transmitters(i)]);
        extra.spectra(:,1:9) = slask';

               figure(6)
               subplot(5,1,1);
               semilogx(extra.spectra(:,2),extra.spectra(:,3),'*');
                  axis([10000 350000 0 40]); grid on;

         % filter the frequencies below 15 kHz (by removing them from data)
        lowin = find(extra.spectra(:,1) <=5000);
        extra.spectra(lowin,:) = [];

        % filter the frequencies above 330 kHz (by removing them from data)
        lowup = find(extra.spectra(:,1) >=105000);
        extra.spectra(lowup,:) = [];

        if X == 2
            extra.removed = 0;

            %Remove noise
            extra = RemoveIndices(extra, StaticTable);
            new_num_transmitters(i) = length(extra.spectra);

               subplot(5,1,2);
               semilogx(extra.spectra(:,2),extra.spectra(:,3),'*');
                  axis([10000 350000 0 40]); grid on;

            %Calculations of ampitude of each component
            Hxamp = abs(extra.spectra(:,4)+sqrt(-1)*extra.spectra(:,5));
            Hyamp = abs(extra.spectra(:,6)+sqrt(-1)*extra.spectra(:,7));
            Hzamp = abs(extra.spectra(:,8)+sqrt(-1)*extra.spectra(:,9));

            minplot = min(min([Hxamp;Hyamp;Hzamp]));
            maxplot = max(max([Hxamp;Hyamp;Hzamp]));

               subplot(5,1,3);
               loglog(extra.spectra(:,2),Hxamp,'.'); axis([10000 350000 1 1000]); grid on;
               subplot(5,1,4);
               loglog(extra.spectra(:,2),Hyamp,'.'); axis([10000 350000 1 1000]); grid on;
               subplot(5,1,5);
               loglog(extra.spectra(:,2),Hzamp,'.'); axis([10000 350000 1 1000]); grid on;
               pause(0.1)

        elseif X==1
            %Remove data over a certain threshold from spectra file
            %OBS! extra.thresh is chosen in FilterAirData/PickNoise
            %extra.thresh = 50;
            noiseindex = find(StaticTable(:,4)*100 >= extra.thresh);

            if noiseindex>0
                extra.removed = 0;

                % Remove noise
                extra = RemoveNoise(extra, noiseindex, StaticTable);
                new_num_transmitters(i) = length(extra.spectra);

            else
                disp(['RunSpectra: No values above ', num2str(extra.thresh) ,' % can be
found']);
                new_num_transmitters(i) = extra.num_transmitters(i);
            end;

        end;    %END if X == 2...
```

```
        %Save information to new filtred spectra file
        %fprintf(fid2,'%8d %7.1f %5.2f %10.5f %10.5f %10.5f %10.5f %10.5f %10.5f
\n',extra.spectra(:,1:9)');
        IndexRout(i) = length(extra.spectra);
        Results(add:add+IndexRout(i)-1,1:9) = extra.spectra(:,1:9);
        add = add+IndexRout(i);
        fprintf('Segment number :%d \n',i)

        %Reading new "noise"-frequencies and save as Table
        Temp = Addtable(extra,i);
        Table(:,2) = Table(:,2)+ Temp(:,2);
        Table(:,3) = Table(:,3)+ Temp(:,3);

        extra.spectra =[];
    else
        %fprintf('End of file reached \n');
        break;

    end         %END if ~feof(fid1)
end             %END for i=1:(N)

EndInd = i;
fclose(fid1);

% Save information header about the transmitters
add = 1;
for i =1:EndInd-1
    fprintf(fid2,'%10d ',extra.segment_counter(i));
    fprintf(fid2,'%10d ',extra.timestamp_tv_sec(i));
    fprintf(fid2,'%10d ',extra.timestamp_tv_usec(i));
    fprintf(fid2,'%10.5f ',extra.latitude(i));
    fprintf(fid2,'%10.5f ',extra.longitude(i));
    fprintf(fid2,'%10.1f ',extra.X(i));
    fprintf(fid2,'%10.1f ',extra.Y(i));
    fprintf(fid2,'%10.3f ',extra.altitude(i));
    fprintf(fid2,'%1d ',extra.position_quality(i));
    fprintf(fid2,'%8.3f ',extra.heading(i));
    fprintf(fid2,'%8.3f ',extra.pitch(i));
    fprintf(fid2,'%8.3f ',extra.roll(i));
    fprintf(fid2,'%1d ',extra.orientation_quality(i));
    fprintf(fid2,'%9.3f ',extra.sn_treshold(i));
    fprintf(fid2,'%d \n',new_num_transmitters(i));
    fprintf(fid2,'%8d %7.1f %5.2f %10.5f %10.5f %10.5f %10.5f %10.5f %10.5f
\n',Results(add:add+IndexRout(i)-1,1:9)');
    add = add+IndexRout(i);
end
fclose(fid2);

Table(:,4) = Table(:,2)./Table(:,3);
StaticTable = Table;

disp('function:Runspectra - ready')

if X == 1
    figure(2)
    %Plot occurance after filtering data
    semilogx(dataf,StaticTable(:,4)*100);
    axis([10000 350000 0 100]); grid on;
end;


% ************************************************
% Subfunction: RemoveIndices
% Remove Noise Frequencies from spectra file when
% manually filtering
%
% Input variables:
%   extra       = struct array
%   StaticTable = list of frequencies to be removed
%
% Output variables:
%   extra       = struct array
%
% ************************************************
function extra = RemoveIndices(extra, StaticTable)
```

```
index = [];

% Make a list for indicies to remove
% OBS! extra.dk is chosen in FilterAirData
if length(StaticTable)>0
    kmin = 1;
    for kk = 1:length(StaticTable)
        %min = index(kk)-extra.dk;
        %max = index(kk)+extra.dk;
        kmax = kmin + 2*extra.dk;
        IndexList(kmin:kmax) = (StaticTable(kk)-extra.dk):(StaticTable(kk)+extra.dk);
        Indmin(kk) = StaticTable(kk)-extra.dk;
        Indmax(kk) = StaticTable(kk)+extra.dk;
        kmin = kmax+1;
     end;
end;

lenold = length(extra.spectra);
% finds indicies within the interval Indmin-Indmax
in = find((extra.spectra(:,1) >= Indmin(1)) & (extra.spectra(:,1) <= Indmax(1)));
    if ~isempty(in)
        extra.spectra(in,:) = [];
    else
        %fprintf('Empty matrix of indices for freq.: %f \n', StaticTable(k)*3.1);
        nnnn = 1;
    end
lennew = length(extra.spectra);
lendiff = lenold-lennew;
inmax = in(length(in))-lendiff;

% Find index from file
for k = 2:length(StaticTable)
    lenold = length(extra.spectra);
    in = find((extra.spectra(inmax:lenold,1) >= Indmin(k)) & (extra.spectra(inmax:lenold,1) <=
Indmax(k)));
    in = in+inmax-1;
    %pause
            if ~isempty(in)
                extra.spectra(in,:) = [];
                lennew = length(extra.spectra);
                lendiff = lenold-lennew;
                inmax = in(length(in))-lendiff;
                in=[];
            else
                %fprintf('Empty matrix of indices for freq.: %f \n', StaticTable(k)*3.1);
                nnnn = 1;
            end
    %fprintf('k = %d index = %d freq = %f\n',k,index(k),extra.spectra(index(k),1)*df);
end
index = index';

% Remove index from file
index(any(isnan(index),2),:) = [];

% Totaly removed number of indicies
extra.removed = (extra.dk*2 +1)*length(index);


% ************************************************
% Subfunction: RemoveNoise
% Remove Noise Frequencies from spectra file when
% automatically filtering
%
% Input variables:
%   extra       = struct array
%   noiseindex  = list of frequencies above a threshold value
%   StaticTable = list of frequencies to be removed
%
% Output variables:
%   extra       = struct array
%
% ************************************************
function extra = RemoveNoise(extra, noiseindex, StaticTable)

index = [];
```

```
% Find index for frequencies to be removed in "old" data
for k = 1:length(noiseindex)
    index(k) = find(extra.spectra(:,1) == StaticTable(noiseindex(k),1));
end

% Choosing bandwith to remove from file
width = input('Choose bandwidth to remove (in Hz): ');
df = 800000/(2^18);
dk = round(width/df);
%dk = 6;                            % 6 index * 3Hz = 18 Hz

if length(index)>0
    for kk = 1:length(index)
        % Give the data to be removed the value NaN
        % and an interval of dk around it...
        extra.spectra(index(kk)-dk:1:index(kk)+dk,:) = NaN;
     end;
end;

% Remove any rows containing NaNs from a matrix X
extra.spectra(any(isnan(extra.spectra),2),:) = [];

% Totaly removed number of frequencies
extra.removed = (dk*2 +1)*length(index);
```

D-4 Main function: ChangeSign.m

```
function ChangeSign

% ************************************************
% Read the filtered files, change sign (and components)
% and save it as a new filtered file in a chosen
% directory

% Input variables:
%
% Output variables:
%
% Called functions:
%   lmax        (mainfunction)
%   lmin        (mainfunction)
%
% Comment:
% Detailed information of the content in the spectra files
% can be found in file documentation 'files_info.doc'.
% ************************************************

datapath    = uigetdir('C:\','Select the data directory to read')
resultpath  = uigetdir('C:\','Select the results directory to write')
files = dir(datapath);
NoofFiles = size(files);

for kk =3:NoofFiles

    file = files(kk).name;
    fprintf(' The data file being processed: %s \n',file)

    % open files
    fid1 = fopen([datapath '\' file]);
    fid2 = fopen([resultpath '\' 'new_' file], 'wt');

    % Reading the spectra file header:
    extra.first_segment = fscanf(fid1,'%d ',1);
    extra.last_segment  = fscanf(fid1,'%d ',1);
    extra.used_channels = fscanf(fid1,'%d ',1);
    extra.project_name  = fscanf(fid1,'%s ',1);
    extra.line_number   = fscanf(fid1,'%d ',1);
    extra.station_number= fscanf(fid1,'%d ',1);

    % Number of stations in file
    N = extra.last_segment - extra.first_segment;

    extra.spectra = [];
    extra.num_transmitters = [];
    ind_change = [];
    XX = [];
    test1 = []; test2 = [];

    add = 1;
    % Reading information for the transmitters
    for i = 1:N
        if ~feof(fid1)

            %Reading information header about the transmitters
            extra.segment_counter(i)   = fscanf(fid1,'%f',1);
            extra.timestamp_tv_sec(i)  = fscanf(fid1,'%f',1);
            extra.timestamp_tv_usec(i) = fscanf(fid1,'%f',1);
            extra.latitude(i)          = fscanf(fid1,'%f',1);
            extra.longitude(i)         = fscanf(fid1,'%f',1);
            extra.X(i)                 = fscanf(fid1,'%f',1);
            extra.Y(i)                 = fscanf(fid1,'%f',1);
            extra.altitude(i)          = fscanf(fid1,'%f',1);
            extra.position_quality(i)  = fscanf(fid1,'%f',1);
            extra.heading(i)           = fscanf(fid1,'%f',1);
            extra.pitch(i)             = fscanf(fid1,'%f',1);
            extra.roll(i)              = fscanf(fid1,'%f',1);
            extra.orientation_quality(i)  = fscanf(fid1,'%f',1);
            extra.sn_treshold(i)       = fscanf(fid1,'%f',1);
            extra.num_transmitters(i)  = fscanf(fid1,'%d',1);
```

```
            %Reading information from spectra data
            slask = fscanf(fid1,'%f %f %f %f %f %f %f %f %f \n',[9,extra.num_transmitters(i)]);
            extra.spectra(:,1:9) = slask';

%             % Shift columns for Hx and Hz *************************
%             shift_Hx_re = extra.spectra(:,4);
%             shift_Hx_im = extra.spectra(:,5);
%
%             extra.spectra(:,4) = extra.spectra(:,8);    % Hx_re --> Hz_re
%             extra.spectra(:,5) = extra.spectra(:,9);    % Hx_im --> Hz_im
%             extra.spectra(:,8) = shift_Hx_re;           % Hz_re --> Hx_re
%             extra.spectra(:,9) = shift_Hx_im;           % Hz_im --> Hx_im
%             % ****************************************************

            % Save information to spectra data
            IndexRout(i) = length(extra.spectra);
            Results(add:add+IndexRout(i)-1,1:9) = extra.spectra(:,1:9);
            add = add+IndexRout(i);

            XX = [XX extra.X(i)];
            test1 = [test1 extra.spectra(100,4)];

            extra.spectra = [];

        else
            %fprintf('End of file reached \n');
            break;
        end         % END if ~feof(fid1)
    end             % END for i=1:(N)

    EndInd = i;
    fclose(fid1);

%     % Shift sign on Hx and Hy ***************
%     % by calculation with gradient
%     % ***********************************
%
%     % Check of direction
%     FX = gradient(X);
%
%     % Interpolation to get ride of zero-values
%     for p = 2:length(FX)-1;
%       if FX(p) == 0
%           %FX(p) = interp1(extra.segment_counter, FX, extra.segment_counter(p));
%
%           % Calculates the mean for the "zeros"
%           FX(p) = (FX(p+1)+FX(p-1))/2;
%       end;
%     end;
%
%     % (if grad of X is negative --> change sign on both Hx and Hy)
%     for m = 1:length(FX)
%       if  FX(m) <0
%           for mm = 1:10
%               extra.spectra(mm,3,m) = -extra.spectra(mm,3,m); %Hx_real
%               extra.spectra(mm,4,m) = -extra.spectra(mm,4,m); %Hx_im
%               extra.spectra(mm,6,m) = -extra.spectra(mm,6,m); %Hy_real
%               extra.spectra(mm,7,m) = -extra.spectra(mm,7,m); %Hy_im
%           end;
%       end;
%     end;

    % Shift sign on Hx and Hy ***************
    % by finding extrem minima and maxima
    %
    % Called functions:
    %   lmax    (mainfunction)
    %   lmin    (mainfunction)
    %
    % ***********************************

    % Find extrem minima and extrem maxima
    df = 120;                                   % intervall
    [b,a]=lmax(XX,df);                          % b = value, a = index
    [d,c]=lmin(XX,df);                          % d = value, c = index
```

```
len_max = length(a)
len_min = length(c)
len = min(len_max, len_min)

if (len_max > 0) && (len_min >0)
        % Check if first max is before or after first min
        % if (first maxima - first minima) is negative then it is ok!
        % --> change sign for Hx and Hy for index to the right of maxima
        % else change sign for Hx and Hy for index to the left of maxima
        ind_check = a(1) - c(1);

        ind_change = [];
        for i=1:len;
            if ind_check < 0
                ind_change = [ind_change a(i):c(i)];
            else
                ind_change = [ind_change c(i):a(i)];
            end;
        end;

        % add indicies for the ends
        if len_min == len_max
            ind_change = ind_change;

        elseif len_min < len_max;
            add_index = a(len_max):length(XX);
            ind_change = [ind_change add_index];

        elseif len_min > len_max;
            add_index = 1:a(1);
            ind_change = [ind_change add_index];
        end;

elseif (len_max > 0) && (len_min ==0);
        % i.e. a negative slope
        ind_change = a(len_max):length(XX);

elseif (len_max == 0) && (len_min > 0);
        % i.e. a positive slope
        ind_change = 1:c(1);

elseif (len_max == 0) && (len_min == 0);
        % Check if the slope is negative or positive
        % with help of the 10 first values in XX
        FX = XX(1:10);
        GradX = gradient(FX);
        if sum(GradX) < 0
            ind_change = 1:length(XX);
        else
            ind_change = [];
        end;

end;    %END if (len_max > 0) && (len_min >0)

% Change of sign
for k = 1:length(ind_change)

        ii = ind_change(k);
        if ii > 1
            L1 = sum(IndexRout(1):IndexRout(ii-1));
            L2 = sum(L1 + IndexRout(ii));

            Results(L1+1:L2,4) = -Results(L1+1:L2,4);   %Hx_real
            Results(L1+1:L2,5) = -Results(L1+1:L2,5);   %Hx_im
            Results(L1+1:L2,6) = -Results(L1+1:L2,6);   %Hy_real
            Results(L1+1:L2,7) = -Results(L1+1:L2,7);   %Hy_im

        else
            L1 = IndexRout(ii);

            Results(1:L1,4) = -Results(1:L1,4);         %Hx_real
            Results(1:L1,5) = -Results(1:L1,5);         %Hx_im
            Results(1:L1,6) = -Results(1:L1,6);         %Hy_real
            Results(1:L1,7) = -Results(1:L1,7);         %Hy_im
        end;
end;
```

```
    % Save the spectra file header in the new file:
    fprintf(fid2,'%10d ',extra.first_segment);
    fprintf(fid2,'%10d ',extra.last_segment);
    fprintf(fid2,'%10d ',extra.used_channels);
    fprintf(fid2,'%s ',extra.project_name);
    fprintf(fid2,'%10d ',extra.line_number);
    fprintf(fid2,'%10d \n',extra.station_number);

    % Save information header about the transmitters in new file
    add = 1;
    for i =1:EndInd-1
        fprintf(fid2,'%10d ',extra.segment_counter(i));
        fprintf(fid2,'%10d ',extra.timestamp_tv_sec(i));
        fprintf(fid2,'%10d ',extra.timestamp_tv_usec(i));
        fprintf(fid2,'%10.5f ',extra.latitude(i));
        fprintf(fid2,'%10.5f ',extra.longitude(i));
        fprintf(fid2,'%10.1f ',extra.X(i));
        fprintf(fid2,'%10.1f ',extra.Y(i));
        fprintf(fid2,'%10.3f ',extra.altitude(i));
        fprintf(fid2,'%1d ',extra.position_quality(i));
        fprintf(fid2,'%8.3f ',extra.heading(i));
        fprintf(fid2,'%8.3f ',extra.pitch(i));
        fprintf(fid2,'%8.3f ',extra.roll(i));
        fprintf(fid2,'%1d ',extra.orientation_quality(i));
        fprintf(fid2,'%9.3f ',extra.sn_treshold(i));
        fprintf(fid2,'%d \n',extra.num_transmitters(i));
        fprintf(fid2,'%8d %7.1f %5.2f %10.5f %10.5f %10.5f %10.5f %10.5f %10.5f
\n',Results(add:add+IndexRout(i)-1,1:9)');
        add = add+IndexRout(i);
    end;

end;              % END for kk =3:NoofFiles
fclose(fid2);
```

D-5 Main function: RunTensor.m

```
function RunTensor

% ************************************************
% Reading all tensor-files in a directory (processed
% after mfr2nd) and save them as 10 different
% stacked frequecy files (.xyz) for further processing
% in the software 'Oasis Montaj'
%
%
% Comment 1:
% The tensor files consist of 2 headers and 10 lines
% of data for each station.
% Detailed information of the content in the files
% can be found in file documentation 'files_info.doc'.
%
% Comment 2:
% For some reason the files in the chosen directory is
% read with hundreds (100-tal) before dozens (10-tal).
% Due to this the processing has to be done in two steps:
% First by reading the dozens and then the hundreds.
% The result from the second processing is added in the
% "old" file.
%
% Comment 3: OBS!!!
% Due to the processing in two steps the saving of the
% header must be removed in the second processing step!
% (See marking in code below)
%
% ************************************************

datapath    = uigetdir('C:\','Select the data directory to read')
resultpath  = uigetdir('C:\','Select the results directory to write')
files       = dir(datapath);
NoofFiles   = size(files);

for num = 1:10  %Number of stacked frequencies in the tensor-file.
    for kk =3:NoofFiles

        fprintf(' The data file being processed: %s \n',files(kk).name)

        %Open files
        fid1 = fopen([datapath '\' files(kk).name]);
        nr = num2str(num);
        fid3 = fopen([resultpath '\' 'Torsby_tensor', nr, '.xyz'], 'at');

        % Reading the 1st tensor file header:
        extra.first_segment = fscanf(fid1,'%d ',1);
        extra.last_segment  = fscanf(fid1,'%d ',1);
        extra.used_channels = fscanf(fid1,'%d ',1);
        extra.project_name  = fscanf(fid1,'%s ',1);
        extra.line_number   = fscanf(fid1,'%d ',1);
        extra.station_number= fscanf(fid1,'%d ',1);

        % Number of stations in file
        N = extra.last_segment - extra.first_segment;

        for i=1:N
            if ~feof(fid1)

                %Reading information header
                extra.segment_counter(i)   = fscanf(fid1,'%f',1);
                extra.timestamp_tv_sec(i)  = fscanf(fid1,'%f',1);
                extra.timestamp_tv_usec(i) = fscanf(fid1,'%f',1);
                extra.latitude(i)          = fscanf(fid1,'%f',1);
                extra.longitude(i)         = fscanf(fid1,'%f',1);
                extra.X(i)                 = fscanf(fid1,'%f',1);
                extra.Y(i)                 = fscanf(fid1,'%f',1);
                extra.altitude(i)          = fscanf(fid1,'%f',1);
                extra.position_quality(i)  = fscanf(fid1,'%f',1);
                extra.heading(i)           = fscanf(fid1,'%f',1);
                extra.pitch(i)             = fscanf(fid1,'%f',1);
                extra.roll(i)              = fscanf(fid1,'%f',1);
                extra.orientation_quality(i)  = fscanf(fid1,'%f',1);
```

```
                extra.sn_treshold(i)       = fscanf(fid1,'%f',1);
                extra.num_transmitters(i)  = fscanf(fid1,'%d',1);

                %Reading information from tensor data
                slask(:,:,i) = fscanf(fid1,'%f %f %f %f %f %f %f %f \n',[8,10]);
                extra.spectra(:,:,i) = slask(:,:,i)';

                if i < N
                    % Reading the tensor file header:
                    extra.first_segment = fscanf(fid1,'%d ',1);
                    extra.last_segment  = fscanf(fid1,'%d ',1);
                    extra.used_channels = fscanf(fid1,'%d ',1);
                    extra.project_name  = fscanf(fid1,'%s ',1);
                    extra.line_number   = fscanf(fid1,'%d ',1);
                    extra.station_number= fscanf(fid1,'%d ',1);
                end;

            else
                %fprintf('End of file reached \n');
            end
        end

        XX = extra.X;

        %*********************************************
        % THIS PART HAS TO BE REMOVED IF THE PROCESSING IS
        % DONE IN MORE THAN ONE STEP!

        if num == 1
            % Save header in new file
            if kk == 3
                fprintf(fid3, ' %s ', ' X ');
                fprintf(fid3, ' %s ', ' Y ');
                fprintf(fid3, ' %s ', ' Z ');
                fprintf(fid3, ' %s '  ,' AR ');
                fprintf(fid3, ' %s '  ,' AI ');
                fprintf(fid3, ' %s '  ,' AE ');
                fprintf(fid3, ' %s '  ,' BR ');
                fprintf(fid3, ' %s '  ,' BI ');
                fprintf(fid3, ' %s '  ,' BE ');
                fprintf(fid3,'\n');
                fprintf(fid3,' %s \n', 'Line 1');
            end;
        end;
        %*********************************************


        % Save information to new file
        for k = 1:(N-1)
            fprintf(fid3,'%10.1f ',XX(k));
            fprintf(fid3,'%10.1f ',extra.Y(k));
            fprintf(fid3,'%5.1f ',extra.altitude(k));
            fprintf(fid3,'%10.6f\t %10.6f\t %10.6f\t %10.6f\t %10.6f\t
%10.6f\n',extra.spectra(num,3:8,k)');
        end;
    end;

    n = num2str(num);
    fprintf('Data file %s is ready! \n', n);
    pause(0.01);

end;
disp('function:RunTensor - ready!')
fclose all;
```

APPENDIX B

UPPSALA UNIVERSITET
Institutionen för Geovetenspaker – Geofysik

UNIVERSIDAD SIMÓN BOLÍVAR
Departamento de Ciencias de la Tierra – Ingeniería Geofísica

Post-processing of Airborne data using the Broadband Frequency Receiver instrument ADU07

Miguel Ángel Alfonzo Carmona.

Uppsala, June 2009.

ABSTRACT

In August 2008 and June 2009 two sets of airborne measurements were made in Falun and Börlänge, respectively, by the Geological Survey of Sweden (SGU). The purpose of these campaigns was to test the new Multi Frequency Receiver (MFR) instrument called ADU07 for the collection of airborne data in the VLF and LF bands. This system was designed by Metronix and adapted by Uppsala University together with the SGU in the frame of a joint research project.

The SGU in its bedrock mapping program routinely records VLF signals from only two transmitters in the frequency band of 14-30 kHz. The RMT technique also makes use of electromagnetic signals in both the VLF and LF bands in the frequency range of 10-250 kHz. By measuring all the three magnetic field components in this broader band, the data acquired by the new MFR system can provide high lateral and vertical resolution compared to the VLF data. This can be done by applying the concepts used for the EnviroMT. The joint research therefore aims at extending the VLF technique currently used by the SGU for geophysical investigations and whereby generating improved and more detailed anomaly maps.

The airborne measurements with the ADU07 system were performed by continuously recording the three magnetic field components with a sampling frequency of 512 kHz in three channels. The prior evaluation of the data gave good results in the beginning. However, later tests showed that there were some near field sources onboard the aeroplane that contaminated the data and highly affected the estimation of transfer functions from the radio transmitters' signals. The noise was basically generated by other measuring instrumentation and the common power supply used to feed both the ADU07 and the PC controller. The main aim of the present project is to develop a processing method that identifies frequencies from these near field sources and filters them out from the spectral ADU07 data. This work has been carried out by writing MATLAB routines. After the filtering, more reliable transfer functions that provide relevant information about the Earth's resistivity structure can be estimated.

Different methods were applied in order to detect the noise in the data. The mean value of the real part of the vertical magnetic field component (H_z) and the scalar tippers were firstly calculated along the profiles. These values should normally be close to zero. These methods did not give any valuable information since no patterns could be seen in the results. Afterwards, the vertical signal-to-noise ratio (VSNR) was calculated for every frequency at each station. This criterion showed that, for the first campaign, there were practically two sets of noise frequencies in the spectra: the first group corresponds to the even and odd harmonics of frequency 8 kHz, and the second group to frequency 23.47 kHz and its harmonics. For the last campaign, frequency 10.28 kHz and its harmonics were identified. The band averaging technique that splits the main frequency band into 9 overlapping sub-bands with 1 octave of width was used. Finally, Prediction Errors (PE's) were estimated to detect the remaining noise. A threshold was then chosen in order to remove from the spectra those frequencies with a PE above 3 and up to 20% of the number of transmitters in the sub-bands. These processing steps improved considerably the tipper behaviour for the VLF band along the profiles, although some noise was also added. For the LF band, the filtering steps seem to have worsened the data quality and therefore the tipper estimation.

The removal of important frequencies that were hidden in the high noise levels and the use of some other instruments during the data collection could be the causes of these responses.

ACKNOWLEDGEMENTS

First of all, I would like to thank my family for giving me all the support I have needed during my life. Special thanks must go to my mum for always encouraging me to keep walking even in the most difficult situations.

Thanks to my supervisor Laust B. Pedersen for introducing me to this project.

Many thanks to my supervisor Mehrdad Bastani for all the hours of teaching and help throughout the project and always trying to find a solution when everything seemed to have no way out.

I am especially grateful to Universidad Simón Bolívar, my home university, for giving me the opportunity to come as an exchange student and making me live one of the most wonderful experiences of my life. Likewise, thanks to Uppsala University for opening me up its doors and contributing significantly in my academic and personal formation.

Finally, special thanks go to my good friends Luis Gavidia, Jennifer Love, Ramón Bruzual and Gorka Fagilde for giving me their invaluable friendship and making my days here in Uppsala and Europe more fun.

Contents

Chapter 1

Introduction

In August 2008 a set of airborne measurements were made in Falun, an area located about 95 kilometres in the northwest of Gävle in Sweden. Later, in June 2009, a new set of airborne data was collected in the area between Uppsala and Börlänge. The purpose of these campaigns was to test the new Multi Frequency Receiver (MFR) system called ADU07 for airborne measurements in the VLF and LF bands. The instrument was developed by Metronix. The software for data acquisition and processing was designed by Uppsala University in collaboration with the Geological Survey of Sweden (SGU). Thus, the system was tuned for measurements in the frequency band of 10-250 kHz in order to extend the VLF technique currently used by the SGU for geophysical investigations.

The VLF method practically measures the signals from only one transmitter in the VLF band (14-30 kHz). This generates problems since there are very few transmitters working in this frequency range and the responses from geological discontinuities are dependent on the strike direction. Therefore, the vertical resolution reached by the SGU's VLF instrument is very poor and sometimes structures cannot be resolved at all.

On the other hand, the Radio Magnetotelluric (RMT) technique works in the frequency range of 10-250 kHz, thus using both the VLF and LF bands. This makes it possible to accomplish higher lateral and vertical resolution than the VLF method itself. For this reason, the construction of the new MFR instrument was suggested by Uppsala University as a joint project with the SGU. This system would be based on the concepts used for the EnviroMT in order to improve the measurements by extending the frequency band up to 250 kHz and making a user-friendly instrument that could be operated by only one person in the field.

The MFR system was used in November 2007 onboard the SGU's aeroplane to test the concept. However, the measurements were not useful due to strong effects from the electronics on the aeroplane and the low number of bits (16). On the other hand, the ADU07 system from Metronix GmbH in Germany is a 24-bit instrument and can therefore be used in noisy environments. It was thus adapted by Uppsala University together with the SGU to continuously collect the data with a sampling frequency of 512 kHz in the three magnetic channels. Two airborne test measurements were then carried out with the ADU07. In either of them the data were highly contaminated by the local noise sources on the aeroplane, the so-called near field sources.

The main aim of this project is to develop a method that identifies the near field sources and filters them out from the ADU07 data. The processing is done by MATLAB routines in order to efficiently eliminate the noise from the spectra. Afterwards, reliable transfer functions giving useful information about the Earth's resistivity structure are meant to be calculated.

Chapter 2

Electromagnetic Theory

The electromagnetic methods are based on the relation between electric and magnetic fields. The understanding of the basic concepts and principles governing the interaction of these fields with the Earth is of paramount importance in order to successfully interpret the electromagnetic data collected in a studied area. Therefore, the fundamentals of the electromagnetic theory are briefly explained below.

2.1 Maxwell's equations.

The basic theory of electromagnetic fields originates in the works of the Scottish mathematician James Clerk Maxwell. His most significant discovery was to prove that electric and magnetic fields and fluxes are coupled and governed by four fundamental laws. Assuming a time dependence of $e^{i\omega t}$ in the frequency domain, these relations can be expressed as:

$$\nabla \times \mathbf{E} = -i\omega\mathbf{B} \qquad \text{Faraday's law} \qquad (2.1)$$

$$\nabla \times \mathbf{H} = \mathbf{J} + i\omega\mathbf{D} \qquad \text{Ampère's law} \qquad (2.2)$$

$$\nabla \cdot \mathbf{D} = \rho \qquad \text{Gauss's law for electricity} \qquad (2.3)$$

$$\nabla \cdot \mathbf{B} = 0 \qquad \text{Gauss's law for magnetism} \qquad (2.4)$$

where, in the SI system:

E = electric field intensity (V/m).

B = magnetic induction (Wb/m^2 or T).

H = magnetic field intensity (A/m).

D = dielectric displacement (C/m^2).

J = electric current density (A/m^2).

$\omega = 2\pi f$ = angular frequency (Hz).

ρ = electric charge density (C/m^3).

The above expressions are related to one another by the following **constitutive equations**. These relations set the foundation of the classic electromagnetic field theory.

$$\mathbf{D} = \varepsilon\mathbf{E} \tag{2.5}$$

$$\mathbf{B} = \mu\mathbf{H} \tag{2.6}$$

$$\mathbf{J} = \sigma\mathbf{E} \tag{2.7}$$

Where:

ε = electric permittivity (F/m).

μ = magnetic permeability (H/m).

σ = conductivity (S/m).

The parameters ε, μ and σ describe the intrinsic properties of the materials through which electromagnetic waves propagate.

2.2 Electromagnetic wave equations.

The general wave relations for electric and magnetic fields can be derived from Maxwell's equations. With a time variation of $e^{i\omega t}$, expressions (2.1), (2.2), (2.5) and (2.6) can be written as:

$$\nabla \times \mathbf{E} = -i\omega\mu\mathbf{H} \tag{2.8}$$

$$\nabla \times \mathbf{H} = \sigma\mathbf{E} + i\omega\varepsilon\mathbf{E} \tag{2.9}$$

Assuming no free charges (ρ=0) and using the vector identity $\nabla \times \nabla \times \mathbf{A} = \nabla(\nabla.\mathbf{A}) - \nabla^2\mathbf{A}$, the solution for an electromagnetic wave travelling in homogeneous regions becomes:

$$\nabla^2\mathbf{E} + k^2\mathbf{E} = 0 \tag{2.10}$$

$$\nabla^2\mathbf{H} + k^2\mathbf{H} = 0 \tag{2.11}$$

These expressions are also known as Helmholtz's equations and represent the electromagnetic wave relations in a linear, source free and homogeneous medium (Bastani, 2001). The complex wave number k is defined as:

$$k=(\mu\varepsilon\omega^2 - i\mu\sigma\omega)^{1/2} \tag{2.12}$$

For the frequency range used in most of the electromagnetic techniques for geophysical investigations (less than 300 kHz), it is possible to assume that $\mu\varepsilon\omega^2 \ll \mu\sigma\omega$ for typical earth materials. This is known as the quasi-static approximation and indicates that the

displacement current flow is negligible compared to the conduction current flow (Persson, 2001).

Thus, the parameter k can be simplified as:

$$k=(-i\mu\sigma\omega)^{1/2} \tag{2.13}$$

In such condition, expressions (2.10) and (2.11) are considered now as diffusion equations (Bastani, 2001).

It is important to highlight that special care must be exercised when applying the quasi-static approximation in the case where the resistivities of Earth materials are very high (Oskooi, 2004).

2.3 Plane waves.

In order to simplify field calculations significantly, the plane wave assumption can be considered. This states that if the wavelength is much larger than the penetration depth, then the wave front propagation is assumed to be planar (Hjärten, 2007). In the presence of a source, this situation is only valid at sufficiently large distances, where the wavelength λ of the primary field is much longer than the distance from the source itself.

A plane wave travels in one direction and has no dependence on other directions. This indicates that the electric and magnetic fields are perpendicular to the direction of propagation. The solutions of a plane wave travelling in the positive z-direction (down into the Earth) are given by:

$$\mathbf{E}(z,t) = \mathbf{E}_0 e^{-i(kz-\omega t)} \tag{2.14}$$

$$\mathbf{B}(z,t) = \mathbf{B}_0 e^{-i(kz-\omega t)} \tag{2.15}$$

Where $\mathbf{E}_0$ and $\mathbf{B}_0$ are the amplitudes of the electric and magnetic fields respectively.

2.4 Plane waves in a 1-D model.

This model consists of a homogeneous half space where the conductivity is constant along the different axes.

Equations (2.14) and (2.15) represent the solutions for plane waves in this model. The imaginary part of k results in an attenuation of the wave, that is, a decrease of the amplitude when increasing z (Gustavsson, 2008).

2.4.1 Skin depth.

The depth at which the amplitude is reduced by a factor of 1/e of its original value is called **skin depth**, and is a measure of how far waves penetrate into the ground. Equation (2.14) can be solved for the amplitude at the surface of the Earth (z=0), given that the complex wave number is:

$$k = -(i\mu\sigma\omega)^{1/2} = \alpha(1-i) \tag{2.16}$$

Where α is a real quantity defined as:

$$\alpha = \left(\frac{\omega\mu\sigma}{2}\right)^{1/2} \tag{2.17}$$

By substituting the obtained solution into equation (2.14) and then solving for z, the skin depth is found as:

$$\delta = \left(\frac{2}{\omega\mu\sigma}\right)^{1/2} \approx 503\left(\frac{1}{f\sigma}\right)^{1/2}[m] = 503\left(\frac{\rho}{f}\right)^{1/2}[\mathrm{m}] \tag{2.18}$$

This expression states that low frequencies and high resistivities cause a deeper wave penetration into the ground.

Another quantity of paramount importance is the **depth of investigation** or **penetration depth** (δ_p), which is defined as the maximum depth at which an anomalous body can be detected by a particular technique and frequency (Spies, 1989). He considers that, in the Magnetotelluric case, a satisfactory depth of investigation estimate is given by 1.5 skin depths:

$$\delta_p = 1.5\left(\frac{2}{\omega\mu\sigma}\right)^{1/2} \tag{2.19}$$

2.4.2 Impedance and phase.

The complex **impedance Z** is the resistance of the ground to electromagnetic fields. Z is a function of the angular frequency, electric conductivity and magnetic permeability, and is, in the simplest case, linearly related to the electric and magnetic fields (Hjärten, 2007).

For a 1-D model, the impedance is calculated by setting the derivatives with respect to x and y to zero, thus expanding the curl in equation (2.9). The obtained expressions are:

$$\frac{\partial E_x}{\partial z} = -i\omega\mu H_y \tag{2.20}$$

$$\frac{\partial E_y}{\partial z} = i\omega\mu H_x \tag{2.21}$$

By substituting the z derivative for the operator– ik, the impedance in a homogeneous half space is found as:

$$Z = \frac{\omega\mu}{k} = \frac{E_x}{H_y} = -\frac{E_y}{H_x} \cong \left(\frac{\omega\mu}{\sigma}\right)^{1/2} e^{i\pi/4} \tag{2.22}$$

This shows that the impedance increases as the square root of the frequency and the **phase** (ϕ) for a homogeneous half space is 45°. Thus, in a homogenous ground, the fields diffuse as an exponentially damped wave with E_x 45° ahead of H_y (Persson, 2001).

If the ground is non-homogenous, the phase difference between E_x and H_y depends on the resistivity of the horizontally layered Earth. If the top layer has a higher resistivity than the lower, the phase will be greater than 45°. Otherwise, it will be less than 45°.

The general expression for the phase is then given by:

$$\phi = \arctan\left(\frac{Im(Z)}{Re(Z)}\right) = \arctan\left(\frac{Im(E_x/H_y)}{Re(E_x/H_y)}\right) \tag{2.23}$$

Where *Re* and *Im* denote the real and imaginary part, respectively.

2.4.3 Apparent resistivity.

If the medium is homogeneous, the measured resistivity will be the true resistivity of the ground. However, heterogeneities in a medium give rise to an apparent resistivity. This is defined as the resistivity of a homogeneous half-space which produces the same response as that measured over the real Earth with the same acquisition parameters: position, transmitted current, etc. (Spies and Eggers, 1986).

By substituting the definition of the resistivity in the ground:

$$\rho = \frac{1}{\sigma} \tag{2.24}$$

Into equation (2.22), the apparent resistivity is defined as:

$$\rho_a = \frac{1}{\omega\mu}|Z^2| = \frac{1}{\omega\mu}\left|\frac{E_x}{H_y}\right|^2 \tag{2.25}$$

2.5 Plane waves in a 2-D model.

In practice, the Earth is generally approximated as a 2-D model. This means that the conductivity variation is negligible along one axis in the coordinate system, the so-called **strike direction** (Figure 2.1).

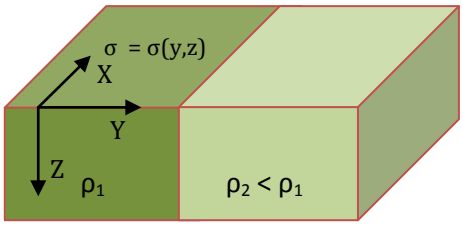

Figure 2.1: 2-D model where the geological strike is in the x-direction, indicating that the conductivity σ is a function of y and z. The y-direction is defined as the profile direction and z is pointing downwards into the ground. In this case $\rho_1 > \rho_2$.

By considering a vertical discontinuity with strike in the x-direction, a profile made in the y-direction, and the ideal 2-D case where the electric and magnetic fields are orthogonal, equations (2.1) and (2.2) can be decoupled into two different modes:

2.5.1 Transverse Magnetic (TM) mode.

In the TM-mode the magnetic field is in the strike direction and the electric field is perpendicular to it (Figure 2.2).

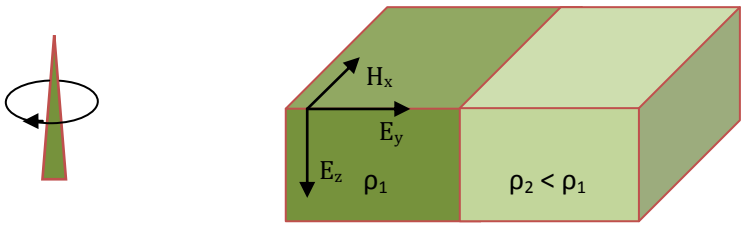

Figure 2.2: 2-D model showing the TM-mode or H-polarization. The plane wave from the transmitter is propagating perpendicularly to the strike. Thus, Hz = 0.

The magnetic field shows no variation over the contact since this field points along the strike direction and the current flow lies in the y- and z- directions. However, the horizontal electric field changes discontinuously across the boundary and charges are induced at the interface in order to account for this discontinuity.

In the case where $\rho_1 > \rho_2$, the apparent resistivity decreases rapidly and the phase shows a peak over the boundary (Persson, 2001).

2.5.2 Transverse Electric (TE) mode.

In the TE-mode, the electric field component is in the strike direction causing a flow of currents in the x-direction. This means that there is no accumulation of charges at the boundary and the electric field varies continuously across the interface (Figure 2.3).

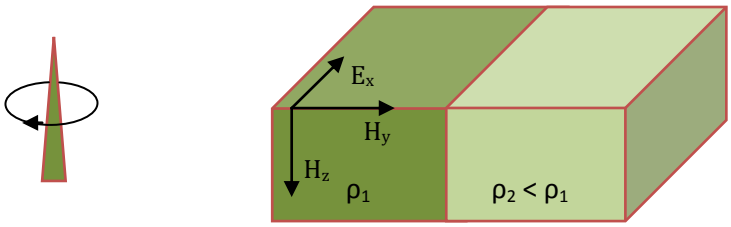

Figure 2.3: 2-D model showing the TE-mode or E-polarization. The plane wave from the transmitter is propagating parallel to the strike. Thus, Ez = 0.

However, in the case where $\rho_1 > \rho_2$, currents are magnified when entering the more conductive medium and the magnetic field changes considerably. Moreover, the induced current at the interface generates a vertical magnetic field in the vicinity of the contact and the resultant magnetic field is elliptically polarized.

The apparent resistivity shows a continuous decay over the boundary. This decay is frequency dependent and becomes more rapid when the frequency increases. Furthermore, the phase behaviour is almost completely reversed compared to its behaviour in the TM-mode.

2.6 Induction of secondary electromagnetic fields.

The radio signals which are far from a transmitter can be considered as plane waves propagating in all directions. If a wave propagates in the x-direction, the electromagnetic field of this wave will have a vertical electric field component E_z and a horizontal magnetic field component H_y (Gustavsson, 2008). At very large distances from the transmitter this primary field may be considered uniform.

According to equation (2.1) the magnetic field from the transmitter will induce a current in the Earth (Figure 2.4). These eddy currents will likewise create a secondary magnetic field which can be shifted in phase and oriented in another direction depending on the conductivity contrast and shape of the conductor.

Whereas the horizontal magnetic field is a mixture of the primary field and the secondary field, the vertical magnetic field is entirely of secondary origin.

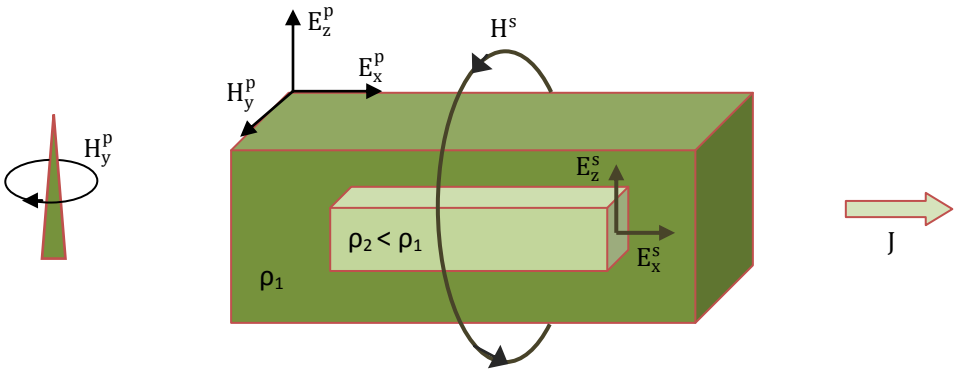

Figure 2.4: Induction of electromagnetic fields due to a conductor in the ground. The superscript p means primary and the superscript s means secondary. The magnetic field from the transmitter creates a current J in the Earth which produces electric field components E_x^s and E_z^s . Modified from Gustavsson (2008).

2.7 Near field and far field.

The behaviour of electromagnetic fields depends on some parameters, such as the distance to the source and the frequency. These fields are especially affected when the distance to the source increases. This fact allows making some approximations in three different zones: the near field, the far field and the transition zone (Hannes, 2009).

In the near field, the source receiver distance R is much shorter than the skin depth δ (R « δ). Here, the electric field **E** decays as $1/R^3$ and the magnetic field **H** as $1/R^2$. In the far field region, where the source receiver distance is much longer than the skin depth (R » δ or at least R ≈ 5δ), either the electric field **E** or the magnetic field **H** decays as $1/R^3$ and the plane wave assumption can be considered. The dielectric displacement **D** is also affected and changes from being frequency independent and geometry dependent to being frequency and resistivity dependent when changing from the near field to the far field.

In the transition zone (R ≈ δ) the fields vary very fast and either of the above cases is true for **E** and **H**. Likewise, **D** depends on frequency, resistivity and geometry.

2.8 Impedance tensor and tipper vector.

For plane waves, the horizontal components of the electric field (E_x, E_y) are related to the horizontal components of the magnetic field (H_x, H_y) by the following expression:

$$\begin{bmatrix} E_x \\ E_y \end{bmatrix} = \mathbf{Z} \begin{bmatrix} H_x \\ H_y \end{bmatrix} \tag{2.26}$$

where **Z** is a 2x2 matrix known as the complex **impedance**. This quantity is given by:

$$\mathbf{Z} = \begin{bmatrix} Z_{xx} & Z_{xy} \\ Z_{yx} & Z_{yy} \end{bmatrix} \tag{2.27}$$

The determinant of the impedance tensor, which is also called the effective impedance Z_{DET}, is defined as:

$$\mathbf{Z}_{DET} = \sqrt{Z_{xx} Z_{yy} - Z_{xy} Z_{yz}} \tag{2.28}$$

The advantage of using determinant data is that they provide a useful average of the impedance for all the current directions that can be inverted to provide robust 1-D and 2-D models. Moreover, no mode identifications (TE- and TM-mode) are required, static shift corrections are not made, and the dimensionality of the data is not considered (Oskooi, 2004).

Likewise, the vertical component of the magnetic field (H_z) is related to the horizontal components of the magnetic field (H_x, H_y) by:

$$H_z = \mathbf{T}^{\mathrm{T}} \begin{bmatrix} H_x \\ H_y \end{bmatrix} \tag{2.29}$$

where the superscript $^{\mathrm{T}}$ denotes transposition and **T** is a vector known as the complex **tipper**. This parameter is given by:

$$\mathbf{T} = (A, B)^T \tag{2.30}$$

where A and B are the complex components in the x- and y-directions respectively. These quantities are independent of the actual source of current and thereby only depend on the internal conductivity of the Earth (Pedersen et al. 1994).

The tipper is a complex quantity with real and imaginary parts. This is due to the fact that the underlying electromagnetic induction process in the Earth produces a time lag between the horizontal and vertical fields.

By substituting equation (2.30) into (2.29), the final expression for the vertical magnetic field component at sufficiently large distances from the source is found as:

$$H_z = AH_x + BH_y \tag{2.31}$$

Z and **T** are then known as Magnetotelluric Transfer functions. These parameters are dependent on the distance from the source, the wave number k and the angular frequency ω (Hellsborn, 2009).

Tipper data are not normally used quantitatively together with impedance data, but are used for dimensionality analysis and quantitative interpretation. Furthermore, tipper data are very useful for a qualitative identification of major lateral changes in electrical conductivity away from the profile. This is due to the fact that they represent the effect of currents over a much larger volume than impedances, which have more local support (Bastani, 2001).

The interpretation of the tipper can be made either by mapping or modelling. In the case of mapping, the tipper values are transformed into apparent resistivity and phase with which electrical resistivity maps can be generated (Becken and Pedersen, 2003). Modelling is made with least square inversion thereby generating resistivity depth sections.

The previous relations for the transfer functions are the general expressions for a 3-D Earth model. In the cases of 2-D and 1-D models some constraints can be applied in order to simplify the equations for the limited structure considered.

2.8.1 Analysis of the transfer functions.

2.8.1.1 1-D model.

In this case there are not preferred directions for the field components. This gives rise to the following simplifications of equations (2.27) and (2.30) for the impedance and the tipper:

$$\mathbf{Z} = \begin{bmatrix} 0 & \mathrm{Z} \\ -\mathrm{Z} & 0 \end{bmatrix} \tag{2.32}$$

where **Z** is given by (2.22).

$$\mathbf{T} = \begin{bmatrix} 0 \\ 0 \end{bmatrix} \tag{2.33}$$

2.8.1.2 2-D model: general case.

In practice, measurements are often performed in a coordinate system which is different from the strike coordinate system. In this case, the impedance and tipper have the following forms (Zhang et al., 1987):

$$\mathbf{Z} = \begin{bmatrix} \mathrm{Z_{xx}} & \mathrm{Z_{xy}} \\ \mathrm{Z_{yx}} & \mathrm{Z_{yy}} \end{bmatrix} \quad , \quad Z_{xx} = -Z_{yy} \tag{2.34}$$

$$\mathbf{T} = \begin{bmatrix} A \\ B \end{bmatrix} \tag{2.35}$$

Thus, the expression for $\mathrm{H_z}$ is the same as in the 3-D case.

2.8.1.3 2-D model: strike coordinate system.

In the strike coordinate system (principal coordinate system) the impedance tensor and the tipper vector have particularly simple structures (Bastani, 2001). Thus, equations (2.27) and (2.30) can be defined as:

For the impedance:

$$\mathbf{Z} = \begin{bmatrix} 0 & Z_{xy} \\ -Z_{yx} & 0 \end{bmatrix}, \ |Z_{xy}| \neq |Z_{yx}| \tag{2.36}$$

For the tipper:

$$\mathbf{T} = \begin{bmatrix} 0 \\ B \end{bmatrix} \tag{2.37}$$

The expression for H_z is now given by:

$$H_z = BH_y \tag{2.38}$$

The tipper therefore varies along the profile showing the strongest variation close to a resistivity contrast (Gustavsson, 2008).

It is important to highlight that these constraints are theoretical and in real field measurements the components do not have exact zero responses. This is especially due to noise and the fact that a natural subsurface always has some 3-D inhomogeneities.

2.8.2 Tipper vector in TE-mode.

The real part of the tipper always points away from a conductor in the far field. This means that, for a given frequency, the real part changes its sign when crossing a conductive body. The imaginary part, on the other hand, is more complex since it is dependent on the depth of the body. Therefore, when there is a conductor at a given depth, the imaginary part changes its sign from positive to negative when decreasing frequency (Pedersen et al., 2005).

The reason why the imaginary part of the tipper vector is more complex is that it contains the response from two wavelengths with two different polarizations. The first has a short-wavelength response with same polarity as the real component. The second has a long-wavelength response with opposite polarity compared to the real component. This makes the imaginary component dependent on the depth. If the depth increases, the short wavelength response disappears and the long wavelength takes over with its reversed polarity.

For this reason, in the case of small resistivity variations near the surface, anomalies with the same polarity can be seen for both the real and the imaginary components. If there is a conductive target or deep low-resistive structures instead, anomalies with reversed polarity in the imaginary part can be observed (Persson, 2001).

2.8.3 Rotation of the coordinate system.

As said before, measurements are generally made in a coordinate system other than the strike coordinate system (Figure 2.5). This fact influences considerably the measured responses. In order to have an interpretable result, the components of the electromagnetic field must be rotated so the conductive anomaly is aligned along one of the horizontal coordinate axes.

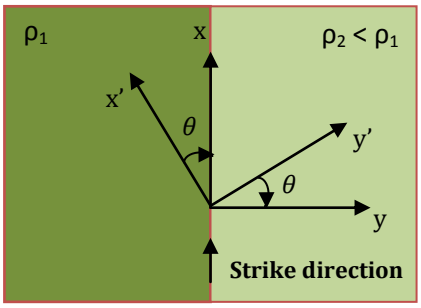

Figure 2.5: Representation of the used coordinate system and the strike coordinate system.

Assuming that θ is the angle between the horizontal axes of the used coordinate system (x',y') and the horizontal axes of the strike coordinate system (x, y), the measured electromagnetic field components (H_x', H_y', H_z', E_x', E_y') and the electromagnetic field components (H_x, H_y, H_z, E_x, E_y) are related by the following expressions:

$$\begin{bmatrix} H_x' \\ H_y' \end{bmatrix} = \mathbf{R} \begin{bmatrix} H_x \\ H_y \end{bmatrix} \tag{2.39}$$

$$\begin{bmatrix} E_x' \\ E_y' \end{bmatrix} = \mathbf{R} \begin{bmatrix} E_x \\ E_y \end{bmatrix} \tag{2.40}$$

Where **R** is the **rotation matrix** defined as:

$$\mathbf{R} = \begin{bmatrix} \cos(\theta) & -\sin(\theta) \\ \sin(\theta) & \cos(\theta) \end{bmatrix} \tag{2.41}$$

The rotation matrix **R** needs to be two-dimensional since the rotation is usually applied to the horizontal plane.

In the used coordinate system, equations (2.26) and (2.29) are expressed as:

$$\begin{bmatrix} E'_x \\ E'_y \end{bmatrix} = \mathbf{Z}' \begin{bmatrix} H'_x \\ H'_y \end{bmatrix} \tag{2.42}$$

$$H'_z = \mathbf{T}'^{\mathrm{T}} \begin{bmatrix} H'_x \\ H'_y \end{bmatrix} \tag{2.43}$$

Considering that the rotation is not applied to the vertical component H_z, that is, $H_z' = H_z$, the rotated impedance tensor and tipper vector can be written as:

$$\mathbf{Z} = \mathbf{R}^{\mathrm{T}} \mathbf{Z}' \mathbf{R} \tag{2.44}$$

$$\mathbf{T} = \mathbf{R}^{\mathrm{T}} \mathbf{T}' \tag{2.45}$$

Equation (2.44) indicates that the trace of the impedance tensor is invariant to the rotation of the coordinate axes (Bastani, 2001).

Chapter 3

Radio Magnetotelluric (RMT) method

3.1 Background.

Plasma processes in the Earth's magnetosphere and the lightning discharges in the ionosphere produce significant natural electromagnetic fluctuations in the frequency range of 10^{-6} to 10^{4} Hz (Oskooi and Pedersen, 2005). The method which makes use of magnetic field components and natural currents in order to image the resistivity of the Earth's structure from depths of only tens of metres stretching as far as several hundred kilometres is called Magnetotellurics (MT).

The Magnetotelluric method is the oldest amongst the plane wave frequency domain electromagnetic (PWEM) techniques and is specially used to map conductivity structures in the Earth crust and mantle. However, due to weak source fields at higher frequencies than 1000 Hz and man-made noise below 1000 Hz in industrialised areas, considerable efforts must be made in order to suppress these influences on the impedance estimates (Bastani, 2001).

Therefore, from the 1960s artificial sources have been widely used in electromagnetic techniques for geophysical investigations. Some of these methods are the Controlled Source Audio Magnetotelluric (CSAMT), Very Low Frequency (VLF) and Radio Magnetotelluric (RMT). The differences between them are based basically on the nature of the source, the field layout and the used frequency range (Table 3.1).

The electromagnetic spectrum is divided into 26 bands or frequency ranges that are named in alphabetical order. The lowest bands of interest are: Extra Low Frequency or Voice Frequency (VF: 300 Hz-3 kHz), Very Low Frequency (VLF: 3-30 kHz), Low Frequency (LF: 30-300 kHz) and Medium Frequency (MF: 300-3000 kHz).

Method	Source	Frequency range	Application
MT	Natural	10^{-4} – 1000 Hz	Lithosphere studies.
CSAMT	Artificial controlled source	Variable	Shallow investigations to deep crust sounding.
VLF	VLF transmitters	14 – 30 kHz	Low resolution shallow investigations.
RMT	VLF and LF transmitters	10 – 250 kHz	Shallow investigations and environmental studies.

Table 3.1: Comparison between the different PWEM methods. Modified from Bastani (2001).

Two of the most popular techniques which work in lowest frequency ranges are briefly explained as follows:

3.1.1 Very Low Frequency (VLF) method.

VLF is a method used to quickly map near-surface structures in the Earth. It was used for the first time in the 1960s after discovering that VLF signals could be used for geophysical investigations besides submarine communication. This method was first applied in Sweden by the Geological Survey of Sweden (SGU) in Lapland, where the results showed that the technique was very useful for mineral exploration (Persson, 2001).

The VLF method works in the frequency range of 14-30 kHz and is divided into two categories based on the measured parameters (Oskooi, 2004). In the conventional VLF method (VLF-Z or VLF-EM) the two horizontal and the vertical components of the magnetic field are measured. The transfer function between them reflects the lateral changes in conductivity along the area.

In the VLF Resistivity (VLF-R), one horizontal magnetic component and one horizontal electric component are measured. Thereby, either the phase or the scalar apparent resistivity can be calculated for each station by using equations (2.23) and (2.25) respectively.

The sources for VLF are powerful transmitters preferably located at long distances from the profile. The best response for geological discontinuities in the ground is obtained with a transmitter located in the strike direction. Structures perpendicular to the strike are not imaged at all.

Ground VLF surveys provide a quick and powerful tool for the study of geological structures to a maximum depth of about 100 metres. However, since the VLF data have a very narrow bandwidth, the recorded signal may be very weak and in some cases structures are not resolved in detail (Oskooi and Pedersen, 2005). Nowadays, the Radio Magnetotelluric (RMT) method is used to overcome this problem.

3.1.2 Radio Magnetotelluric (RMT) method.

The Radio Magnetotelluric (RMT) method is a technique that makes use of both the VLF and LF bands and is similar to the VLF technique. However, since the RMT has a broader frequency range, it resolves upper and lower parts of the ground better than the VLF method itself.

RMT works in the frequency range of 10-250 kHz and consists basically of measuring the ratio between the horizontal electric field component (E_x) and the corresponding orthogonal magnetic field component (H_y) generated by radio transmitters. Similarly to VLF, the phase and the apparent resistivity are calculated by equations (2.23) and (2.25), respectively, in order to provide a rough estimate of the resistivity in the ground.

Likewise, after measuring the three magnetic field components from at least two transmitters, the tensor VLF data can be calculated to provide the values of tipper A and tipper B (Pedersen and Oskooi, 2004).

Nowadays, the RMT method is widely used in shallow depth investigations providing high lateral and/or vertical resolution.

3.2 RMT far field sources.

The far field sources for VLF measurements are fixed VLF transmitters specially used for submarine communication. In RMT, either VLF transmitters or LW (Long Wave Band, 30-300 kHz) Radio transmitters are used. This broader frequency range makes it possible to gain high lateral and even vertical resolution.

In Europe, there are about 25 transmitters operating in the VLF range and more than 500 transmitters in the LW band (Oskooi, 2004). Figure 3.1 shows the location of these transmitters.

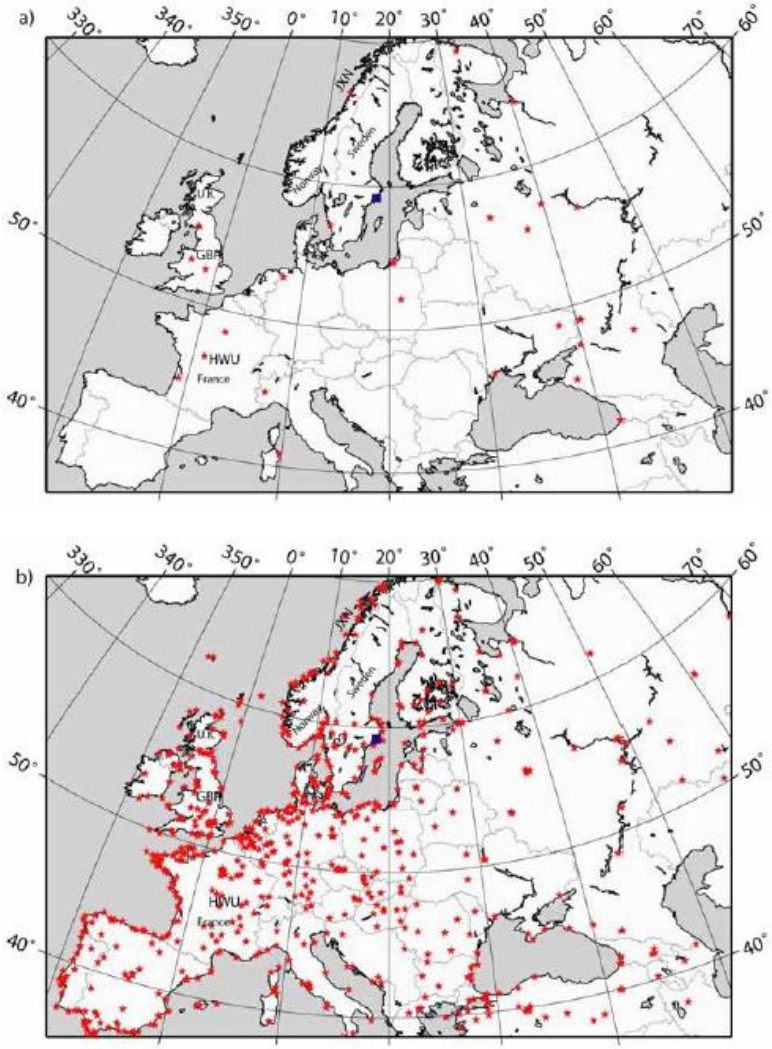

Figure 3.1: Location of a) VLF transmitters (14-30 kHz) and b) additional RMT transmitters (30-300 kHz). From Oskooi (2004).

The transmitters are normally operating as vertical electric dipoles with a transmitting power of the order of 1 MW (Pedersen and Oskooi, 2004). The radio signals are propagated either as ground or reflected waves in the wave-guide made up by the solid Earth and the conducting ionosphere. The wavelength is considered to be infinitely large compared to the penetration depth since the transmitters are generally located very far from the area where the measurements are performed. In this case, signals can be approximated as plane waves.

When measurements are being made in the field, different transmitters are detected with different signal intensities. The ratio between the total horizontal magnetic field energy and the background energy is defined as the signal-to-noise ratio (SNR). This important parameter is a function of the transmitter strength, the distance to the transmitter and the used bandwidth.

3.3 Near field sources.

Although signals from the far field region can be considered as plane waves, the fields near to the source are more complex and the previous analysis and normal equations are no longer valid. Near field sources can be of different origin such as noise in the instrumentation, unbalanced power consumption and cables. Therefore, the collected data can include a combination of far and near influences.

In order to use the normal plane wave equations, the far field sources must be separated from those in the near field. This can be done by analysing the behaviour of the tipper data.

The real part of the tipper vector generally points away from conductors under far field conditions. For near field sources, the tipper points towards the transmitter in the case of electric dipole sources and away from the transmitter in the case of magnetic dipole sources (Pedersen et al., 2005). This means that, for far field transmitters, the real and imaginary parts of the tipper vector are changing smoothly since they are a function of the conductive structure below the profile. For the near field sources, the tipper points almost towards or from a fixed location instead, namely, the source location. Therefore, near field frequencies may be easily detected by calculating the scalar tipper along the measured line.

To remove frequencies from the near field, a digital notch filter can be used prior to the main transfer functions calculation. Another method consists of using the tensor tippers and then calculating the prediction errors for each individual index in the band of interest. Those indices whose prediction errors are greater than a certain value can be eliminated from the data.

3.4 RMT data processing.

The data collected in the field are saved as raw time series by digitalising the analogue signals with an A/D converter and a Digital Signal Processor (DSP). Several processing steps must then be performed in order to estimate the transfer functions. These procedures follow Bastani (2001).

3.4.1 Preliminary steps.

In this stage a filter is used to reduce edge effects, such as Gibbs phenomenon or ringing. Posteriorly, an automatic or manual gain adjustment is applied with the purpose of amplifying or reducing the signal to acceptable levels by calculating the Root Mean Square (RMS) for each channel.

In order to increase the SNR at a particular station or site, a certain measurement must be stacked for a predefined number of times, the so-called number of stacks. Before doing this, the outliers (spikes) have to be detected and their effect reduced by using a time domain notch filter with a certain length. This notch is applied to all the channels.

3.4.2 Fast Fourier Transform (FFT) and spectral matrix.

The relations between the input and output channels are much simpler in the frequency domain than in the time domain. If the raw time series are divided into a number of time segments, then the FFT can be used to transform each of them to find the complex spectrum of the channel. Since the RMT signals lie in the frequency range of 10-250 kHz, only the spectrum in the band of interest is analysed.

In practice, some signals are not in complete phase stability over the total measurement interval. Therefore, the spectra are converted into auto and cross powers which are defined as the products of the field components and their complex conjugates. Subsequently, these are stored in a three dimensional spectral matrix **S** that contains 25 elements corresponding to the contribution of all the segments (real and imaginary parts of the auto and cross powers) for each frequency index.

3.4.3 Transmitter picking.

As said before, radio transmitters appear in the spectra with different signal-to-noise ratios depending on their location and transmitting power. For this reason, the following processing steps must be performed in order to detect the transmitters automatically.

3.4.3.1 Finding the signal-to-noise ratio to pick radio transmitters.

In this step, the electric and magnetic noise levels are defined as the median filtered horizontal fields (Figure 3.2). Thus, the SNR for each frequency in the band of interest, which is defined as the ratio between the horizontal power and the estimated noise, can be obtained.

The radio transmitters are then picked by choosing a total horizontal magnetic SNR threshold. This is due to the fact that the magnetic field is usually less noisy than the electric field. The data with a SNR above this threshold are subsequently saved in the spectra file.

As the transmitting power is more or less stable, the threshold can be determined by making a preliminary test in the whole survey area.

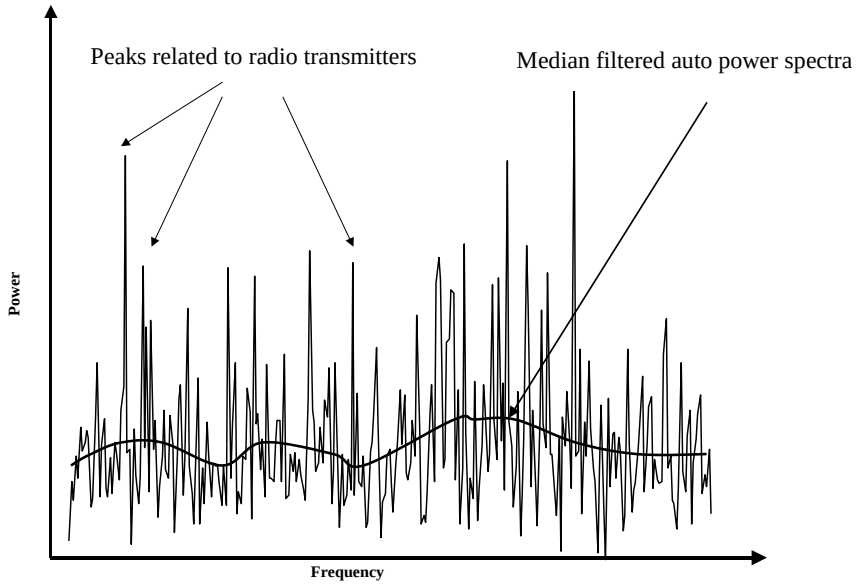

Figure 3.2: Synthetic example of an auto power spectrum and its median filtered spectrum. The noise level is found from the latter. From Bastani (2001).

3.4.3.2 Automatic determination of directions to radio transmitters.

As mentioned in section 2.6, the primary signal from transmitters induces secondary currents in the Earth. These currents generate a small horizontal electric field approximately along the transmitter direction and a horizontal magnetic field that is rotated 90 degrees with respect to the electric field.

Since the magnetic field is usually less distorted by lateral conductivity changes compared to the electric field, it can therefore be used to estimate the direction to the radio transmitters. Considering the fact that the transmitters azimuths are measured from the magnetic north towards the east, the azimuth can be obtained by rotating the coordinate system about a vertical axis such that the power of the magnetic field in the transmitter direction is minimized. Thus, this azimuth ϕ_{Az} is given by:

$$\phi_{Az} = \frac{k\pi}{2} + 0.5 \tan^{-1}\left[\frac{2Real\,(S_{12})}{S_{11}-S_{22}}\right],\ k = 0,1. \tag{3.1}$$

where the S_{ij}'s are the auto and cross powers of channels *i* and *j*. Here, channel 1 corresponds to the magnetic north and channel 2 to the magnetic east.

Equation (3.1) yields a minimum and a maximum value in the horizontal magnetic field powers. The angle of the minimum is therefore found by calculating the second derivative of S_{11} in the rotated coordinate, thus obtaining:

$$2(S_{22} - S_{11})\cos(2\phi_{Az}) - 4[Real(S_{12})\sin(2\phi_{Az})] \tag{3.2}$$

Finally, the angle with a positive second derivative is taken into account.

3.4.3.3 Detection of near field sources.

Near field sources with high signal-to-noise ratios may be detected as radio transmitters generating biased transfer functions. One way to remove the effect of these strong local sources is by using a digital notch filter which acts on the SNR before the transmitter selection. If the central frequency and bandwidth are specified, the filter forces the measured values to zero for the central frequency and those frequencies that lie within half a bandwidth around it.

3.4.4 Locked estimating.

A great number of frequencies within the VLF and LF bands are saved when performing measurements in the field. However, only a few of them corresponding to the detected transmitters are needed to calculate the transfer functions. In this phase, a new spectral matrix is formed to only contain the selected frequencies. The subsequent stacking is then *locked* to the spectral matrix in order to make the processing faster and estimate the transfer functions together with their standard errors after the following steps.

3.4.4.1 Band splitting.

The band splitting is a technique used in the natural source MT method and consists of dividing the frequency spectrum into 9 or 10 narrower sub-bands in order to calculate the transfer functions within each of them. Figure 3.3 shows that, in the first case, the main frequency band is split into 10 sub-bands with a bandwidth of half an octave. In the other case, the spectrum is divided into 9 overlapping sub-bands with a bandwidth of one octave. One octave is by definition the interval between two points where the frequency at the second point is twice the frequency of the first. Thus, two sets of transfer functions can be estimated.

It is important to highlight that in each sub-band the geometric mean of the minimum and maximum frequencies is defined as the nominal target frequency.

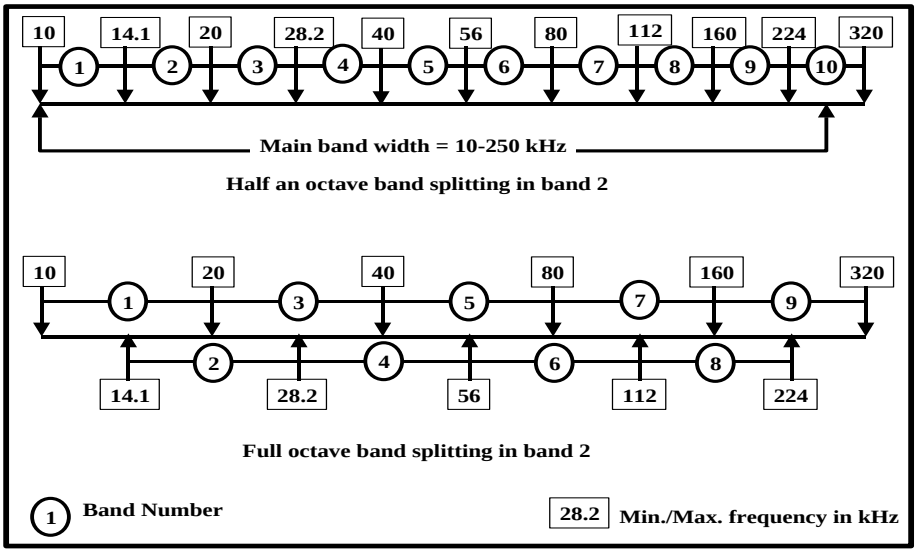

Figure 3.3: Band splitting technique in RMT processing. From Bastani (2001).

3.4.4.2 Band averaging.

Band averaging consists of estimating the transfer functions by using the least squares approach. The transfer functions in each sub-band are therefore assumed to be constant and independent of the frequency. For all *n* frequencies in a narrow sub-band, the relations between the input and output channels can be written as:

$$H_z(\omega_i) = A(\omega_t)H_x(\omega_i) + B(\omega_t)H_y(\omega_i) \quad (3.3)$$

$$E_x(\omega_i) = Z_{xx}(\omega_t)H_x(\omega_i) + Z_{xy}(\omega_t)H_y(\omega_i) \quad (3.4)$$

$$E_y(\omega_i) = Z_{yx}(\omega_t)H_x(\omega_i) + Z_{yy}(\omega_t)H_y(\omega_i) \quad (3.5)$$

Where *i*= 1, 2, ..., n and $\omega_t = \sqrt[n]{\omega_1\omega_2 \dots \omega_n}$ is the nominal target frequency.

These equations can be written as:

$$\mathbf{H_z}(\omega_t) = \tilde{\mathbf{H}}(\omega_t)\mathbf{T}(\omega_t) \quad (3.6)$$

$$\mathbf{E_x}(\omega_t) = \tilde{\mathbf{H}}(\omega_t)\mathbf{Z_x}(\omega_t) \quad (3.7)$$

$$\mathbf{E_y}(\omega_t) = \tilde{\mathbf{H}}(\omega_t)\mathbf{Z_y}(\omega_t) \quad (3.8)$$

Where:

$$\tilde{\mathbf{H}}(\omega_t) = \begin{pmatrix} H_x(\omega_1) & H_y(\omega_1) \\ H_x(\omega_2) & H_y(\omega_2) \\ \vdots & \vdots \\ H_x(\omega_n) & H_y(\omega_n) \end{pmatrix} \quad (3.9)$$

$$\mathbf{Z}_x(\omega_t) = \begin{bmatrix} Z_{xx}(\omega_t) \\ Z_{xy}(\omega_t) \end{bmatrix} \quad (3.10)$$

$$\mathbf{Z}_y(\omega_t) = \begin{bmatrix} Z_{yx}(\omega_t) \\ Z_{yy}(\omega_t) \end{bmatrix} \quad (3.11)$$

In practice, the input channels corresponding to the horizontal components of the magnetic field (H_x and H_y) are assumed to be noise free. Thus, all the transfer functions can be calculated by minimizing the total prediction error energy of each output channel over the entire sub-band.

Considering $\mathbf{O}$ as the vector of the measured output channels ($\mathbf{H}_z$, $\mathbf{E}_x$ or $\mathbf{E}_y$) and $\mathbf{m}$ the model parameter vector or the target transfer function ($\mathbf{T}$, $\mathbf{Z}_x$ or $\mathbf{Z}_y$), the least square estimate $\breve{\mathbf{m}}$ can be written as:

$$\breve{\mathbf{m}} = \left[\left(\tilde{\mathbf{H}}^*\right)^{\mathrm{T}}\tilde{\mathbf{H}}\right]^{-1}\left(\tilde{\mathbf{H}}^*\right)^{\mathrm{T}}\mathbf{O} \quad (3.12)$$

Where the superscripts $^{\mathrm{T}}$ and * denote transposition and complex conjugation respectively.

As said before, in the RMT method the frequencies from the transmitters in each sub-band are chosen. If the number of independent transmitters is greater than or equal to two, then the equation system is no longer underdetermined and the unknown transfer functions can be calculated. In the case of the electric field in the x-direction, equation (3.12) is given by:

$$\hat{Z}_{xx}(\omega_t)=\frac{\sum_{i=1}^{n} S_{22}^{i}\times\sum_{i=1}^{n} S_{14}^{i}-\sum_{i=1}^{n} S_{12}^{i}\times\sum_{i=1}^{n} S_{24}^{i}}{\sum_{i=1}^{n} S_{11}^{i}\times\sum_{i=1}^{n} S_{22}^{i}-\sum_{i=1}^{n} S_{21}^{i}\times\sum_{i=1}^{n} S_{12}^{i}} \tag{3.13}$$

$$\hat{Z}_{xy}(\omega_t)=\frac{\sum_{i=1}^{n} S_{11}^{i}\times\sum_{i=1}^{n} S_{24}^{i}-\sum_{i=1}^{n} S_{21}^{i}\times\sum_{i=1}^{n} S_{14}^{i}}{\sum_{i=1}^{n} S_{11}^{i}\times\sum_{i=1}^{n} S_{22}^{i}-\sum_{i=1}^{n} S_{21}^{i}\times\sum_{i=1}^{n} S_{12}^{i}} \tag{3.14}$$

Where the S_{ij}'s are the spectral matrix elements defined as:

$$S_{ij} = C_i^* C_j \tag{3.15}$$

In this case, C_i stands for one of the measured electric or magnetic field components numbered from 1 to 5 corresponding to H_x, H_y, H_z, E_x, and E_y, respectively.

3.4.4.3 Estimation of the random errors of transfer functions.

The random errors can be estimated after the calculation of the transfer functions. These errors are rather insensitive to noise in the magnetic field but increase when the SNR increases in the electric field (Pedersen, 1982).

To decide whether the noise in the measured data is small or not it is necessary to distinguish between the input and output channels (Müller, 2000). This is done by assuming that the input channel is noise free. The output channel, however, can be estimated by adding Gaussian noise to the output data.

The data fit can then be calculated as the coherence between the predicted and the measured output data. If this coherence is close to one, the data fit between the measured and the predicted data is good. This means that the error is small and thus there is little noise. However, if the coherence is much smaller than one, the noise in the data is large.

The general expression for the coherence between two input channels (where i,j = x,y,z) can be written as:

$$\gamma_{ij}^2 = \frac{\sum_{k=1}^{n} \left| S_{ij}^k \right|^2}{\sum_{k=1}^{n} S_{ii}^k \sum_{k=1}^{n} S_{jj}^k} \tag{3.16}$$

Moreover, the coherence between the input and the output channels, *m*, is:

$$\gamma_{mij}^2 = \frac{\sum_{k=1}^{n} \left(S_{mm}^{(p)} \right)^k}{\sum_{k=1}^{n} S_{mm}^k} \tag{3.17}$$

where $(S_{mm}^{(p)})^k$ is the auto power of channel m as predicted from the horizontal magnetic field. As an example, these two expressions can be used to estimate the variance of the impedance $\mathbf{Z}_{xx}$ where the two input channels are H_x and H_y. The result is given by:

$$\sigma_{Z_{xx}}^2 = \frac{1}{N-4} \frac{1-\gamma_{412}^2}{1-\gamma_{12}^2} \frac{\sum_{i=1}^{n} S_{44}^i}{\sum_{i=1}^{n} S_{11}^i} \tag{3.18}$$

In this expression, $N = 2n * N_s$ is the number of degrees of freedom and N_s is the number of stacks.

3.4.4.4 Estimation of Prediction Errors (PE's).

If transmitters are located in the far field, the plane wave assumption is valid and equations (3.3), (3.4) and (3.5) can be used. In the case where sources are close to the recording site, the collected data will obey different linear relations. If these near field sources are relatively few, their effect on the data can be removed by using prediction errors (PE's) as follows (Bastani and Pedersen, 2001).

Firstly, the magnitude of the individual prediction errors is calculated by:

$$e_i = \left(\frac{\left(d_i^{obs} - d_i^{est} \right)^* \left(d_i^{obs} - d_i^{est} \right)}{\sigma_i^2} \right)^{1/2} \tag{3.19}$$

where d_i^{obs} and d_i^{est} are the measured and estimated data (output), respectively, and σ_i^2 is the data variance. The superscript * denotes the complex conjugate.

Assuming that the data variances are well estimated and the impedance elements are not very distorted, the PE's are of the order of 1 for plane wave signals. However, if the transfer functions are generated by a local source, the corresponding prediction errors may be much larger.

Secondly, a threshold for the PE's is chosen and all the frequencies whose prediction errors supersede this value are deleted from the data. This is done because those signals are very likely generated by a nearby source. Later, a new improved estimate of impedance tensor and tipper can be made.

In the real case, due to the difficulty in estimating the data variance accurately, the best choice of the threshold is that a maximum 20% of all transmitters are rejected.

3.4.4.5 Estimation of scalar transfer functions.

In traditional RMT studies the scalar transfer functions are estimated and used due to instrumental limitations and the irregular distribution of radio transmitters. These quantities are calculated in the transmitter coordinate system in which the y-axis coincides with the horizontal magnetic field direction (perpendicular to the transmitter). Thus, the general expression for the scalar transfer functions is given by:

$$T_{ij} = \frac{S_{ij}}{S_{ii}} \tag{3.20}$$

Where *i*= 1, 2 and *j*= 3, 4, 5.

By using equation (3.20) it is possible to estimate the scalar tipper. The significance of this quantity is different depending on whether the measurements are made with two or three magnetic components (Pedersen and Oskooi, 2004).

In the first case, two magnetic components are available, that is, one horizontal (H_y) and one vertical component (H_z) of the magnetic field were measured as occurs in standard VLF measurements. If the strike direction is in the x-direction, then the component A is equal to zero and the derived scalar transfer function is identical to the unique tipper component B. This scalar quantity is given by:

$$B_{scalar} = \frac{H_z}{H_y} \tag{3.21}$$

If the strike direction differs from that of the x-axis, it is not possible to compensate for the rotation by some correction factor. This means that the true transfer function cannot be recovered from the measured scalar transfer function B_{scalar} .

In the case where the three magnetic components are measured, a 2-D structure having a strike angle θ with respect to the x-axis can be constructed since the horizontal components of the magnetic field are used to calculate the field in an arbitrary direction. In this case, the scalar transfer function is defined as:

$$B_{scalar}(\theta) = \frac{H_z}{-sin(\theta)H_x + cos(\theta)H_y} \tag{3.22}$$

Where B_{scalar} is identical to the 2-D tipper element along a profile perpendicular to

the strike.

Finally, if three magnetic field components from two transmitters with slightly different frequencies and a nearly orthogonal direction are measured simultaneously, the total field for each transmitter is given by:

$$T = (|H_x|^2 + \left|H_y\right|^2 + |H_z|^2)^{1/2} \tag{3.23}$$

Maps of T contain useful information about the conductivity structure in a survey area. For example, the maxima of T describe the conductive structures, especially those with a strike direction parallel to the transmitter.

Chapter 4

The MFR instrument

The Geological Survey of Sweden (SGU) currently uses an instrument called Wadi, designed by ABEM instrument AB, for investigations of the bedrock quality and the electrical resistivity variation in the ground along some selected profiles. This system measures the signals from only one transmitter in the VLF band. As mentioned before, this fact generates problems since there are very few transmitters working in this band and the responses from geological discontinuities are dependent on the strike direction. Therefore, the vertical resolution reached by Wadi is very poor and sometimes structures cannot be resolved at all.

In order to overcome this problem, an instrument called EnviroMT was developed by Uppsala University (Bastani, 2001) under the EU 4th Framework programme 1997-2000. This system improves the measurements by using the RMT method instead, detecting the signals from many transmitters and choosing those with a signal-to-noise ratio (SNR) above a certain threshold. Measurements are then independent of the direction to the transmitter because all the three magnetic components are considered.

However, the Wadi has some important advantages over the EnrivoMT, such as its light weight and a short measuring time at every point (about 5 seconds). The EnviroMT, on the other hand, is heavy (about 25 kg), must be handled by at least two persons and has a measuring time of as long as 2 minutes.

The construction of the new MFR instrument, also called multi frequency VLF/LF receiver, was funded by the SGU. This instrument is based on the concepts used for the EnviroMT system whilst taking into consideration the importance of it being user-friendly as the Wadi.

The MFR system is a portable and low power instrument which can be operated by one person in the field (Figure 4.1). The weight of the complete system, which includes the magnetic sensor, the data acquisition unit and the battery, is less than 12 kg (Dynesius et al., 2004). Likewise, the system provides inputs for electrodes to measure the electric field along two orthogonal directions.

The instrument is mainly a data acquisition system where the processed data are displayed station by station along a profile. When the measurements are completed, the data can be transferred to an external and more powerful computer for further processing (1D or 2D inversion of complete profiles, for example) and data visualisation including pseudo sections of apparent resistivity, phase, tippers and results from the inversions (Dynesius et al., 2004).

Figure 4.1: The MFR system for ground measurements. Photograph taken by Mehrdad Bastani.

Furthermore, the system operates in two data acquisition modes: automatic and manual. In the automatic mode the acquisition of the data is continuous when the instrument is being moved by a person or a vehicle. In the manual mode the data are manually acquired at discrete equidistant points along a profile by the operator. The positioning in either case is governed by a differential GPS receiver, so the positioning data can be stored together with the results. Likewise, the system has a resolution of 3 Hz with a sampling frequency of 800 kHz (Pedersen and Dynesius, 2008).

The electric field sensors are steel sticks that can be mounted in a rig with dimensions of 1 metre by 1 metre (Figure 4.2). This creates a dipole length of 1.4 metres along two orthogonal directions.

The magnetic sensor consists of a three components induction coil magnetometer of 15 cm long configured in an orthogonal system. Its orientation (roll, tilt and heading) and the electrode rig (heading) are measured during the acquisition by an electronic compass with a tiltmeter included. As the magnetometer operates in the broad frequency band of 14-350 kHz, it can be used for both ground measurements as well as in the stinger of an airborne platform.

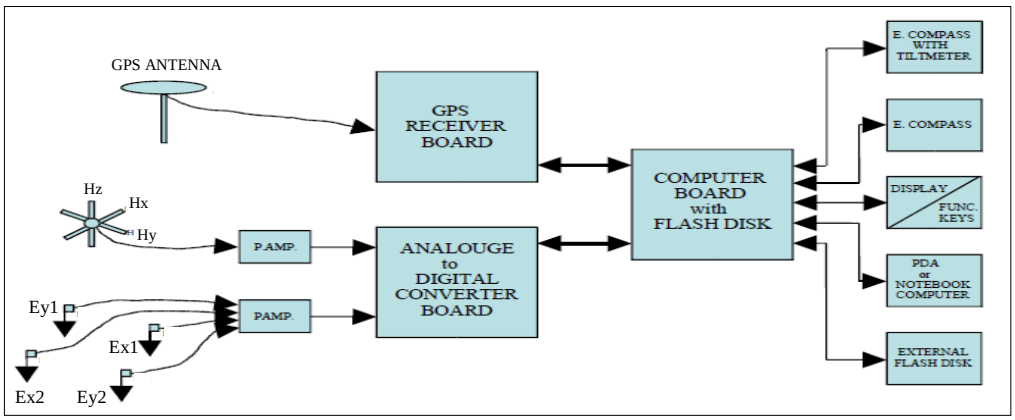

Figure 4.2: Diagram of the Multi Frequency Receiver (MFR). From Dynesius et al. (2004).

Chapter 5

Airborne data from the MFR system

5.1 Background.

The Geological Survey of Sweden (SGU) has performed airborne magnetic measurements since 1960 which initially aimed at exploring iron ores. From 1973 the VLF method has been routinely used in the airborne electromagnetic measurements as part of the SGU's bedrock mapping programme. For this reason, the airborne VLF data available at this institute now cover about half of the Sweden's area and provide detailed information about soils and structural features of the bedrock (Pedersen et al., 2009).

In order to make airborne electromagnetic measurements, the aeroplane normally flies in straight lines from north to south or east to west at intervals of 200 metres. This means that the data during the post-processing must be interpolated between the profiles. The flight speed is about 240 km/h and the sampling distance is around 16 metres. Therefore, according to the Nyquist theorem, the minimum wavelength that can be investigated is 32 metres.

Some important considerations about the flight height must be taken into account since anomalies attenuate quite rapidly with increasing the altitude and practically disappear at 100 metres (Oskooi and Pedersen, 2006). Until 1994 measurements were made at an altitude of 30 metres due to the fact that this height provided a better resolution. Nowadays, most of the measurements are made at an altitude of about 60 metres, which is considered as the minimum safety height for an aeroplane.

In the field, a GPS system and radar altimeters are used to ensure correct positioning of the measurements. The sensor (magnetometer) can be placed on a wing tip, in a nose stinger or a towed so called "bird" to record the field in three directions: H_x, H_y and H_z. These data are then saved as raw time series together with the information containing the position and orientation of the aeroplane.

It is important to highlight that measurements of the electric field are very difficult in the air. Therefore, only the magnetic field components are measured when collecting airborne data.

5.2 Airborne measurements with the MFR system.

Three airborne measurements were made by the SGU between 2007 and 2009 in order to test the new MFR instrument. These campaigns are explained as follows:

5.2.1 Campaign 1: November 2007.

The first airborne measurements were made in Torsby and Falun, Sweden, on the 6th and 7th of November 2007. These areas were chosen since they have been well documented by the SGU and the new results could be compared with the old maps. The installation of the magnetometer and the MFR system was done at Wermlandsflyg facilities in Torsby. The latest magnetometer prototype was put in the stinger and the MFR system in the instrument rack of the SGU's aeroplane (Pedersen and Dynesius, 2008).

The measurements were performed along flight lines in the North-South direction with a separation of 100 metres and an altitude of about 60 metres. The speed of flight was approximately 240 km/h giving a sampling distance of about 16 metres (Gustavsson, 2008). Likewise, a continuous time series was recorded with a sampling rate of 800 kHz and a time tagged GPS data stream delivered by the SGU system was used to localise the data geographically.

The primary test measurements were made in Torsby, where the data were recorded with high amplification that then caused signal clipping. This was due to the noise residing from the aeroplane generators which had a fundamental frequency of 120 Hz. After overcoming this difficulty, the real measurements were performed in the Falun area.

The data were processed at Uppsala University and the Geological Survey of Sweden (SGU) by the student Anna Gustavsson in 2008, being supervised by Dr. Mehrdad Bastani and Prof. Laust B. Pedersen. The conclusion of the test was that the airborne MFR data were very noisy when collected in the broad frequency band. This was especially due to the fact that the aeroplane engines generated a very high noise level. These test results therefore showed that proper high pass filters had to be made in order to avoid the engines noise (Pedersen and Dynesius, 2008).

5.2.2 Campaign 2: August 2008.

Due to the previous results, a second test was made in 2008 taking into account the problems and acquired knowledge from the first airborne measurements. For this campaign, Uppsala University recommended SGU to use a commercial data acquisition system with a higher number of bits that could provide a wider dynamic range. Another benefit of using a commercial system was the future support and maintenance provided by the company.

The new instrument called ADU07 and designed by Metronix GmbH was a good alternative. ADU07 is a 24-bit system characterised by a rather high sampling rate (512 kHz) that was later redesigned for continuous time series measurements. The instrument was mounted on the aeroplane and the test was carried out at Gävle airport on the 20th of August 2008. The final measurements were made in Falun on the 22nd of August, the same area where the first set of data was collected in 2007.

The ADU07 software was developed and adapted by Uppsala University and the SGU to continuously collect the data with a sampling frequency of 512 kHz in the three magnetic channels. Furthermore, a high pass filter was used in order to record only frequencies in the band of 10- 250 kHz.

The measurements were made along lines in the North-South and South-North directions with a separation of 200 metres and a flight height of 60 metres. The aeroplane speed was about 240 km/h, which gave a sampling distance of about 17 metres. Likewise, GPS signals were recorded with a frequency of 1 Hz in order to localise the data geographically.

In the beginning, the prior evaluation of the ADU07 data in the time and frequency domain seemed to be promising. However, subsequent results showed that there were some near field sources on the aeroplane that contaminated the signals from the radio transmitters. These sources were basically the common power supply for the PC and the instrument, as well as other measuring systems that ran in parallel with the ADU07. These systems were comprised of a magnetometer and a radar altimeter.

5.2.3 Campaign 3: June 2009.

A third set of airborne measurements was made in the area between Uppsala and Börlänge on the 5th of June 2009. This campaign was aimed to collect better quality data after overcoming some problems that released in Falun.

As in the previous campaign, the ADU07 software was adapted to continuously perform the measurements with a sampling frequency of 512 kHz in the three magnetic channels. In this case, the data were collected along one line in the South-North and North-South directions. The aeroplane speed was about 240 km/h and the flight height was 400 metres. Unfortunately, these data were not geographically localised since the GPS system generated high noise levels when the PC was connected to the ground.

The SGU's instrumentation also generated local noise on the aeroplane that contaminated the signals from the radio transmitters. However, the spectra from these measurements looked initially promising since the noise levels were low compared with those in the previous campaign.

5.3 Objective and methodology of this study.

The main aim of this project is to develop a method that identifies the near field sources and filters them out from the ADU07 data, whereby reliable transfer functions representing the Earth's resistivity structure can be obtained.

The data to use are the raw spectral components from each selected radio transmitter. The idea is to compare the new processing with the old procedures carried out in 2008 in order to show the benefits and improvements made.

In the present situation the amount of data is so large that the manual rejection of noise frequencies is impossible. Therefore, it is necessary to develop a method that automatically identifies the near field sources and then rejects them from the transfer function calculations. For that, programs in MATLAB are designed and created to carry out the task.

Basically, the preliminary steps that should be followed in order to successfully accomplish the aim of the project are:

1. Writing of a processing program in MATLAB for reading and running the raw spectral data.
2. Calculation and visualisation of the scalar transfer functions.
3. Detection of near field sources and their elimination from the data (a Notch filter in the frequency domain).
4. Visualisation of the final tensor and scalar tippers.
5. Quality test of the new tipper function by comparing it with the existing results.
6. Evaluation of any improvements, changes and other issues.

If the goal of the project is successfully reached, the results would represent an important advance in the way airborne measurements are made. This would also allow the SGU to replace its old dual VLF system for the new MFR instrument, which, as said before, could bring more advantages in the processing and interpretation of the data.

5.4 Processing and interpretation of the Airborne MFR data.

The times series recorded for the three components of the magnetic field (H_x, H_y and H_z), the header and the positioning information from the GPS system are all saved in different files during the data collection. In order to have interpretable results that could provide valuable information about the geology of a survey area, such as the transfer functions and apparent resistivities, the ADU07 raw data were processed as follows:

5.4.1 Time series.

During the signal amplification the gain was set in order to avoid signal clipping. In this first step, the recorded raw time series (RTS) were divided into a number of time segments with an adjustable length. The longest number of samples N is 2^{17} (131 k) and the sample frequency F is 512 kHz. Therefore, a frequency resolution $\Delta f = F/N$ of about 4 Hz could be achieved.

In the case of the EnviroMT system, the data segment length of 2^{14} samples (16 k) and the sampling frequency of 2 MHz give rise to a frequency resolution of 122.1 Hz. This means that the MFR instrument is about 30 times more accurate in resolving the peaks from the radio transmitters. The long segments also provide a good control on the SNR since transfer functions are calculated in the frequency domain.

5.4.2 Conversion to the frequency domain and spectra files.

In this step, the Fast Fourier Transform (FFT) was applied to each time segment to convert all the measured field components to the frequency domain. This created a raw spectrum with N/2 frequency indices. The transmitters were then selected as explained in section 3.4.3 and all the information was saved in raw data files.

A median length of 4 kHz that corresponds to about 1000 samples is usually used to process the raw data. In this project, a linear median that makes use of every 10^{th} sample was applied in the median filter in order to calculate the SNR. This gives rise to 100 samples. Posteriorly, a SNR threshold of 10 dB was chosen to select the radio transmitters.

Every spectra file contains many segments in which the index, frequency, SNR and the real and imaginary parts of the magnetic field components are included. These segments correspond to the measured points or stations along the profile. Each spectra file also contains the header with important information such as the number of transmitters, number of stations and their coordinates, etc. (See Appendix A).

In the case of this project, 18 raw data files were provided from Campaign 2. However, only 9 of them contained the data collected when the aeroplane was flying over the survey area. The data in the other files were measured at the airport or on the ground before the take off of the aeroplane and were not considered in the processing steps. Likewise, 8 files were generated from Campaign 3, but only 4 of them were considered for the same reasons.

5.4.3 Filtering of raw data in MATLAB.

A series of programs was designed in MATLAB in order to remove the noise frequencies from the spectra files (Appendices B and C). The main idea was to write user-friendly routines which could carry out the processing stages in the shortest time possible.

Several methods can be applied in order to decide whether or not a frequency must be considered as a noise frequency. For Campaign 2, the first step was to remove all the information below 14 kHz. This was done since in the range of 10-14 kHz the signals had very low SNR values and did not provide useful information.

The processing stages that were subsequently performed to process the data are explained as follows:

5.4.3.1 Mean value of Hz.

As discussed in section 2.6, the vertical magnetic field component H_z is entirely of secondary origin and therefore depends only on the conductive bodies in the ground. When making measurements along a profile, the real component of H_z for a certain frequency has its minimum and maximum values on either side of the conductor and is zero just above it. For this reason, the mean value of H_z^{real} over a certain profile length must be about zero for each

frequency if they are not related to noise. After plotting the results, those frequencies showing a mean value much greater or much less than zero are considered as noise and must be filtered out from the data.

This step was carried out in MATLAB by using the program *plotrawdataRRD*. This routine calls the sub-function *readrawdata* which reads the information from the raw data files and then calculates the mean value of H_z^{real} for each frequency. Finally, the results are plotted against the frequency giving rise to one graph for each file when the sub-function is executed.

5.4.3.2 Calculation of the scalar tipper.

Another way to separate the far field sources from the near field signals is by calculating the scalar tipper components A and B as follows:

$$A_{scalar} = \frac{H_z}{H_x} \tag{5.1}$$

$$B_{scalar} = \frac{H_z}{H_y} \tag{5.2}$$

As explained before, for a given set of far field transmitter frequencies, the real and imaginary parts of the tipper vector are smoothly changing functions that are dependent on the Earth conductivity. However, in the near field, the tipper that moves with the source (in this case, the aeroplane located 60 and 400 metres above the ground) is a rather constant function with a very small imaginary part along the measuring line.

Therefore, by calculating the mean value of the scalar tipper for every single frequency over a certain profile length and then plotting the results, it should be possible to detect the near field frequencies and filter them out from the list of radio transmitters. This is preferably done by using a digital notch filter.

This step was also done in MATLAB by using the program *plotrawdataRRD*. The called sub-routine *readrawdata* calculates the mean value of the real and imaginary parts of the scalar tipper components (A and B) for each frequency in the file. Finally, the results are plotted against the frequency, thus making 4 graphs for each file when the sub-function finishes the calculations.

5.4.3.3 The VSNR criterion.

The SNR values in the raw data files correspond to the horizontal signal-to-noise ratio (HSNR). In this processing step, the vertical signal-to-noise ratio (VSNR) was calculated for each frequency assuming that it had the same noise level as the HSNR. The used expressions were:

$$V_{noise} = \left(\frac{abs\,(H_x)^2 + abs\,(H_y)^2}{10^{\frac{HSNR}{10}}} \right) / 4 \tag{5.3}$$

$$VSNR = 10\log_{10}\left(\frac{abs\,(H_z)^2}{V_{noise}}\right) \tag{5.4}$$

The VSNR may be very useful when detecting noise frequencies in the data. For this, its median value and standard deviation are calculated at every station. The number of occurrences is the number of times one certain frequency has a VSNR above the median value + one standard deviation along the file (blue line in Figure 5.1). The division of this quantity by the number of times the frequency has been found in the file gives rise to its occurrence or probability. This last parameter is usually multiplied by 100 to obtain the occurrence percentage.

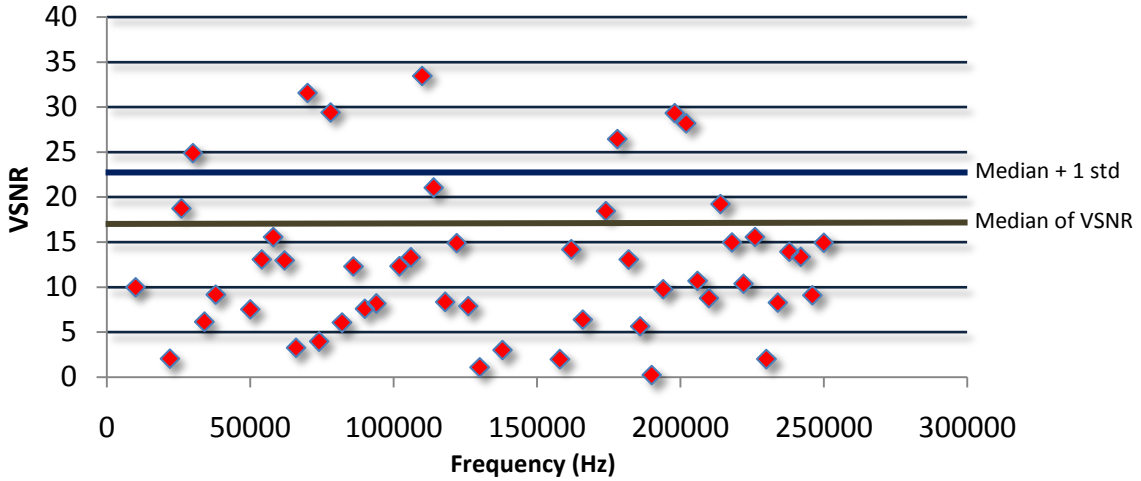

Figure 5.1: Detection of noise frequencies by using the VSNR criterion. The green line corresponds to the median VSNR value for a certain station. The blue line corresponds to the median value plus one standard deviation.

A table consisting of four columns is created in order to analyse each frequency separately. The first column contains all the frequencies in the file. The second column has the number of occurrences for each frequency. The third contains the number of times the frequency has been detected in the file and the last column has the percentage. Those frequencies with an occurrence value above a chosen threshold are saved in a separate file. In this project, a threshold of 50% was selected.

An automatic removal of the frequencies with an occurrence above 50% can be done directly in the processing program. However, this method might eliminate frequencies corresponding to radio transmitters. The information was manually analysed instead.

The conclusion was that, for Campaign 2, there were two sets of noise frequencies affecting the data. The first group corresponds to frequency 8 kHz (16 kHz is the first frequency in the RMT band) and its even and odd harmonics, and the second to frequency 23.47 kHz and its harmonics. In the case of Campaign 3, frequency 10.28 kHz and its harmonics were identified. If a certain noise frequency belonging to one of these groups was detected in all the files, this would then be added to a frequency list saved in a text-file. This file contains all the central frequencies that would be subsequently removed by a notch filter. However, there were some frequencies which did not belong to any of the previous sets and were also added to the frequency list since they appeared in all the files.

The frequencies which were not found in all the files, even though they belonged to any of the previous sets, were not included on the list since they are meant to be detected and removed by other processing methods, such as the calculation of Prediction Errors (PE's).

A digital notch filter was designed to remove the frequencies on the list. The filter has a central frequency and a bandwidth. The central frequency is already on the list and the frequency bandwidth can be given by the user at the beginning of the program. The bandwidth influences the effect of eliminating the noise frequencies and is chosen by using a trial-and-error method to delete the harmonics and obtain the best results. In this project, a bandwidth of 200 Hz was selected.

Finally, the program read the frequencies from the list and eliminated them from the spectra together with their harmonics. The rest of the frequencies were considered as transmitters. The filtered data were then saved in other files for further processing.

An average occurrence table was also created in order to study the behaviour of every frequency in the entire measuring period. The frequencies that were found in all the files were saved in the first column. The subsequent columns contained respectively the number of occurrences for each frequency, the number of times those frequencies were detected in all the files and the average of the occurrence percentage. This table was useful when choosing manually the frequencies that would be added to the list.

The occurrence table was created in MATLAB by using the main routine *plotrawdataIN*. This program calls the function *IdentifyNoise* which reads the data from the files and calls the sub-routine *Addtable*. In this last sub-function, the VSNR is calculated and compared to the value of the calculated median + one standard deviation. Those frequencies having values above this level are counted by a variable. The number of times the frequencies appear in the file is also counted. Then, the occurrence in percentage can be calculated and plotted against the frequency.

The function *IdentifyNoise* saves the frequencies with an occurrence value greater than or equal to 50% in an Excel-file for the subsequent selection of the frequencies to be included on the list.

The chosen noise frequencies were saved in the text file *frequency_list_final.txt*. The main function *FilterAirDataFinal* removes those frequencies from the spectra together with their harmonics. This routine reads the frequency list from the file and the bandwidth from the command line that is used in the notch filter. The function *RunSpectraNewFormatFinal* is then called to read the data from the files and invoke the sub-routine *RemoveIndices* to remove all the indices corresponding to the noise frequencies. Afterwards, the sub-function *CalculateTipper* is called to calculate the new tipper tensor values from the filtered data.

Finally, the new data and tippers are stored in filtered data files and tensor files (Appendix A), respectively, by the function *RunSpectraNewFormatFinal*.

5.4.3.4 Estimation of Prediction Errors (PE's).

As mentioned before, some noise frequencies were not removed from the spectra since they did not appear in all the files. By calculating the PE's it may be possible to detect and eliminate them together with some noise frequencies that the VSNR criterion could not discover.

The detection and removal of frequencies by using the PE criterion was explained in section 3.4.4.4. For this project, the band splitting technique that makes use of 9 overlapping sub-bands with a width of one octave was used to calculate the tensor tipper. By using the tipper values, the data at each frequency can be estimated, namely, H_z^{est}. Expression (3.19) can therefore be written as:

$$e_i = \left(\frac{\left(H_{z_i}^{obs} - H_{z_i}^{est}\right)^* \left(H_{z_i}^{obs} - H_{z_i}^{est}\right)}{\sigma_i^2} \right)^{1/2} \tag{5.5}$$

The vertical noise (V_{noise}) defined by expression (5.3) was used as the data variance due to its direct relation with the vertical magnetic field component H_z error.

The PE's were then calculated for every single frequency at each station. The mean value of the PE's was calculated for each frequency since the same frequency could be found many times at different stations in the same file. Finally, the mean PE values were plotted against the frequency in order to study their behaviour along the profile.

The results showed many frequencies with large PE values that might be considered as noise frequencies. Likewise, the noise frequencies that were detected by the VSNR criterion and not removed also had large PE values. This provided a prior idea about the effectiveness of PE's when detecting frequencies generated by local sources.

After looking at the generated graphs, it was concluded that those frequencies with a PE value above 3 are considered as noise and must be removed from the data. The PE's were then calculated for every frequency in each sub-band. Those frequencies with a PE above 3 were stored. According to Bastani and Pedersen (2001), when using PE analysis, a maximum of 20% of the total number of frequencies (transmitters) in the sub-band can be rejected. This was done by sorting the PE's in descending order and then removing those with the highest values up to the 20% of the number of transmitters.

The calculation of the mean PE values was done in MATLAB by the program *plotrawdataPE*. This function calls the routine *RunSpectraNewFormatPE* to read the data from the files and then invoke the sub-function *CalculateTipperPE* to calculate the tensor tipper and the estimated values of H_z. With this information, the program calculates the PE for every single frequency in the segment and accumulates the values in a variable. After calculating the PE's for all the stations in the file, the routine *RunSpectraNewFormatPE* averages the values for each frequency and saves them in another variable. The results are then plotted against the frequency for the later visualisation of the data.

The removal of frequencies above the PE threshold was done by using the program *FilterAirDataFinalPERemoval*. This function calls the function *RunSpectraNewFormatPERemoval* which reads the filtered data from the files and calls another sub-function called *PEsRemoval*. This sub-routine calculates the PE's for every single frequency and immediately removes from the sub-band those that follow the above explained criterion. After this, the sub-function *CalculateTipper* is called to calculate the tensor tipper for the new filtered data.

Finally, the new data and the tensor tippers were saved by the routine *RunSpectraNewFormatPERemoval* in filtered spectra and tensor files, respectively, for the subsequent visualisation of the results. This set of new data was meant to contain only information from the transmitters without near field sources.

5.4.4 Estimation of new transfer functions.

The tensor tipper was calculated by using the least squares solution as explained in section 3.4.4.2. To do so, the band averaging technique which splits the main band into a number of 9 overlapping sub-bands with a width of one octave was considered.

The tensor tipper calculations and the stacking of the filtered data were done in MATLAB immediately after the removal of noise frequencies. The results were then saved in tensor files which contain the real and imaginary parts of A and B together with their respective errors for every stacked frequency at each station (Appendix A). The number of stacked frequencies was 9 since 9 overlapping sub-bands were used. The header with information about the location of the measured points and the number of transmitters was also saved for each station in the file.

5.4.5 Flight direction dependence.

Before saving the transfer functions in the files, the magnetic field components dependence on the flight direction was considered. This means that, if the aeroplane flies in the North-South direction, the sign of the horizontal components of the magnetic field (H_x and H_y) must be changed when it is heading to the south (Figure 5.2). The vertical magnetic field component H_z, on the other hand, is independent of the flight direction.

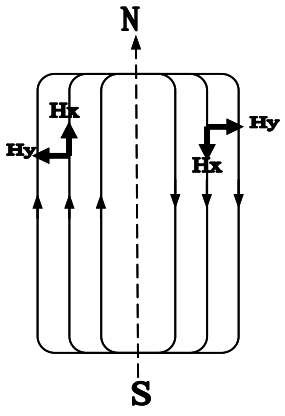

Figure 5.2: Magnetic field dependence on the flight direction. H_z is pointing outside the paper. From Gustavsson (2008).

The effect of the flight direction is considered by the MATLAB routines when the tipper values are being saved in the tensor files. The signs of both the real and imaginary parts of the tipper components A and B change when the aeroplane changes its direction over the area. However, this process was not performed in the case of the tipper from Campaign 3 since the coordinates were not recorded.

5.4.6 Visualization of the data.

The ADU07 system is mainly a data acquisition instrument. An external program must therefore be used to visualise the data by making tipper maps or pseudo-sections of apparent resistivity and phase.

In this project, the software Oasis Montaj was used for the visualization of the obtained results from Campaign 2. In order to import the data to this application, the tensor files were converted to XYZ format by using the program *MakeXYZFile*. This routine saves the information in different files for each stacked frequency. As 9 overlapping sub-bands were used, the number of converted files was also 9.

Tipper maps could not be made for Campaign 3 due to the fact that the coordinates of its stations were not saved during the data collection.

Chapter 6

Results and discussions

6.1 The filtering process.

Figure 6.1 shows the raw spectra from the ADU07 measurements made in Campaign 2. The band of interest starts from 10 kHz.

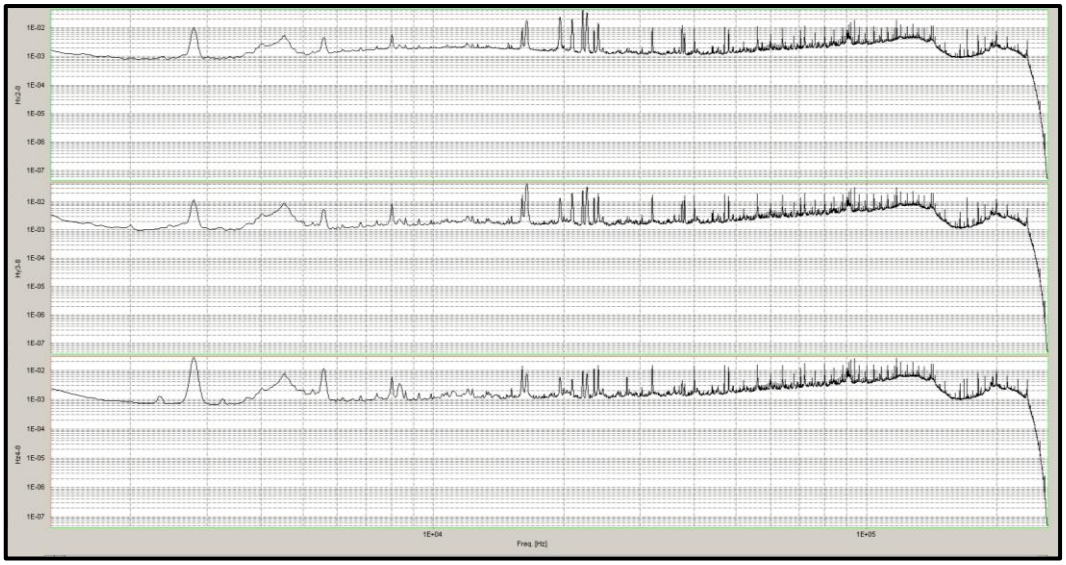

Figure 6.1: Raw spectra from the ADU07 measurements in Campaign 2. The component H_x is shown at the top, H_y in the middle and H_z at the bottom. The vertical axis corresponds to the magnetic field components in $mV/H_z^{1/2}$ and the horizontal axis to the frequency in Hz.

A background noise of approximately $1.0x10^{-3}$ $mV/H_z^{1/2}$ can be seen in the three magnetic channels. As mentioned before, the SGU's instrumentation was the main source of noise on the aeroplane during the data acquisition. In this campaign, the ADU07 and the PC controller were connected to the same power supply. Experience shows that this type of connection has generated very high noise levels, especially from a frequency of about 40 kHz.

At higher frequencies, the local noise starts to take over and rises to values ten times as large as the noise floor in the three components (Figure 6.1). Furthermore, many spikes related to either noise or anomalies in the ground can be seen in the spectra, being very frequent in the LF band. These facts gave an idea about the problem to overcome: very noisy data, mainly for high frequencies.

Figure 6.2 shows the raw spectra from the ADU07 measurements in Campaign 3.

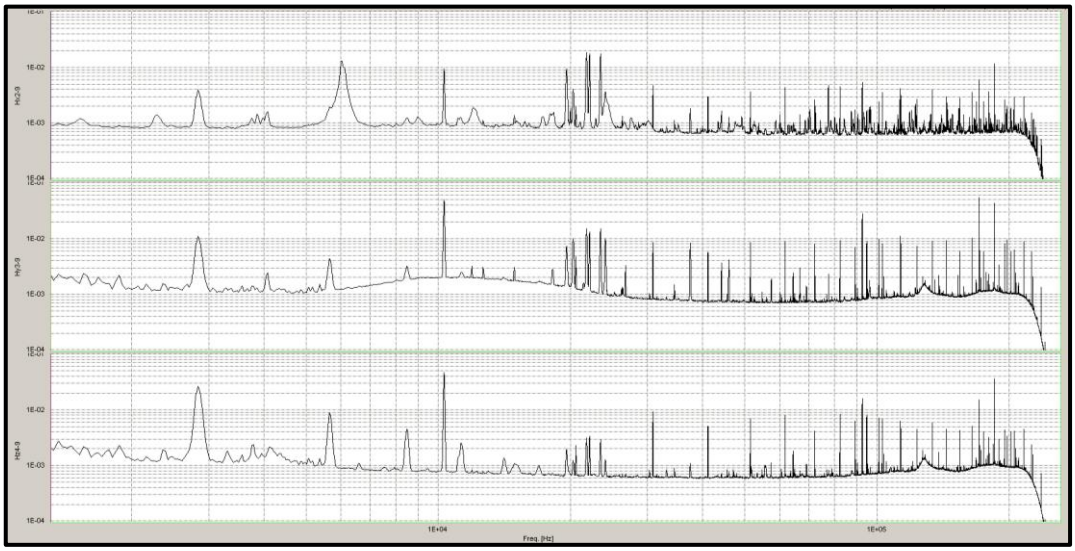

Figure 6.2: Raw spectra from the ADU07 measurements in Campaign 3. The component H_x is shown at the top, H_y in the middle and H_z at the bottom. The vertical axis corresponds to the magnetic field components in $mV/H_z^{1/2}$ and the horizontal axis to the frequency in Hz.

A background noise of approximately $0.6x10^{-3}$ $mV/H_z^{1/2}$ can be seen in the three magnetic channels. The noise levels in this case are lower compared with those in Figure 6.1 since the signals remain most of the time close to the noise floor. However, the local noise rises to higher values from a frequency of about 80 kHz. Many spikes can also be found especially in the LF band. This means that, as in the case of Campaign 2, the data are noisier for the highest frequencies in the spectra.

Several methods were applied in order to identify the near field sources of noise and filter them out from the spectra. The results from all the filtering steps explained in section 5.4.3 are shown below:

6.1.1 Mean value of Hz.

The mean values of the real part of H_z were plotted against the frequency for every raw data file. Figure 6.3 shows the results for file airdata023 from Campaign 2. It can be seen that many frequencies have both positive and negative mean values which are much larger than zero. Likewise, they do not show any pattern along the profile that could help identifying noise frequency harmonics in the data.

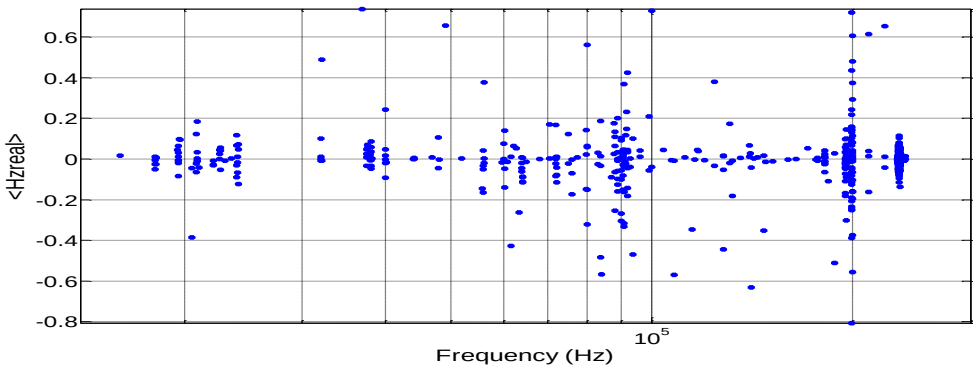

Figure 6.3: Mean H_z^{real} values against the frequency for file airdata023 from Campaign 2.

The results were also plotted in decibel (dB) graphs as another attempt to analyse the behaviour of H_z and detect noise frequencies. For these graphs, the highest value is equal to zero and the rest are negative.

As in the previous case, Figure 6.4 does not give any valuable information about noise frequencies in the data due to the large mean values and their irregularity along the profile.

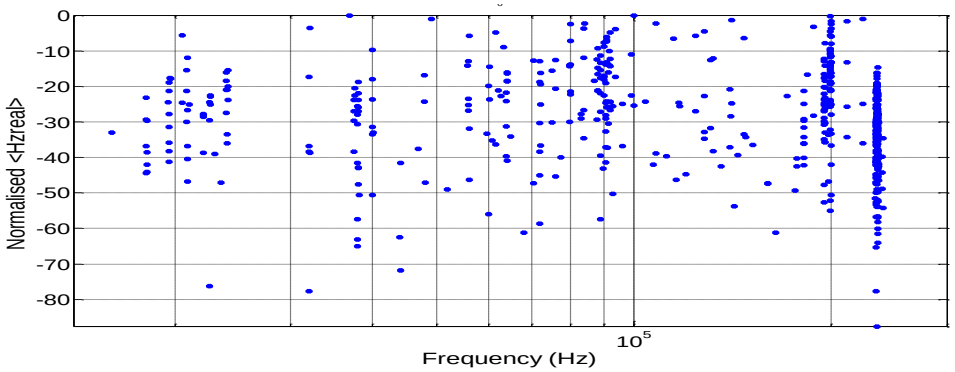

Figure 6.4: Decibel graph of the mean H_z^{real} values against the frequency for file airdata023 from Campaign 2.

A similar situation was found for Campaign 3. Thus, this criterion did not give the expected results since it was not possible to distinguish between good signal and noise frequencies.

6.1.2 Scalar tipper.

The mean values of the real and imaginary parts of the scalar tipper components A and B were also plotted against the frequency in decibel graphs. Figure 6.5 shows the results for the component A along profile airdata023 from Campaign 2.

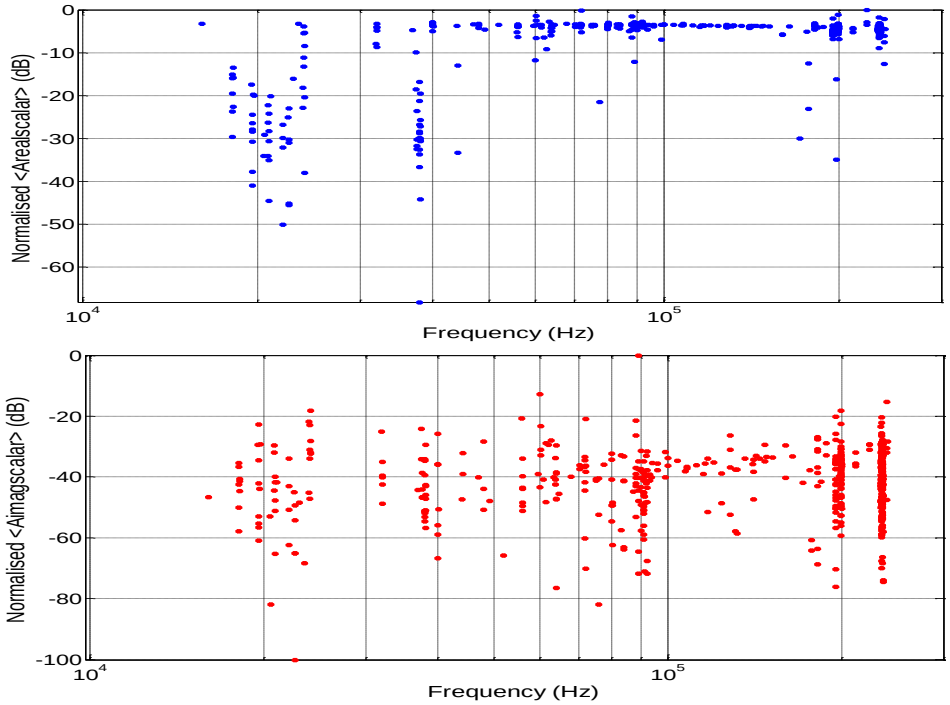

Figure 6.5: Decibel graphs for the mean values of the real and imaginary parts of A against the frequency in file airdata023 from Campaign 2.

Although the real part of A is somewhat constant in some ranges, the imaginary part shows a large variation at almost all the frequencies. This fact was relatively similar in all the files and made it impossible to identify noise frequencies in the data.

Likewise, Figure 6.6 shows the results for the tipper component B in the same file. As in the previous case, the real part of B is constant in some frequency ranges whereas the imaginary part changes considerably and does not show any pattern along the profile. This fact, which was somewhat similar in all the files and in the data from Campaign 3, did not allow identifying noise frequencies.

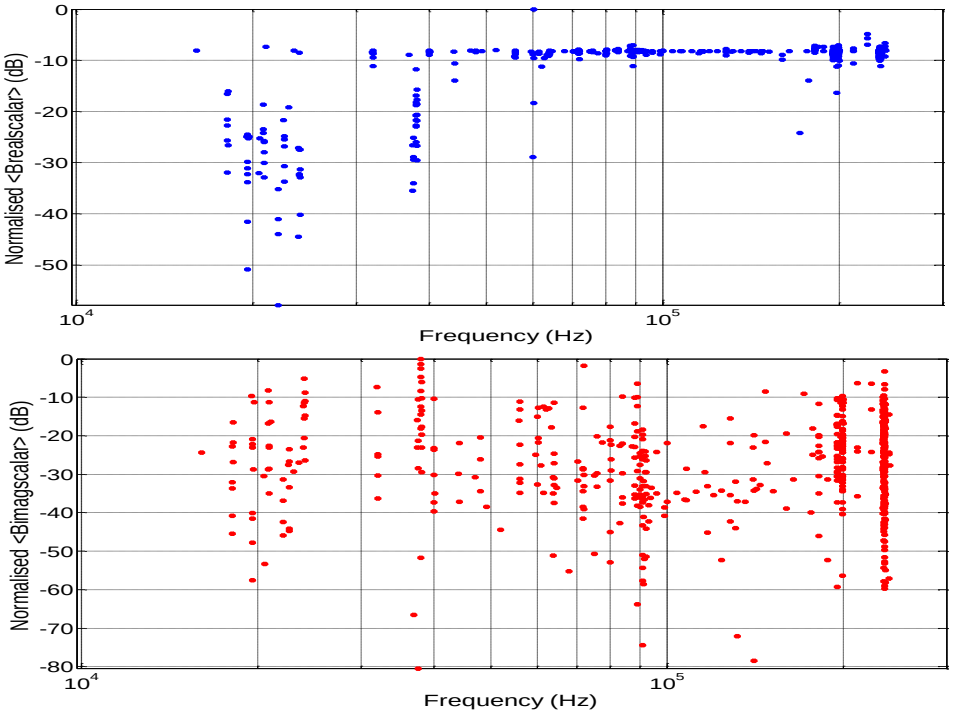

Figure 6.6: Decibel graphs for the mean values of the real and imaginary parts of B against the frequency in file airdata023 from Campaign 2.

Finally, neither H_z^{real} nor the scalar tipper components gave any valuable information. In both cases, the quantities showed large variations without any pattern along the profiles that could have helped identifying noise frequencies in the data. Therefore, improved transfer functions could not be estimated after the application of these criteria.

6.1.3 The VSNR criterion.

6.1.3.1 Campaign 2.

Figure 6.7 shows the occurrence graph for file airdata032 from Campaign 2. As explained in section 5.4.3.3, an occurrence threshold of 50% (green line) was chosen in order to detect noise frequencies and save them in an Excel file. Those frequencies above this value were manually analysed to avoid rejecting valuable information from the transmitters and then create the list of frequencies to remove.

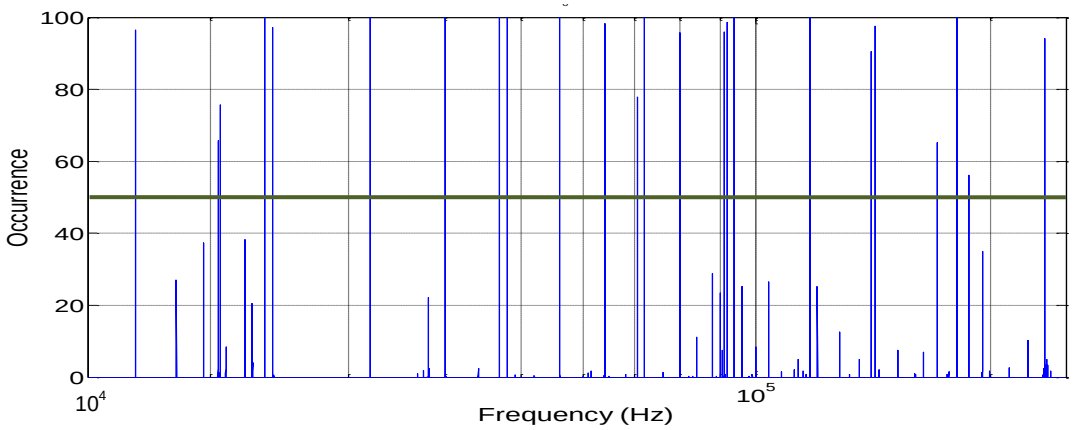

Figure 6.7: Occurrence plot for file airdata032 in Campaign 2. A threshold of 50% (green line) was selected.

Two sets of noise frequencies were found after the analysis. The first group corresponds to the even and odd harmonics of frequency 8 kHz, and the second to frequency 23.47 kHz and its harmonics. Those frequencies that belonged to any of these groups were added to the list if they were found in all the files. Some other frequencies were also added due to their appearance in all the data files. Tables 6.1, 6.2 and 6.3 summarise this selection process.

	Frequency: 8000 Hz.		
Harmonics	**Frequencies (Hz)**	**Found in some files**	**Added to list**
1st	16000	Found	Added
2nd	24000	Found	Added
3rd	32000	Found	Added
4th	40000	Found	Added
5th	48000	Found	Added
6th	56000	Found	Added
7th	64000	Found	Added
8th	72000	Found	Added
9th	80000	Found	Added
10th	88000	Found	Not added
11th	96000	Found	Not added
12th	104000	Found	Not added
13th	112000	Not found	Not added
14th	120000	Not found	Not added
15th	128000	Found	Not added
16th	136000	Not found	Not added
17th	144000	Not found	Not added
18th	152000	Not found	Not added
19th	160000	Not found	Not added
20th	168000	Found	Not added

Table 6.1: Set 1 of noise frequencies for Campaign 2. Frequencies were added to the list if they were found in all the files.

	Frequency: 23470 Hz.		
Harmonics	**Frequencies (Hz)**	**Found in some files**	**Added to list**
1st	23470	Found	Added
2nd	46940	Found	Added
3rd	70410	Found	Added
4th	93880	Found	Added
5th	117350	Found	Added
6th	140820	Found	Added
7th	164290	Not found	Not added
8th	187760	Found	Added
9th	211230	Not found	Not added
10th	234700	Found	Added

Table 6.2: Set 2 of noise frequencies for Campaign 2. Frequencies were added to the list if they were found in all the files.

Other frequencies (Hz)		
91004	92004	142344

Table 6.3: Other frequencies added to the list.

Finally, the list was comprised of the following frequencies:

Frequency list (Hz)									
16000	23470	24000	32000	40000	46940	48000	56000	64000	70410
72000	80000	91004	92004	93880	117360	140820	142344	187760	234700

Table 6.4: Final list of central frequencies to remove for Campaign 2.

This list contains the central frequencies that would be subsequently removed by a notch filter with the selected bandwidth of 200 Hz. These frequencies were then read and eliminated from the spectra together with their harmonics. The rest were considered as transmitters and improved transfer functions were meant to be estimated after this stage.

6.1.3.2 Campaign 3.

Figure 6.8 shows the occurrence graph for file conv_021 from Campaign 3. An occurrence threshold of 50% (green line) was also chosen in order to detect noise frequencies and save them in an Excel file. A manual analysis was also done in order to create the list of frequencies to remove.

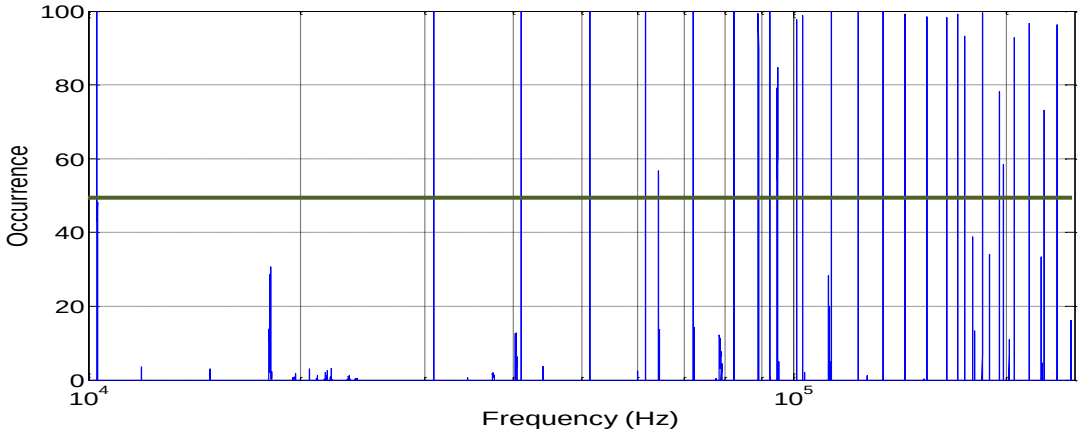

Figure 6.8: Occurrence plot for file conv_21 in Campaign 3. A threshold of 50% (green line) was selected.

One set of noise frequencies was found after the analysis: frequency 10.28 kHz and its harmonics. As in the previous case, those frequencies that belonged to this group were added to the list if they were found in all the files. Some other frequencies were also added. Tables 6.5 and 6.6 summarise this selection process.

	Frequency 10.28 kHz		
Harmonics	**Frequencies (Hz)**	**Found in files**	**Added to list**
1st	10280	Found	Added
2nd	20560	Not found	Not added
3rd	30840	Found	Added
4th	41120	Found	Added
5th	51400	Found	Added
6th	61680	Found	Added
7th	71960	Found	Added
8th	82240	Found	Added
9th	92520	Found	Added
10th	102800	Found	Added
11th	113080	Found	Added
12th	123360	Found	Not added
13th	133640	Found	Not added
14th	143920	Found	Added
15th	154200	Found	Added
16th	164480	Found	Added
17th	174760	Found	Added
18th	185040	Found	Added
19th	195320	Found	Added
20th	205600	Found	Added
21st	215880	Found	Added
22nd	226160	Not found	Not added
23rd	236440	Found	Added

Table 6.5: Set of noise frequencies for Campaign 3. Frequencies were added to the list if they were found in all the files.

Other frequencies (Hz)	
171000	198000

Table 6.6: Other frequencies added to the list.

The final list was comprised by the following frequencies:

Frequency list (Hz)									
10280	30848	41136	51420	61700	71988	82276	92500	102836	113120
143964	154244	164528	171000	174820	185096	195396	198000	205676	215960
236508									

Table 6.7: Final list of central frequencies to remove for Campaign 3.

This list contains the central frequencies that would be subsequently removed by a notch filter with the selected bandwidth of 200 Hz. It can be seen that some of these frequencies are not exactly the same as those in Table 6.5. This is due to the fact that the exact harmonic numbers could not be found in the files. However, they were considered to be the same since they are very similar to one another. Improved transfer functions were meant to be estimated after this stage.

6.1.4 Prediction Errors (PE's).

This method was mainly applied to detect those noise frequencies that were not removed before, and eliminate them together with more frequencies that the VSNR criterion could not identify.

6.1.4.1 Campaign 2.

Figure 6.9 shows the mean PE values for file filtered_new_airdata032 which contains the filtered data after using the VSNR criterion. It can be seen that there is still much noise since most of the frequencies have PE values that are much larger than 1. It is important to highlight that some frequencies detected by the VSNR criterion and not removed also have large PE values. For example, frequency 171 kHz does not belong to either of the identified sets but was found in most of the files. As seen in the figure, this frequency has a very large PE value and must definitely be considered as noise.

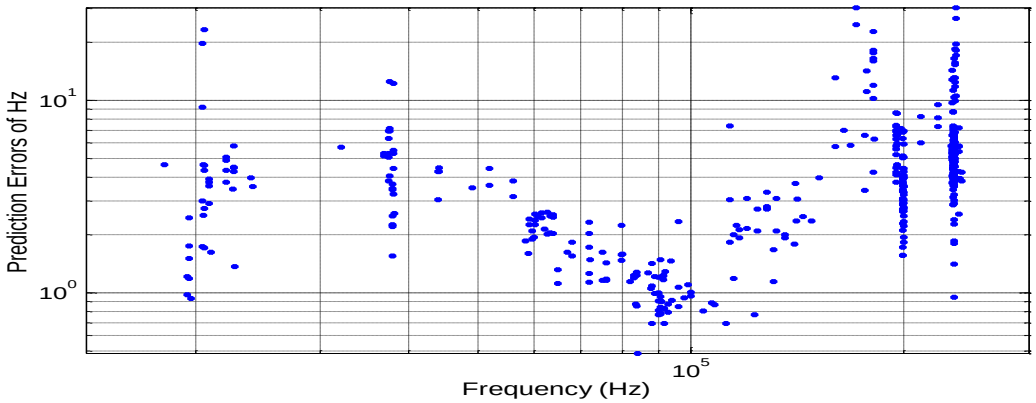

Figure 6.9: Mean PE values for file filtered_new_airdata032 in Campaign 2.

A PE threshold of 3 was then chosen in order to remove those frequencies with PE's above this value and up to 20% of the number of transmitters in each sub-band. Afterwards, the filtered data were saved and the tensor tipper was plotted along the profiles for further analysis.

6.1.4.2 Campaign 3.

Figure 6.10 shows the mean PE values for file filtered_conv_021 which contains the filtered data after using the VSNR criterion. As in the previous case, there is still much noise since most of the frequencies have PE values that are much larger than 1.

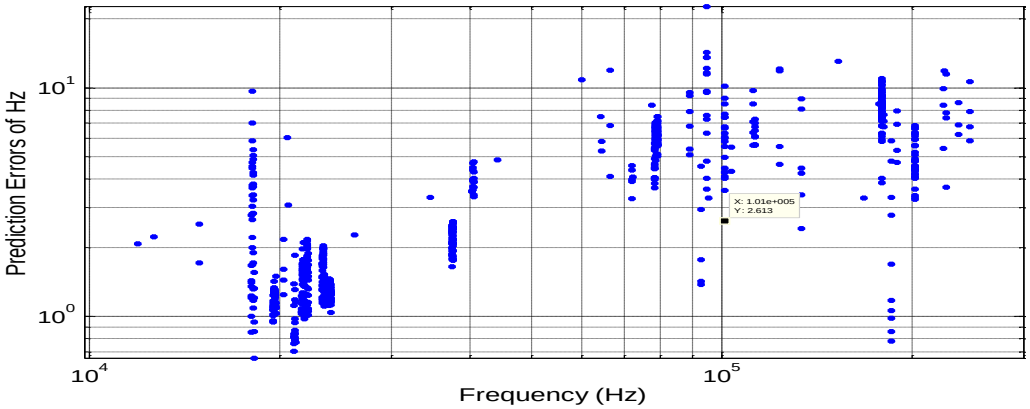

Figure 6.10: Mean PE values for file filtered_conv_021 in Campaign 3.

A PE threshold of 3 was also chosen in order to remove those frequencies with PE's above this level and up to 20% of the number of transmitters in every sub-band. The filtered data were then saved and the tensor tipper was plotted along the profiles for further analysis.

6.2 Tensor tipper along profiles.

The tensor tipper components A and B were plotted along every profile. This was done in order to visualise the results obtained from the filtering steps and thus see the improvements made in the data after these processes.

As the band splitting technique of 9 overlapping sub-bands was used, 9 tipper graphs were obtained for each stacked frequency. These frequencies are: 14142, 20000, 28284, 40000, 56569, 80000, 113137, 160000 and 226274 Hz (Figure 3.3).

According to the theory, for a non-rotated coordinate system as in this case, the real part of the tipper components A and B must fluctuate around zero showing both positive and negative values. The imaginary part is more complex and depth dependent, but basically must also average to zero. Three stacked frequencies were thus chosen in order to analyse the tipper behaviour along the profiles and compare it with the theoretical case: frequency 20000 Hz (Campaign 2) and 28284 Hz (Campaign 3) which lie in the VLF band, and 226274 Hz (for both campaigns) located in the upper part of the LF band.

6.2.1 Raw data.

6.2.1.1 Campaign 2.

Figure 6.11 shows the tipper component A for frequency 20000 Hz along profile airdata043 prior to any filtering process. Likewise, Figure 6.12 shows this component for frequency 226274 Hz along the same profile.

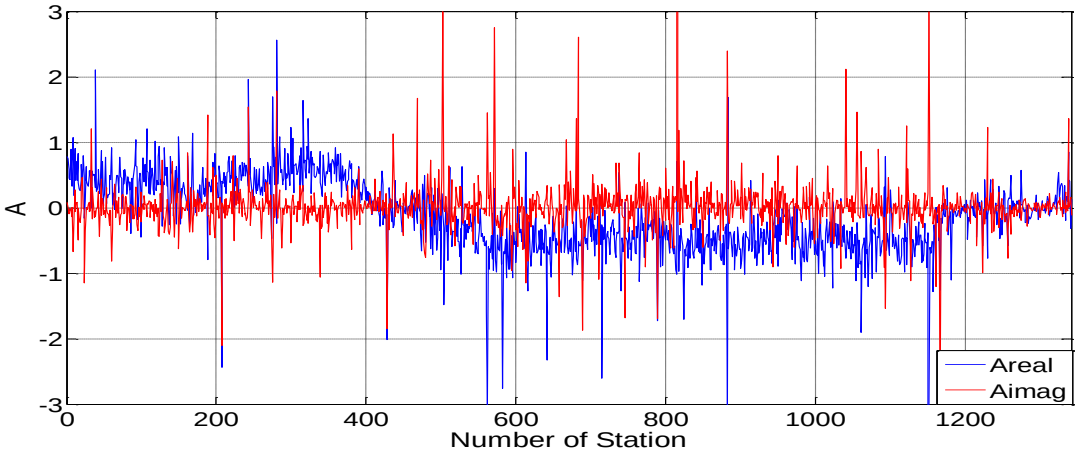

Figure 6.11: Tipper component A along profile airdata043 for Campaign 2 before any filtering process. Stacked frequency: 20000 Hz. The vertical axis corresponds to the A values and the horizontal axis to the number of the stations along the profile.

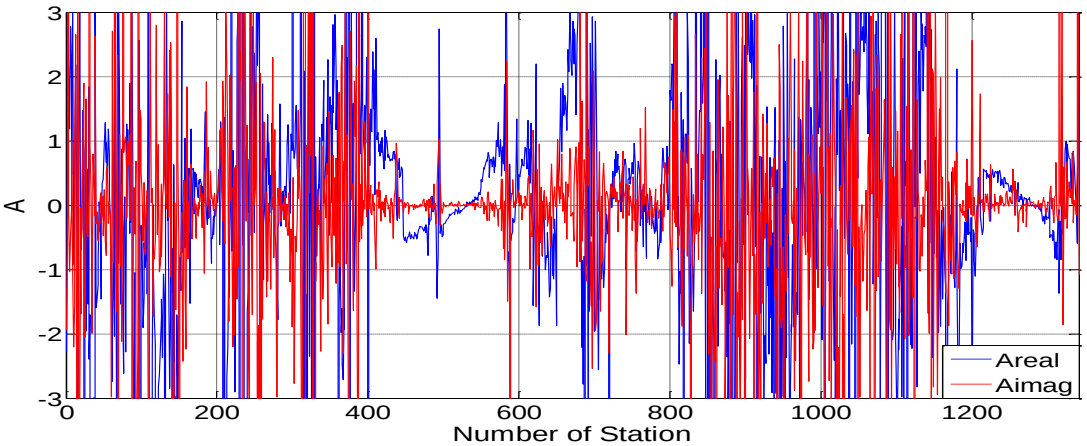

Figure 6.12: Tipper component A along profile airdata043 for Campaign 2 before any filtering process. Stacked frequency: 226274 Hz.

It can be seen that the real part of A for frequency 20000 Hz fluctuates around zero, sometimes showing only positive or negative values at many subsequent stations. This fact may be caused by the change in the flight direction over the area. Likewise, it is clearly observed that the data have very high noise levels due to the rough tipper behaviour and the large number of spikes along the profile. The imaginary part, on the other hand, is always very close to zero without much fluctuation, but also showing many spikes and a rough response.

The tipper component A for frequency 226274 Hz is extremely noisy along the entire profile. It is roughly seen that either the real or imaginary part oscillates around zero. However, the high noise level in the data, represented by large values and the highly rough response, makes it difficult to see the actual tipper behaviour along the profile. This result was expected after looking at the spectra in Figure 6.1, where the fact that high frequencies are more affected by noise than those in the VLF band is easily observed.

Figures 6.13 and 6.14 show the tipper component B along the same profile for frequencies 20000 and 226274 Hz, respectively.

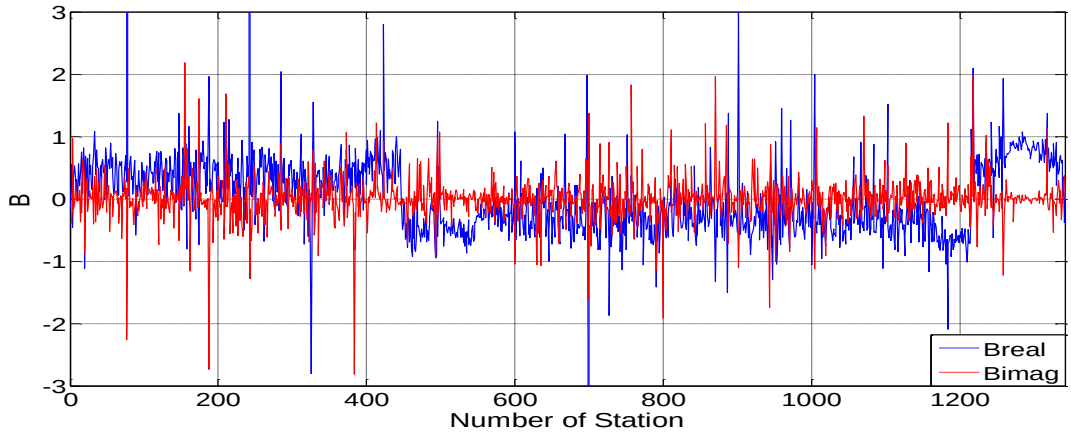

Figure 6.13: Tipper component B along profile airdata043 for Campaign 2 before any filtering process. Stacked frequency: 20000 Hz. The vertical axis corresponds to the B values and the horizontal axis to the number of the stations along the profile.

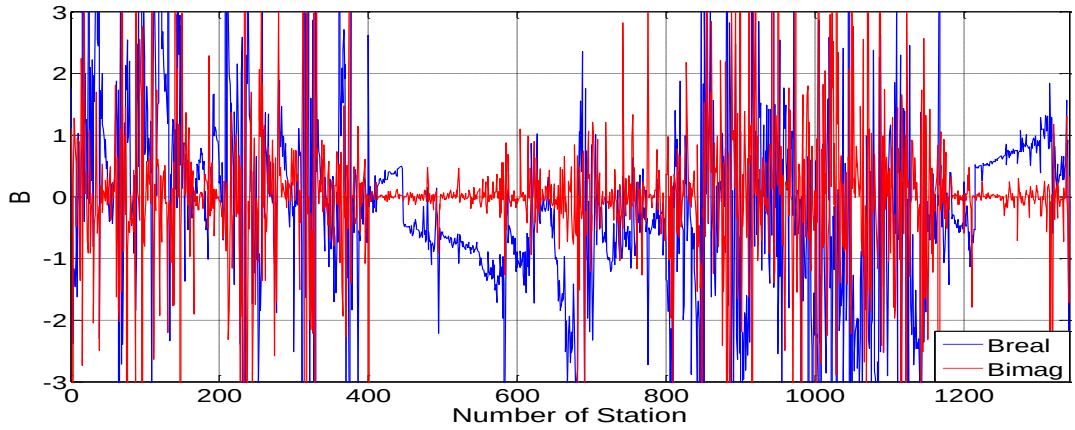

Figure 6.14: Tipper component B along profile airdata043 for Campaign 2 before any filtering process. Stacked frequency: 226274 Hz.

The tipper component B for 20000 Hz has a similar behaviour compared to A. This means that the real part fluctuates around zero as a whole whereas the imaginary part shows a little variation around this value. The fact that the real part has only positive or negative values at many subsequent stations is possibly due to the change in the flight direction. Furthermore, as in the case of A, the tipper component B for frequency 226274 Hz shows an extremely rough behaviour around zero. As said before, this is due to the high noise levels associated with the higher frequencies in the data.

The mean values of both tipper components are not zero due to the cross-talk effect between the sensor components. The results from the calibration of the magnetic sensors have shown that due to the configuration used in the sensor, the signal in one component has a significant influence on the other two directions. This effect appears in the estimated tipper components as a constant shift. The cross-talk effect, which is frequency dependent and has a much stronger effect at higher frequencies, can be easily removed from the data after the system calibration.

6.2.1.2 Campaign 3.

Figure 6.15 shows the tipper component A for frequency 28284 Hz along profile conv_020 before the application of any filtering process. Likewise, Figure 6.16 shows this component for frequency 226274 Hz along the same profile.

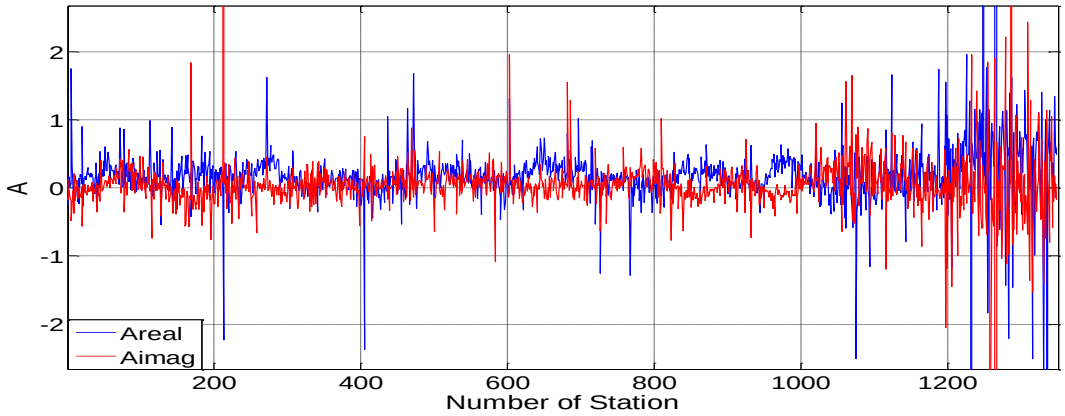

Figure 6.15: Tipper component A along profile conv_020 for Campaign 3 before any filtering process. Stacked frequency: 28284 Hz. The vertical axis corresponds to the A values and the horizontal axis to the number of the stations along the profile.

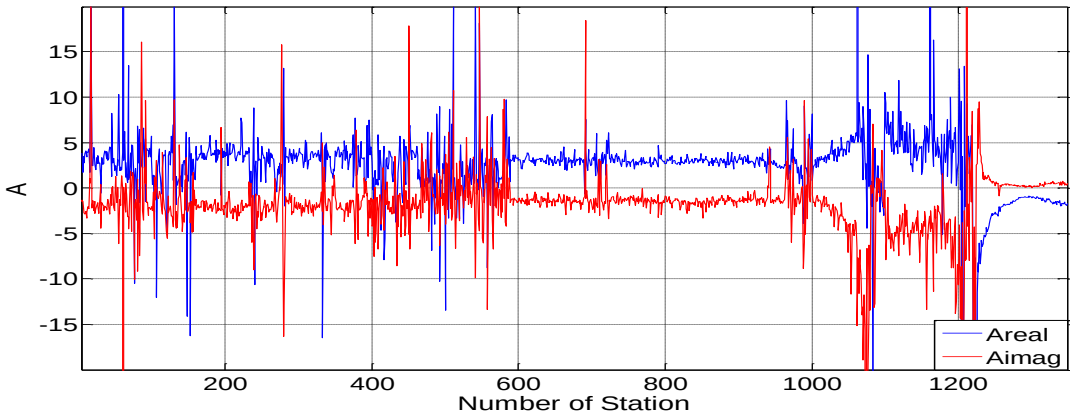

Figure 6.16: Tipper component A along profile conv_020 for Campaign 3 before any filtering process. Stacked frequency: 226274 Hz.

It can be seen that the real part of A for frequency 28284 Hz fluctuates around a value very close to zero showing especially a positive response. The imaginary part, on the other hand, fluctuates around zero showing continuously both positive and negative values. A rough behaviour and many spikes are seen in both curves, mainly from station 1000. Even so, it is evident that this set of data is much less noisy than the one from Campaign 2 (see Figure 6.11).

The tipper component A for frequency 226274 Hz is very noisy along the entire profile. Likewise, many large spikes are frequent particularly at some stations and then they become somewhat scarce. A very rough behaviour similar to this was expected after looking at the spectra in Figure 6.2, where it is seen that the highest frequencies are more affected by noise.

Figures 6.17 and 6.18 show the tipper component B for frequencies 28284 and 226274 Hz, respectively, along the same profile.

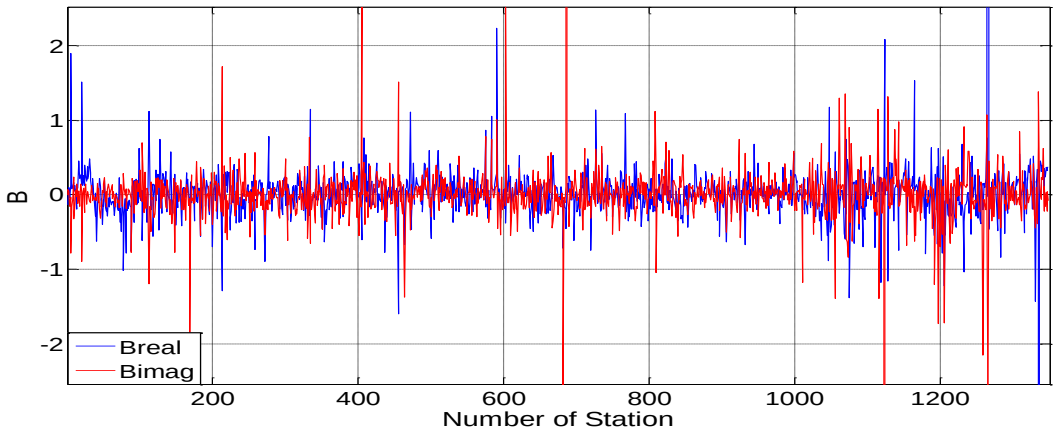

Figure 6.17: Tipper component B along profile conv_020 for Campaign 3 before any filtering process. Stacked frequency: 28284 Hz. The vertical axis corresponds to the B values and the horizontal axis to the number of the stations along the profile.

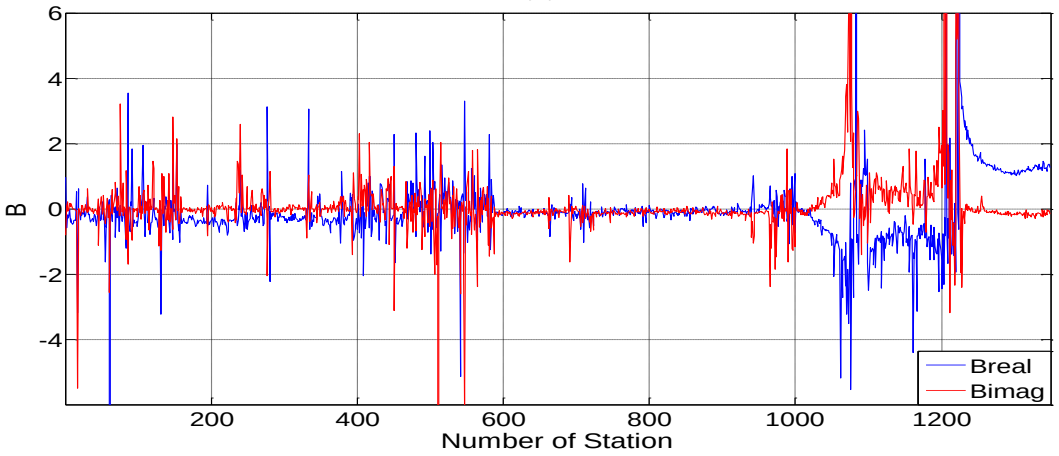

Figure 6.18: Tipper component B along profile conv_020 for Campaign 3 before any filtering process. Stacked frequency: 226274 Hz.

The tipper component B for 28284 Hz fluctuates around zero showing both positive and negative values along the profile. As in the case of the tipper component A, a very rough behaviour and many spikes are also found especially from station 1000. For frequency 226274 Hz the B behaviour is very similar to A in Figure 6.16. However, the tipper values are smaller in this case. Many spikes are also more frequent at some subsequent stations than at others. As before, this fact could be caused by the higher noise for the highest frequencies in the data, although the behaviour is now very particular. Furthermore, it is suspected that at higher frequencies the cross-talk effect plays a more important role.

By comparing the previous figures with those in section 6.2.1.1 it is evident that the data from this campaign is less noisy than the data from Campaign 2. However, much noise is seen in both cases. The idea after the filtering processes was to estimate tipper components that fluctuate as smoothly as possible around zero along all the profiles. This behaviour should be the same for A and B regardless of the change in the flight direction over the area.

6.2.2 VSNR processing results.

6.2.2.1 Campaign 2.

Figure 6.19 shows the tipper component A for frequency 20000 Hz along profile filtered_new_airdata_043 after filtering the data by using the VSNR criterion. Likewise, Figure 6.20 shows this component for frequency 226274 Hz along the same profile.

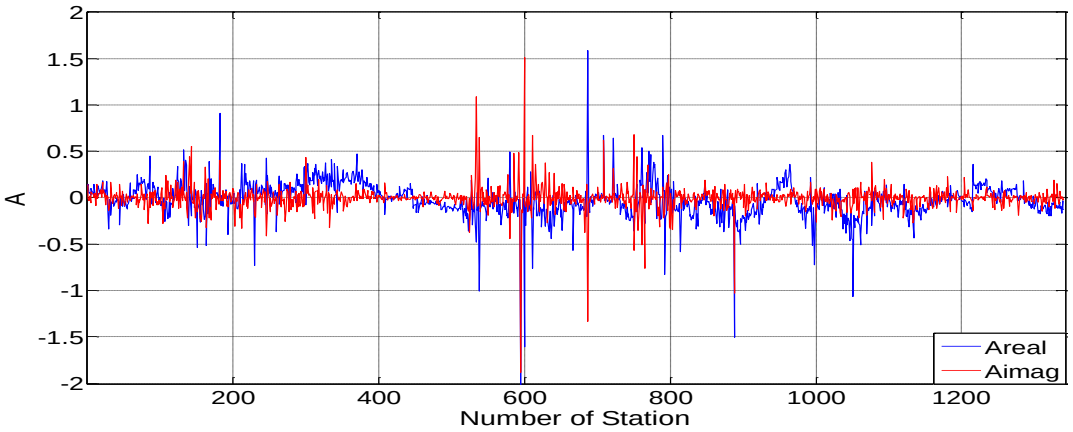

Figure 6.19: Tipper component A along profile filtered_new_airdata_043 for Campaign 2 after applying the VSNR criterion. Stacked frequency: 20000 Hz.

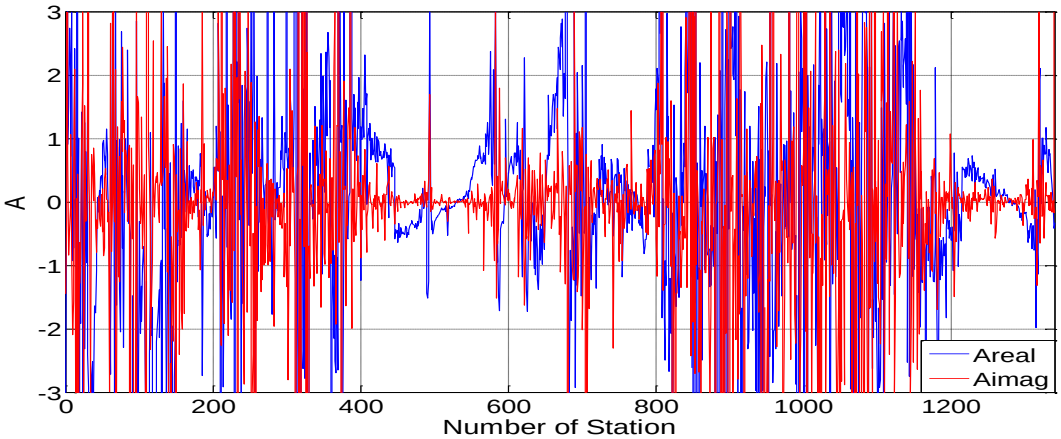

Figure 6.20: Tipper component A along profile filtered_new_airdata_043 for Campaign 2 after applying the VSNR criterion. Stacked frequency: 226274 Hz.

The real part of A for 20000 Hz fluctuates around zero showing either positive or negative values along the profile. Likewise, it shows a smoother behaviour compared to Figure 6.11 since many of the spikes were removed during the processing step. An important improvement was also made in the imaginary part because its values are now closer to zero and most of the spikes were eliminated.

However, in the case of 226274 Hz, no improvements are shown after the data processing since Figures 6.12 and 6.20 are practically alike and the tipper still has an extremely rough behaviour. This means that the noise level for this frequency is so high that the removal of noise by using the VSNR criterion was not enough to properly filter the data. Moreover, the cross-talk effect has a large influence on the results at higher frequencies.

Figures 6.21 and 6.22 show the tipper component B for frequencies 20000 and 226274 Hz, respectively, along the same profile.

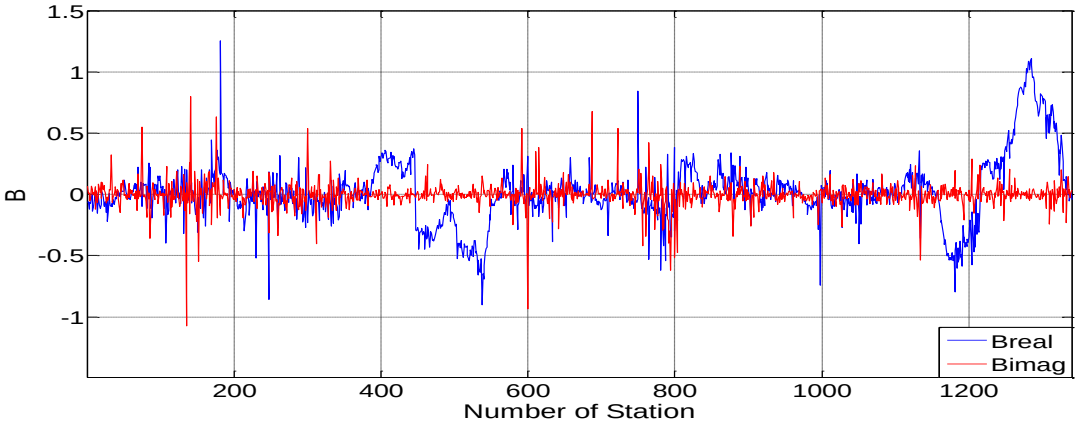

Figure 6.21: Tipper component B along profile filtered_new_airdata_043 for Campaign 2 after applying the VSNR criterion. Stacked frequency: 20000 Hz.

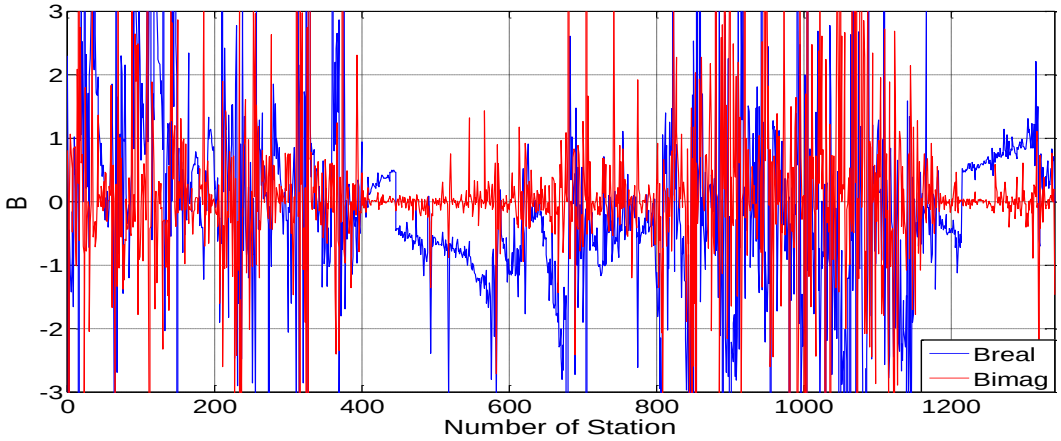

Figure 6.22: Tipper component B along profile filtered_new_airdata_043 for Campaign 2 after applying the VSNR criterion. Stacked frequency: 226274 Hz.

The tipper component B for 20000 Hz was also improved since its real part shows a smoother fluctuation around zero and most of the spikes were eliminated. Likewise, some sharp changes were also removed from its imaginary part, although there are still many of them remaining in the data. As in the case of A, evident improvements could not be seen for frequency 226274 Hz after the filtering due to some new spikes that appeared in the imaginary part between stations 600 and 800. This means that some frequencies of importance could be removed from the data since they were hidden in the high noise floor.

The previous graphs show that there is still much noise affecting the data, even though the tipper in the VLF band was considerably improved after applying the VSNR criterion.

6.2.2.2 Campaign 3.

Figure 6.23 shows the tipper component A for frequency 28284 Hz along profile filtered_conv_020 after filtering the data by using the VSNR criterion. Likewise, Figure 6.24 shows this component for frequency 226274 Hz along the same profile.

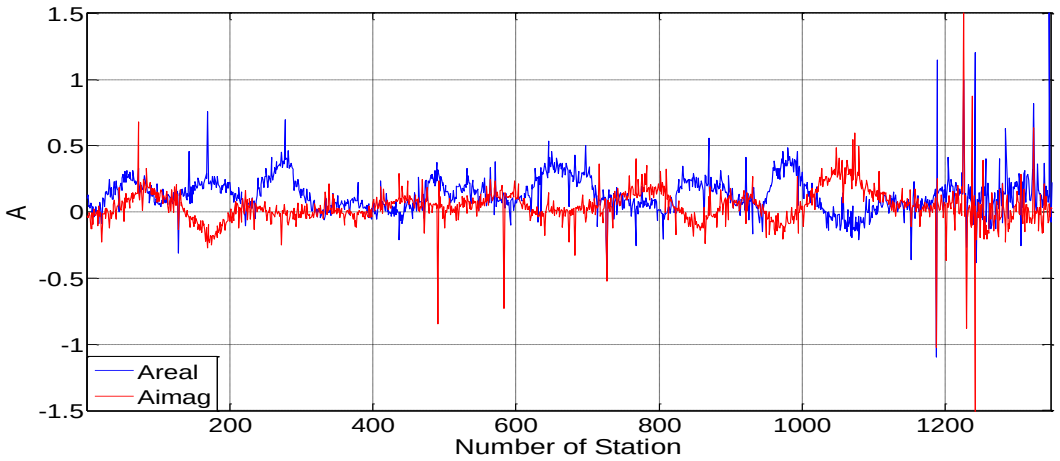

Figure 6.23: Tipper component A along profile filtered_conv_020 for Campaign 3 after applying the VSNR criterion. Stacked frequency: 28284 Hz.

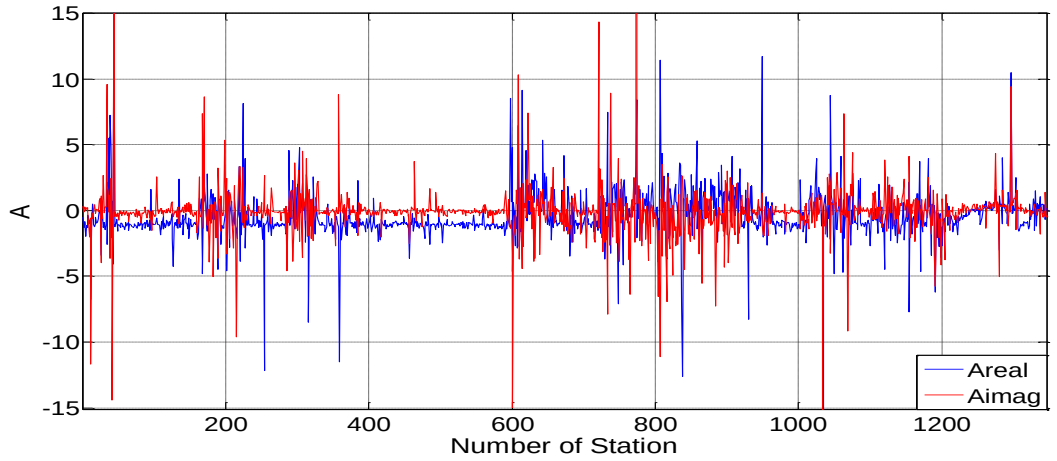

Figure 6.24: Tipper component A along profile filtered_conv_020 for Campaign 3 after applying the VSNR criterion. Stacked frequency: 226274 Hz.

The real part of A for 28284 Hz fluctuates around a value very close to zero showing mainly positive values along the whole profile. Likewise, both parts have a smoother behaviour compared to Figure 6.15 since many spikes were deleted during the processing step and the fluctuation is now more clearly seen. Many large values are still seen, especially from station 1180.

Some noise was also removed for frequency 226274 Hz. Both curves are now closer to each other and show smaller tipper values compared with those in Figure 6.16. An interesting fact is that the processing has created new spikes between stations 600 and 980. This could be caused by the removal of important frequencies (transmitter frequencies) that were hidden in the noise levels, but also by the effect of some other instrumentation used during

the data acquisition. An example could be the instrument used for communication between the pilot and the control tower.

Figures 6.25 and 6.26 show the tipper component B along the same profile for frequencies 28284 and 226274 Hz, respectively.

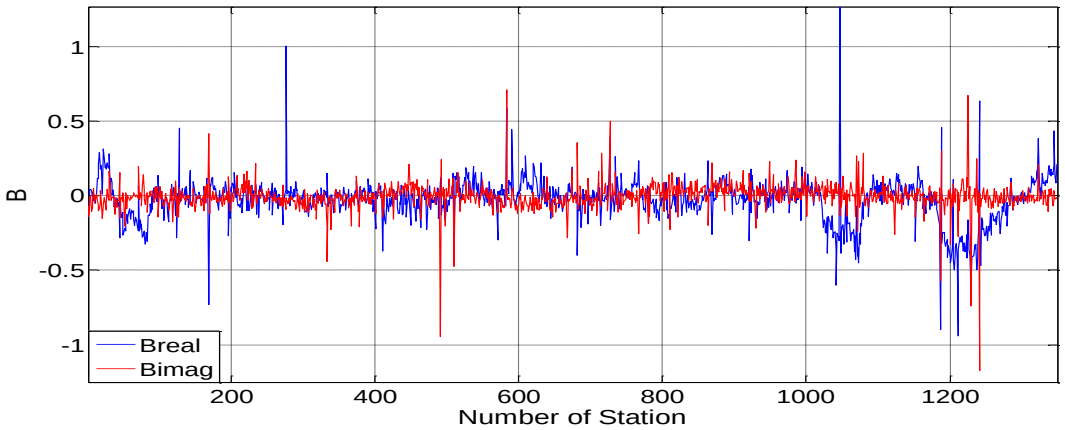

Figure 6.25: Tipper component B along profile filtered_conv_020 for Campaign 3 after applying the VSNR criterion. Stacked frequency: 28284 Hz.

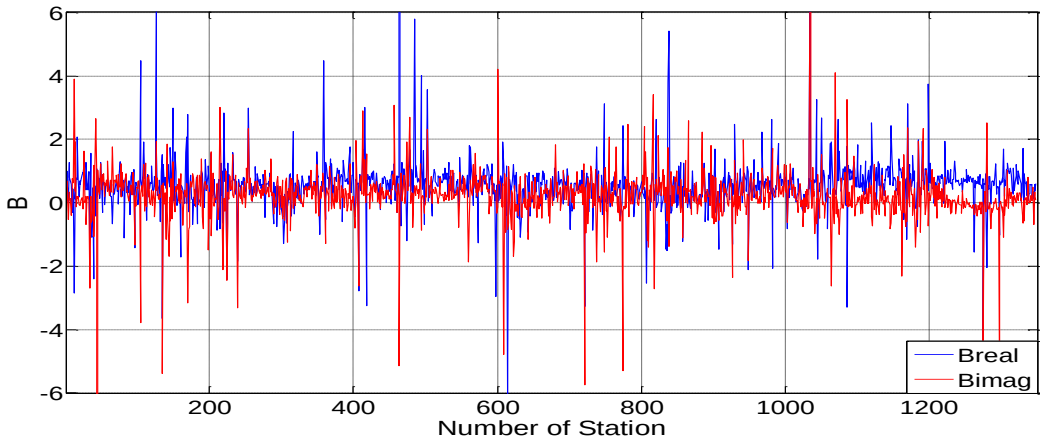

Figure 6.26: Tipper component B along profile filtered_conv_020 for Campaign 3 after applying the VSNR criterion. Stacked frequency: 226274 Hz.

The tipper component B for 28284 Hz was improved since both parts show now a smoother fluctuation around zero and many spikes were removed. However, there are still many of them remaining in the data. Some isolated spikes also appeared along the profile possibly due to the removal of transmitter frequencies that were hidden in the high noise floor.

For frequency 226274 Hz the tipper behaviour was worsened since many new spikes appeared along the whole profile. It seems that the filtering process did not make any improvement on the tipper component B. This strange response, however, could also be caused by an external agent during the collection of the data. As mentioned before, some artefacts used for communication could have been run in parallel with the SGU's instrumentation.

6.2.3 PE processing results.

6.2.3.1 Campaign 2.

Figure 6.27 shows the tipper component A for frequency 20000 Hz along profile filteredPE3_filtered_airdata_043 after filtering the data by using the PE criterion. Likewise, Figure 6.28 shows this component for frequency 226274 Hz along the same profile.

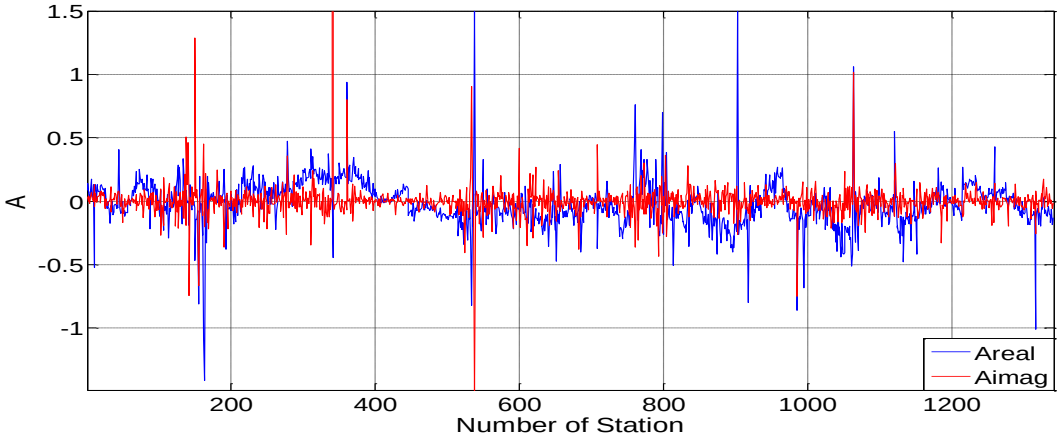

Figure 6.27: Tipper component A along profile filteredPE3_filtered_airdata_043 for Campaign 2 after applying the PE criterion. Stacked frequency: 20000 Hz.

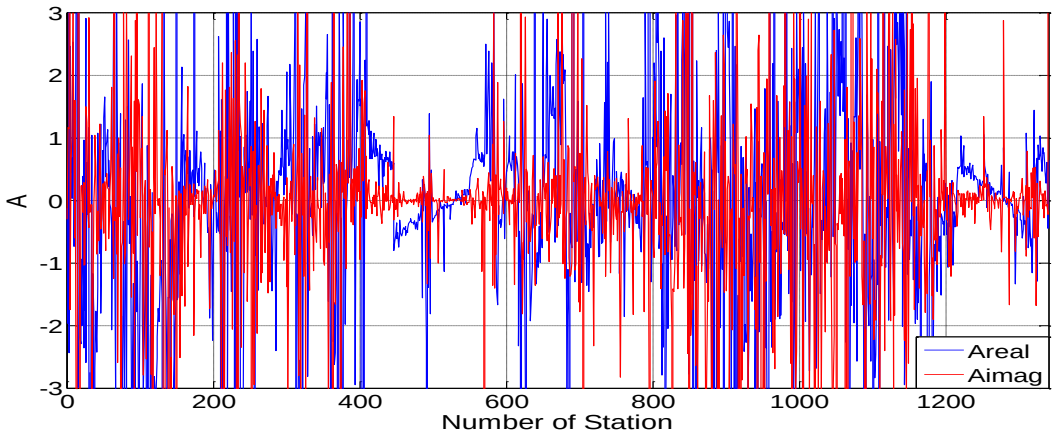

Figure 6.28: Tipper component A along profile filteredPE3_filtered_airdata_043 for Campaign 2 after applying the PE criterion. Stacked frequency: 226274 Hz.

The tipper component A for 20000 Hz also fluctuates around zero showing both positive and negative values along the profile. However, an evident improvement was not made in this case because the number of new spikes is higher than the number of large values deleted by the PE criterion in the real part. This is especially seen at stations 560 and 900. In the imaginary part, some spikes were removed but large ones also appeared on the profile. This might also be explained by the fact that frequencies of interest were deleted from the data since they were hidden in the high noise levels.

The results were worse for frequency 226274 Hz where many new spikes appeared along the profile. This is especially seen for both the real and imaginary parts between

stations 600 and 800. The much higher noise levels in this case may be the cause of this response.

Figures 6.29 and 6.30 show the tipper component B along the same profile for frequencies 20000 and 226274 Hz, respectively.

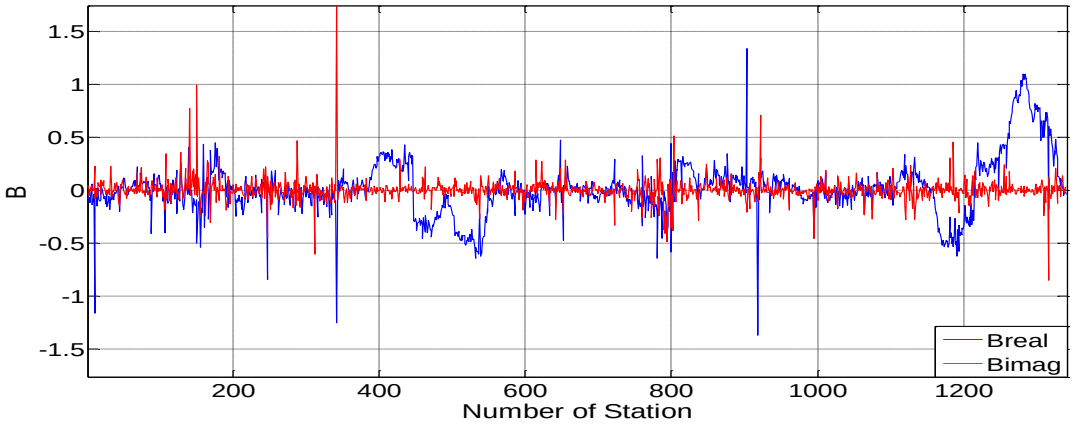

Figure 6.29: Tipper component B along profile filteredPE3_filtered_airdata_043 for Campaign 2 after applying the PE criterion. Stacked frequency: 20000 Hz.

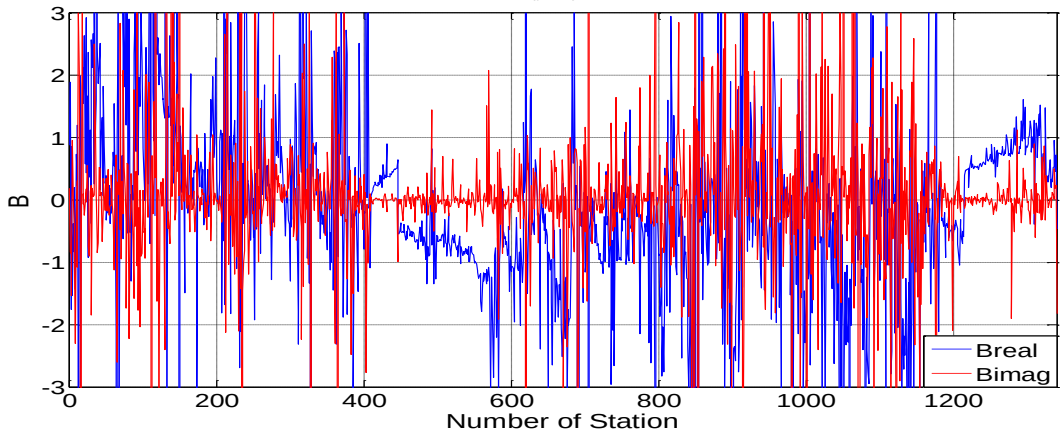

Figure 6.30: Tipper component B along profile filteredPE3_filtered_airdata_043 for Campaign 2 after applying the PE criterion. Stacked frequency: 226274 Hz.

The tipper component B for 20000 Hz shows the same behaviour as A. Likewise, some spikes were also removed but other large values were added for both the real and imaginary parts. The same argument used for A can be applied to this case. The tipper component B for 226274 Hz also shows the same response. However, the number of new spikes is higher in this case due to the very noisy data at higher frequencies. This is especially seen in the real part at stations from 200 to 400 and from 600 to 700.

In conclusion, the PE criterion was able to remove some noise frequencies from the data. However, an important improvement was not made because some transmitter frequencies could be eliminated due to the high noise levels. This affected the tipper behaviour by introducing more spikes along the profiles.

6.2.3.2 Campaign 3.

Figure 6.31 shows the tipper component A for frequency 28284 Hz along profile filteredPE3_filtered_conv_020 after filtering the data by using the PE criterion. Likewise, Figure 6.32 shows this component for frequency 226274 Hz along the same profile.

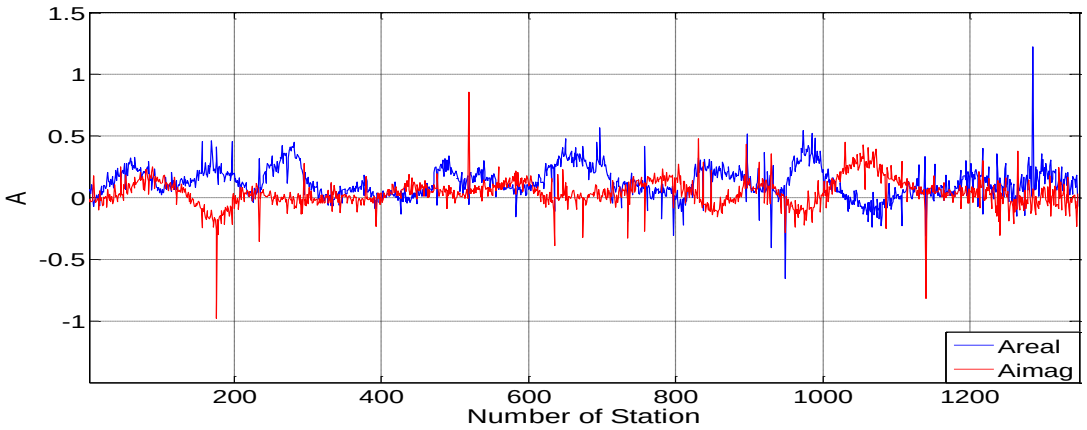

Figure 6.31: Tipper component A along profile filteredPE3_filtered_conv_020 for Campaign 3 after applying the PE criterion. Stacked frequency: 28284 Hz

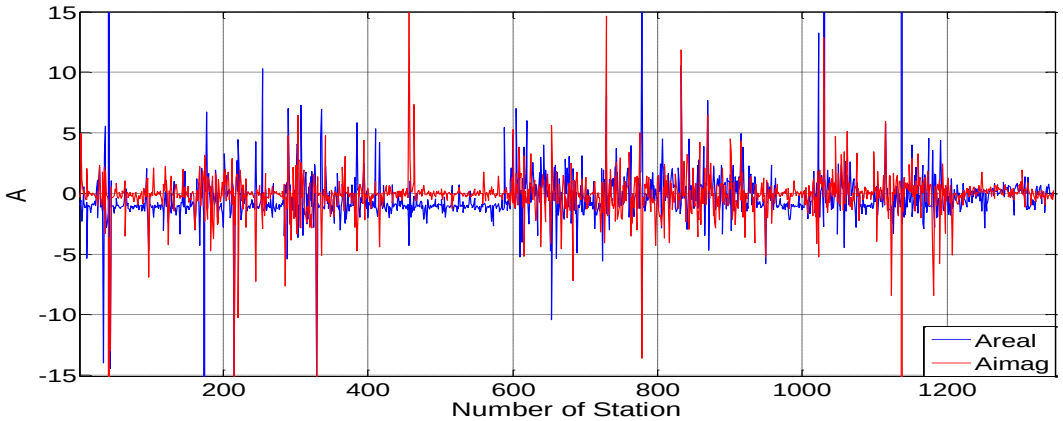

Figure 6.32: Tipper component A along profile filteredPE3_filtered_conv_020 for Campaign 3 after applying the PE criterion. Stacked frequency: 226274 Hz.

The real part of A for 28284 Hz still fluctuates around a value very close to zero. The imaginary part, on the other hand, varies around zero showing both positive and negative values along the profile. Some spikes were removed especially from station 1180, although some others appeared. This is seen, for example, between stations 1000 and 1200. As in the other measurements, this fact might also be caused by the rejection from the data of frequencies of interest since they were hidden in the high noise levels.

Although some large values were removed, evident improvements were not made for frequency 226274 Hz. This is seen because the data are still very noisy and many new spikes appeared along the profile during the processing step. The high noise levels in this case could also be the cause of this response.

Figures 6.33 and 6.34 show the tipper component B along the same profile for frequencies 28284 and 226274 Hz, respectively.

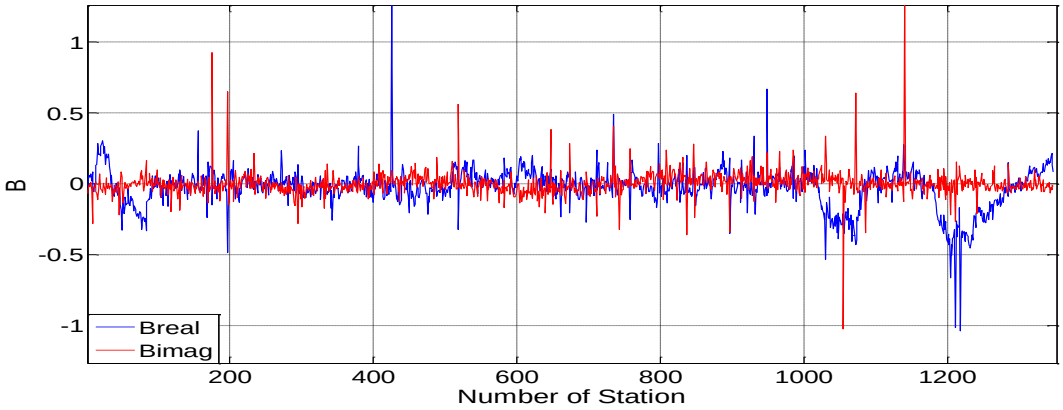

Figure 6.33: Tipper component B along profile filteredPE3_filtered_conv_020 for Campaign 3 after applying the PE criterion. Stacked frequency: 28284 Hz

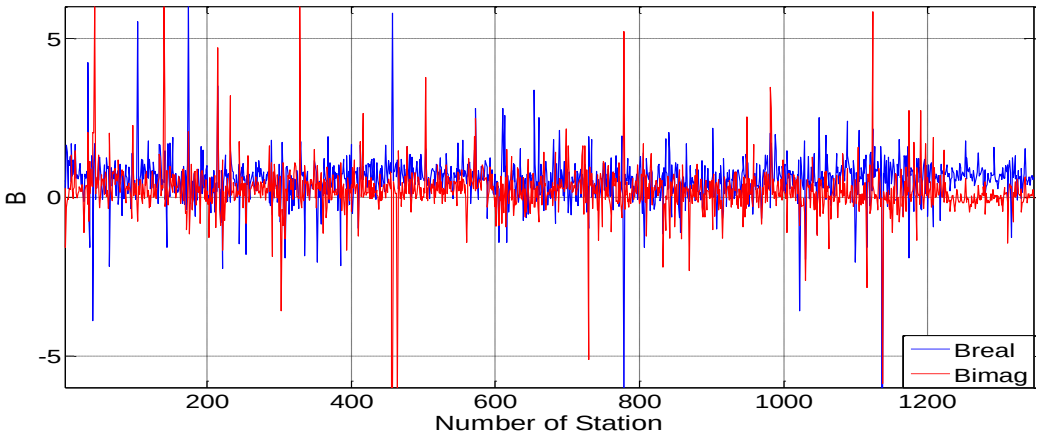

Figure 6.34: Tipper component B along profile filteredPE3_filtered_conv_020 for Campaign 3 after applying the PE criterion. Stacked frequency: 226274 Hz

The tipper component B for 28284 Hz shows practically the same behaviour as in Figure 6.25. An improvement was made since some spikes were removed, although some others appeared for both the real and imaginary parts along the profile. The explanation used for A can be applied to this case. The tipper component B for 226274 Hz was much more improved in this case than with the application of the VSNR criterion. It is evident that many spikes were removed, although more new large values appeared compared to the case of 28284 Hz. This can also be explained by the fact that the noise levels and the cross-talk effect are higher for the high frequencies in the spectra.

6.2.4 Comparison between the filtering steps.

The tipper components A and B before and after the application of the VSNR criterion and the PE criterion were also plotted together in order to more easily visualise the results from each processing step.

6.2.4.1 Campaign 2.

Figure 6.35 shows the real part of A for frequency 20000 Hz along profiles airdata043, filtered_new_airdata_043 and filteredPE3_filtered_airdata_043. These correspond to the raw data, the data after filtering with the VSNR criterion and after applying the PE criterion, respectively.

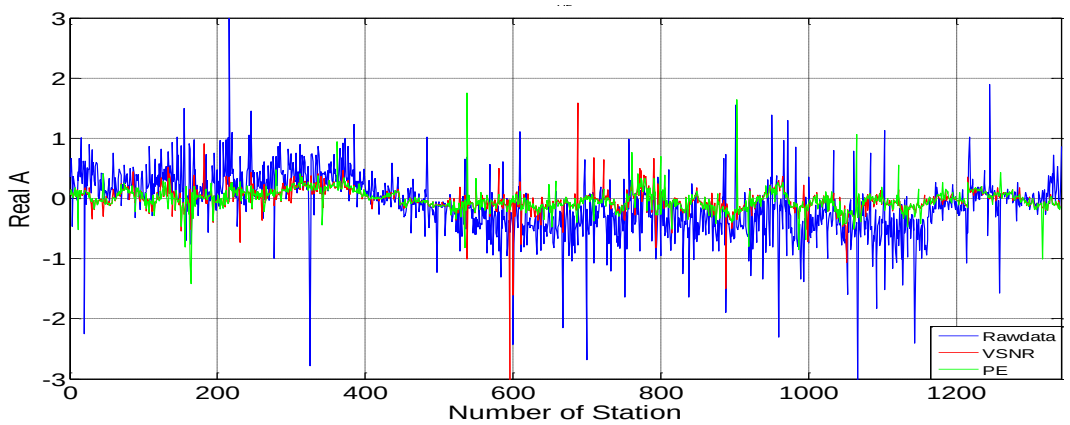

Figure 6.35: Real part of the tipper component A before any filtering (blue line), after applying the VSNR criterion (red line) and after filtering the data with the PE criterion (green line) for Campaign 2. Stacked frequency: 20000 Hz.

This figure shows that the processing steps smoothed considerably the tipper behaviour along the profiles since many spikes were deleted. Likewise, the tipper component now fluctuates closer to zero showing both positive and negative values. This is more clearly seen in Figure 6.36 which represents a zoom made from Figure 6.35 between stations 600 and 790.

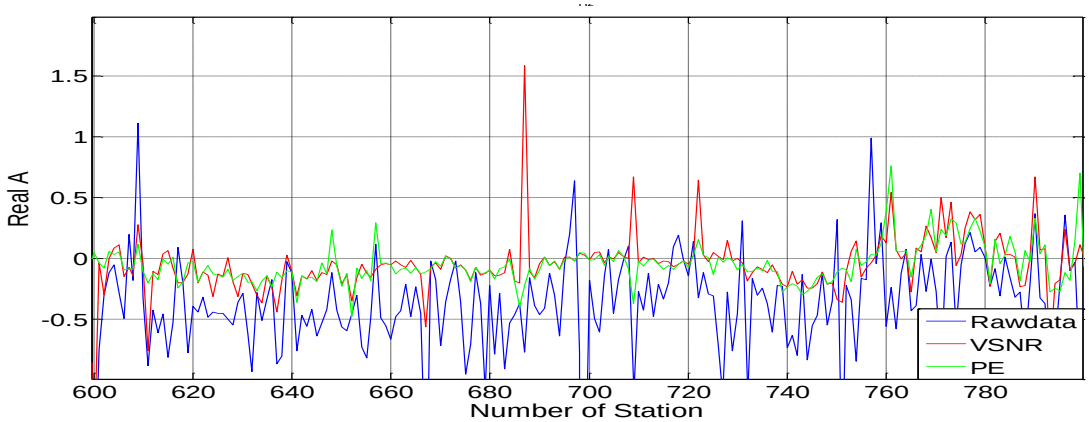

Figure 6.36: Zoom made from Figure 6.35 between stations 600 and 790 for the real part of the tipper component A. Stacked frequency: 20000 Hz.

This figure shows that the tipper behaviour is certainly much smoother after the filtering processes. However, it can be seen that some new spikes were created along the profile after applying the VSNR criterion. In this range of stations the PE criterion did not generate more spikes. Figure 6.35 shows, on the other hand, that this step gave rise to new larger values compared to the previous criterion. The possible cause of this fact was

explained previously in this chapter. Even so, many noise frequencies were removed from the data and a more reliable tipper functions could be estimated for the VLF band.

Figure 6.37 shows the real part of A for 226274 Hz along the same profiles. It can be seen that the very high noise levels for this frequency make it impossible to visualise any improvement made on the data after the filtering process. Figure 6.38, on the other hand, shows a zoom from Figure 6.37 between stations 400 and 800.

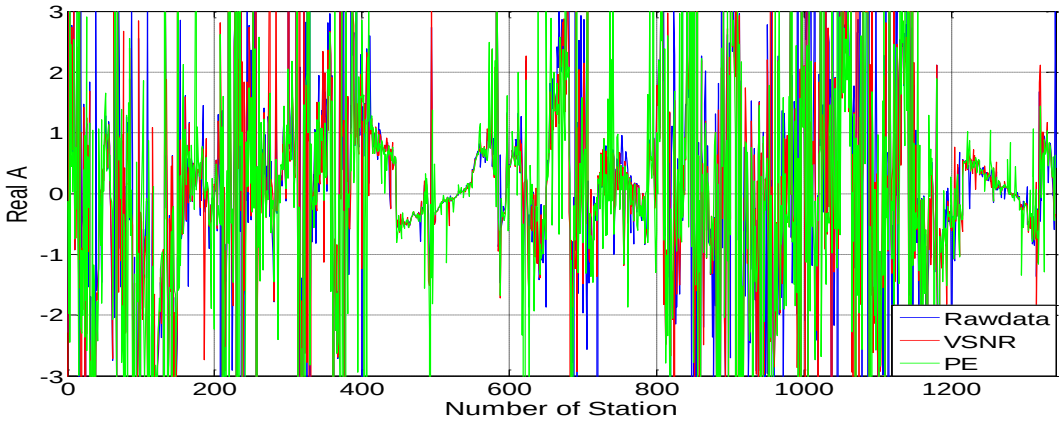

Figure 6.37: Real part of the tipper component A before any filtering (blue line), after applying the VSNR criterion (red line) and after filtering the data with the PE criterion (green line) for Campaign 2. Stacked frequency: 226274 Hz.

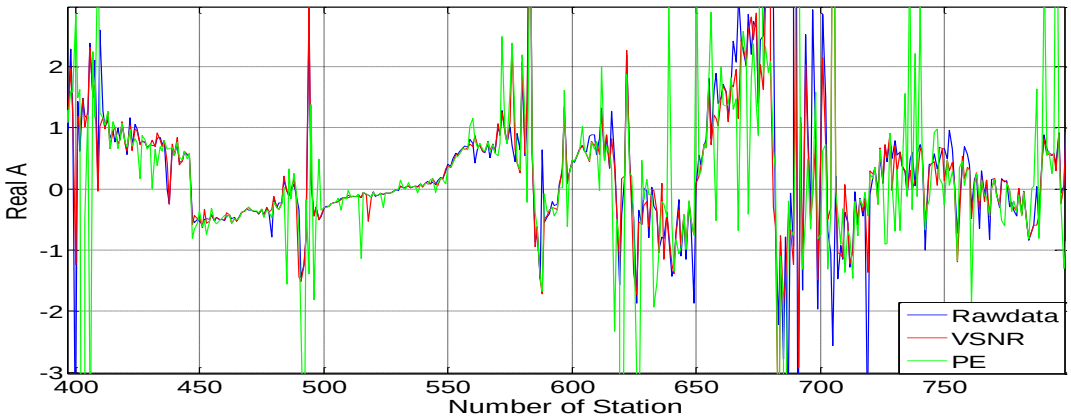

Figure 6.38: Zoom made from Figure 6.37 between stations 400 and 800 for the real part of the tipper component A. Stacked frequency: 226274 Hz.

This figure shows that the processing steps, especially the PE criterion, generated much more new spikes than those existing originally in the raw data. The extremely high noise levels for the higher frequencies in the spectra made it impossible to reach any improvement after the filtering processes. On the contrary, the data and tipper qualities were worsened since many transmitter frequencies seem to have been eliminated.

Similar responses were obtained for both frequencies in the imaginary part of A.

Figure 6.39 shows the real part of B for frequency 20000 Hz along profiles airdata043, filtered_new_airdata_043 and filteredPE3_filtered_airdata_043. As in the case of A, the tipper component B has a much smoother fluctuation around zero along the profiles since many spikes were removed. However, some new large values were added during the processing steps.

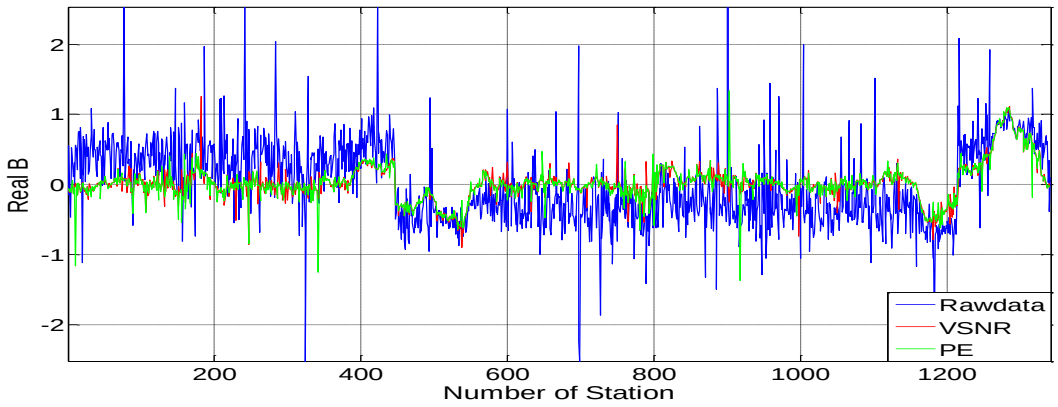

Figure 6.39: Real part of the tipper component B before any filtering (blue line), after applying the VSNR criterion (red line) and after filtering the data with the PE criterion (green line) for Campaign 2. Stacked frequency: 20000 Hz.

Figure 6.40 shows a zoom made from Figure 6.39 between stations 200 and 400. It can be seen that, although some new spikes appeared after the filtering steps, the resulting tipper is much smoother and most of the large and sharp values were removed. For this reason, more reliable tipper functions could be calculated along the profiles for the VLF band.

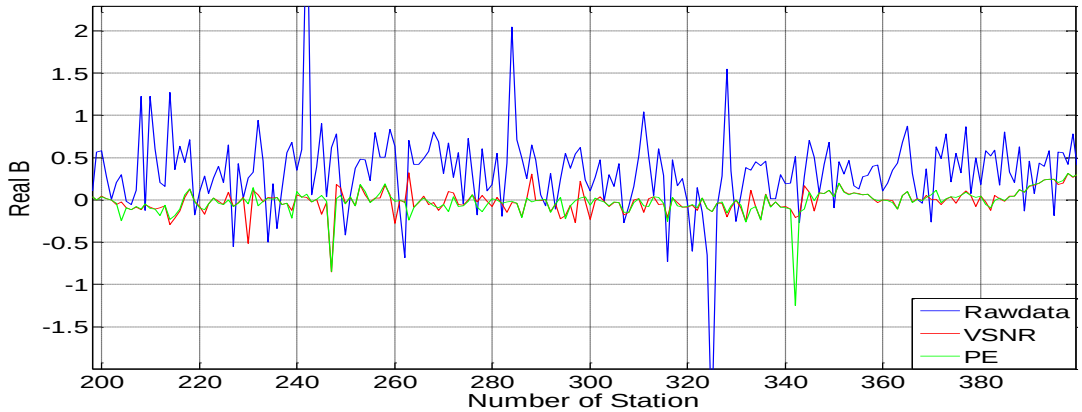

Figure 6.40: Zoom made from Figure 6.39 between stations 200 and 400 for the real part of the tipper component B. Stacked frequency: 20000 Hz.

Figure 6.41 shows the real part of B for 226274 Hz along the same profiles. As in the case of the tipper component A, the high noise makes it impossible to visualise any improvement. Figure 6.42 shows a zoom made from Figure 6.41 between stations 400 and 600.

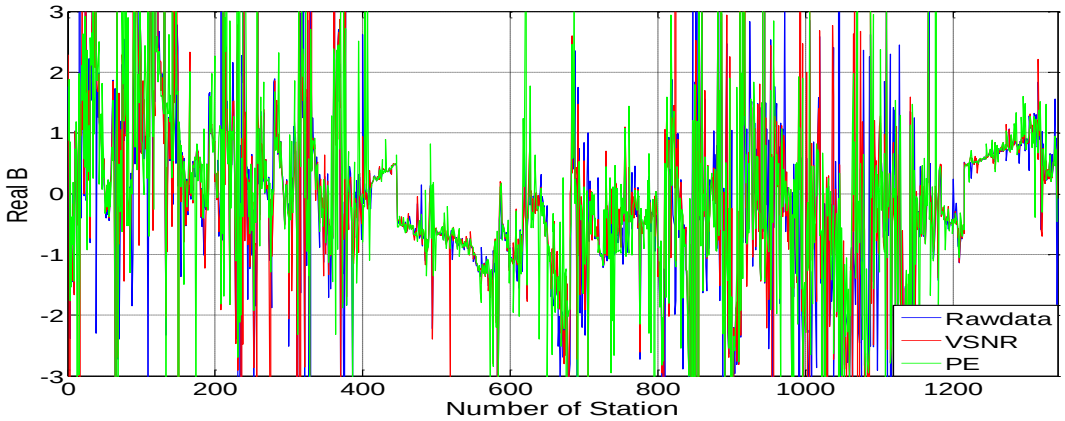

Figure 6.41: Real part of the tipper component B before any filtering (blue line), after applying the VSNR criterion (red line) and after filtering the data with the PE criterion (green line). Stacked frequency: 226274 Hz.

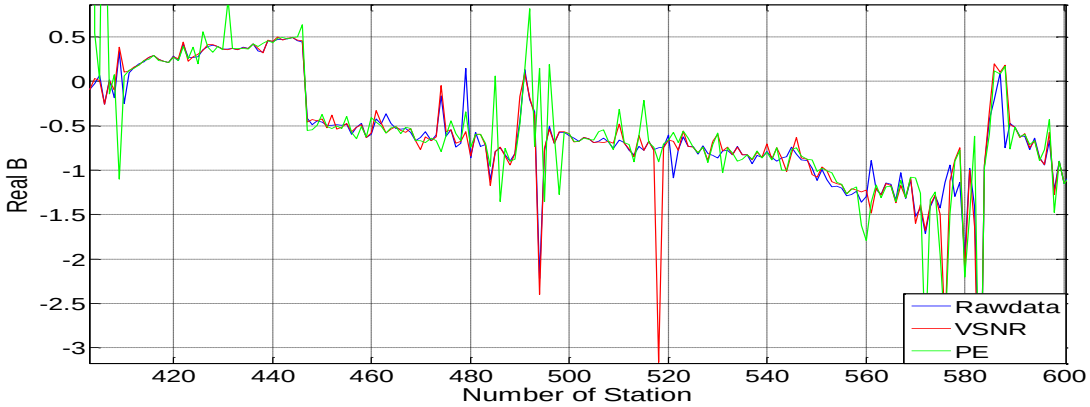

Figure 6.42: Zoom made from Figure 6.41 between stations 400 and 600 for the real part of the tipper component B. Stacked frequency: 226274 Hz.

This figure shows that the processing steps also generated more new spikes than those existing in the raw data. As in the case of A, no improvements were reached after the processing steps since many frequencies of importance seem to have been eliminated and the data and tipper qualities were worsened.

Similar results were obtained for both frequencies in the imaginary part of B.

In conclusion, the processing steps seem to have worked well on the data for the VLF frequency, although some noise was also added. Even so, much more reliable tipper functions could be subsequently estimated. For the LF frequency, on the other hand, the processing did not make any improvements on the results. The filtering steps seem to have worsened the data quality and therefore the tipper behaviour along the profiles. As explained previously in this chapter, this may be caused by the removal of transmitter frequencies that were hidden in the high noise level associated with the higher frequencies in the spectra.

6.2.4.2 Campaign 3.

Figure 6.43 shows the real part of A for frequency 28284 Hz along profiles conv_020, filtered_conv_020 and filteredPE3_filtered_conv_020. It is evident that the processing steps smoothed considerably the tipper behaviour along the profiles since many spikes were deleted. This is especially seen from station 1000, where most of the large values have been eliminated.

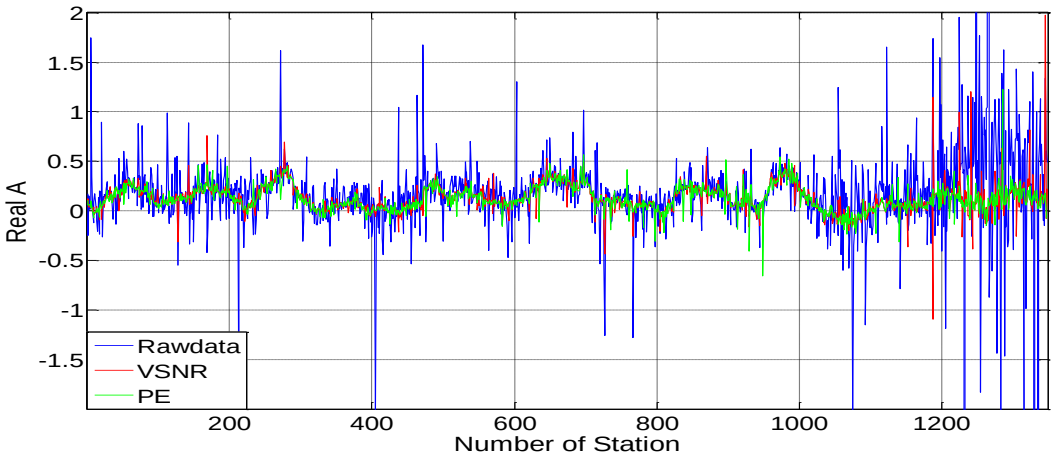

Figure 6.43: Real part of the tipper component A before any filtering (blue line), after applying the VSNR criterion (red line) and after filtering the data with the PE criterion (green line) for Campaign 3. Stacked frequency: 28284 Hz.

The improvement reached is more clearly seen in Figure 6.44 which represents a zoom made from Figure 6.43 between stations 200 and 600. This figure shows that the tipper behaviour is certainly much smoother after the filtering processes. However, some new spikes appeared on the profile after applying the VSNR and PE criteria. Similar results were obtained for the imaginary part of A. The possible cause of this fact was explained previously in this chapter. Even so, many noise frequencies were removed from the data and more reliable tipper functions could be estimated for the VLF band.

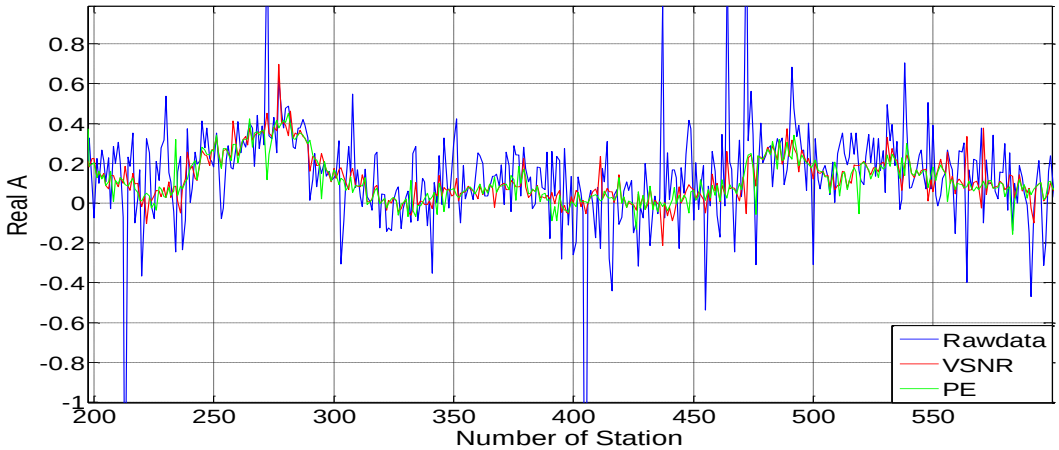

Figure 6.44: Zoom made from Figure 6.43 between stations 200 and 600 for the real part of the tipper component A. Stacked frequency: 28284 Hz.

Figure 6.45 shows the real part of A for 226274 Hz along the same profiles. This figure shows that the tipper component was not clearly improved. Although many spikes were deleted, many others appeared along the profile during the processing steps, especially the PE criterion.

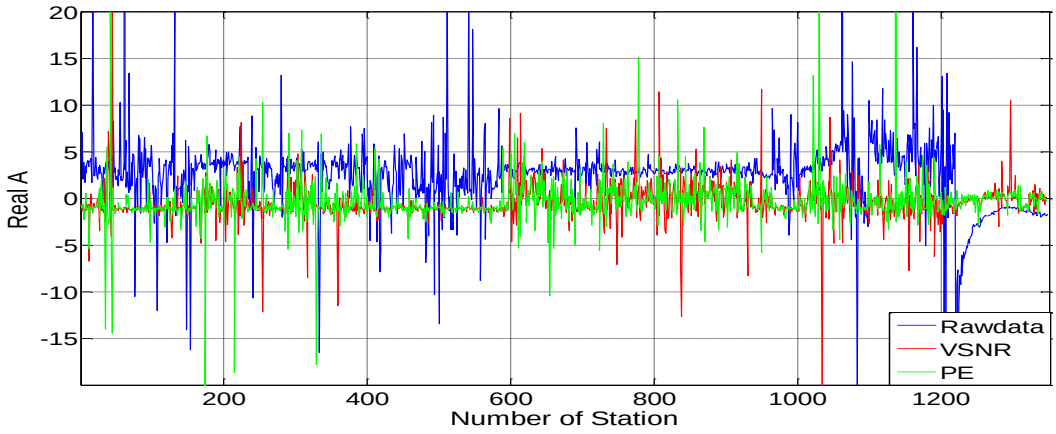

Figure 6.45: Real part of the tipper component A before any filtering (blue line), after applying the VSNR criterion (red line) and after filtering the data with the PE criterion (green line) for Campaign 3. Stacked frequency: 226274 Hz.

Figure 6.46 represents a zoom made from Figure 6.45 between stations 790 and 910. It is seen that the remaining tipper values are very high although they seem to be closer to zero after the processing steps. A similar response was obtained for the imaginary part. The new spikes can also be explained by the removal of transmitter frequencies that were hidden in the high noise floor.

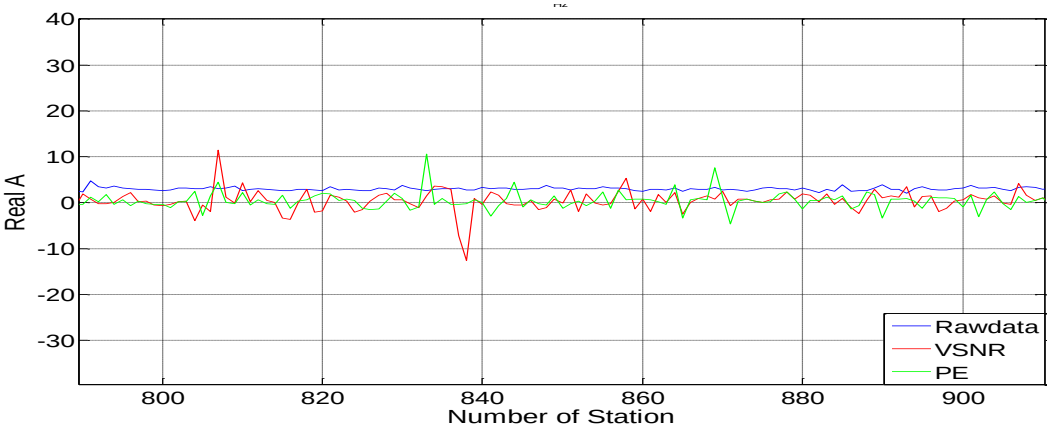

Figure 6.46: Zoom made from Figure 6.45 between stations 790 and 910 for the real part of the tipper component A. Stacked frequency: 226274 Hz.

In conclusion, evident improvements were not made on A in the case of the LF frequency. Besides the removal of transmitter frequencies, a strange behaviour was seen along the profiles. As mentioned before, this could have been caused by the use of some additional instrumentation on the aeroplane during the data collection. The cross-talk effect had also a large influence on the results. However, the processing steps seem to have worked well on the data for the VLF frequency, although some noise was also added. Even so, more reliable tipper functions could be subsequently estimated.

Figure 6.47 shows the real part of B for frequency 28284 Hz along profiles conv_020, filtered_conv_020 and filteredPE3_filtered_conv_020. This figure shows that an important improvement was made on the tipper estimation after the processing. The tipper component has a much smoother fluctuation around zero along the profiles since many spikes were deleted. However, some new large values were also added during the processing steps.

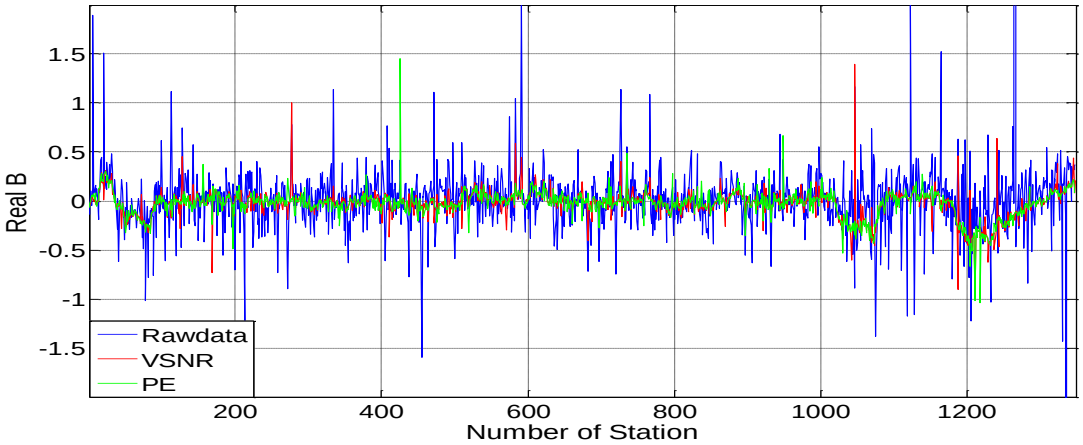

Figure 6.47: Real part of the tipper component B before any filtering (blue line), after applying the VSNR criterion (red line) and after filtering the data with the PE criterion (green line) for Campaign 3. Stacked frequency: 28284 Hz.

Figure 6.48 shows a zoom made from Figure 6.47 between stations 500 and 900. It can be seen that, although some new spikes appeared after the filtering steps, the resulting tipper is much smoother and many outliers (spikes) were removed. For this reason, more reliable tipper functions could be calculated along the profiles for the VLF band. Similar results were obtained for the imaginary part of B.

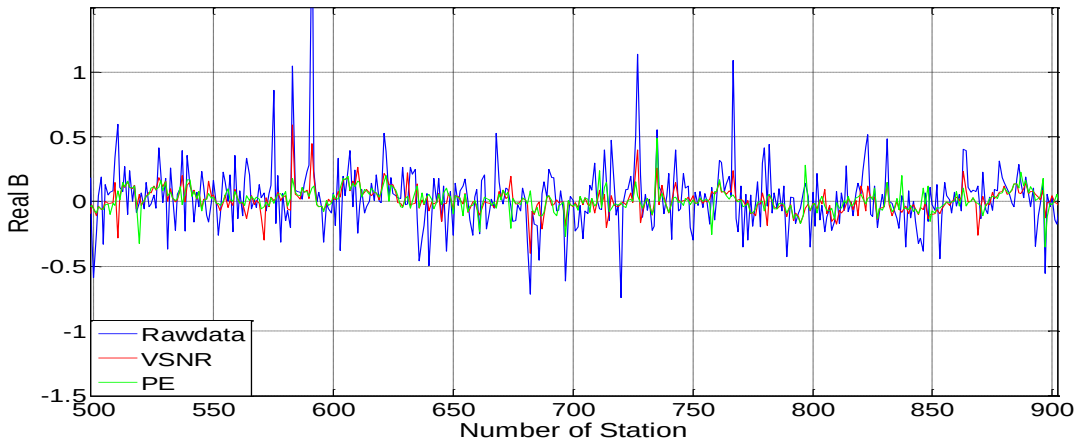

Figure 6.48: Zoom made from Figure 6.47 between stations 500 and 900 for the real part of the tipper component B. Stacked frequency: 28284 Hz.

Figure 6.49 shows the real part of B for 226274 Hz along the same profiles. The very rough tipper behaviour makes it impossible to visualise any improvement in this case.

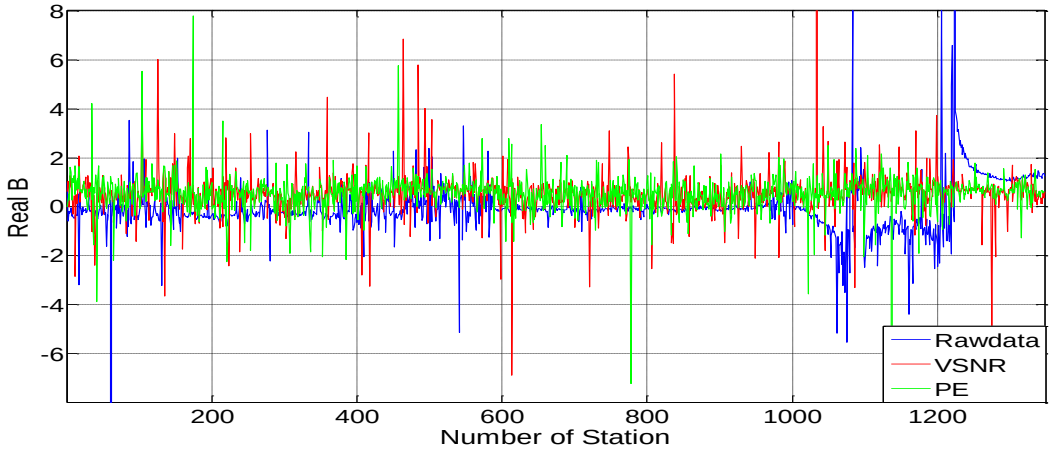

Figure 6.49: Real part of the tipper component B before any filtering (blue line), after applying the VSNR criterion (red line) and after filtering the data with the PE criterion (green line) for Campaign 3. Stacked frequency: 226274 Hz.

Figure 6.50 shows a zoom made from Figure 6.49 between stations 210 and 400. This figure shows that the processing steps introduced more new spikes than those existing in the raw data. Thus, many frequencies of importance were possibly eliminated and the data and tipper qualities therefore worsened. Similar results were obtained for the imaginary part of B.

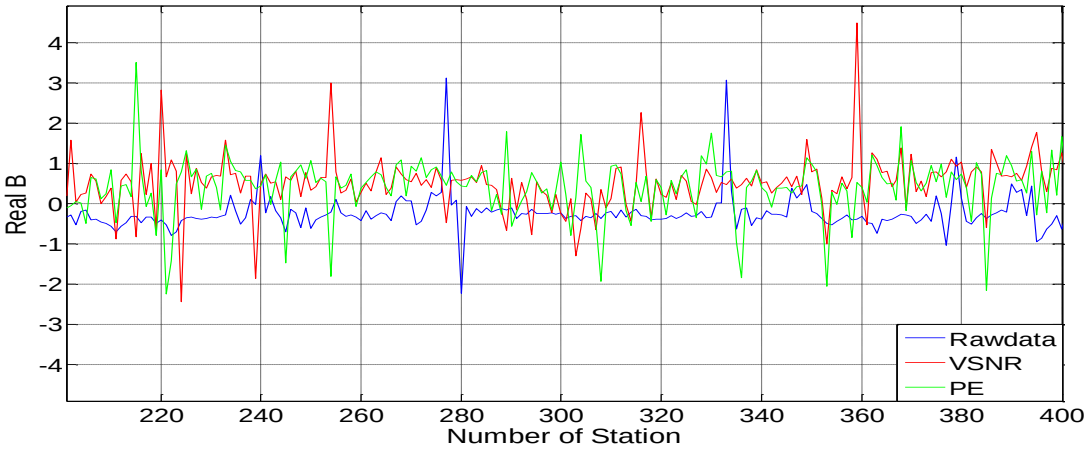

Figure 6.50: Zoom made from Figure 6.49 between stations 210 and 400 for the real part of the tipper component B. Stacked frequency: 226274 Hz.

In conclusion, the processing steps made evident improvements on the tipper component B for the VLF frequency, although some noise was also added. Even so, more reliable tipper functions could be estimated. For the LF frequency, on the other hand, the filtering steps seem to have worsened the data quality and therefore the tipper behaviour along the profiles. As mentioned before, this could have been caused by the removal of transmitter frequencies that were hidden in the high noise level associated with the higher frequencies, and the influence of the cross-talk effect. Likewise, some other instrumentation was possibly operated during the data collection. The tipper component B for the higher frequencies was thus more affected by these facts.

6.3 Tipper maps.

The software Oasis Montaj was used to make tipper maps over the survey area for frequency 20000 Hz in the VLF band and 226274 Hz in the LF band. Only the real part of A from Campaign 2 was mapped. In order to better visualise the results from the processing steps, these maps were created for the data without any filtering, after the application of the VSNR criterion and after using the PE criterion. The tipper mean value or trend generated on the profiles by a polynomial of zero order was previously removed from the raw data along each flight line. This was done in order to reduce the cross-talk or calibration effect. Later, the maps were compared with the SGU's map for old VLF measurements in Falun.

6.3.1 Raw data.

Figure 6.51 shows the map for the real part of A, made from the raw data, together with the SGU's dual VLF frequency map. The central frequency is 20000 Hz and the grid size is 50 metres.

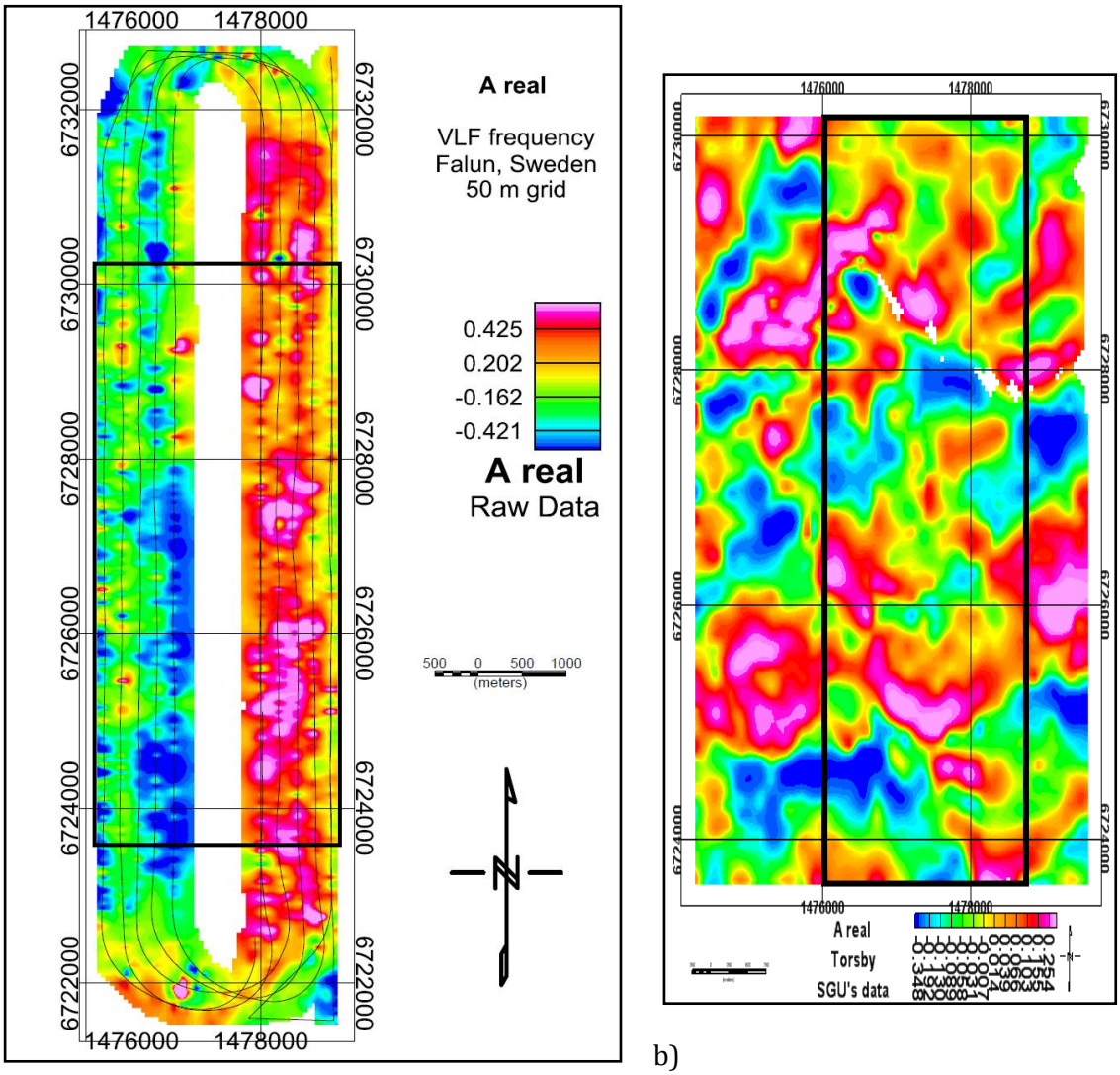

a) b)

Figure 6.51: Tipper map for the real part of A for a) the raw data at 20000 Hz, b) SGU's dual VLF map over the same area. Grid size: 50 m.

The thin black lines in Figure 6.51a correspond to the flight path over the area. Likewise, the zone within the black rectangle in Figure 6.51b corresponds to the area where the measurements were made using the ADU07. It is important to highlight that red colours represent high tipper values and blue colours show low tipper values. Although these figures do not have exactly the same colour scales, they are similar enough to allow making a comparison between the maps.

Generally speaking, this figure shows that the tipper map is not similar to the one from the SGU. This is especially due to the fact that positive values predominate on the right side of Figure 6.51a whereas only negative values are found on its left side. This corresponds with Figure 6.11, where it is clearly seen that the real part of A is only positive or negative at many subsequent stations without any local fluctuation around zero. Likewise, these values are so large compared with those on the SGU's map that the colour scales are very different from each other. This made it impossible to properly compare both maps.

Nevertheless, some very general features can be correlated. For example, some high tipper and low tipper areas between 6724000 and 6726000, and one small high tipper zone between 6728000 and 6730000.

Figure 6.52 shows the map for the real part of A, before the application of any filtering process, together with the SGU's dual VLF map. The frequency is 226274 Hz and the grid size 50 metres.

In this case there are many different tipper values that change sharply and rapidly with distance. These generated many fictitious features that cannot be correlated with those on the SGU's map. This result was expected since the noise levels are very high for the higher frequencies in the data. Furthermore, the signal has different penetration depths since the used frequencies are different.

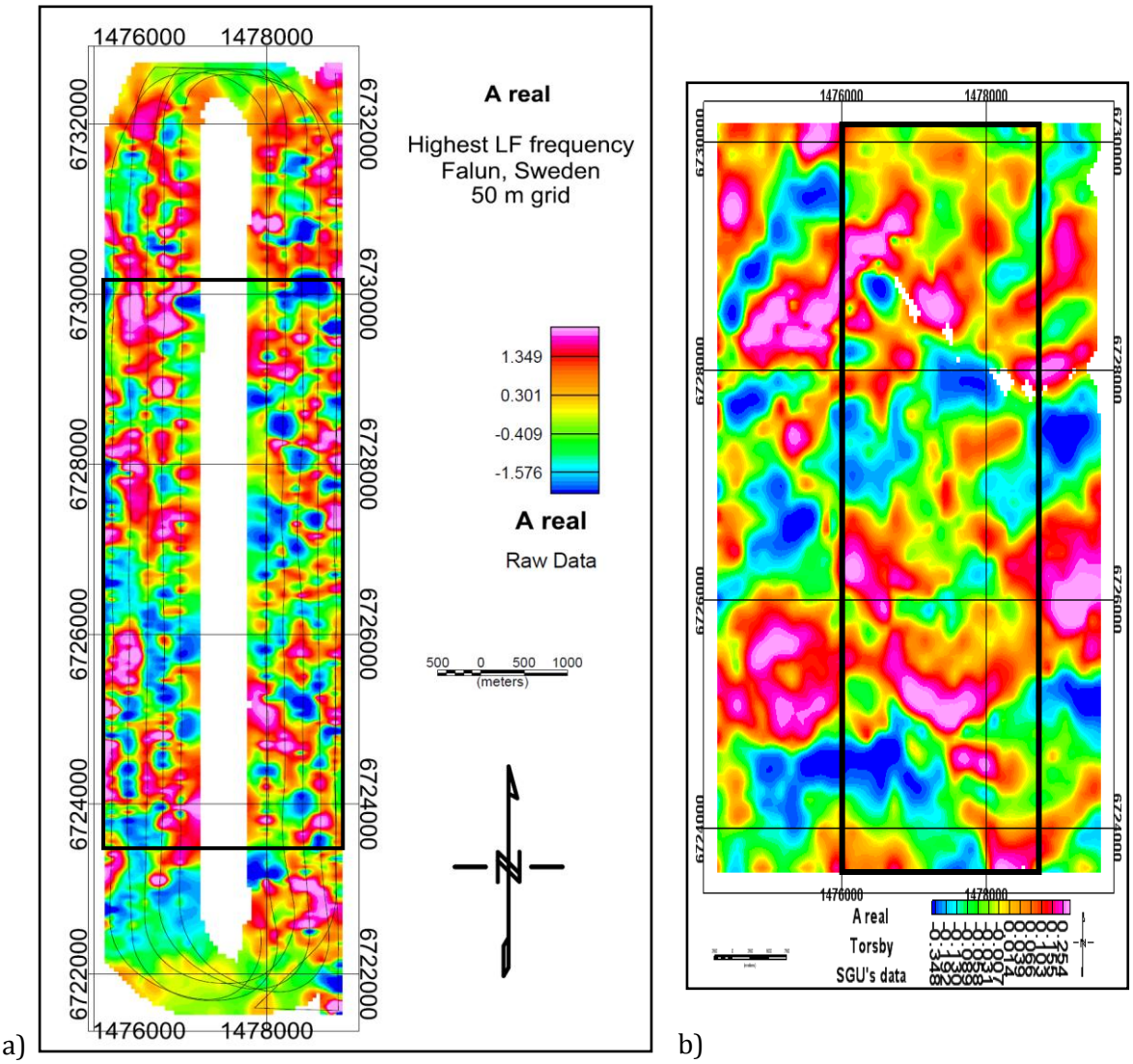

a) b)

Figure 6.52: Tipper map for the real part of A for a) the raw data at 226274 Hz, b) SGU's dual VLF map over the same area. Grid size: 50 m.

6.3.2 Maps after the VSNR processing.

Figure 6.53 shows the map for the real part of A, after applying the VSNR criterion, together with the SGU's dual VLF map. The stacked frequency is 20000 Hz and the grid size 50 is metres.

This figure shows that, despite of some values that change abruptly with distance, both maps are very similar since most of the features in Figure 6.53b can be found in Figure 6.53a. For example, the three red zones and the dark blue area between 6723600 and 6726000 are easily seen on the tipper map. Three blue zones between 6726000 and 6728000 together with one red area and one small blue zone below it between 6728000 and 6730000 can also be correlated.

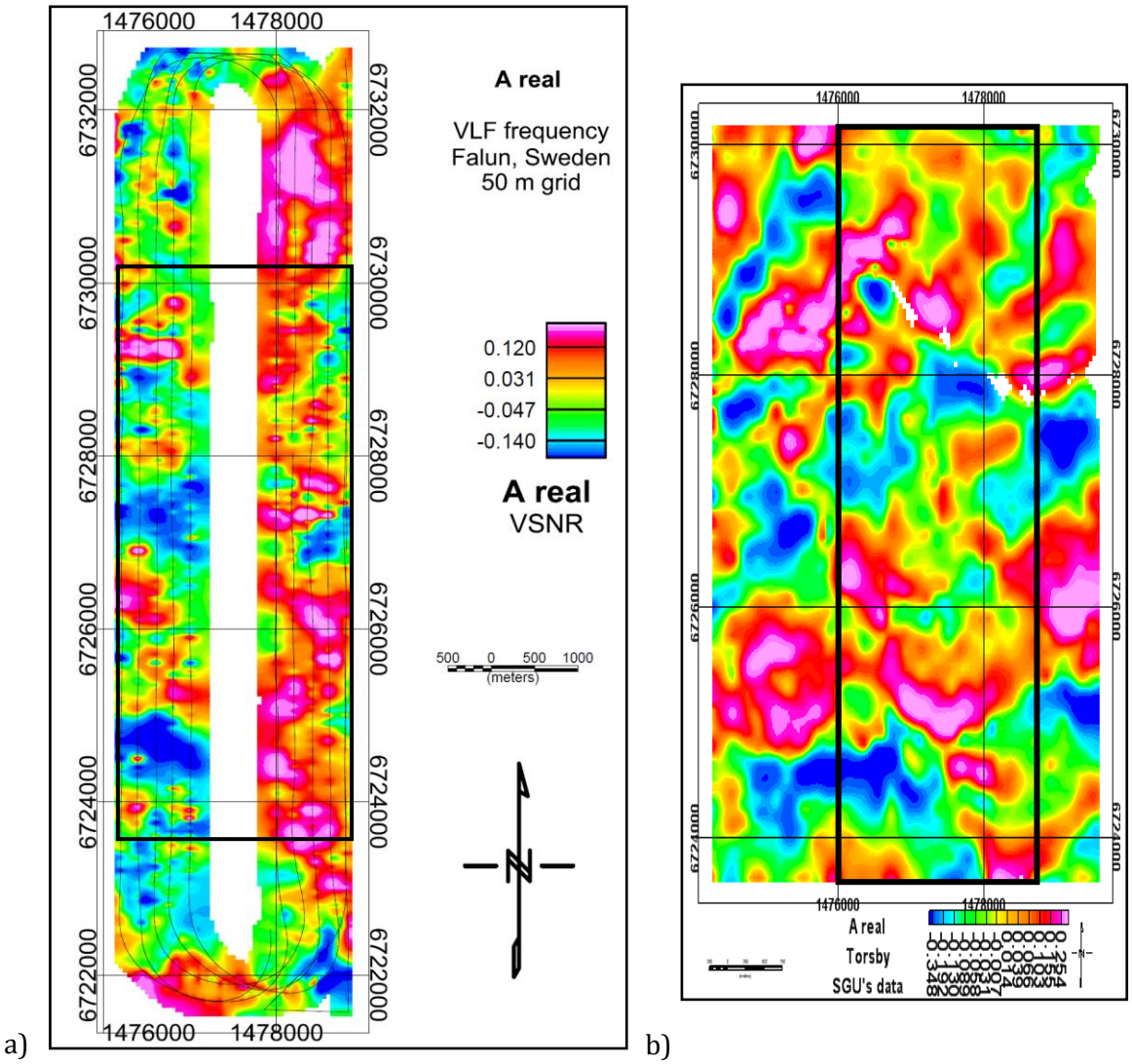

Figure 6.53: Tipper map for the real part of A for a) the filtered data after the VSNR criterion at 20000 Hz, b) SGU's dual VLF map over the same area. Grid size: 50 m.

Figure 6.54 shows the map for the real part of A after applying the VSNR criterion, together with the SGU's dual VLF map. The frequency is 226274 Hz and the grid size 50 metres.

This figure shows that the VSNR criterion could not help improving the tipper map for this frequency. Although the values are now smaller, there are still many sharp and abrupt changes that can be seen on the map. Likewise, important features cannot be correlated with those on the SGU's map. These facts make Figure 6.54a very little reliable when studying the tipper behaviour in the area. Moreover, the signal has different penetration depths since the used frequencies are different.

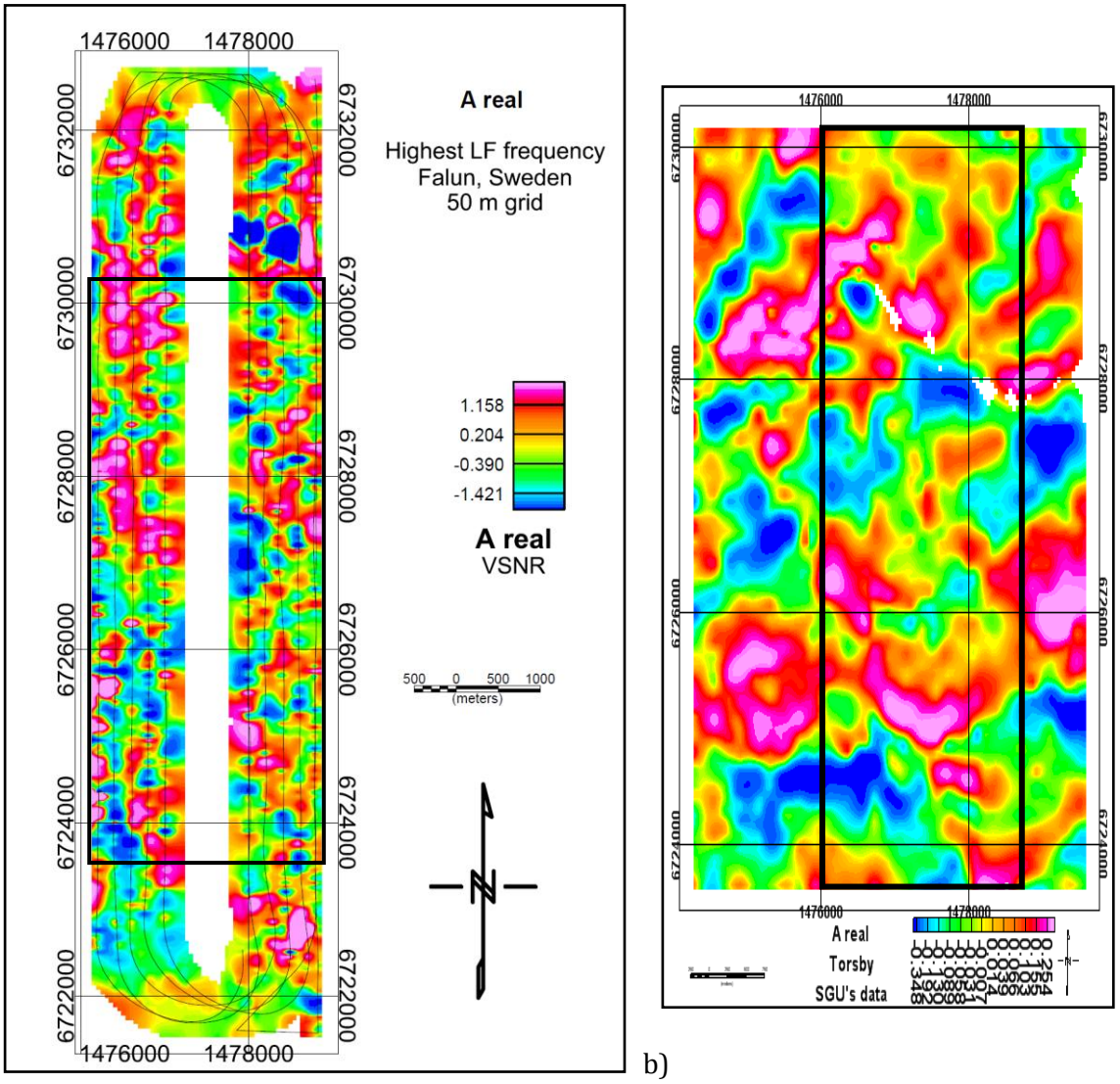

a) b)

Figure 6.54: Tipper map for the real part of A from a) the filtered data after the VSNR criterion at 226274 Hz, b) SGU's dual VLF map over the same area. Grid size: 50 m.

6.3.3 Maps after the PE processing.

Figure 6.55 shows the map for the real part of A, after applying the PE criterion, together with the SGU's dual VLF map. The frequency is 20000 Hz and the grid size is 50 metres.

This figure shows that both maps are very similar since most of the features in Figure 6.55b can be found in Figure 6.55a. This is especially evident for the three red zones and the blue area located between 6723600 and 6726000, the four red areas and the three blue zones between 6726000 and 6728000, and the rest of red areas and the small blue zone between 6728000 and 6730000. Despite this, the tipper map is not completely reliable since there are still some fictitious features along it.

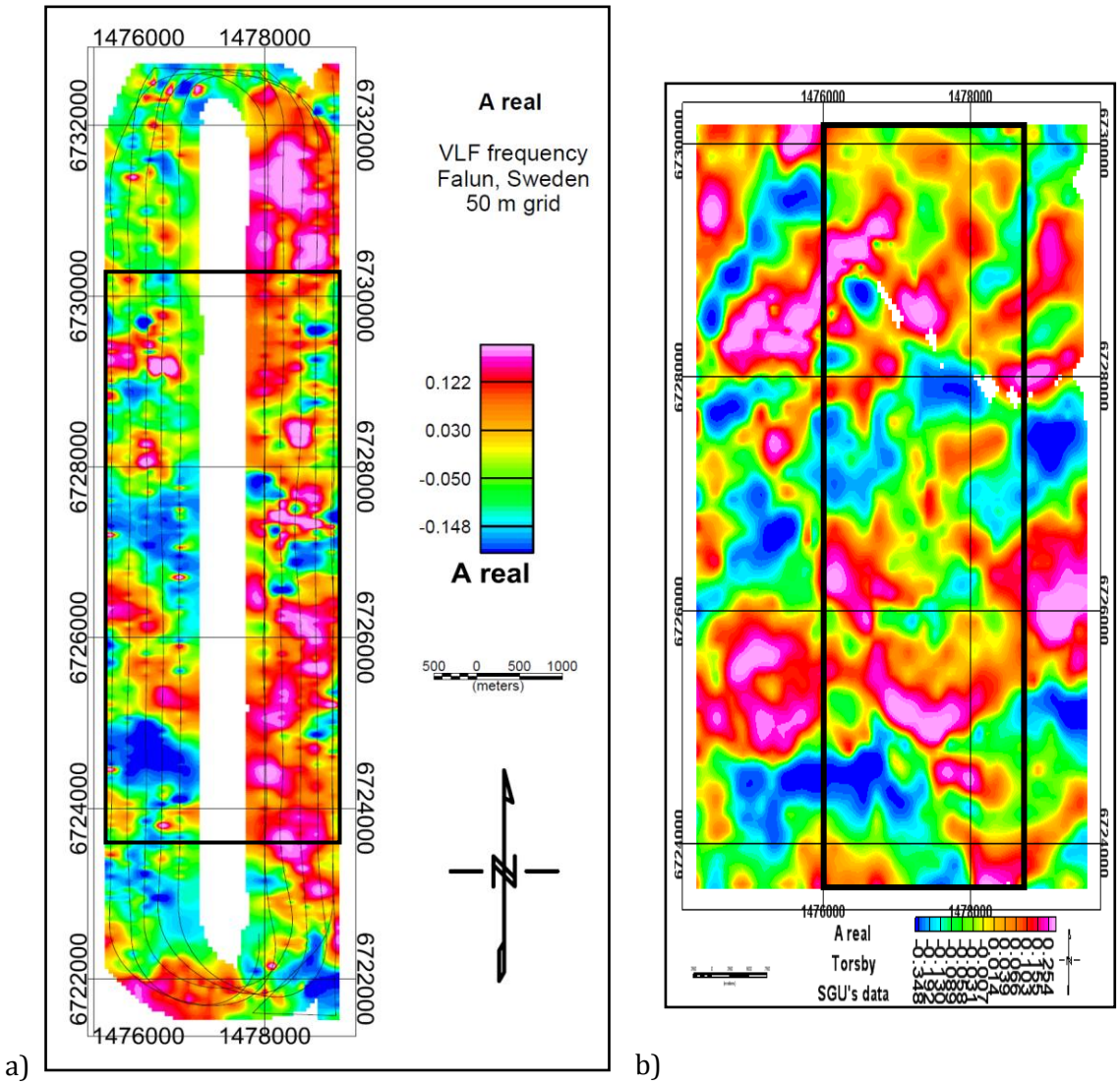

Figure 6.55: Tipper map for the real part of A for a) the filtered data after the PE criterion 20000 Hz, b) SGU's dual VLF map over the same area. Grid size: 50 m.

Figure 6.56 shows the map for the real part of A after applying the PE criterion, together with the SGU's dual VLF map. The frequency is 226274 Hz and the grid size 50 metres.

As in the previous case for this frequency, there are many features on the tipper map that cannot be correlated with those on the SGU's map. This fact makes this figure very little reliable when studying the tipper behaviour in the area. As mentioned before, this result was expected since the PE criterion was not able to improve the data quality for the higher frequencies in the spectra. Furthermore, the signal has different penetration depths since the used frequencies are different.

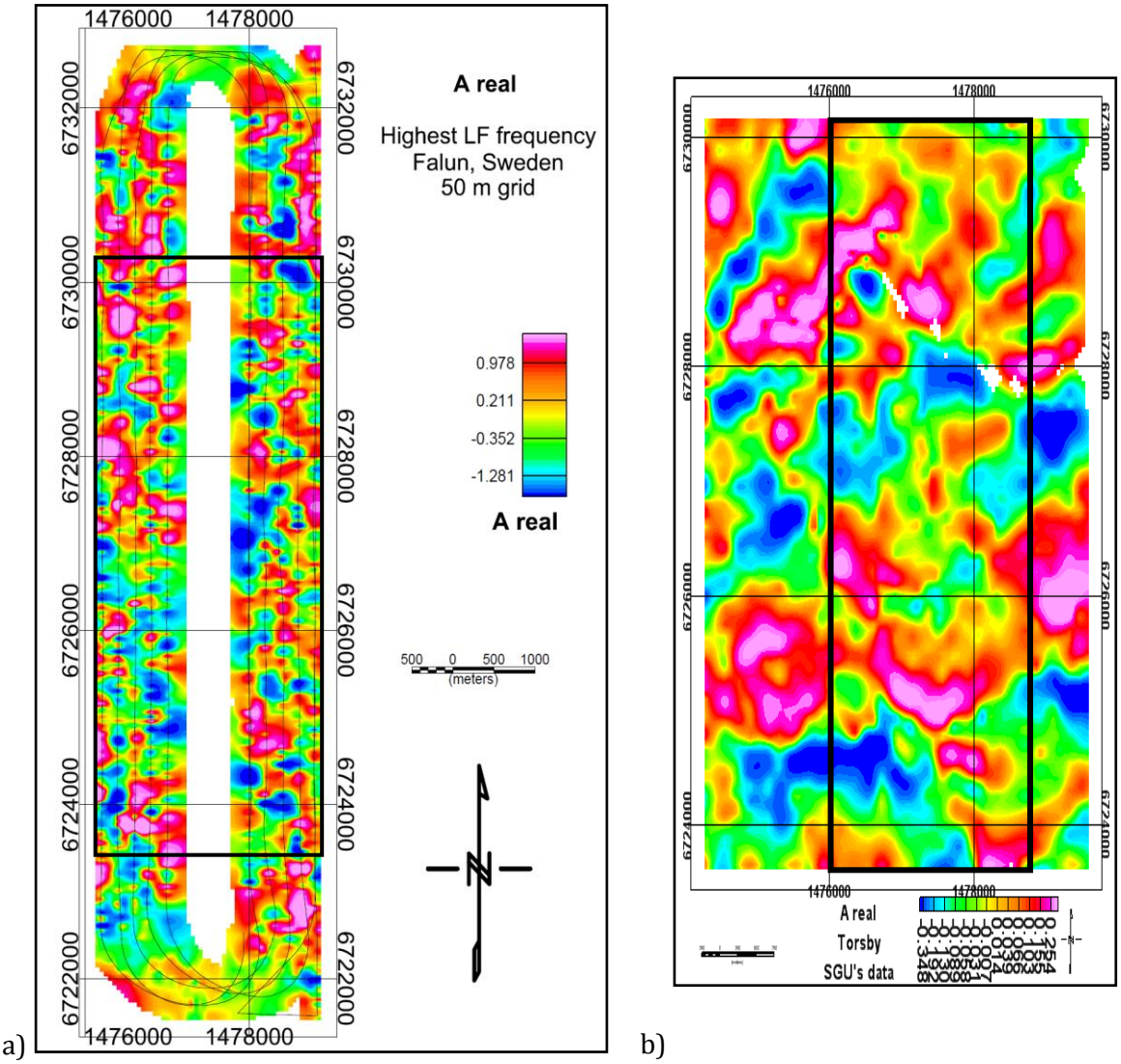

Figure 6.56: Tipper map for the real part of A from a) the filtered data after the PE criterion at 226274 Hz, b) SGU's dual VLF map over the same area. Grid size: 50 m.

When comparing Figure 6.55a with Figure 6.53a it is possible to observe that the former has some more features that cannot be found on the SGU's map. An example of this can be the small blue low tipper zones located between 6726000 and 6728000. However, the PE map also shows some important structures that cannot be seen on the VSNR map and correlate better with those on the SGU's. For example, the red high tipper zone between 6728000 and 6730000 and the differentiation of two different red areas in this range.

Despite of these fictitious features, the PE map correlates well with the one made by the SGU. Additionally, by using a larger grid size of 200 metres, a very good but less detailed (smoother) map can be made. The new map in Figure 6.57a reflects the most important structures seen on the SGU's dual VLF map.

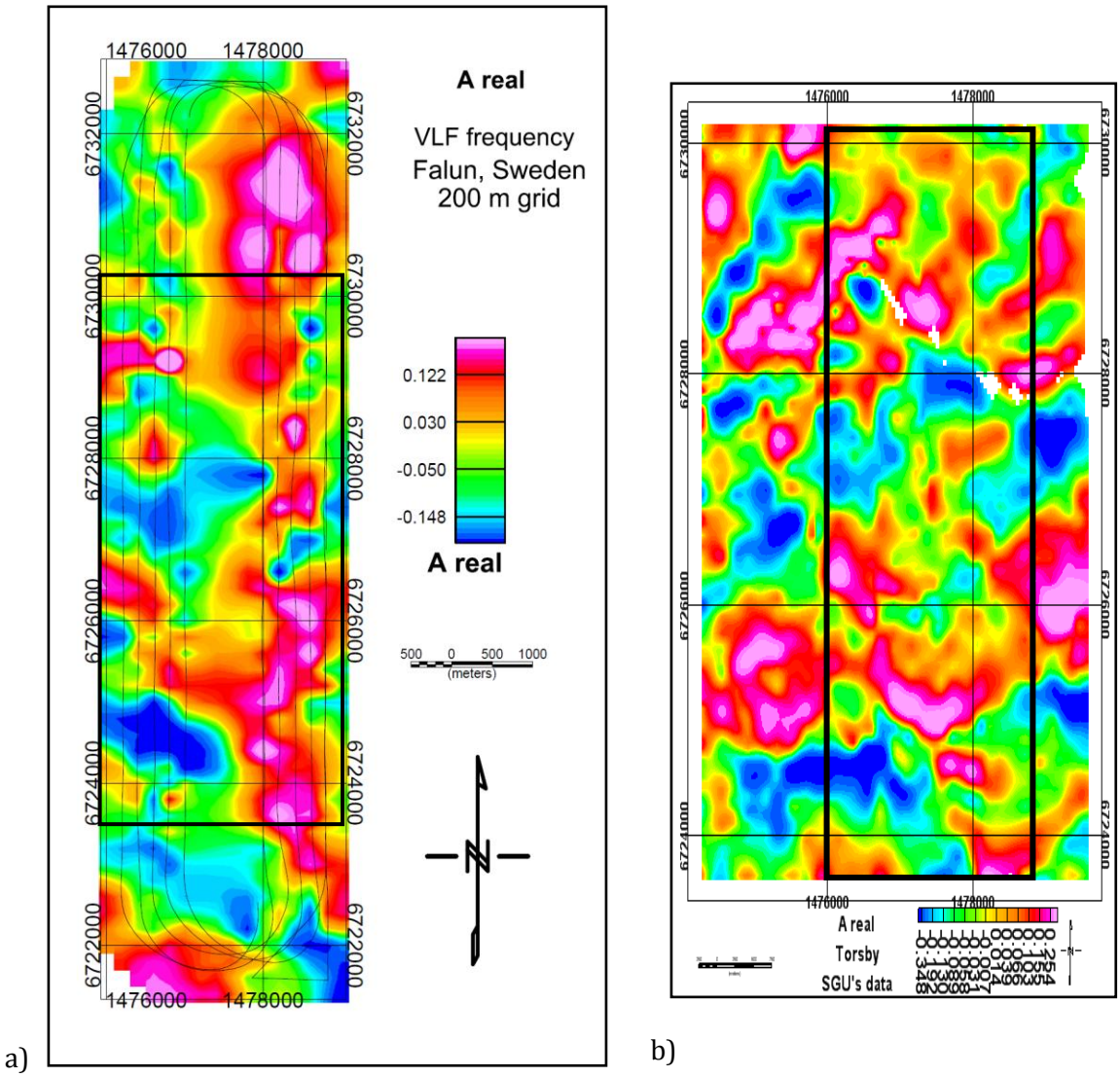

Figure 6.57: Tipper map for the real part of A for a) the filtered data after the PE criterion 20000 Hz, b) SGU's dual VLF map over the same area. Grid size: 200 m.

All the previous maps show that important improvements were made in the data quality for frequencies in the VLF band. Therefore, the results obtained from the filtering processes were somehow satisfactory for the lower frequencies in the spectra.

Chapter 7

Conclusions

Two cases of airborne measurements using the broadband measuring system were presented in this thesis. In the first case (Campaign 2), high noise levels were generated by the SGU's instrumentation and the common power supply connection. In the second case (Campaign 3), the SGU's instrumentation was the main source of noise on the aeroplane during the data collection. As seen in Figure 6.1, for Campaign 2, this especially affected the high frequencies from 40 kHz, where the local noise rises to large values in the spectra. Much more spikes related to noise were also found for these frequencies compared with those in the VLF band. In general terms, the available data were initially very noisy, mainly at the higher frequencies.

In Figure 6.2 it is seen that the data from Campaign 3 are less noisy than in the previous case. However, the local noise rises to higher values from a frequency of about 80 kHz. Many spikes can also be found especially in the LF band. This means that, as in Campaign 2, the data were noisier for the higher frequencies in the spectra.

7.1 The filtering process and estimated tipper.

The VSNR and PE criteria improved considerably the data quality in the VLF band since many noise frequencies were successfully removed from the spectra in both campaigns. This was reflected during the tipper calculation when smoother and less noisy transfer functions could be estimated. The main problem was found at high frequencies for which the processing steps were not able to effectively reduce the very high noise levels. As seen in Figure 6.1, the local noise is much stronger than the signal itself in the LF band. Figure 6.2 also shows this fact but with lower noise levels. The cross-talk effect could also have a very big influence on the data since it is much higher at high frequencies.

The calculation of the mean value of H_z^{real} and the scalar tipper components could not help detecting noise frequencies in the spectra. The improvement made by the VSNR criterion, on the other hand, is clearly evident for the VLF band as seen in section 6.2.2. After the PE criterion some improvements were also reached. However, both processing steps also introduced a few new spikes on the tipper profiles. This fact was seen in the VLF band, but especially in the LF band. The removal of frequencies of interest which were hidden in the high noise levels may explain this effect.

In the case of Campaign 3, the strange behaviour of the tipper components for the LF frequency, especially for B, could have also been caused by the use of some instrumentation, besides the SGU's equipment, during the data collection. A good example can be the

instrument used for communication between the pilot and the control tower. This fact is considered since many large spikes appeared on the profile at stations where they had not been seen before.

Although the PE criterion removed some noise from the spectra, more new spikes appeared after its application than those generated by the VSNR criterion. This is especially seen for Campaign 2. This fact can be explained by the removal of more transmitter frequencies during this processing step. For example, Figures 6.9 and 6.10 show that frequency 171 kHz has a very large PE value. For this reason, it was then considered as noise when applying the PE criterion. However, this frequency corresponds to a very well known radio transmitter signal that contains valuable information. The removal of this and other frequencies of interest hidden in the high noise levels worsened the data quality and therefore affected the tipper calculations.

Despite of these problems, the smoother and less noisy tipper functions along the profiles reflect that the filtering processes generated satisfactory results for the lower frequencies in the spectra. The high frequencies, however, represent a problem that must be overcome in the future.

7.2 Tipper maps.

The improvement made on the data quality after the application of the processing steps is also reflected on the tipper maps for Campaign 2. The cross-talk effect in the magnetic sensor used a constant value (shift) that, as seen in the estimated tipper values, increases with frequency. This phenomenon is directional dependent and generates a stripe pattern on the tipper maps. In order to eliminate this effect, the mean value (trend) of the estimated tipper was removed from the raw data along each flight line. This considerably eliminated the stripe patterns on the obtained maps.

The map generated for the raw data at the VLF frequency was very different from the one created by the SGU for VLF measurements in Falun. In fact, the real part of the tipper component A seemed to be highly affected by the change in the flight direction over the area. This is because only large positive values were found on the right side of the map whereas large negative values predominated on its left side. The similarity was much less in the case of the LF frequency. The noise levels were so high that many fictitious features could be seen on the map. This made it impossible to compare it with the one created by the SGU.

The application of the VSNR criterion improved considerably the quality of the generated map for the VLF frequency since a good correlation of its features with those on the SGU's map could be accomplished. In fact, the calculated tipper component seemed to have no dependence on the flight direction. However, there were still some abrupt variations that cast doubt on the complete reliability of the map. The same results were not obtained for the LF frequency. In this case, although the tipper values were smaller, the very high noise levels did not allow the VSNR criterion to improve the data quality. Actually, the generated map is very similar to the one created by using the raw data. This fact makes it completely unreliable when studying the tipper behaviour along the area.

The PE criterion made some improvements for the VLF frequency since many features on the SGU's map are now more easily seen in the new figure. Despite this, the tipper map is not completely reliable since there are a few more fictitious features on it compared with those on the VSNR map. As expected, no improvements were made for the LF frequency since the PE criterion was not able to improve the data quality in this case.

A very important conceptual point in the differences between the new VLF maps and the SGU's dual VLF map lies in the number and direction of the used transmitters. SGU's maps are made by using the signals from only the two strongest selected VLF transmitters. The maps from the ADU07 data, on the other hand, were made with the signals from all the selected and acceptable VLF transmitters. There is more control on the direction and therefore more details are resolved on the new maps (see Figures 6.55a and 6.55b).

7.3 Unanswered questions and improvements.

It is not possible to say that all the aims of this project were successfully accomplished. The fact that the high noise levels in the LF band did not allow the processing steps to make any improvement in this range is still something that has to be shortly solved in future. Likewise, less noisy data in the VLF band will also generate more benefits. This would avoid the removal of transmitter frequencies and more reliable transfer functions could therefore be estimated.

One way to overcome this problem is by using the information about the frequencies of radio transmitters from the international frequency list IFL published by the ITU (International Telecommunications Union). This is done in order to check if any of those transmitters are available in our list. Posteriorly, the tipper functions can be calculated by selecting the spectra from only those frequencies. This could not be done in this project due to time constraints, but it is highly recommended to perform this process and see if any improvement is reached.

An important fact is that the airborne MFR system will be calibrated soon. The first and most important step is to apply the calibration to the spectral data and run all the processes once again. This will be particularly important for the higher frequencies.

Chapter 8

References

Bastani, M. (2001). EnviroMT - A New Controlled Source/Radio Magnetotelluric System. *Uppsala Dissertations from the Faculty of Science and Technology* 32. Uppsala University.

Bastani, M. and Pedersen, L. B. (2001). Estimation of Magnetotelluric transfer functions from radio transmitters. *Geophysics,* 66 (4): 1038-1051.

Becken, M. and Pedersen, L. B. (2003). Transformation of VLF anomaly maps into apparent resistivity and phase. *Geophysics,* 68 (2): 497-505.

Dynesius, L., Smirnov, M. and Pedersen, L. B. (2004). Multifrequency VLF/LF receiver. A new tool for fast and detailed mapping of near surface geology. *Report for the Geological Survey of Sweden, March 31, 2004*. Uppsala University.

Gustavsson, A. (2008). Master thesis on Post-processing of airborne data from Multi Frequency Receiver (MFR) System. Uppsala University.

Hellsborn, H. (2009). A note on electromagnetic field theory and 1D Modeling of synthetic CSAMT data. Uppsala University.

Hjärten, M. (2007). Master thesis on Interpretation of controlled-source radiomagnetotelluric data from Hallandåssen. Uppsala University.

Müller, A. (2000). A new method to compensate for bias in Magnetotellurics. *Geophysical Journal International,* 142: 257-269.

Oskooi, B. (2004). A broad view on the Interpretation of Electromagnetic Data (VLF, RMT, MT, CSTMT). *Uppsala Dissertations from the Faculty of Science and Technology* 959. Uppsala University.

Oskooi, B. and Pedersen, L. B. (2005). Comparision between VLF and RMT methods. A combined tool for mapping conductivity changes in the sedimentary cover. *Journal of Applied Geophysics* 57: 227-241.

Oskooi, B. and Pedersen, L. B. (2006). Resolution of airborne VLF data. *Journal of Applied Geophysics* 58: 158-175.

Pedersen, L.B. (1982). The magnetotelluric impedance tensor – Its random and bias errors. *Geophysical Prospecting* 30: 188–210.

Pedersen, L.B., Qian, W., Dynesius, L. and Zhang, P. (1994). An airborne tensor VLF system. From concept to realization. *Geophysical Prospecting* 42. 863-883.

Pedersen, L. B. and Oskooi, B. (2004). Airborne VLF measurements and variations of ground conductivity: A tutorial. *Surveys in Geophysics* 25: 151-181.

Pedersen, L. B., Bastani, M. and Dynesius, L. (2005). Groundwater exploration using combined controlled-source and radiomagnetotelluric techniques. *Geophysics,* 70 (1): G8-G15.

Pedersen, L. B. and Dynesius, L. (2008). Final report on the Multi Frequency VLF/LF receiver (MFR) project, September 2008. Uppsala University.

Pedersen, L. B., Persson, L., Bastani, M. and Byström, S. (2009). Airborne VLF measurements and mapping of ground conductivity in Sweden. *Journal of Applied Geophysics,* 67: 250-258.

Persson, L. (2001). Plane Wave Electromagnetic Measurements for Imaging Fracture Zones. *Uppsala Dissertations from the Faculty of Science and Technology 30*. Uppsala University.

Spies, B.R. and Eggers, D. (1986). The use and misuse of apparent resistivity in electromagnetic methods. *Gephyisics,* 51 (7): 1462-1471.

Spies, B. R. (1989). Depth of investigation in electromagnetic sounding methods. *Geophysics*, 54 (7): 872–888.

Zhang, P., Roberts, R.G. and Pedersen, L. B. (1987). Magnetotelluric strike rules. *Geophysical Journal International,* 52 (3): 267-278.

Chapter 9

Appendix

9.1 Appendix A: Files format.

9.1.1 Spectra File format.

SPECTRA FILES

Header 1: This header only appears at the beginning of the file.

File-header:

first_segment segment_length project_revision project_name project_client observer method have_stations line_number station_number positioning_mode coord_sys t_start_sec t_start_usec t_end_sec t_end_usec number_of_segments.

Acquisition parameters:

num_ch used_channels sample_encoding voltage_range postamp_gain_Hx postamp_gain_Hy postamp_gain_Hz postamp_gain_Ex postamp_gain_Ey sampling_frequency electrode_distance.

Processing parameters:

frequency_averaging coherence_threshold NSTACK selected_band WIDTH MEDTYPE MEDWIDTH MEDINT PERFORM_MEDIAN_INTERVAL TRAC min_number_of_transmitters.

Header 2: This header appears at the beginning of every segment (station).

Segment-header:

time_end_tv_sec time_start_tv_usec time_end_tv_sec time_end_tv_usec sn_threshold num_transmitters.

Positioning-header:

latitude longitude altitude X Y Z position_quality t_gps_sec t_gps_usec t_update_sec t_update_usec.

Orientation-header:

heading pitch roll t_update orient_quality.

Data: The number of lines for each segment is given by the num_transmitters in Header 2.

Index Frequency SNR Hx_real Hx_imag Hy_real Hy_imag Hz_real Hz_imag.

TENSOR FILES

Header 1: This header only appears at the beginning of the file.

File-header:

first_segment segment_length project_revision project_name project_client observer method have_stations line_number station_number positioning_mode coord_sys t_start_sec t_start_usec t_end_sec t_end_usec number_of_segments.

Acquisition parameters:

num_ch used_channels sample_encoding voltage_range postamp_gain_Hx postamp_gain_Hy postamp_gain_Hz postamp_gain_Ex postamp_gain_Ey sampling_frequency electrode_distance.

Processing parameters:

frequency_averaging coherence_threshold NSTACK selected_band WIDTH MEDTYPE MEDWIDTH MEDINT PERFORM_MEDIAN_INTERVAL TRAC min_number_of_transmitters.

Header 2: This header appears at the beginning of every segment (station).

Segment-header:

time_end_tv_sec time_start_tv_usec time_end_tv_sec time_end_tv_usec sn_threshold num_transmitters.

Positioning-header:

latitude longitude altitude X Y Z position_quality t_gps_sec t_gps_usec t_update_sec t_update_usec.

Orientation-header:

heading pitch roll t_update orient_quality.

Data: There are 9 lines corresponding to every stacked frequency.

Frequency Stacked frequency A_real A_imag A_error B_real B_imag B_error.

9.2 Appendix B: Programs flowchart.

The following flowchart describes the relation between the different programs designed in MATLAB in order to perform the processing steps for the ADU07 data, especially the filtering process.

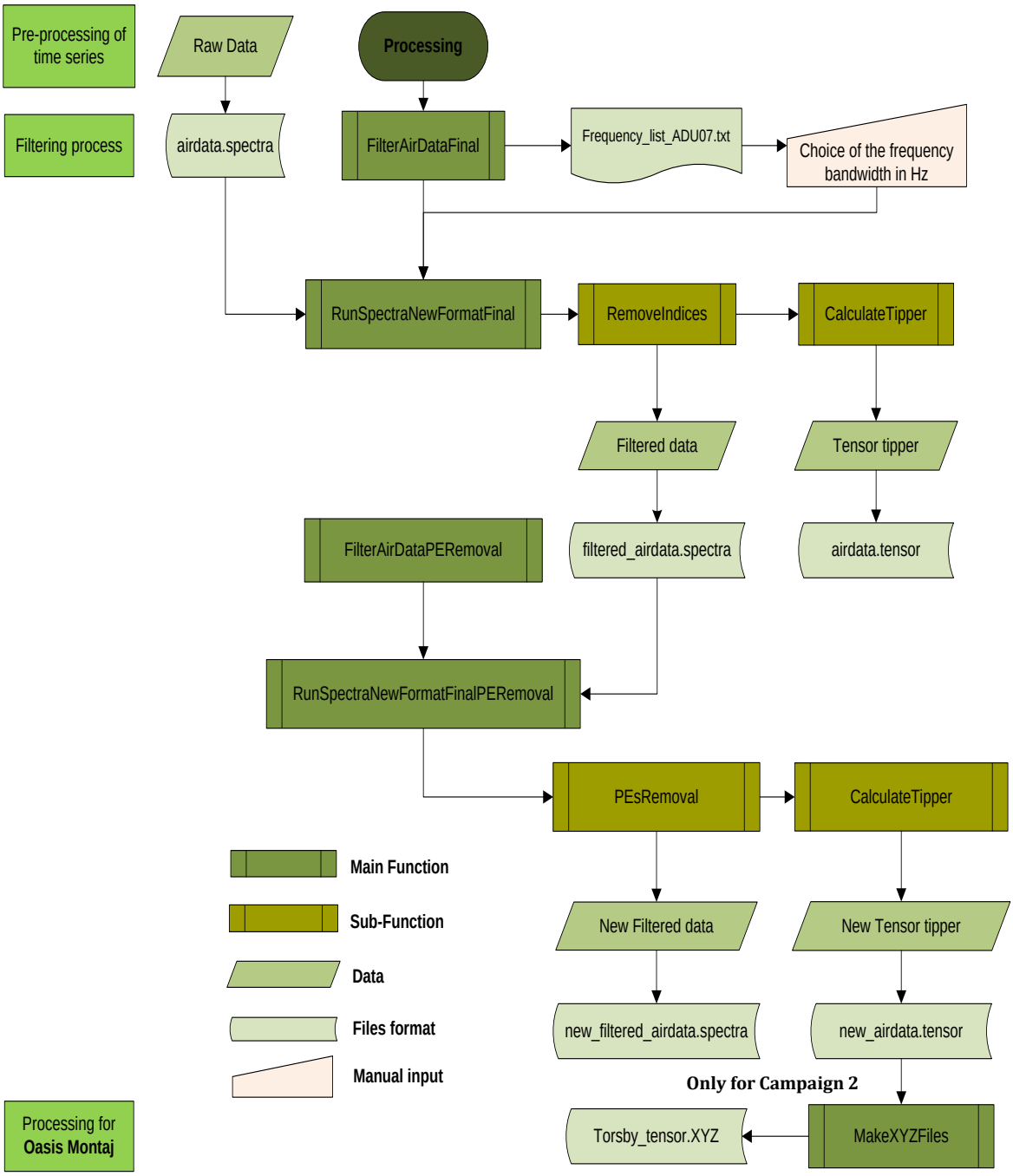

9.3 Appendix C: MATLAB scripts.

The most important functions and sub-functions written in MATLAB for this project are shown as follows:

9.3.1 Function *IdentifyNoise*.

```
% ************************************************************************
% This program reads spectra-files and calculates statitics.
%
% Called functions:
%   AddTable (sub-function).
% ************************************************************************

function IdentifyNoise(datapath,file,rr)

fprintf(' The data file being processed: %s \n',file)

% Open files.
fid1 = fopen([datapath '/' file]);

% Creating StatiticTable.
datadf=4; %4Hz.
lengthf = round((250000-10000)/datadf);
stind = round(10000/datadf);
StaticTable = zeros(lengthf,4);
StaticTable(:,1) = stind:1:lengthf+stind-1;
dataf = StaticTable(:,1)*datadf;

extra = [];
extra = ReadSpecFileHeader(fid1,extra,1,0);

% Number of stations in file.
N = extra.first_segment;
extra.spectra = [];
extra.num_transmitters = [];

IntCount = 1;
totdiff  = 0;
for i=1:N
    if ~feof(fid1)
     % Reading segment header.
     extra = ReadSpecFileHeader(fid1,extra,2,i);

     if(i>1)
       xdiff = extra.X(i)- extra.X(i-1);
       ydiff = extra.Y(i)- extra.Y(i-1);
       totdiff = xdiff + ydiff;
       if(abs(totdiff) > 0)
             dx = xdiff/IntCount;
             dy = ydiff/IntCount;
             for jj=1:IntCount
                    extra.X(i-jj) = extra.X(i-jj)+ (IntCount-jj)*dx;
                    extra.Y(i-jj) = extra.Y(i-jj)+ (IntCount-jj)*dy;
                    extra.totdiff(i-jj) = totdiff;
             end
```

```
                IntCount = 1;
                totdiff = 0;
        else
             IntCount = IntCount+1;
        end
        if(i == N)
             if(abs(dx)> abs(dy))
                 if(dx > 0)
                      dx = 17.0;
                      dy = 0.0;
                  else
                       dx = -17.0;
                       dy = 0.0;
                  end
              else
                  if(dy>0)
                       dx = 0.0;
                       dy = 17.0;
                   else
                       dx = 0.0;
                       dy = -17.0;
                   end
              end
              for jj=1:IntCount-1
                    extra.X(i-jj) = extra.X(i-jj)+ (IntCount-jj)*dx;
                    extra.Y(i-jj) = extra.Y(i-jj)+ (IntCount-jj)*dy;
                    extra.totdiff(i-jj) = totdiff;
              end
        end
    end

        % Calculates statistics for occurrence.
        Temp = Addtable(extra);
        StaticTable(:,2) = StaticTable(:,2)+ Temp(:,2);
        StaticTable(:,3) = StaticTable(:,3)+ Temp(:,3);

        fprintf('Ready segment number :%d \n',i)
        extra.spectra =[];

    else
        fprintf('End of file reached \n');
    end

end

IndexZero=find(StaticTable(:,3)~=0);
StaticTable(IndexZero,4)=StaticTable(IndexZero,2)./StaticTable(IndexZero,
3);

% Plots frequency probability.
figure('Name','Probability vs. Frequency (Hz)','NumberTitle','off')
semilogx(dataf,StaticTable(:,4)*100)
title({'Probability vs. Frequency (Hz) for file:', num2str(file)})
xlabel('Frequency (Hz)'), ylabel('Probability')
axis([10000 250000 0 100]), grid on

FinalTable=[dataf(IndexZero)                    StaticTable(IndexZero,2)
StaticTable(IndexZero,3) StaticTable(IndexZero,4)*100];
xlswrite('FinalTable',FinalTable,rr)
```

```
% Removes frequencies whose occurrences are greater than or equal to 50%.
noiseindex = find(StaticTable(:,4)*100 >= 50);
if noiseindex>0
    StaticTest = StaticTable;
    datafTest  = dataf;
    StaticTest(noiseindex,:) = NaN;
    xlswrite('NoiseFrequencies',datafTest(noiseindex),rr)
    datafTest(noiseindex) = NaN;

    % Removes any rows containing NaNs from a matrix X.
    StaticTest(any(isnan(StaticTest),2),:) = [];
    datafTest(any(isnan(datafTest),2),:) = [];

    % Plots when occurrence > threshold is removed.
    figure('Name','Probability vs. Frequency (Hz) ','NumberTitle','off')
    semilogx(datafTest,StaticTest(:,4)*100)
    title({'Probability vs. Frequency (Hz) after removing noise
    frequencies for file:', num2str(file)})
    xlabel('Frequency (Hz)'), ylabel('Probability')
    axis([10000 250000 0 100]), grid on
else
    disp('PickNoise: No values above 50% can be found');
end

StaticTable=[];
fclose(fid1);
```

9.3.2 Sub-function *Addtable*.

```
% ************************************************************************
% This program makes the statistical table for all the indices in the
% range (10 kHz-250 kHz).
% ************************************************************************

function StaticTable = Addtable(extra)

% Creating StaticTable.
datadf=4; %4Hz.
lengthf = round((250000-10000)/datadf);
stind = round(10000/datadf);
StaticTable = zeros(lengthf,4);
StaticTable(:,1) = stind:1:lengthf+stind-1;

% Defines Hx, Hy and Hz as complex numbers.
Hx  = extra.spectra(:,4) + sqrt(-1.0).*extra.spectra(:,5);
Hy  = extra.spectra(:,6) + sqrt(-1.0).*extra.spectra(:,7);
Hz  = extra.spectra(:,8) + sqrt(-1.0).*extra.spectra(:,9);

% Calculates the vertical S/N ratio (VSNR) assuming that it has the same
% noise level as the horizontal S/N ratio (HSNR).
HSNR = extra.spectra(:,3);
Vnoise  =  ((abs(Hx).^2  +  abs(Hy).^2)./(10.^(HSNR./10))./4.0;  %Vertical
                                                                  noise.
Hnoise = 10.^(HSNR./10); %Horizontal noise.
VSNR  = 10*log10((abs(Hz).^2)./Vnoise);
extra.Vnoise = Vnoise;
```

```
% Calculation of CrossSN to compare it against threshold in a later step.
CrossN = sqrt(Vnoise.*Hnoise);
CrossSN = 10*log10(CrossN);

% Calculation of mean and standard deviation for CrossSN and VSNR.
MnCross = mean(CrossSN);
%MnCross = median(CrossSN);
MnV = median(VSNR);
CrossSt = std(CrossSN);
CrossStV = std(VSNR);

Midd = MnCross*ones(length(CrossSN));
StdMidd = (MnCross+CrossSt)*ones(1,length(CrossSN));
MiddV = MnCross*ones(length(VSNR));
StdMiddV = (MnV+CrossStV)*ones(1,length(VSNR));
limit = mean(StdMidd);
limitV =mean(StdMiddV);

% Finds values for CrossSN above limit.
aboveStdMidd = find(CrossSN>=limit );
aboveStdMiddV = find(VSNR>=limitV);
listme = extra.spectra(aboveStdMidd,1);
listmeV = extra.spectra(aboveStdMiddV,1);

Len = length(listmeV);
if(Len>0)
    % Creates index for frequencies with crossSN above limit.
    for kk = 1:1:Len
      staticindex(kk) = find(StaticTable(:,1)== listmeV(kk));
    end

    % Creates index for frequencies that appear in the file.
    inlen=length(extra.spectra(:,1));
    for s3=1:1:inlen
        static3index(s3)=find(StaticTable(:,1)==extra.spectra(s3,1));
    end

    % Adds to list frequencies with crossSN above threshold.
    StaticTable(staticindex,2) =  StaticTable(staticindex,2)+1;

    % Counts the number of times frequencies are in the file.
    StaticTable(static3index,3) = StaticTable(static3index,3)+1;

    StaticTable(:,4) = StaticTable(:,2)./StaticTable(:,3);
    staticindex = [];
    static3index = [];
    listme = [];
    listmeV = [];
end
```

9.3.3 Function *FilterAirDataFinal*.

```
% ********************************************************************
%  This program removes frequencies by reading a list where noise
%  frequencies detected by the VSNR criterion were saved.
%
% Called functions:
%   RunSpectraNewFormatFinal(main function).
% ********************************************************************
```

```
function FilterAirDataFinal

format long

% Selects file for processing.
datapath    = uigetdir('C:\','Select the data directory to read');
resultpath  = uigetdir('C:\','Select the results directory to write');
files = dir(datapath);
NoofFiles = size(files);

% Selects the file where the noise frequencies were saved.
[filename path] = uigetfile('*.txt','Select a file for frequencies to
remove');
file2 = [path filename];

% Choosing bandwith to remove from file.
width = input('Choose bandwith to remove (in Hz): ');
df=4; %Resolution: 4Hz.
dk = round(width/df);
fid2 = fopen(file2);

% Reading frequencies from file and save them as StaticTable.
freq_list = [];
j = 0;
while ~feof(fid2)
     j = j+1;
     freq_list(j) = fscanf(fid2,'%10d \n',1);
end;
StaticTable = freq_list./4; % Converts the frequencies into indices,
                            % where 4 Hz is the frequency resolution.
fclose(fid2);

for kk =3:NoofFiles
    rr=kk-2;
    RunSpectraNewFormatFinal(datapath,resultpath,files(kk).name,dk,Static
    Table,rr);
end
```

9.3.4 Function *RunSpectraNewFormatFinal*.

```
% ********************************************************************
% Reading spectra-files from a directory, filter them and save the
% filtered files in a new directory.
%
% Called functions:
%   RemoveIndicies (sub-function).
%   CalculateTipper (sub-function).
% ********************************************************************

function
RunSpectraNewFormatFinal(datapath,resultpath,file,dk,StaticTable,rr)

fprintf(' The data file being processed: %s \n',file)

% Opens files.
fid1 = fopen([datapath '/' file]);
out_filename = [resultpath '/' 'filtered_' file];
fid2 = fopen(out_filename, 'wt');
```

```
out_filename = [resultpath '/'  file(1:length(file)-7) 'tensor'];
fid3 = fopen(out_filename, 'wt');

extra = [];
extra = ReadSpecFileHeader(fid1,extra,1,0);

% Number of stations in file.
N = extra.first_segment;
extra.spectra = [];
extra.num_transmitters = [];
add = 1;

% Makes overlapping bands of 1 octave for tensor calculations.
StartingFrequency = 10000;
NoOfBands = 9;
Inc = sqrt(2.0);
extra.StF(1) = StartingFrequency;
extra.EnF(1) = extra.StF(1)*2.0;
extra.TarF(1)= sqrt(extra.EnF(1)*extra.StF(1));
for i = 2:NoOfBands
    extra.StF(i) = extra.StF(i-1)*Inc;
    extra.EnF(i) = extra.StF(i)*2.0;
    extra.TarF(i)= sqrt(extra.EnF(i)*extra.StF(i));
end

IntCount = 1;
totdiff  = 0;
addSNR=1;
addFRET=1;
for i=1:N
    if ~feof(fid1)

        %Reading segment header.
        extra = ReadSpecFileHeader(fid1,extra,2,i);

         if(i>1)
           xdiff = extra.X(i)- extra.X(i-1);
           ydiff = extra.Y(i)- extra.Y(i-1);
           totdiff = xdiff + ydiff;
           if(abs(totdiff) > 0)
                 dx = xdiff/IntCount;
                 dy = ydiff/IntCount;
                 for jj=1:IntCount
                        extra.X(i-jj) = extra.X(i-jj)+ (IntCount-jj)*dx;
                        extra.Y(i-jj) = extra.Y(i-jj)+ (IntCount-jj)*dy;
                        extra.totdiff(i-jj) = totdiff;
                 end
                    IntCount = 1;
                    totdiff = 0;
            else
                 IntCount = IntCount+1;
            end
            if(i == N)
                 if(abs(dx)> abs(dy))
                     if(dx > 0)
                          dx = 17.0;
                          dy = 0.0;
                      else
                           dx = -17.0;
                           dy = 0.0;
```

```
                    end
                else
                    if(dy>0)
                        dx = 0.0;
                        dy = 17.0;
                     else
                        dx = 0.0;
                        dy = -17.0;
                     end
                end
                for jj=1:IntCount-1
                      extra.X(i-jj) = extra.X(i-jj)+ (IntCount-jj)*dx;
                      extra.Y(i-jj) = extra.Y(i-jj)+ (IntCount-jj)*dy;
                      extra.totdiff(i-jj) = totdiff;
                end
            end
         end

        % Filtering of frequencies below 14 kHz (by removing them from
        the data).
        lowin = find(extra.spectra(:,1) <=3500);
        extra.spectra(lowin,:) = [];

        % Filtering of frequencies by using the StaticTable.
        extra = RemoveIndices(extra,StaticTable);

        % New number of transmitters after removing frequencies.
        extra.new_num_transmitters(i) = length(extra.spectra);

        IndexRout(i) = length(extra.spectra);
        Results(add:add+IndexRout(i)-1,1:9) = extra.spectra(:,1:9);
        add = add+IndexRout(i);

        Tippers = CalculateTipper(extra,NoOfBands);
        TippTot(1:NoOfBands,:,i) = Tippers;

        fprintf('Ready segment number :%d \n',i)

        extra.spectra =[];
    else

        break;

    end
end

extra.first_segment=i;

% Saves the spectra file header into the new filtered spectra file:
WriteSpecFileHeader(fid2,extra,1,0)

% Saves the spectra file header into the tensor tipper file:
WriteSpecFileHeader(fid3,extra,1,0)

EndInd = i-1;
fclose(fid1);

add = 1;
```

```
IntCount = 1;
totdiff  = 0;
for i=1:1:EndInd

    % Writing of segment header into the filtered spectra file.
    WriteSpecFileHeader(fid2,extra,2,i);

    % Writing of the new filtered data into the file.
    fprintf(fid2,'%8d  %7.1f  %5.2f  %10.5f  %10.5f  %10.5f  %10.5f  %10.5f
     %10.5f \n',Results(add:add+IndexRout(i)-1,1:9)');
    add = add+IndexRout(i);

    % Writing of segment header into the tensor tipper file.
    WriteSpecFileHeader(fid3,extra,2,i);

    % Making a packed tensor matrix.
    if(extra.totdiff(i) >= 0)
          TensorPack = [extra.TarF' extra.TarF' ...
                        real(TippTot(1:NoOfBands,1,i)) ...
                        imag(TippTot(1:NoOfBands,1,i)) ...
                        ones(9,1)*0.01 ...
                        real(TippTot(1:NoOfBands,2,i)) ...
                        imag(TippTot(1:NoOfBands,2,i)) ...
                        ones(9,1)*0.01 ];
     else
          TensorPack = [extra.TarF' extra.TarF' ...
                        -real(TippTot(1:NoOfBands,1,i)) ...
                        -imag(TippTot(1:NoOfBands,1,i)) ...
                        ones(9,1)*0.01 ...
                        -real(TippTot(1:NoOfBands,2,i)) ...
                        -imag(TippTot(1:NoOfBands,2,i)) ...
                        ones(9,1)*0.01 ];
    end

    % Writing of the packed results into the file
    fprintf(fid3,'  %8.1f  %8.1f  %8.5f  %8.5f  %8.5f  %8.5f  %8.5f  %8.5f
     \n',TensorPack');

end
fclose(fid2);
fclose(fid3);

disp('function:Runspectra - ready')
```

9.3.5 Sub-function *RemoveIndices*.

```
% ***********************************************************************
% This program removes the indices of noise frequencies from the spectra
% file.
% ***********************************************************************

function extra = RemoveIndices(extra,StaticTable)

% Make a list for indices to remove.
if ~isempty(StaticTable)
    kmin = 1;
    for kk = 1:1:length(StaticTable)
        kmax = kmin + extra.dk;
```

```
        IndexList(kmin:kmax)=(StaticTable(kk)-
        (extra.dk)/2):(StaticTable(kk)+(extra.dk)/2);
        Indmin(kk)=StaticTable(kk)-(extra.dk)/2;
        Indmax(kk)=StaticTable(kk)+(extra.dk)/2;
        kmin = kmax+1;
     end
end

lenold = length(extra.spectra);

% Finds indices within the interval Indmin-Indmax.
in = find((extra.spectra(:,1) >= Indmin(1)) & (extra.spectra(:,1) <=
Indmax(1)));
    if ~isempty(in)
        extra.spectra(in,:) = [];
        lennew = length(extra.spectra);
        lendiff = lenold-lennew;
        inmax = in(length(in))-lendiff;
    else
        inmax = 1;
    end
    if(inmax == 0)
        inmax = 1;
    end

% Finds indices from file.
for k = 2:1:length(StaticTable)
    lenold = length(extra.spectra);
    in = find((extra.spectra(inmax:lenold,1) >= Indmin(k)) &
    (extra.spectra(inmax:lenold,1) <= Indmax(k)));
    in = in+inmax-1;
            if ~isempty(in)

                extra.spectra(in,:) = [];
                lennew = length(extra.spectra);
                lendiff = lenold-lennew;
                inmax = in(length(in))-lendiff;
                in=[];
            end
end
```

9.3.6 Sub-function *CalculateTipper*.

```
% ************************************************************************
% This function calculates the tipper values using the least squares
% solution for the airborne measurements.
************************************************************************

function Tippers=CalculateTipper(extra,NoOfBands)

% Makes overlapping bands of 1 octave wide.

Hx = (extra.spectra(:,4)+sqrt(-1)*extra.spectra(:,5));
Hy = (extra.spectra(:,6)+sqrt(-1)*extra.spectra(:,7));
Hz = (extra.spectra(:,8)+sqrt(-1)*extra.spectra(:,9));

Tippers = -1000.0*(ones(2,NoOfBands)+sqrt(-1.0)*ones(2,NoOfBands));
Tippers = Tippers';
for i = 1:NoOfBands
```

```
    in = find(( extra.spectra(:,2) >= extra.StF(i) & extra.spectra(:,2)
     <= extra.EnF(i) ));
    if (~isempty(in) && length(in)>1)
                HH = [Hx(in) Hy(in)];
                Tippers(i,:) = inv(conj(HH')*HH)*(conj(HH')*Hz(in));
    else
                Tippers(i,:) = -1000;
    end
end
```

9.3.7 Function *RunSpectraNewFormatPE.*

```
% ************************************************************************
% This program calculates the PE mean values for every frequency at each
% station.
%
% Called functions:
%CalculateTipperPE(subfunction).
************************************************************************

function RunSpectraNewFormatPE(datapath,file,rr)

fprintf(' The data file being processed: %s \n',file)

% Opens files.
fid1 = fopen([datapath '/' file]);
extra = [];
extra = ReadSpecFileHeader(fid1,extra,1,0);

% Number of stations in file.
N = extra.first_segment
extra.spectra = [];
extra.num_transmitters = [];

% Makes overlapping bands of 1 octave for tensor calculations.
StartingFrequency = 10000;
NoOfBands = 9;
Inc = sqrt(2.0);
extra.StF(1) = StartingFrequency;
extra.EnF(1) = extra.StF(1)*2.0;
extra.TarF(1)= sqrt(extra.EnF(1)*extra.StF(1));
for i = 2:NoOfBands
    extra.StF(i) = extra.StF(i-1)*Inc;
    extra.EnF(i) = extra.StF(i)*2.0;
    extra.TarF(i)= sqrt(extra.EnF(i)*extra.StF(i));
end

IntCount = 1;
totdiff  = 0;
cerrfret=1;
tr=1;
for i=1:N
    if ~feof(fid1)

        % Reading segment header.
        extra = ReadSpecFileHeader(fid1,extra,2,i);
     if(i>1)
       xdiff = extra.X(i)- extra.X(i-1);
       ydiff = extra.Y(i)- extra.Y(i-1);
```

```
    totdiff = xdiff + ydiff;
    if(abs(totdiff) > 0)
          dx = xdiff/IntCount;
          dy = ydiff/IntCount;
          for jj=1:IntCount
                extra.X(i-jj) = extra.X(i-jj)+ (IntCount-jj)*dx;
                extra.Y(i-jj) = extra.Y(i-jj)+ (IntCount-jj)*dy;
                extra.totdiff(i-jj) = totdiff;
          end
             IntCount = 1;
             totdiff = 0;
     else
          IntCount = IntCount+1;
     end
     if(i == N)
          if(abs(dx)> abs(dy))
              if(dx > 0)
                   dx = 17.0;
                   dy = 0.0;
               else
                    dx = -17.0;
                    dy = 0.0;
               end
           else
               if(dy>0)
                    dx = 0.0;
                    dy = 17.0;
                else
                    dx = 0.0;
                    dy = -17.0;
                end
           end
           for jj=1:IntCount-1
                 extra.X(i-jj) = extra.X(i-jj)+ (IntCount-jj)*dx;
                 extra.Y(i-jj) = extra.Y(i-jj)+ (IntCount-jj)*dy;
                 extra.totdiff(i-jj) = totdiff;
           end
     end
end

     % Filtering of frequencies below 14 kHz (by removing them from
     the data).
     lowin = find(extra.spectra(:,1) <=3500);
     extra.spectra(lowin,:) = [];

     ResultsErrFre = CalculateTipperPE(extra,NoOfBands);

     murrot=size(ResultsErrFre);
     IndexErrFreT(i) = murrot(1);
     ResultsErrFreT(cerrfret:cerrfret+IndexErrFreT(i)-1,1:2)=
     ResultsErrFre(:,1:2);
     cerrfret = cerrfret+IndexErrFreT(i);

     if i==N

         inErrFreT=unique(ResultsErrFreT(:,1));
         leninErrFreT=length(inErrFreT);
         for luiet=1:1:leninErrFreT;
             ind=find(ResultsErrFreT(:,1)==inErrFreT(luiet));
             InSaErrFre=ResultsErrFreT(ind,1:2);
```

```
                % Mean of the PEs for the profile length (file).
                PreMeT(luiet)=mean(InSaErrFre(:,2));
            end

        % Plots of the means of Prediction errors for new formula.
        figure('Name','Prediction Errors of Hz vs. Frequency
        (Hz)','NumberTitle','off')
        loglog(inErrFreT,PreMeT,'*b','MarkerSize',3)
        title({'Prediction Errors of Hz vs. frequency (Hz) for file:';
        num2str(file)})
        xlabel('Frequency (Hz)'), ylabel('Prediction Errors of Hz'), grid
        on
        axis([9800 300000 min(PreMeT) max(PreMeT)])

        ResultsErrFreT=[];
        end

        fprintf('Ready segment number :%d \n',i)
        extra.spectra =[];
    else
        break;

    end
end
fclose(fid1);
```

9.3.8 Sub-function *CalculateTipperPE.*

```
% ************************************************************************
% This function calculates the mean of the prediction errors over a
certain profile length.
% ************************************************************************

function ResultsErrFre = CalculateTipperPE(extra,NoOfBands)

% Makes overlapping bands with 1 octave wide.
Hx = (extra.spectra(:,4)+sqrt(-1)*extra.spectra(:,5));
Hy = (extra.spectra(:,6)+sqrt(-1)*extra.spectra(:,7));
Hz = (extra.spectra(:,8)+sqrt(-1)*extra.spectra(:,9));

% Calculates the Vertical noise.
HSNR = extra.spectra(:,3);
Vnoise = ((abs(Hx).^2 + abs(Hy).^2)./(10.^(HSNR./10))./4.0; % Sigma^2.
ErrPEs=sqrt(Vnoise);
extra.Vnoise = Vnoise;
cerrfre=1;
for i = 1:NoOfBands
    in = find(( extra.spectra(:,2) >= extra.StF(i) & extra.spectra(:,2)
<= extra.EnF(i) ));
    if (~isempty(in) && length(in)>1)
                HH = [Hx(in) Hy(in)];
                Tippers(i,:) = inv(conj(HH')*HH)*(conj(HH')*Hz(in));
                Hzest = HH*conj(Tippers(i,:)');
                % Estimation of Prediction Errors.
                preerrorT=sqrt(((conj(Hz(in)-Hzest)).*(Hz(in)-
                 Hzest))./((ErrPEs(in)).^2));
```

```
                ErrFre=[extra.spectra(in,2) preerrorT];
                siErrFre=size(ErrFre);
                IndexErrFre(i) = siErrFre(1);
                ResultsErrFre(cerrfre:cerrfre+IndexErrFre(i)-1,1:2)=
                 ErrFre(:,1:2);
                cerrfre = cerrfre+IndexErrFre(i);
                in=[];
    else
                Tippers(i,:) = -1000;
    end
end
```

9.3.9 Function *FilterAirDataFinalPERemoval*.

```
% ********************************************************************
% This program remove frequencies by using the Prediction Error criterion
%
% Called functions:
%   RunSpectraNewFormatPERemoval (mainfunction).
% ********************************************************************

function FilterAirDataFinalPERemoval

format long

% Select file for processing.
datapath    = uigetdir('C:\','Select the data directory to read');
resultpath  = uigetdir('C:\','Select the results directory to write');
files = dir(datapath);
NoofFiles = size(files);

for kk =3:NoofFiles
    rr=kk-2;
    RunSpectraNewFormatPERemoval(datapath,resultpath,files(kk).name,rr);
end
```

9.3.10 Function *RunSpectraNewFormatPERemoval*.

```
% ********************************************************************
% Reading spectra-files from a directory, filter them and save the
% filtered files in a new directory.
%
% Called functions:
%   PEsRemoval      (subfunction).
%   CalculateTipper (subfunction).
% ********************************************************************

function RunSpectraNewFormatPERemoval(datapath,resultpath,file,rr)

fprintf(' The data file being processed: %s \n',file)

% Opens files.
fid1 = fopen([datapath '/' file]);
out_filename = [resultpath '/' 'filteredPE3_' file];
fid2 = fopen(out_filename, 'wt');
out_filename = [resultpath '/'  file(1:length(file)-7) 'tensor'];
fid3 = fopen(out_filename, 'wt');
```

```
extra = [];
extra = ReadSpecFileHeader(fid1,extra,1,0);

% Number of stations in file.
N = extra.first_segment;

extra.spectra = [];
extra.num_transmitters = [];
add = 1;

% Makes overlapping bands of 1 octave for tensor calculations.
StartingFrequency = 10000;
NoOfBands = 9;
Inc = sqrt(2.0);
extra.StF(1) = StartingFrequency;
extra.EnF(1) = extra.StF(1)*2.0;
extra.TarF(1)= sqrt(extra.EnF(1)*extra.StF(1));
for i = 2:NoOfBands
    extra.StF(i) = extra.StF(i-1)*Inc;
    extra.EnF(i) = extra.StF(i)*2.0;
    extra.TarF(i)= sqrt(extra.EnF(i)*extra.StF(i));
end

IntCount = 1;
totdiff  = 0;
cerrfret=1;
contador=0;
for i=1:N
    if ~feof(fid1)
        %Reading segment header
        extra = ReadSpecFileHeader(fid1,extra,2,i);

     if(i>1)
       xdiff = extra.X(i)- extra.X(i-1);
       ydiff = extra.Y(i)- extra.Y(i-1);
       totdiff = xdiff + ydiff;
       if(abs(totdiff) > 0)
             dx = xdiff/IntCount;
             dy = ydiff/IntCount;
             for jj=1:IntCount
                    extra.X(i-jj) = extra.X(i-jj)+ (IntCount-jj)*dx;
                    extra.Y(i-jj) = extra.Y(i-jj)+ (IntCount-jj)*dy;
                    extra.totdiff(i-jj) = totdiff;
             end
                IntCount = 1;
                totdiff = 0;
        else
             IntCount = IntCount+1;
        end
        if(i == N)
             if(abs(dx)> abs(dy))
                 if(dx > 0)
                      dx = 17.0;
                      dy = 0.0;
                  else
                       dx = -17.0;
                       dy = 0.0;
                  end
              else
                  if(dy>0)
```

```
                    dx = 0.0;
                    dy = 17.0;
                else
                    dx = 0.0;
                    dy = -17.0;
                end
            end
            for jj=1:IntCount-1
                extra.X(i-jj) = extra.X(i-jj)+ (IntCount-jj)*dx;
                extra.Y(i-jj) = extra.Y(i-jj)+ (IntCount-jj)*dy;
                extra.totdiff(i-jj) = totdiff;
            end
        end
    end

        % Filtering of frequencies below 14 kHz (by removing them from
        the data).
        lowin = find(extra.spectra(:,1) <= 3500);
        extra.spectra(lowin,:) = [];

        % Filtering of frequencies above a specific PE value.
        extra = PEsRemoval(extra,NoOfBands);

        sizSE=size(extra.spectra);
        if (sizSE(1)>1)
        contador=contador+1;

        % New number of transmitter after removing frequencies.
        newtranssize=size(extra.spectra);
        extra.new_num_transmitters(contador) = newtranssize(1);

        % Saves information into a new filtered spectra file.
        sizespe=size(extra.spectra);
        IndexRout(contador) = sizespe(1);
        Results(add:add+IndexRout(contador)-1,1:9)=extra.spectra(:,1:9);
        add = add+IndexRout(contador);

        Tippers = CalculateTipper(extra,NoOfBands);
        TippTot(1:NoOfBands,:,i) = Tippers;

        else
            disp('extra.spectra with not enough data')
        end

        fprintf('Ready segment number :%d \n',contador)

        extra.spectra =[];
    else
        break;

    end
end
extra.first_segment=contador;
% Saves the spectra file header in the new filtered spectra file:
WriteSpecFileHeader(fid2,extra,1,0)

% Saves the spectra file header in the  tensor tipper file:
WriteSpecFileHeader(fid3,extra,1,0)
```

```
EndInd = contador-1;
fclose(fid1);

% Saves information header about the transmitters
add = 1;
IntCount = 1;
totdiff  = 0;
for i=1:1:EndInd
    % Writing of segment header into the filtered spectra file.
    WriteSpecFileHeader(fid2,extra,2,i);

    % Writing of the new filtered data into the file.
    fprintf(fid2,'%8d  %7.1f  %5.2f  %10.5f  %10.5f  %10.5f  %10.5f  %10.5f
%10.5f \n',Results(add:add+IndexRout(i)-1,1:9)');
    add = add+IndexRout(i);

    % Writing of the segment header into the tensor tipper file.
    WriteSpecFileHeader(fid3,extra,2,i);

    % Making a packed tensor matrix.
    if(extra.totdiff(i) >= 0)
          TensorPack = [extra.TarF' extra.TarF' ...
                        real(TippTot(1:NoOfBands,1,i)) ...
                        imag(TippTot(1:NoOfBands,1,i)) ...
                        ones(9,1)*0.01 ...
                        real(TippTot(1:NoOfBands,2,i)) ...
                        imag(TippTot(1:NoOfBands,2,i)) ...
                        ones(9,1)*0.01 ];
     else
          TensorPack = [extra.TarF' extra.TarF' ...
                        -real(TippTot(1:NoOfBands,1,i)) ...
                        -imag(TippTot(1:NoOfBands,1,i)) ...
                        ones(9,1)*0.01 ...
                        -real(TippTot(1:NoOfBands,2,i)) ...
                        -imag(TippTot(1:NoOfBands,2,i)) ...
                        ones(9,1)*0.01 ];
    end

    % Writing of the packed results into the file.
    fprintf(fid3,'  %8.1f  %8.1f  %8.5f  %8.5f  %8.5f  %8.5f  %8.5f  %8.5f
    \n',TensorPack');

end

fclose(fid2);
fclose(fid3);

disp('function:Runspectra - ready')
```

9.3.11 Sub-function *PEsRemoval.*

```
% ************************************************************************
%  This function removes those frequencies with PE vales above a
%threshold.
************************************************************************

function extra=PEsRemoval(extra,NoOfBands)
```

```
% First step is to make bands of overlapping with 1 octave width.
Hx = (extra.spectra(:,4)+sqrt(-1)*extra.spectra(:,5));
Hy = (extra.spectra(:,6)+sqrt(-1)*extra.spectra(:,7));
Hz = (extra.spectra(:,8)+sqrt(-1)*extra.spectra(:,9));

% Calculates the Vertical noise.
HSNR = extra.spectra(:,3);
Vnoise = ((abs(Hx).^2 + abs(Hy).^2)./(10.^(HSNR./10))./4.0; % Sigma^2.
ErrPEs=sqrt(Vnoise);
extra.Vnoise = Vnoise;

Tippers = -1000.0*(ones(2,NoOfBands)+sqrt(-1.0)*ones(2,NoOfBands));
Tippers = Tippers';

for i = 1:NoOfBands
    in = find(( extra.spectra(:,2) >= extra.StF(i) & extra.spectra(:,2)
     <= extra.EnF(i) ));

    if (~isempty(in) && length(in)>1)
                HH = [Hx(in) Hy(in)];
                Tippers(i,:) = inv(conj(HH')*HH)*(conj(HH')*Hz(in));
                Hzest = HH*conj(Tippers(i,:)');

                % Estimation of Prediction Errors.
                 preerrorT=sqrt(((conj(Hz(in)-Hzest)).*(Hz(in)-
                 Hzest))./((ErrPEs(in)).^2));

                % Calculates the 20% of the number of transmitters in the
                 sub-band.
                LPET=length(preerrorT);
                RejectPE=round(LPET/5);

                % Determines those PEs larger than or equal 3.
                inPEAb=find(preerrorT>=3);

                if ((~isempty(inPEAb)) && (length(in)>2))

                    % Case where the number of noise frequencies is
                    % greater than the 20% of the transmitters.
                    if ((length(inPEAb))>=RejectPE)

                        PEsttf=sort(preerrorT(inPEAb),'descend');
                        PEstt=PEsttf(1:1:RejectPE);

                        for ch=1:1:length(PEstt)

                       inpruebb(ch)=find(preerrorT(inPEAb)==PEstt(ch));
                        end
                        extra.spectra(in(inPEAb(inpruebb)),:)=[];
                        inpruebb=[];

                    % Case where the number of noise frequencies is
                    % less than the 20% of the transmitters.
                    elseif ((length(inPEAb)<RejectPE))
                        extra.spectra(in(inPEAb),:)=[];
                    end

                else
                    disp('No values could be found')
```

```
                end
    else
                Tippers(i,:) = -1000;
    end
end
```

9.3.12 Function *MakeXYZFile*.

```
% ************************************************************************
% This function reads all the tensor-files in a directory and save them
% as 9 different stacked frequency files (.xyz) for further processing
% in the software 'Oasis Montaj'
% ************************************************************************

function MakeXYZFile

datapath    = uigetdir('C:\','Select the data directory to read');
resultpath  = uigetdir('C:\','Select the results directory to write');
files       = dir(datapath);
NoofFiles   = size(files);

extra = [];

for num = 1:9  %Number of stacked frequencies in the tensor-file.
    fc = 1;
    for kk =3:NoofFiles

        fprintf(' The data file being processed: %s \n',files(kk).name)

        % Opens files.
        fid1 = fopen([datapath '\' files(kk).name]);
        nr = num2str(num);
        fid3 = fopen([resultpath '\' 'Torsby_tensor', nr, '.xyz'], 'at');

        % Reads the 1st tensor file header:
        extra = ReadTensorFileHeader(fid1,extra,1,0);
        N = extra.first_segment;
        cnt = 0;
        for i=1:N
            if ~feof(fid1)

                %Reading information header
                extra = ReadTensorFileHeader(fid1,extra,2,i);
                cnt = cnt+1;

            else
                %fprintf('End of file reached \n');
            end
        end

        %*********************************************
        % THIS PART HAS TO BE REMOVED IF THE PROCESSING IS
        % DONE IN MORE THAN ONE STEP!

        if fc == 1
            % Save header in new file.
            if kk == 3
                fprintf(fid3, ' %s ', '/ X ');
```

```
                fprintf(fid3, ' %s ', ' Y ');
                fprintf(fid3, ' %s ', ' Z ');
                fprintf(fid3, ' %s '  ,' AR ');
                fprintf(fid3, ' %s '  ,' AI ');
                fprintf(fid3, ' %s '  ,' AE ');
                fprintf(fid3, ' %s '  ,' BR ');
                fprintf(fid3, ' %s '  ,' BI ');
                fprintf(fid3, ' %s '  ,' BE ');
                fprintf(fid3,'\n');
                fprintf(fid3,' %s \n', 'Line 1');
                fc = 0;
            end
        end;
        %*********************************************

        % Saves information to new file.
        for k = 1:(N-1)
            %fprintf('%d %d %d \n',k,N,cnt)
            fprintf(fid3,'%10.1f ',extra.X(k));
            fprintf(fid3,'%10.1f ',extra.Y(k));
            fprintf(fid3,'%5.1f ',extra.altitude(k));
            fprintf(fid3,'%10.6f\t %10.6f\t %10.6f\t %10.6f\t %10.6f\t
            %10.6f\n',extra.spectra(num,3:8,k)');
        end;
    end;

    n = num2str(num);
    fprintf('Data file %s is ready! \n', n);
    pause(0.01);
    fclose(fid3)

end;
disp('function:RunTensor - ready!')
fclose all;
```